Automotive Lubricant Testing and Additive Development

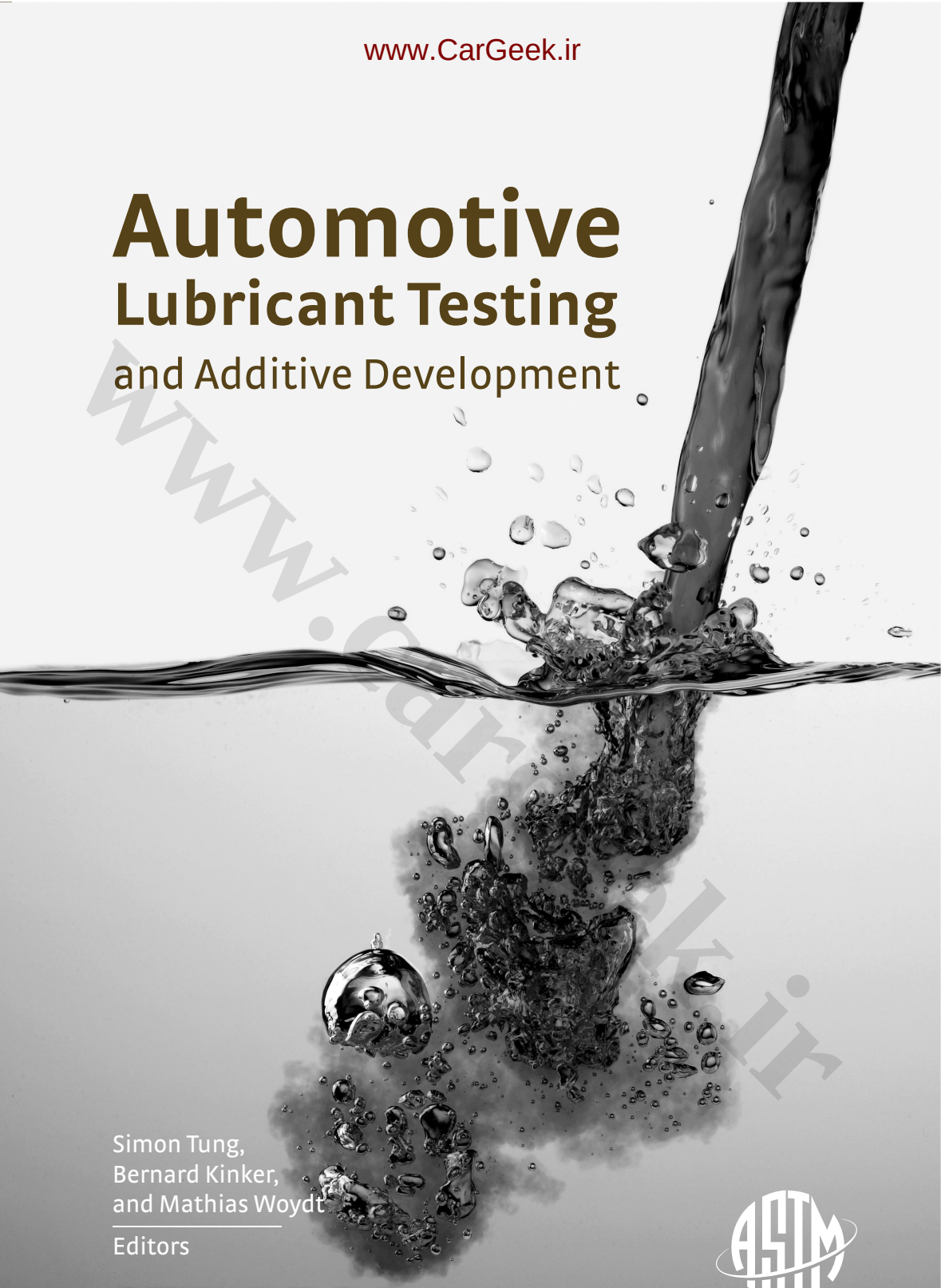

Simon Tung,
Bernard Kinker,
and Mathias Woydt
Editors

STP 1501

ASTM INTERNATIONAL
Standards Worldwide

STP 1501

Automotive Lubricant Testing and Advanced Additive Development

Dr. Simon Tung, Mr. Bernard Kinker, and Dr. Mathias Woydt, editors

ASTM Stock Number: STP1501

ASTM
100 Barr Harbor Drive
PO Box C700
West Conshohocken, PA 19428-2959

Printed in the U.S.A.

Library of Congress Cataloging-in-Publication Data

Automotive lubricant testing and additive development / Simon Tung, Bernard Kinker, and Mathias Woydt, editors.
p. cm. — (ASTM stock number: STP1501)
ISBN: 978-0-8031-4505-4
1. Automobiles--Motors--Lubrication systems. 2. Automobiles--Lubrication. I. Tung, Simon. II. Kinker, Bernard, 1945- III. Woydt, Mathias, 1963- IV. ASTM International.
TL214.O5A98 2008
629.25'5--dc22

2007051559

Peer Review Policy

Each paper published in this volume was evaluated by two peer reviewers and at least one editor. The authors addressed all of the reviewers' comments to the satisfaction of both the technical editor(s) and the ASTM International Committee on Publications.

The quality of the papers in this publication reflects not only the obvious efforts of the authors and the technical editor(s), but also the work of the peer reviewers. In keeping with long-standing publication practices, ASTM International maintains the anonymity of the peer reviewers. The ASTM International Committee on Publications acknowledges with appreciation their dedication and contribution of time and effort on behalf of ASTM International.

Printed in Mayfield, PA
April, 2008

Foreword

This publication, *Automotive Lubricant Testing and Advanced Additive Development*, contains peer reviewed papers from the above symposium, organized by committee D02, in December, 2006 at Lake Buena Vista, Florida. This symposium was in conjunction with the D02 sub-committee “Fuels and Lubricants”. The symposium Co-Chairs were Dr. Simon Tung, General Motors, Warren, MI, Mr. Bernard Kinker, Rhomax, USA, Horsham, PA, and Dr. Mathias Woydt, BAM, Federal Institute for Materials Research and Testing, Berlin, Germany.

Contents

Overview

This book represents the work of several authors at the 1st Symposium organized by D02 to focus on automotive lubricant testing and advanced additive development. This symposium was held at Lake Buena Vista, Florida, in conjunction with the meeting in December 2006 of the ASTM D02 sub-committee “Fuels & Lubricants”.

In order to help automotive industry meet lower emission standards, higher fuel economy goals, and loger drain intervals associated with a minimization of any adverse effects of lubricants to the environment, the petroleum industries and the additive suppliers are developing low SAPS (sulfated ash, phosphorus and sulfur) and high tribological performance lubricants to meet these challenges. New developments in powertrain system design and advanced additive formulation are essential in addressing these problems. This ASTM symposium has provided an outstanding forum to discuss how OEMs and lubricant companies are solving real engineering problems to increase fuel economy and meet emissions legislation together. This symposium publication is focused on both the chemical and tribological aspects of the functional performance of automotive lubricant and testing. In this symposium, recent advances in additive and base oil chemistry and function have been covered in details; product formulation for engine performance and the link between additive chemistry and emissions have been discussed. Tribological performance issues such as fuel economy retention, wear protection and friction reduction as well as their retention over drain, engine durability, and future challenges, including advanced powertrain developments, new lubricant test methods outside of the application, lubricant formulations, and correlation between lubricant formulation and engine performance are the key subjects.

Papers and presentations are targeted to provide a comprehensive overview of various lubrication test methods for a typical engine system including the oxidation tests for screening antioxidants and base oils, bench wear tests, engine sequence test development, and oil condition monitoring techniques, as well as the major technical issues on lubricant degradation and the surface mechanisms of ZDDP tribofilms interacted with advanced DLC coatings.

Several papers describes the low SAP lubricant development and testing, the impact of additive and base oil on engine oil characteristics, the current industrial standard tests methods for lubricant oxidation stability, surface pitting, and alternative engine oil development. Some of the papers discuss the synergistic effects of lubricant additive formulation and surface coatings while others concentrated on the coverage of various surface engineering applicators in practice. This particular surface engineering area continues to be the major activity of many industrial researchers.

As in the past ASTM lubricant symposium lubricant formulation technology was always a critical focus theme. This ASTM symposium was no exception. The diversity demonstrated in this symposium exemplified the critical role of the lubricant formulation issues which was influenced by recent automotive hardware changes. Papers ranged from a discussion of low SAP lubricants and validation of oxidation stability for factory fill and alternative engine oils used in new automotive emission system. Impact of emission regulations and hardware changes on lubricant formulations also was discussed this symposium. In addition, the additive development addressing surface interaction studies between advanced materials and lubricants plays an important role for automotive hardware changes.

On the behalf of all editors and chairs, we would like to thank the outstanding contributions from all authors and speakers in this symposium for making our 1st automotive lubricant testing and additive development symposium very successful. Thank you for your participation. We hope we will organize another symposium in the near future.

Dr. Simon Tung
General Motors
Warren, MI

Mr. Bernard Kinker
Rhomax, USA
Horsham, PA

Dr. Mathias Woydt
BAM, Federal Institute for Materials Research and Testing
Berlin, Germany

Journal of ASTM International, Vol. 4, No. 7
Paper ID JAI100849
Available online at www.astm.org

Vincent Gatto,[1] *William Moehle,*[1] *Emily Schneller,*[1] *Thalan Burris,*[1]
Tyler Cobb,[1] *and Mark Featherstone*[1]

A Review of Engine Oil Oxidation Bench Tests and Their Application in the Screening of New Antioxidant Systems for Low Phosphorus Engine Oils

ABSTRACT: A review of current oxidation and deposit bench tests used for the evaluation of engine oil performance will be presented. Some of the more meaningful tests will be utilized to evaluate a number of antioxidant systems for oxidation and deposit control capabilities in engine oils formulated with 470 ppm of ZDDP-derived phosphorus. The antioxidant components are selected from a series of commonly used and commercially available materials plus one new developmental component. These components include an organo-molybdenum compound (MoDTC), an alkylated diphenylamine (NDPA), a conventional hindered phenolic (HPE), a high performance hindered phenolic (MBDTBP), and a new multi-functional boronated MBDTBP. The performance of these fully formulated engine oils will be ranked in the selected bench tests in order to highlight the benefits of each antioxidant system under evaluation. The results point to significant benefits with the molybdenum- and boronated-systems, or mixed molybdenum-/boronated-systems, for oxidation control, while systems containing NDPA and MBDTBP are favored more for deposit control. Unique and superior performing antioxidant systems will be recommended for screening in fired engine and bench wear tests.

KEYWORDS: oxidation, viscosity increase, stabilization, deposits, antioxidants, engine oil, bench tests

Introduction

In recent years greater performance demands have been placed on engine oils to deliver superior oxidation and deposit control protection. This has occurred concurrently with the mandated reductions of phosphorus driven by concerns to protect engine catalyst systems. This has forced the use of lower levels of zinc dalkyldithiophosphate (ZDDP) in modern engine oils. Such formulation changes have had a number of negative impacts on engine oil performance. ZDDP is known to be one of the most cost effective antioxidants and antiwear additives available. Reductions in its use must be compensated for by the use of other phosphorus-free components. A challenge exists for the engine oil formulator to identify the most cost effective alternatives to ZDDP using inexpensive yet meaningful bench test techniques.

Figure 1 illustrates one example of the technical challenge lubricant formulators must address when moving to lower phosphorus engine oils. The chart shows TEOST MHT® results for two 5W-30 engine oils containing varying amounts of phosphorus from ZDDP. The chart also highlights the GF-3 and proposed GF-5 passing limits for maximum deposits in the TEOST®. Note that the passing limits have dropped from 45 to 25 mg with the advance of the category, while the deposit forming tendency of the test oil has increased from 30 to 64 mg. This observed change is due exclusively to the reduction in ZDDP level.

Deposit formation is just one aspect associated with lubricant oxidation. Parameters such as viscosity increase and varnish formation are critical performance measures in a variety of fired sequence engine tests. While it is conceivable to develop engine oils around TEOST® performance, it becomes impractical from a cost and time standpoint to use sequence engine tests to optimize for all oxidation parameters. This has recently led to increased interest in oxidation bench tests to optimize engine oil formulations for

Manuscript received October 16, 2006; accepted for publication July 9, 2007; published online August 2007. Presented at ASTM Symposium on Automotive Lubricant Testing and Additive Development on 3–5 December 2006 in Lake Buena Vista, FL; Simon Tung, Bernard Kinker, and Mathias Woydt, Guest Editors.
[1] Albemarle Corporation, P.O. Box 341, Baton Rouge, LA 70821.

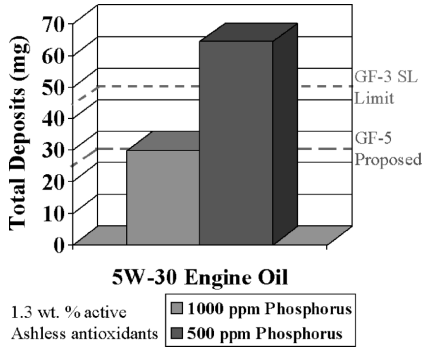

FIG. 1—*Effects of phosphorus reduction on the TEOST MHT.*

eventual evaluation in fired engines [1]. A number of reports focus on designing bench tools to model engine oil performance in engine tests [2–4]. A drawback to this approach is that changes in engine tests make the associated bench tests obsolete. Another approach involves using a variety of oxidation bench tests to evaluate different aspects of lubricant oxidation. The purpose of this paper is to review the types of oxidation bench tests that are available for monitoring different aspects of lubricant oxidation. A brief review of oxidation mechanisms will be presented and related to a few of the more commonly used oxidation bench test tools. A combination of tests will be presented to show how engine oil formulations can be optimized for all aspects of lubricant oxidation.

Mechanism of Lubricant Oxidation and Stabilization

The mechanisms of lubricant oxidation and stabilization have recently been reviewed [5,6]. As this report will deal more with testing methods, only a brief discussion will be presented.

Figure 2 provides a schematic representation showing the chemical transformations that take place during lubricant oxidation. In this scheme the various *R* groups represent different hydrocarbon chains of the lubricant. The oxidation process produces hydroperoxides that are somewhat unstable at elevated temperatures. These hydroperoxides will cleave to form alkoxy radicals that can undergo one of two possible fates. It is possible they can react with hydrocarbon molecules in the lubricant to produce alcohols. Alternatively, they can undergo a chain scission reaction to produce two lower molecular weight hydrocarbon fragments, a carbonyl compound which can be an aldehyde or ketone, and an alkyl radical. The aldehydes and ketones are known to undergo condensation reactions that eventually lead to the formation of polymerization products. These aldehydes and ketones can also undergo further oxidation to produce organic acids.

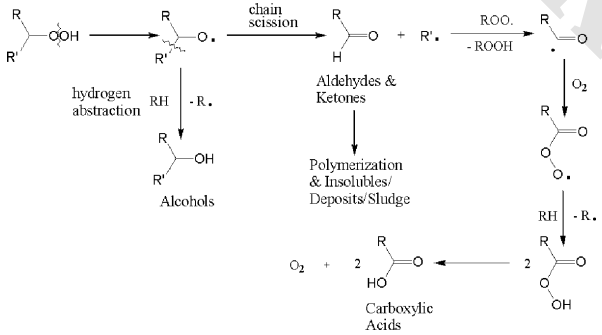

FIG. 2—*Mechanism of lubricant degradation.*

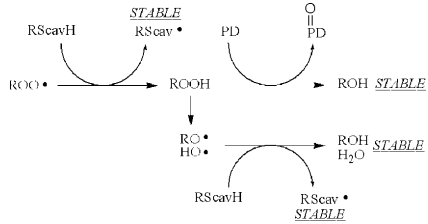

FIG. 3—*Mechanism of radical scavenger (RScavH) and peroxide decomposer (PD) antioxidant function.*

The polymerization products cause a number of physical changes in the lubricant that result in fluid thickening, sludge and volatiles formation, and eventually varnish and deposit formation. These changes can be monitored by measuring viscosity increase of the lubricant, by using FT-IR to determine the increase in carbonyl compounds that are present during the oxidation process, or by measuring the increase in acid number. Some of these condition monitoring tools will be discussed in detail in the experimental section.

Antioxidants are used to inhibit oxidation and protect the lubricant from the degradation processes described above. In general, two types of oxidation inhibitors are available to the lubricant formulator, the radical scavengers, of which hindered phenolics and alkylated diphenylamines are the most common; and peroxide decomposers, of which sulfur and phosphorus compounds, and organomolybdenum compounds are the most common. The chemistry of all these antioxidant types, and their mechanism of function, has been extensively studied [7–9]. Figure 3 shows a generalized mechanism of antioxidant function for radical scavengers and peroxide decomposers. Synergism between different antioxidant types is also an important contributor to the overall stabilization effect observed when combinations of antioxidants are utilized. Detailed discussions on the mechanisms and types of antioxidant synergism can be found in the literature [5,6,10,11].

Engine Oil Oxidation Bench Tests

The complexity of lubricant degradation and antioxidant function makes it a challenge when trying to select a single bench test for evaluating an engine oils oxidation resistance. Many tests have been developed to study different aspects of engine oil oxidation [12]. The diversity and complexity of test methods can be illustrated in the oxidation bench test matrix shown in Table 1. This matrix lists a variety of different oxidation tests in terms of the mode of oxidation (thin-film or bulk), and the physical or chemical changes that occur during the degradation process (chemical oxidation or deposit/varnish formation).

Thin-film oxidation tests generally use very small sample sizes to produce small lubricant film thicknesses. This approach maximizes oxygen diffusion and allows for a greatly accelerated test. The rate of oxidation can be accelerated further by elevating the temperature or by utilizing an oil soluble oxidation catalyst. These thin-film tests can be broken down into two types, those that monitor chemical oxidation, and those that produce a varnish or deposit from oxidation of the thin-lubricant film. Examples of thin-film type tests that monitor chemical changes in the engine oil are Pressurized Differential Scanning Calorimetry (PDSC) [13–15] and the Thin-Film Oxygen Uptake test (TFOUT) [16,17]. A well known example of

TABLE 1—*Oxidation bench test matrix.*

	Thin-Film Oxidation	Bulk Oil Oxidation
Chemical Oxidation (O_2 Absorption)	PDSC - D 6186 [13–15] TFOUT - D 4742 [16,17]	AIBOT/D 2893 [22,34] FOAT [23] IP-48 [24], D 2893 [34] CVIT/IP-280 [4]
Deposit or Varnish Formation (Surface Promoted)	CMOT [18] PSMOT [19–21]	Panel coker [29,30] HTT [31] TEOST MHT [26,28] TEOST 33C [25,27]

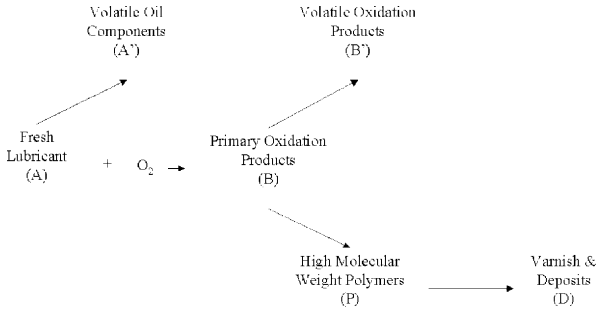

FIG. 4—*Kinetic model of lubricant deposit formation under thin-film conditions.*

a thin-film engine oil test that produces deposits on a carbon steel surface is the Caterpillar Micro-Oxidation Test (CMOT) [18]. This latter test was originally developed by researchers at Penn State University and is also called the Penn State Micro-Oxidation Test [19–21].

Bulk oil oxidation tests generally involve aging larger reservoirs of engine oil at an elevated temperature, and usually for a longer period of time. The use of greater lubricant volumes allows for monitoring the degradation of the engine oil by a variety of analytical techniques. Thickening or oil polymerization can be monitored by viscosity increase. Oxidation can be monitored by acid formation and the increase of carbonyl compounds by FT-IR. The depletion of additives, especially antioxidant depletion, can be monitored using FT-IR or potentiometric methods. The versatility of these tests to easily change temperature, the oxidant (air, oxygen, or air containing NOx), oxidation catalyst type, and analysis parameters makes them very popular to additive researchers and engine oil formulators. Typical examples of chemical oxidation bulk oil tests are the Albemarle Bulk Oxidation Test (AlBOT) [22], the Ford Oil Aging Test (FOAT) [23], the Ciba Viscosity Increase Test (CVIT) [4], and the IP-48 Oxidation Test [24].

A unique group of bulk oil tests deserve special description as they encompass characteristics of the traditional bulk oil oxidation tests combined with thin-film oxidation conditions. These tests are listed in the bottom right quadrant of the oxidation bench test matrix shown in Table 1. Examples of these tests are the Thermo-Oxidation Engine Oil Simulation Test (TEOST MHT® or TEOST 33C®) [25–28], the Panel Coker Test [29,30], and the Komatsu Hot Tube Test (HTT) [31]. These tests all pass a reservoir of oil over a metal or glass surface heated at temperatures generally over 200°C. In the TEOST and Panel Coker the stressed oil is continually recirculated or splashed over the heated surface for the length of the test, while in the Hot Tube Test the oil passes over the heated surface only once. The flow of oil is used to generate a thin-oil film on the heated surface that results in the formation of a varnish or deposit. The degree of varnish formation is usually determined by establishing a rating scale, while the degree of deposit formation is often measured by a weight increase on the surface where the thin-film is produced.

The physical and chemical transformations taking place in any given oxidation bench test can be described by the flow chart shown in Fig. 4. This diagram has been reported earlier to describe a multi-step mechanism for deposit formation in the micro-oxidation test [1,19,32,33]. The principles can be used to describe most oxidation tests if the individual steps are properly weighed. For example, a typical bulk oil oxidation test will likely not contain the varnish or deposit component D. Alternatively, it's known that the TEOST® encompasses a significant contribution from volatile oil components A′ and volatile oxidation products B′. A proper understanding of how an oxidation bench test relates to Fig. 4 is important if one is to fully understand the benefits and limitations of that test relative to engine tests or real world use.

Referring back to Table 1, a reasonable selection of oxidation bench tests might include PDSC, the AlbOT, the CMOT, and the TEOST MHT® as this covers all of the quadrants shown in the matrix. Below we report an oxidation study where a variety of mixed antioxidant systems are screened in these bench tests in order to identify the most effective, or robust, system for use in low phosphorus passenger car engine oils.

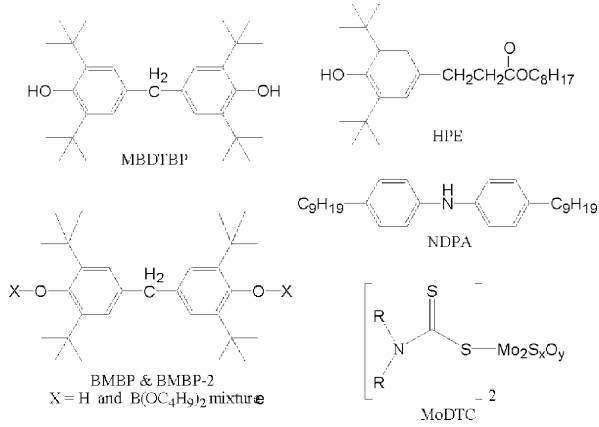

FIG. 5—*Antioxidants chosen for evaluation of low phosphorus engine oils.*

Experimental

Antioxidants

The antioxidants chosen for this study are shown in Fig. 5. The additives HPE and MBDTBP represent two different hindered phenolics commonly used in engine oils. The dimer MBDTBP possesses a high total phenolic content with the two hindered-phenolic groups connected by a single methylene (CH_2) bridge. The ester HPE represents a mono-cyclic hindered phenolic that possesses a much lower phenolic content compared to MBDTBP. All of these phenolics are of low volatility and considered effective antioxidants in high temperature lubricant applications. The nonylated diphenylamine (NDPA) and molybdenum dithiocarbamate (MoDTC) chosen for this study are commonly used commercial lubricant additives. Finally, a new multi-functional antioxidant BMBP has been included in this study. This new antioxidant combines boron with the hindered phenolic functionality of MBDTBP. Two versions of BMBP were used. The material designated BMBP contained 22.3 wt. % MBDTBP and 79.2 % of borate esters as determined by high pressure liquid chromatography (HPLC), and had a boron content of 1.8 wt. %. The material designated BMBP-2 contained 38.4 wt. % MBDTBP and 55.5 % of borate esters as determined by HPLC, and had a boron content of 1.4 wt. %.

Passenger Car Engine Oil Formulations

An engine oil preblend was prepared by mixing additives and base oil so that the finished oil contained 4.80 wt. % succinimide dispersant, 1.80 wt. % overbased calcium detergent, 0.5 wt. % neutral calcium detergent, and 0.60 wt. % secondary zinc dialkyldithiophosphate, with the balance composed of Group II base oil. The Group II base oil had a kinematic viscosity @100°C of 6.1 cSt, a viscosity index of 114, and a Noack volatility of 8 wt. %. The nonylated diphenylamine (NDPA), hindered phenolics (HPE and MBDTBP), and boronated phenolics (BMBP and BMBP-2) were added to the preblend as indicated in the graphed results where percentages are by weight. The Group II base oil was used as the diluent to complete the blend. The organo-molybdenum compound MoDTC, when used, was added to deliver either 360 ppm molybdenum ion (indicated as Mo in the graphed results) or 180 ppm molybdenum ion (indicated as 1/2 Mo in the graphed results) to the finished engine oil. All of the finished engine oil blends contained 470 ppm of phosphorus, 520 ppm of zinc, and 2400 ppm of calcium.

Oxidation Bench Test Conditions

A brief description of the oxidation bench test conditions used in this study, including some improvements or modifications that have been made to the tests, are provided below.

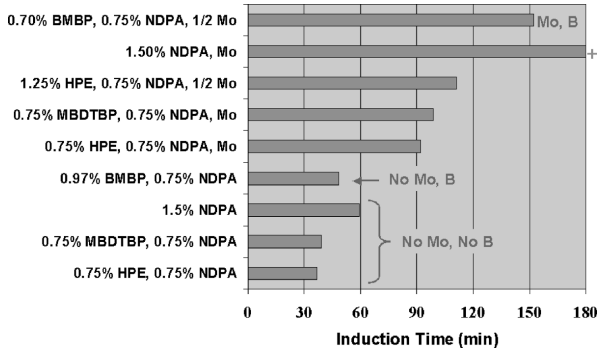

FIG. 6—*Evaluation of low phosphorus engine oils by PDSC.*

Pressurized Differential Scanning Calorimetry (PDSC)

The general test operation is described in ASTM D 6186 [13]. Details of the tests utility can be found in the literature [14,15]. In this study an oil sample size of approximately 3.0 mg was employed. Oxidation of the oils was carried out in the presence of 50 ppm iron from an iron(III)naphthenate oxidation catalyst. Testing was performed at 180°C under 500 psig oxygen and an oxygen purge rate of 100 mL/min. Test results are reported as the oxidation induction time (OIT) resulting from an exothermic release of heat caused by oxidation of the thin-film of oil. The method of calculating OIT is provided in the ASTM procedure. Each engine oil was evaluated in duplicate and the average determined. The OIT results are shown in Fig. 6.

Albemarle Oxidation Test (AlbOT)

This bulk oil oxidation test is similar to ASTM D 2893 [34], but has been modified for studying the oxidation properties of low phosphorus engine oils. In this modification 300 mL of engine oil is treated with 110 ppm iron from an iron(III)naphthenate oxidation catalyst. The treated oil is heated at 150°C while dry oxygen is bubbled through the oil at a flow rate of 10 L/h. Aged oil samples are removed from the test at specified time intervals. Kinematic viscosities of the aged oils are determined at 40°C. The aged oils are also tested by FT-IR for the formation of carbonyl oxidation products using the Peak Area Increase (PAI) method reported by Obiols [35]. Results are reported as percent viscosity increase versus the fresh oil (% Visc. Inc.), or PAI, and are plotted as a function of test time. In this study samples were removed for analysis every 24 h until the 168-h sample was reached, or until a breakpoint caused by rapid viscosity increase or rapid carbonyl oxidation was reached. The percent viscosity increase and PAI results are shown in Figs. 7 and 8.

Modified Caterpillar Micro-Oxidation Test (CMOT)

A variety of modifications to the CMOT have been reported in the literature. The procedure followed in this study has been modified from that reported by Caterpillar [18]. In the Caterpillar procedure the carbon steel coupon is placed in the impinger tube and the apparatus stabilized for 20 min in the heating bath. The oil sample is then applied to the coupon with a syringe. The weight of oil applied is determined by the change in weight of the syringe before and after sample application. This approach suffers from a number of problems. First, a direct determination of the amount of oil on the coupon surface is not possible. Second, application of the oil sample on the coupon surface cannot be visually confirmed since the coupon is submerged with the impinger in the heating bath. It was felt that these conditions would negatively impact test repeatability because small losses of the sample during application could not be controlled or even detected. In order to address this limitation a modification was made where the oil sample was weighed directly on the carbon steel surface. This involved, (1) placing the coupon in the impinger tube, (2) accurately weighing the impinger tube/coupon assembly, (3) carefully applying the oil sample to the coupon via a syringe while the impinger tube/coupon assembly is still on the balance, (4) reweighing the

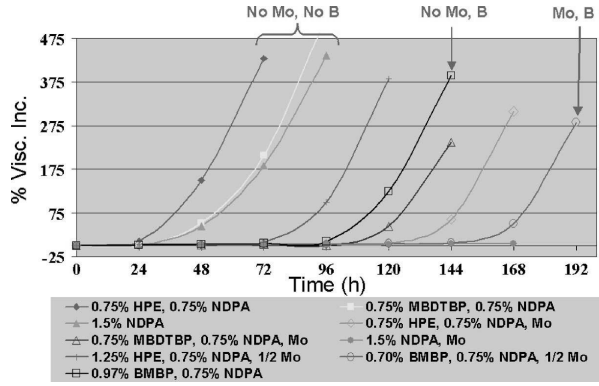

FIG. 7—*Evaluation of low phosphorus engine oils in the AlBOT (Visc. Inc.).*

impinger tube/coupon assembly after the oil sample has been added, and (5) placing the sample/impinger tube/coupon system in the heated bath. This approach has been successful in improving test repeatability.

The following test conditions were used: engine oil sample size, approximately 20 μL accurately weighed; temperature, 230°C; and air flow, 20 mL/min. Sampling was performed at 10-min intervals. However, the time range for sampling depended upon the oxidative stability of the engine oil. Less stable oils were sampled between 50 and 120 min, while more stable oils were sampled between 110 and 180 min. In two cases oils were sampled over a broader range of 50 to 160 min. Each engine oil was evaluated in triplicate and the results averaged. Results are reported as weight percent deposits formed as a function of time, and as the onset time to a rapid increase in deposit formation. Onset time is determined by calculating the intercept between the baseline formed where minimal deposits are seen, and the slope produced when a rapid increase in deposit formation is observed. The percent deposit results are shown in Fig. 9 and the onset time results are shown in Fig. 10.

Thermo-Oxidation Engine Oil Simulation Test (TEOST MHT®)

The TEOST MHT-4® is a standard lubricant industry test for the evaluation of the oxidation and carbonaceous deposit-forming characteristics of engine oils. The test is designed to simulate high-temperature deposit formation in the piston ring belt area of modern engines. The test utilizes a patented instrument with the MHT-4 protocol being a relatively new modification to the test. Details of the test operation and specific MHT-4 conditions appear in ASTM D 7097 [26]. Test results are reported as total rod deposits.

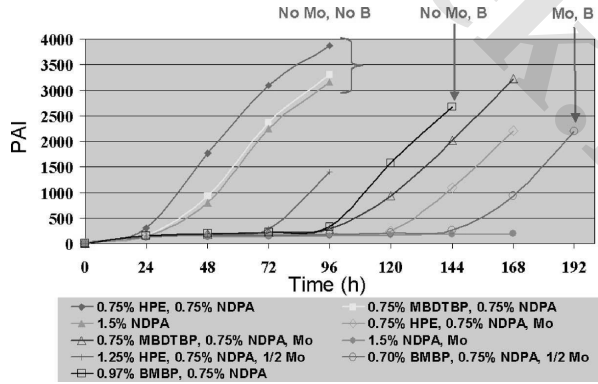

FIG. 8—*Evaluation of low phosphorus engine oils in the AlBOT (PAI).*

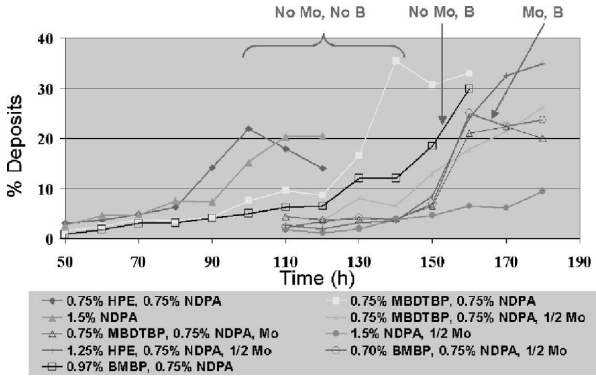

FIG. 9—*Evaluation of low phosphorus engine oils in the CMOT (% deposits).*

Engine oils were tested in duplicate and the average determined. The total rod deposit results for the engine oils in this study are shown in Fig. 11.

Certain additional precautions within the scope of the ASTM method were followed to improve TEOST® precision and repeatability. First, laboratory humidity was closely monitored and tests were only performed if the relative humidity in the lab was below 70 %. In the past we have found that higher humidity levels can result in higher test variability for certain types of weakly stabilized engine oils.

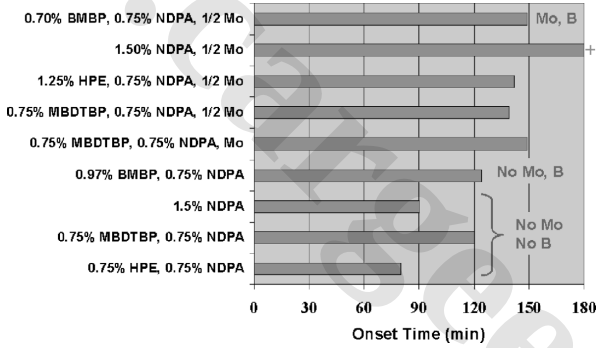

FIG. 10—*Evaluation of low phosphorus engine oils in the CMOT (onset time).*

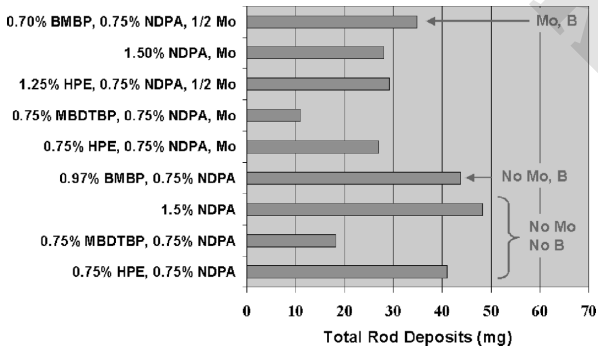

FIG. 11—*Evaluation of low phosphorus engine oils in the TEOST MHT.*

Second, each test was closely monitored to ensure oil flow ran evenly down the coiled deposit rod. Tests producing uneven or sporadic flow were terminated. Finally, a Teflon washer has recently been developed by the TEOST® manufacturer to prevent contamination of the test sample while in the sample flask. This washer was used to protect the test sample in this study.

Results and Discussion

Antioxidant System Selection

The antioxidants chosen for this study are described in the experimental section. The materials HPE, MBDTBP, NDPA, and MoDTC all represent commercial antioxidants that have seen widespread use in engine oils for many years. The specific additive combinations and the chosen treat levels were selected in order to achieve defined performance levels and detect synergies that might be apparent in the various bench tests under investigation. For example, there are reports in the literature of alkylated diphenylamine/molybdenum combinations, and alkylated diphenylamine/hindered phenolic combinations, showing enhanced viscosity or deposit control performance in certain bench and engine tests [9,36]. It has also been reported that molybdenum has beneficial antiwear properties in low phosphorus engine oils [37]. It's believed that reductions in ZDDP will require higher treat levels of both ashless antioxidants and organomolybdenum compounds.

A new multi-functional antioxidant system has been included in this study. The boronated phenolic antioxidants BMBP and BMBP-2 represent the reaction product of MBDTBP with a boron source [38,39]. This class of antioxidant was developed many years ago but did not see widespread use at the time because high levels of ZDDP were sufficient to provide both oxidation and antiwear protection. We have decided to revisit this class of chemistry to determine if it has any utility in modern low phosphorus engine oils. The benefits of boron in engine oils are well established [40]. Traditionally boron is added to engine oils through the dispersant. This new class of additive represents a new approach that combines the benefits of boron with antioxidancy. Recently, there have been reports of molybdenum/boron additive combinations providing antiwear benefits to low phosphorus engine oils [41]. The use of a boronated hindered phenolic antioxidant with organomolybdenum represents a new formulation approach that may provide oxidation, wear, and friction reduction benefits. In this study only the oxidation and deposit control aspects will be evaluated.

Oxidation Bench Test Results

PDSC

The ability to extend oxidation induction time in the PDSC is illustrated in Fig. 6 where OIT is plotted for the low phosphorus engine oils. The weakest performing system is the combination of HPE and NDPA, while the strongest performing system is the combination of NDPA and molybdenum. All the molybdenum-containing systems appear to significantly outperform the molybdenum-free systems. The systems containing boron tend to outperform similar boron-free systems, but this effect is more pronounced when molybdenum is present in the formulation. Referring only to the PDSC test, one would recommend one of two possible antioxidant systems; the one composed of NDPA and molybdenum, or a system containing BMBP, NDPA, and molybdenum.

AlbOT

The ability to control viscosity increase or the formation of carbonyl oxidation products is illustrated in Figs. 7 and 8 where the degree of oxidation is plotted as a function of test time for the low phosphorus engine oils. A shift to the right in these plots represents an improvement in oxidation performance. The trends seen here are similar to those seen in the PDSC, however, there are a few interesting differences. First, there is a significant improvement in oxidation control when increasing molybdenum and decreasing HPE in the mixed HPE/NDPA/molybdenum antioxidant system. This response is reversed in the PDSC results. Second, the molybdenum-free BMBP/NDPA combination significantly outperforms one of the

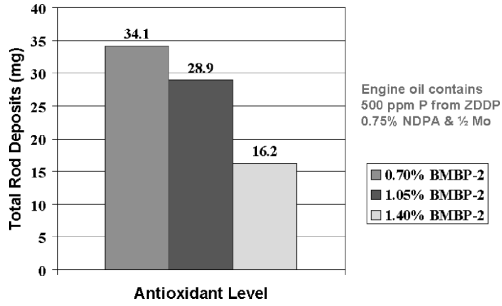

FIG. 12—*Effect of BMBP-2 treat level on TEOST deposit performance.*

molybdenum-containing systems, while this response is reversed in the PDSC results. As with the PDSC results, the best performing systems are either NDPA/molybdenum or BMBP/NDPA/molybdenum. Note that for the NDPA/molybdenum system no viscosity or PAI break was observed even after 168 h.

Modified CMOT

The ability to control deposit formation in the CMOT is illustrated in Figs. 9 and 10. In Fig. 9 the degree of deposit formation is plotted as a function of test time, while in Fig. 10 the onset time to a rapid increase in deposit formation is plotted for the low phosphorus engine oils. A shift to the right in Fig. 9 represents an improvement in deposit control, while an increase in onset time in Fig. 10 represents the resistance of an oil to undergo a rapid increase in deposit formation. These results are clustered into four groups. The weakest performing are the molybdenum-free systems consisting of NDPA or HPE/NDPA. A significant improvement is seen when shifting to the MBDTBP/NDPA or BMBP/NDPA antioxidant combinations. A further improvement is seen when shifting to the hindered phenolic/NDPA/molybdenum antioxidant combinations. Finally, the most significant performance increase is seen when formulating with the NDPA/molybdenum combination. For this latter system the onset time exceeds the 180 h test time.

TEOST MHT®

The ability to control deposit formation in the TEOST MHT® is illustrated in Fig. 11 where total rod deposits are plotted for the low phosphorus engine oils. These results provide a different picture regarding the most effective antioxidant systems for deposit control. The antioxidant systems containing a combination of NDPA and MBDTBP are the better performing. This is true in the presence or in the absence of molybdenum. The NDPA/molybdenum system, which performed exceptionally well in the other three bench tests, is showing only modest performance in the TEOST®. The low deposit result for the MBDTBP/NDPA system relative to the all NDPA or mixed HPE/NDPA systems illustrates a very unique and powerful antioxidant synergism that exists in the presence or absence of molybdenum. This effect has been reported in much greater detail in an earlier TEOST® study [42].

An additional set of TEOST experiments were performed using a sample of BMBP-2 containing a very high level of MBDTBP. These results are shown in Fig. 12. The treat level of BMBP-2 was varied from 0.70 wt. % to 1.40 wt. %. The results show exceptional TEOST deposit control at the highest level. BMBP-2 is expected to deliver approximately 0.55 wt. % of the highly effective antioxidant MBDTBP when used at 1.40 wt. % in the engine oil. Note these TEOST results are consistent with the MBDTBP/NDPA results in Fig. 11. This suggests the TEOST performance of BMBP and BMBP-2 can be attributed to the level of free MBDTBP present in the engine oil.

Antioxidant System Assessment Using the Oxidation Bench Test Matrix

A summary of the best performing antioxidant systems in each of the oxidation bench tests used in this study is provided in Table 2. This tool clearly shows that antioxidant system selection is very much dependent on the type of test being performed. This is probably equally true when evaluating antioxidant

TABLE 2—*Antioxidant system assessment using the oxidation bench test matrix.*

	Thin-Film Oxidation	Bulk Oil Oxidation
Chemical Oxidation (O_2) Absorption	*PDSC - D 6186* #1 - NDPA/Mo #2 - BMBP/NDPA/Mo	*AIBOT/D 2893* #1 - NDPA/Mo #2 - BMBP/NDPA/Mo
Deposit or Varnish Formation (Surface Promoted)	*CMOT* #1 - NDPA/Mo #2 - BMBP/NDPA/Mo or MBDTBP/NDPA/Mo	*TEOST MHT* #1 - NDPA/MBDBP/Mo #2 - NDPA/MBDTBP

systems in fired engines. In the case of bench tests, however, the time and cost necessary for performing the evaluations is relatively small.

While NDPA/molybdenum appears to do well in the PDSC, AlBOT, and CMOT, Table 2 shows the combination is weak with regard to TEOST® deposit control. Figure 11 shows this system cannot achieve the proposed 25 mg maximum spec being considered for GF-5 passenger car engine oils. Alternatively, Fig. 11 shows two MBDTBP/NDPA formulations that can achieve the 25 mg maximum specification, but these systems are less effective in the other tests. One promising candidate for further investigation is the mixed system consisting of BMBP-2/NDPA and molybdenum, especially if higher levels of BMBP-2 can be used.

Conclusions

This review has shown that a variety of bench tools are available for evaluating the oxidation properties of low phosphorus engine oils. By considering the different modes of operation, the number of tests can be narrowed down to a few that provide the most diverse range of oxidation conditions. Considerations of bulk versus thin-film oxidation conditions, and chemical oxidation versus deposit formation parameters, are useful in narrowing the range of screeners for more detailed bench testing.

In this study PDSC, AlBOT, CMOT, and TEOST MHT® were selected for a detailed screening program. A variety of engine oils containing 470 ppm phosphorus, and containing different antioxidant systems, were screened in these tests to determine the optimum antioxidant system. No single system stands out as being superior in all the tests utilized. However, a number of candidates show promise for further testing and optimization. NDPA/molybdenum looks promising but requires the use of very high levels of molybdenum in order to achieve reasonable TEOST® results. A new antioxidant system composed of BMBP-2/NDPA/molybdenum can achieve excellent TEOST® results but requires the use of high levels of BMBP-2. Finally, a traditional antioxidant combination of MBDTBP/NDPA is exceptionally effective in the TEOST®, with or without molybdenum, but appears weak in some of the other tests. Further optimization of these antioxidant systems should take into consideration the overall needs of the lubricant by considering the antiwear and friction reduction properties of the boron and molybdenum containing additives.

References

[1] Hutchings, M., Chasan, D., Burke, R., Odorisio, P., Rovani, M., and Wang, W., “Heavy Duty Diesel Deposit Control…Prevention as a Cure,” *SAE* Paper No. 972954, 1997, pp. 155–165.

[2] Lakatos, L. K., Jones, R. N., Roby, S. H., and Sukys, D. J., “Modeling of ASTM Sequence IIIE Piston Ring Land Deposit Formation,” *SAE* Paper No. 922293, 1992, pp. 15–22.

[3] Gunsel, S., Lockwood, F. E., and Westmoreland, T. D., “Engine Oil Oxidation Correlation of the ASTM III-D and III-E Sequence Engine Tests to Bench Tests,” *SAE* Paper No. 892164, 1989, pp. 1320–1328.

[4] Mazzamaro, G. A., Hutchings, M., Vargo, M. W., Evans, S., and Cassidy, D., “Proper Antioxidant Selection for API SH by Statistical Evaluation in a New Sequence IIIE Screening Test,” *SAE* Paper No. 940793, 1994, pp. 1–6.

[5] Rasberger, M., “Oxidative Degradation and Stabilization of Mineral Oil Based Lubricants,” *Chemistry and Technology of Lubricants*, R. M. Motier and S. T. Orszulik, Eds., Blackie Academic and

Professional, London, 1997, pp. 98–143.
[6] Gatto, V. J., Moehle, W. E., Cobb, T. W., and Schneller, E. R., "Oxidation Fundamentals and Its Application to Turbine Oil Testing," *J. ASTM Int.*, Vol. 3(4), 2006.
[7] Gatto, V. J. and Grina, M. A., "Effects of Base Oil Type, Oxidation Test Conditions and Phenolic Antioxidant Structure on the Detection and Magnitude of Hindered Phenolic/Diphenylamine Synergism," *Lubr. Eng.*, Vol. 55(1), 1999, pp. 11–20.
[8] Migdal, C. A., "Antioxidants," *Lubricant Additives Chemistry and Applications*, L. R. Rudnick, Ed., Marcel Dekker, Inc., New York, 2003, pp. 1–28.
[9] Gatto, V. J. and Bezjak, Y. L., "The Antioxidant Properties of Organomolybdenum Compounds in Engine Oils," *Tribology and Lubrication Technology*, Vol. 62(1), 2006, pp. 32–39.
[10] Scott, G., *Atmospheric Oxidation and Antioxidants*, Elsevier Publishing Company, Amsterdam, 1965, pp. 203–218.
[11] Scott, G., "Synergism and Antagonism," *Atmospheric Oxidation and Antioxidants Volume II*, G. Scott, Ed., Elsevier Science Publishers B. V., Amsterdam, 1993, pp. 431–459.
[12] Wang, J. C., "High Temperature Liquid Lubricant Development Part II: Bench Test Development," *SAE* Paper No. 932843, 1993.
[13] ASTM Standard D 6186-98, "Standard Test Method for Oxidation Induction Time of Lubricating Oils by Pressure Differential Scanning Calorimetry (PDSC)," *Annual Book of ASTM Standards*, Vol. 05-03, ASTM International, West Conshohocken, PA, 1998.
[14] Hsu, S. M., Cummings, A. L., and Clark, D. B., "Evaluation of Automotive Crankcase Lubricants by Differential Scanning Calorimetry," *SAE* Paper No. 821252, 1982.
[15] Walker, J. A. and Tsang, W., "Characterization of Lubricating Oils by Differential Scanning Calorimetry," *SAE* Paper No. 801383, 1980.
[16] ASTM Standard D 4742-96, "Standard Test Method for Oxidation Stability of Gasoline Automotive Engine Oils by Thin-Film Oxygen Uptake (TFOUT)," *Annual Book of ASTM Standards*, Vol. 05.02, ASTM International, West Conshohocken, PA, 1996.
[17] Ku, C.-S., and Hsu, S. M., "A Thin-Film Oxygen Uptake Test for the Evaluation of Automotive Crankcase Lubricants," *Lubr. Eng.*, Vol. 40(2), 1984, pp. 75–83.
[18] Zerla, F. N. and Moore, R. A., "Evaluation of Diesel Engine Lubricants by Micro-Oxidation," *SAE* Paper No. 890239, 1989, pp. 193–199.
[19] Palekar, V., Duda, J. L., Klaus, E. E., and Wang, J., "Evaluation of High Temperature Liquid Lubricants Using the Penn State Micro-Oxidation Test," *Lubr. Eng.*, Vol. 52(4), 1996, pp. 327–334.
[20] Perez, J. M., Kelley, F. A., and Klaus, E. E., "Development and Use of the PSU Microoxidation Test for Diesel Engine Oils," *SAE* Paper No. 872028, 1987.
[21] Klaus, E. E., Cho, L., and Dang, H., "Adaptation of the Penn State Microoxidation Test for the Evaluation of Automotive Lubricants," *SAE* Paper No. 801362, SAE Sp. Pub. 80-473, 1980, pp. 83–92.
[22] Gatto, V. J., Elnagar, H. Y., Moehle, W. E., and Schneller, E. R., "Redesigning Alkylated Diphenylamine Antioxidants for Modern Lubricants," *Lubr. Sci.*, Vol. 19, 2007, pp. 25–40.
[23] Korcek, S., Jensen, R. K., and Johnson, M. D., "Assessment of the Useful Life of Current Long-Drain and Future Low-Phosphorus Engine Oils," *TriboTest*, Vol. 9(3), 2003, pp. 197–207.
[24] "Determination of Oxidation Characteristics of Lubricating Oil," Institute of Petroleum Test Method IP 48, 1997, 61 New Cavendish Street, London W1G 7AR.
[25] ASTM Standard D 6335-036, "Standard Test Method for Determination of High Temperature Deposits by Thermo-Oxidation Engine Oil Simulation Test," *Annual Book of ASTM Standards*, Vol. 05-03, ASTM International, West Conshohocken, PA, 2003.
[26] ASTM Standard D 7097-05, "Standard Test Method for Determination of Moderately High Piston Deposits by Thermo-Oxidation Engine Oil Simulation Test—TEOST MHT," *Annual Book of ASTM Standards*, Vol. 05.04, ASTM International, West Conshohocken, PA, 2005.
[27] Selby, T. W. and Florkowski, D. W., "The Development of a Thermo-Oxidation Engine Oil Simulation Test (TEOST)," *SAE 1993 Transactions, J. of Fuels and Lubricants*, Vol. 102, Section 4, 1994, pp. 1870–1887.
[28] Selby, T. W. and Florkowski, D. W., "The Development of the TEOST MHT Bench Test of Engine Oil Piston Deposit Tendency," *Proceedings, 12th Int. Coll. Trib., Technische Akademie Esslingen*,

Ostfildern, Germany, Supplement, 2000, pp. 55–62.

[29] "Coking Tendency of Oil," Federal Test Method Standard No. 791B, Method 3462, January 15, 1969.

[30] Brown, G., Barr, D., Calder, R., Durham, J., McAtee, R., and Sutton, M., "A New Screening Test for the Thermo-Oxidative Stability of Engine Oils – The Glass Panel Coker," SAE Sp. Pub. *SP-1885, Engine Lubricants, Effects of Fuels & Lubricants on Automotive Devices, and Lubricant Applications & New Test Methods*, 2004, pp. 235–245.

[31] Ohkawa, S., Seto, K., Nakashima, T., and Takase, K., "Hot Tube Test—Analysis of Lubricant Effect on Diesel Engine Scuffing," *SAE* Paper No. 840262, 1984, pp. 1–13.

[32] Wang, J. C., Duda, J. L., and Klaus, E. E., "A Kinetic Model of Lubricant Deposit Formation Under Thin Film Conditions," *Tribol. Trans.*, Vol. 37(1), 1994, pp. 168–174.

[33] Wang, J. C., "Deposit Formation Tendency of Lubricants at High Temperatures," *Lubr. Eng.*, Vol. 51(5), 1995, pp. 413–419.

[34] ASTM Standard D 2893-03, "Standard Test Method for Oxidation Characteristics of Extreme-Pressure Lubrication Oils," *Annual Book of ASTM Standards*, Vol. 05.01, ASTM International, West Conshohocken, PA, 2003.

[35] Obiols, J., "Lubricant Oxidation Monitoring Using FTIR Analysis—Application to the Development of a Laboratory Bulk Oxidation Test and to In-Service Oil Evaluation," JSAE Technical Paper No. *20030124*, JSAE, Tokyo, Japan, 2003.

[36] Hamblin, P. C., and Rohrbach, P., "Piston Deposit Control Using Metal-Free Additives," *Lubr. Sci.*, Vol. 14(1), 2001, pp. 3–22.

[37] Hartley, R. J. and Waddoups, M., "Lubricating Oil Compositions With Reduced Phosphorus Content," European Patent Application EP 1 321 506 A2, June 25, 2003.

[38] Hinkamp, J. B., "Liquid Hydrocarbon Compositions of Boron Esters," U.S. Patent 3,509,054, April 28, 1970.

[39] Wright, W. E., Davis, B. T., Matteson, D. S., and Knapp, G. G., "Haze-Free Boronated Antioxidant," U.S. Patent 4,927,553, May 22, 1990.

[40] Choudhary, R. B., and Pande, P. P., "Lubrication Potential of Boron Compounds: An Overview," *Lubr. Sci.*, Vol. 14(2), 2002, pp. 211–221.

[41] Brown, A. J., Chung, S.-S. M., and Arrowsmith, S., "Boron Containing Lubrication Oil Compositions with Low Sulfur and Low Phosphorus Content," European Patent Application EP 1 310 549 B1, May 31, 2006.

[42] Moehle, W. E., Cobb, T. W., Schneller, E. R., and Gatto, V. J., "Utilizing the TEOST MHT to Evaluate Fundamental Oxidation Processes in Low Phosphorus Engine Oils," *Tribol. Trans.*, Vol. 50, 2007, pp. 96–103.

Journal of ASTM International, Vol. 4, No. 10
Paper ID JAI100894
Available online at www.astm.org

Kenneth O. Henderson[1] *and C. Patrick Maggi*[1]

Viscometric Temperature Sensitivity of Engine Lubricants at Low Temperature and Moderately High Shear Conditions

ABSTRACT: Low-temperature viscosity of engine oils is a key indication of a lubricant's capacity to provide wear protection during starting and subsequent operation of an engine. Some 40 years ago the Cold Cranking Simulator (CCS) was developed to measure the low-temperature viscosity of engine oil with viscometric conditions similar to a starting engine. The importance of cranking viscosity has grown since the test was originally developed and is now one of two low-temperature viscosity measurements that define the SAE grades for engine oils. Previous studies evaluating viscosities determined by the CCS have focused on test precision and correlation to engine starting performance. This study evaluates the effects small offsets from the indicated temperature have on the measured apparent viscosity of engine oils. Interest in this topic was driven by the observation that some engine oil formulations have abnormally high variation in viscosity. All the low-temperature viscosity measurements were made in the CCS in accord with ASTM D 5293-04. A small temperature offset was achieved by adjusting the CCS temperature probe calibration so that the indicated test operating temperature was offset from the true temperature. The viscosity data were collected using automatic thermoelectrically cooled CCS instruments. Comparative viscosity data were collected on instruments using cold methanol to control the sample temperature. The oil samples in this study consisted of base oils, a selection of commercial engine oils of the API performance category SL, recent ASTM Interlaboratory Crosscheck Program (ILCP), and from the Low Temperature Engine Performance (LTEP) study which was conducted in the 1990s. The LTEP oils are of an earlier performance category and thus have a different composition than either the API SL commercial engine oils or the ASTM ILCP program oils. Results of this study show that when the CCS stator and sample are warmer than the indicated temperature, the measured viscosities are higher than when the viscosity is measured at the correct (true) temperature. As would be expected, the opposite response is seen when the offset is in the opposite direction. This response to the temperature offset is opposite of what would be traditionally expected—lower temperatures typically result in higher measured viscosities. As seen in the study, this is a result of the way the instrument is calibrated and not a fluid anomaly. Some of the API SL oils exhibited more than a 5 % change in measured viscosity from a 0.5°C shift in temperature. Base oils and synthetic formulations only had a change of around 1 % due to a 0.5°C shift in temperature. The samples of API SG oils have temperature sensitivity lower than the API SL oils tested. This study compares data obtained on instruments using two different methods of controlling sample temperature. For the samples evaluated in this program, the data indicated no relative bias between the two methods (thermoelectric and cold methanol) of stator temperature control.

KEYWORDS: cranking viscosity, ccs, low-temperature viscosity, engine lubricants, SAE J300, temperature sensitivity

Introduction

The Cold-Cranking Simulator (CCS) was developed nearly 40 years ago in response to an industry need for a more accurate low-temperature viscosity measurement which approximated the actual conditions an engine experienced when cranking at low temperatures. Before the CCS instrument, low-temperature viscosity of engine oils was determined by extrapolating from higher-temperature kinematic viscosity data as well as other techniques. The CCS was designed to measure the viscosity of engine lubricants at low temperature under conditions that approximate the conditions in an engine journal bearing during starting [1–4]. An engine's cranking speed is a critical factor in starting an engine at low temperatures. The cranking speed is directly related to the lubricant's viscosity, and thus CCS viscosity is referred to as the cranking viscosity (CV). Cranking speed had a great impact on starting when the engine was fitted with a

Manuscript received November 2, 2006; accepted for publication October 5, 2007; published online October 2007. Presented at ASTM Symposium on Automotive Lubricant Testing and Additive Development on 3–5 December 2006 in Lake Buena Vista, FL; Simon Tung, Bernard Kinker, and Mathias Woydt, Guest Editors.
[1] Cannon Instrument Company, State College, PA

carburetor and mechanical timing advance. With the advent of electronic ignition and fuel injection, the impact of CV on low-temperature starting has eased somewhat in its criticality. In the past, an engine designer could overcome a lubricant's low-temperature viscosity by adding cranking power to the engine design or by decreasing engine friction.

During these 40 years, the fundamental design of the rotor stator for the CCS has remained constant. Many improvements have been made to the instrument's components that translate the rotor stator response into a viscosity value. These improvements have improved the accuracy of CV measurements. This improvement has been timely as CV has grown to become an important factor in defining engine lubricant formulations. A part of this increased need for better accuracy of CV determinations was driven by the increasingly strict engine oil performance requirements. Today, CV of an engine oil formulation can be a critical constraint in the equation a formulator has to balance during the formulation's design. A new formulation's CV can directly influence the choice of components ultimately used for the formulation. In a blend plant, correcting the viscosity of a product because of an inaccurate cranking viscosity could require inclusion of more expensive components to meet industry specifications. Additionally, accurate measurement of CV is necessary to ensure the formulation is correctly labeled.

For the first 30 years, the temperature of the rotor stator was managed by flowing cold methanol around the CCS stator. Cold methanol, while easy to handle and readily available in the laboratory, has several shortcomings as a low-temperature heat transfer media. When methanol is held at a temperature much below 0°C, it easily absorbs water from the ambient environment. It will continue to absorb water until the mixture crystallizes. As the concentration of water increases, the physical properties of the mixture change. The transfer fluid's viscosity increases and its heat capacity decreases. This increased viscosity reduces flow. To counter the reduced heat capacity, the flow needs to be increased to maintain the same level of control. A response to this can be to either increase the methanol flow or to reduce the fluid temperature. Unfortunately, the thicker bath fluid also tends to increase the thermal gradients in the circulating fluid. The net effect is a stator sample temperature that is unstable. This leads to having an effective sample temperature that is different from the temperature during instrument calibration. This combination increases measurement variability.

The evolution of CCS temperature control began with the original manually controlled instruments. These were cooled to test temperature by using a dry ice-methanol bath to cool the circulated methanol which flowed around the stator. Maintaining a constant stator temperature, which was manually adjusted by the operator, was difficult because of the difficulty in holding the dry ice-methanol mixture at a constant temperature [4]. The advent of using mechanical refrigeration systems improved the operator's ability to maintain a stable cold source temperature when the methanol was dry. All the difficulties in maintaining a constant methanol coolant temperature combine to increase the variability in CV measurements between instruments with methanol coolant. Recent advances in solid-state thermoelectric (TE) devices have made it possible to move away from the circulating liquid as the heat removal media. The newer TE modules now have the necessary thermal capacity in a compact form factor so they can directly cool the stator. This approach provides a uniform heat sink around the periphery of the stator. This provides a nearly constant delta between the stator wall and the surface of the heat sink—independent of ambient temperature. Considering the mechanics of heat flow, this should lead to a more uniform test temperature, which should translate into improved test repeatability. Current CCS designs employ this cooling technology and potentially reduce the CV measurement variance between instruments.

In the early 1980″s, the CCS test method and related specifications were modified to determine CV at multiple temperatures [5]. Using this multi-temperature test method, most users of the test adjusted the methanol bath to a temperature at least 7°C below the lowest test temperature. For example, if the lowest test temperature occurred at −30°C, then the methanol temperature was set to about −37°C. The methanol temperature could be lower, depending on how the methanol had been piped to the instrument. However, by using a bath temperature offset from the lowest test temperature, a different temperature gradient between the coolant and sample was observed at each test temperature. ASTM D 5293 [5] achieved a partial compensation for the multiple temperature gradients by calibrating the instrument at each test temperature. The authors have found that this works well when the calibration oils and test oils all have similar temperature sensitivities or viscosity indexes.

Over the past 20 years, the industry has seen several changes in engine lubricant formulations. These changing requirements, combined with the viscometric characteristics of the components used in engine

oils, have made cranking viscosity a significant criterion when developing formulations. Fortunately, several improvements to the CCS were made during that time to address the more demanding requirements. These included the arrival of microprocessor control, automated data collection, and improved speed resolution. The combination of these changes yields improved measurement precision by removing the variability introduced by operator intervention.

In the early 1990s, ASTM D02.07 was requested to launch a study of low-temperature performance of engine lubricants in modern engines. This study was conducted by ASTM D02.07.C Low Temperature Engine Performance Task Force and evaluated engine starting and pumping requirements at low temperatures. This study found that modern engines started at lower temperatures. The study also found that engine starting strongly correlated with cranking viscosity as measured by the CCS [6]. Most importantly, it showed that modern engines start at lower temperatures than were found in the previous correlation work conducted in the early 1970s. This ability to start at lower temperatures is in part because of changes in ignition design, fuel/air management, and fuel quality. As a result, the specification requirements [7] for cranking viscosity were altered by the SAE Task Force on Engine Oil Viscosity Classification. They increased the viscosity limit by a factor of approximately 1.9 while reducing the test temperature by 5°C. In the CCS, this had the effect of increasing the viscosity range of the instrument, and therefore required some adjustments in the motor-speed to rotor-speed relationship. The reduction of all test temperatures by 5°C exacerbated the thermal gradient between coolant bath and test temperature. With lower test temperatures, a uniform stator temperature between instruments has become a much more critical component when comparing the results between different instruments.

Since the LTEP study, there have been several more changes in the performance requirements of engine oils. The two most recent performance category changes have centered on reducing volatility and increasing fuel economy. These changes in performance requirements have encouraged the use of new Viscosity Index Improver (VII) technology and base oils with higher Viscosity Indexes (VI). These component changes occurred primarily with the introduction of API SL performance category. The characteristics of these new components may have amplified the effect of small differences in instrument operating conditions between laboratories, resulting in greater than anticipated measurement differences or apparent biases.

This study looks at the effect of an error in test temperature on the measured viscosity. This is a topic that has not been covered in previously published papers for CV as determined by the CCS. A temperature error was simulated by altering the temperature sensor calibration to give an offset of ±0.5°C. The viscometric response of the samples measured with the induced temperature offset was atypical. For this project a selection of commercial formulated engine lubricants was used that included the viscosity multigrades SAE 0W-xx, 5W-xx, 10W-xx. The xx of the designation could be 20, 30, 40, or 50 and is the high temperature portion of the Engine Oil Viscosity Classification J300. The selection of samples included both traditional mineral oil formulations and synthetics. The lubricants purchased specifically for this study carried the API SL service classification, as that was the current API service classification at the time of the study. Discussion with several engine oil formulators has indicated that the change from API SL to SM would not likely have an impact on this study.

Experimental Setup

Instrument Description

The CCS is a unique rotational viscometer in terms of its operation. It consists of a rotor stator pair in concentric cylinder geometry. The rotor is connected to the motor by a flexible shaft, two drive pulleys, and a belt. The design concept is fundamentally unchanged from the original CCS instruments. The motor is operated at constant power which is similar to engine operation when starting. The rotor speed is sensed by a speed encoder on the end of the rotor shaft. A temperature sensor in the stator is used for both measuring and controlling temperature.

Temperature Sensor Setup

Sample temperature is sensed by a thermistor. This thermistor is calibrated independently to related resistance to temperature. The following equation was used to relate the CCS thermistor probe resistance to temperature using an SPRT as the thermal reference:

TABLE 1—*Instrument 3054 thermistor probe constants.*

Probe Constant	Temperature Offset +0.5°C	Temperature Offset Zero	Temperature Offset −0.5°C
A0	1.109551	1.109629	1.109751
A1	0.258757	0.258212	0.257667
A2	0.136916E−03	0.134912E−03	0.132928E−03

$$1000/(t + 273) = a_0 + a_1 \ln R + a_2(\ln R)^3 \quad (1)$$

where:

t = temperature in degrees Celsius
R = the resistance of the temperature probe in ohms
$\ln R$ = the natural logarithm of R

a_0, a_1, and a_2 are regression constants.

This study was to evaluate the effect of a temperature offset from true temperature on apparent viscosity. To achieve this offset, the temperatures at which the thermistor resistance was measured were altered so that the instrument would operate either with a warm offset of +0.5°C or with a cold offset of −0.5°C from the indicated temperature. With this approach, the test temperature displayed by the instrument control software would always display the nominal (indicated) operating temperature. This approach was taken so that the testing would use the current version of CCS control software. The probe constants with the different offsets are shown in Table 1 where the "Offset Zero" constants are from the probe certificate.

Instrument

Viscosity measurements were done primarily in current model CCS-2100 instruments which use advanced thermoelectric cooling technology to control the stator temperature. The primary test unit was instrument 3054, with some data being collected on a second instrument, 3127. Instrument 3054 was operated at two different power ratios (PR), which is simply the drive ratio between rotor speed and motor speed. PR1 has a ratio of 98:34, while PR2 has a ratio of 80+40.

PR1 was the drive ratio used in the CCS instruments prior to completing the LTEP study and the resulting change in SAE J300. PR2 drive ratio was used with the CCS to provide the wider viscosity range needed to meet the new SAE J300 requirements with older instruments. With improvements in rotor speed measurement, CCS instruments have reverted to the PR1 drive ratio.

Calibration

The CCS-2100 instrument operation used in this study was managed by ViscPro® for Windows software. Using the most recent version of this software, a sample was tested at multiple temperatures on a single sample injection. All the viscosity data included in this paper used this multi-temperature viscosity measuring ability.

Both 3054 and 3127 instruments were calibrated by first setting the motor current so that the rotor speed was 240±1 r/min, with reference oil CL250 (~3500 mPa(s)) at a −20°C displayed temperature following ASTM D 5293-04 [5]. Before running a test matrix, the instrument was preconditioned by running for three minutes at a speed of approximately 240 r/min. This preconditioning step was done by cooling the sample cell until the rotor speed was ~240 r/min. Once the temperature speed combination was obtained, the rotor was held at that speed for three minutes. This instrument preconditioning is an option in the software. Its purpose is to establish the normal operating thermal gradients in the instrument. This technique can improve the repeatability on the first measurements made in a sample set.

To collect the needed data for calculating the rotor-speed viscosity relationship, the speed for each of the CL reference oils was measured twice at each reference temperature. The calibration test matrix is shown in Appendix A. The calibration constants were then determined by fitting the data according to the following quadratic equation:

$$\eta = B_0/s + B_1 + (B_2 * s) \quad (2)$$

where:

η = apparent dynamic viscosity in mPa(s)
s = rotor speed in KRPM,

B_0, B_1, and B_2 are regression constants.

The calculation of the constants (B_0, B_1, and B_2) was accomplished through the use of the instrument software. These constants were then used to calculate the reference oil viscosities. The first criterion for evaluating a calibration dataset was the coefficient of determination, R^2, which had to be at least 0.99 and preferably greater than 0.995. The lower R^2 was acceptable if the data were distributed on both sides of the line. Next, a comparison of the measured viscosity was made against the certified viscosity of the reference oils to determine if the dataset contained a suspect result. Any calculated CV value that deviated by more than 1.5 % from reference value was rejected and the constants were then recalculated with the remaining dataset. No more than three rejections were permitted for a test temperature. Limiting the rejections ensured that the calibration coefficients were based on a dataset containing at least 10 data pairs (speed and viscosity). If the dataset dropped below 10 data pairs, the calibration was rerun. Note: The current version of ASTM D 5293-04 [5] requires a minimum of four data points per temperature for the calibration and no maximum.

Data Collection

Throughout this study, the sequence of sample testing and the number of test temperatures measured per sample were held constant. The test matrix consisted of 28 test samples (Appendix B.) Of these, four were duplicate samples which were positioned at least five positions apart in the test matrix. Most samples in the test matrix were tested at either four or five temperatures; but a few were tested at only three test temperatures. The test matrix covered the viscosity range of 800 mPa(s) to just over 30 000 mPa(s) and spanned temperatures from −35 to −15°C.

Samples

Samples used in this study consisted of base oils, ASTM Inter Laboratory Check Program (ILCP) oils, commercial engine oils and oils from the LTEP program completed in the late 1990s. Most of the commercial oils (API SL category) were purchased in five quart bottles from a local retail store in Central Pennsylvania. Some of the commercial oil samples were provided by a major engine lubricant manufacturer and these were also API SL category formulations.

Reference material CLNNR is a blend of a nondispersant olefin copolymer (OCP) viscosity index improver (VII) in polyalpha olefin (PAO) base stock. The shear stability index (SSI) for this OCP VII is nominally 50. A high SSI VII was chosen to enhance the formulations sensitivity to shear rate. By using a PAO, the need for pour point depressant was eliminated. The two part composition was chosen to avoid introducing the buffering influence of an engine oils additive package on the viscometric measurement. This composition turned out to be temperature sensitive as well.

Results

Motor Current Setting

Testing for each temperature offset condition began by setting the motor current. The motor current set with reference oil CL250 at true temperatures of −19.5, −20.0, and −20.5°C and a rotor speed of 240±1 r/min provided the information shown in Table 2.

Two power ratios were used with instrument 3054 and one PR with instrument 3127. The current data shown in Table 2 are consistent with the motor in PR1 having a higher mechanical advantage than the motor in PR2 configuration. The motor's higher mechanical advantage of PR1 shows it needs less current to obtain the 240 r/min rotor speed at −20°C with CL250. The relationship between motor current and the true temperature is consistent with the viscosity being less as the temperature increases.

TABLE 2—*Cell temperature versus motor current.*

True Test Temperature, °C	Offset from Indicated Temperature	Indicated Test Temperature, °C	Motor Current, mA		
			3054 PR1	3054 PR2	3127 PR2
−19.5	+0.5	−20.0	446	556	…
−20.0	Zero	−20.0	463	590	554
−20.5	−0.5	−20.0	486	612	…

The use of two PRs with the same constant power source yields slightly different effective shear rates over the instrument's viscosity range of 1500 to 23 000 mPa(s). At a rotor speed of 240 r/min, shear rate for both PRs is equivalent as this is the point where the motor current is set. The data in Fig. 1 show the relationship between viscosity and speed for both PR1 and PR2 in instrument 3054 across the entire operating range of speeds. These data indicate that above 3000 mPa(s) the shear rate is nearly identical between the two power ratios. Below 3000 mPa(s) the shear rate for PR2 is slightly higher than for PR1 at equivalent viscosities. For a given viscosity, the higher speeds with PR2 will result in more viscous heat being created in the rotor-stator gap. This is most noticeable when the viscosity is less than 2000 mPa(s). The shear rate changes by a factor of 10 over the instrument's viscosity range. At 240 r/min, it is approximately 15 600 s^{-1} for both PR1 and PR2. For a viscosity of 10 000 mPa(s), PR1 has a shear rate of ~5900 s^{-1} while PR2 is ~5200 s^{-1}; at 1000 mPa(s), however, PR1 is ~33 800 s^{-1} and PR2 is ~44 000 s^{-1}.

ASTM D 5293-04 [5] specifies setting the motor current with reference oil CL250 at −20°C to achieve a rotor speed of 240 r/min with a tolerance of plus or minus 5 r/min. With the CCS-2100 instruments used in this study, the speed stability over time was observed to be plus or minus 1 r/min. To evaluate the impact of the speed tolerance on measured viscosity, instrument 3054 was configured with a zero temperature offset using PR1. During the current setting step, the speed was set to 245 r/min with CL250 at −20°C and was followed by a full viscosity calibration. The results from the sample matrix showed that the viscosities were all higher by less than 1 % when compared to the viscosities determined when the rotor speed was set correctly at 240 r/min.

Calibration

All the viscosity measurements made in this study were done by making multiple viscosity measurements on a single sample injection into the stator. The acceptability of making multiple viscosity measurements on a single sample was determined in a previous study by the authors. The evaluation was done by making multiple measurements at the same temperature and at multiple temperatures on the same sample. A comparison of the results measured by either criterion showed that making multiple measurements on a

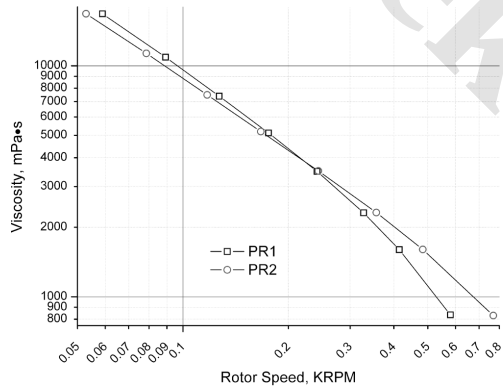

FIG. 1—*Power ratio comparison of calibration oils at −25°C.*

TABLE 3—*−25°C comparison of calibration constants by temperature offset, instrument 3054.*

	Calibration Constants		
Simulated Error	B_0	B_1	B_2
	PR1		
+0.5°C Offset	1060	−775	−461
Zero Offset	1007	−640	−494
Zero Offset 2nd rotor	1032	−661	−435
−0.5°C Offset	967	−364	−684
	PR2		
+0.5°C Offset	897	−131	−305
Zero Offset	890	−71	−335
Zero Offset 2nd rotor	895	−125	−287
−0.5°C Offset	850	43	−378

single sample injection did not significantly impact the results. The variance was well within the stated repeatability of the method and did not show any trend. The study on the impact of multiple measurements included both reference oils and formulated engine lubricants.

The calibration constants for instrument 3054, determined using Eq 2, are shown in Table 3 for the −25°C test temperature. The data in the table include the constants for the two PRs evaluated and the various temperature offsets tested. The B_0 constants for the other test temperatures (−15, −20, −30, and −35°C) varied by 1 to 2 % from those shown; however, the B_1 and B_2 constants varied by 10 % except for −35°C where the variation was larger. The increased variation for −35°C could be the result of not having reference oil with a viscosity below 1700 mPa(s).

The rotor-stator pair was replaced in instrument 3054 toward the end of this study due to a failure of the flexible shaft. The separation of the flexible shaft was caused by the multiple viscosity measurements made beyond the instrument's normal viscosity range, that is greater than 30 000 mPa(s). The calibration constants for this new rotor-stator pair are included in Table 3. The differences between the two rotor-stator pairs exemplify the effect of changing the rotor-stator pair on the calibration constants.

The values of coefficients B_0 and B_1 are the prime contributors to the viscosity calculation. For example, with a rotor speed of 300 r/min and using the constants for PR1 Zero Offset, the viscosity would be:

$$\text{Cranking viscosity} = (1007/0.300) + (-640) + (-494^{*}0.300) = (3357) + (-640) + (-148) = 2569 \text{ mPa(s)}$$

In this example, the second term is 25 % of the result and the third term is a little less than 6 % of the result. As the speed decreases or the viscosity increases, the contributions of the second and third terms become less significant.

Even though there were 15 different formulated oils in this study, we will focus on only four of the oils for most of this paper. These were reference oil CLNNR and engine oils: A34, B1, E1, and H1. A summary of the samples tested is shown in Table 4. It is unfortunate that this work was well underway when API SM oil became available.

Power Ratio

Figure 2 compares the speed data from two measurement sets for CLNNR over a range of temperatures for both the PR1 and PR2 configurations. Based on the difference in mechanical advantage, PR1 and PR2 show slightly different relationships between temperature and rotor speed. This difference is greatest when the temperature was above a −25°C test temperature. However, as seen in Fig. 3 which compares the same data from Fig. 2 but in terms of viscosity, there is little if any difference between measurements made with the two configurations. For the 30 pairs of data for each power ratio, only five data pairs exceeded a 1 % difference between repeat test results and none exceeded 1.6 %. Both configurations are well within the precision of ASTM D5293-04 [5] (2.6 %), with a reproducibility of 7.3 %.

TABLE 4—*Sample oil summary.*

SAE Viscosity Grade	Oil Code	API Category	Formulation Type
0W-30	**A34**	SL	Partial synthetic
0W-30	LTEP 1	SG	Partial synthetic
5W-30	**B1**, C1, D1, S1, A33	SL	Mineral Oil
5W-30	LTEP 2	SG	Mineral Oil
5W-30	**E1**, J1	SL	Synthetic
10W-30	A32, F1, G1, **H1**, T1	SL	Mineral Oil
10W-30	LTEP 3	SG	Mineral Oil
15W-40	A31	SL	Mineral Oil
…	LU 0401	…	Mineral Oil
…	LU 0405	…	Mineral Oil
…	BO 0406	…	Base Oil
…	**CLNNR**	…	PAO/ndVII

Temperature Offset

An interesting characteristic of the instrument's calibration and measurement is the response of the measured viscosity to a temperature offset (Fig. 3). When the temperature is offset in a warmer direction, the

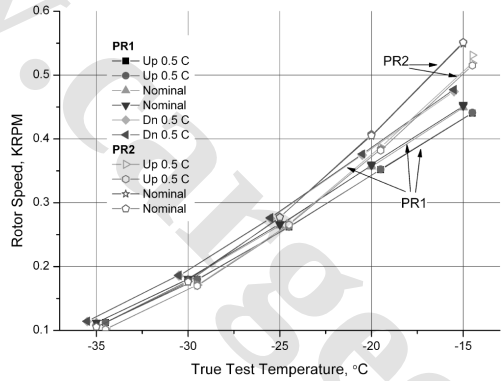

FIG. 2—*Impact temperature offset on rotor speed oil sample—CLNNR.*

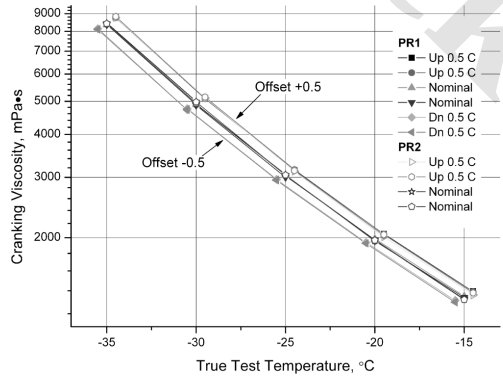

FIG. 3—*Comparison of power ratio on apparent viscosity for oil sample—CLNNR.*

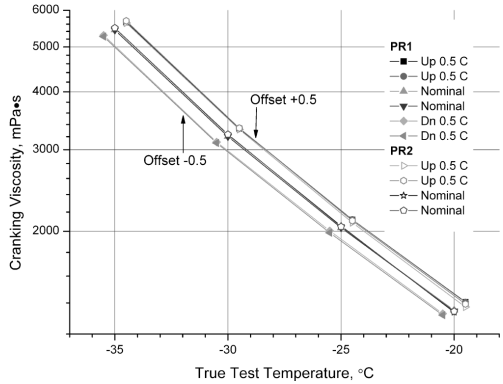

FIG. 4—*Impact of power ratio on apparent viscosity of Oil A34—SAE 0W-30.*

viscosity measured by the CCS is higher than when measured at the correct temperature. This is a reflection of the calibration constants being higher when the temperature error is positive or warmer—essentially the real effect of temperature offset is masked by the calibration.

The viscosity-temperature relationships for three commercial engine oil formulations are shown in Figs. 4–6. The figures include data with both the PR1 and PR2 configurations. Oil A34 (SAE 0W-30) in Fig. 4 indicates that the different power ratio configurations have little effect on the measured viscosity. Oil A34 is presumed to contain either a very good Group 2 base stock or is a partial synthetic product. It can be seen in the figure that the 0.5°C offset uniformly shifts the viscosity by about 5 % at a temperature over the temperature range evaluated.

Oil B1 (SAE 5W-30) in Fig. 5 follows the trend set by Oil A34 in that there is little difference in viscosity at the two different power ratios. This oil is a mineral based formulation and would be expected to have a slightly different VI. While the viscosity at −20°C is nearly identical, the viscosity at −35°C is close to double that of Oil A34.

Similar comparisons of the temperature offset were made for E1, an SAE 5W-30 synthetic formulation, in Fig. 6. The impact of PR ratio on viscosity is hardly noticeable. This oil shows less shift in viscosity from the 0.5°C change than either B1 or A34 samples. At −35°C, the viscosity is about halfway between that of Oils A34 and B1, while at −20°C they are very similar.

All three commercial engine oils, A34, B1, and E1, show the similar responses to temperature offset (error) of ±0.5°C and power ratios that was seen with CLNNR blend in Fig. 3. Figures 4 and 5 both

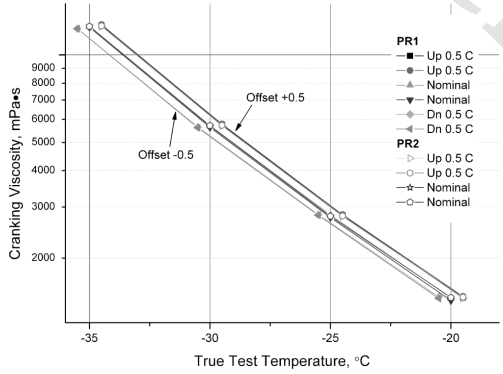

FIG. 5—*Impact of power ratio on apparent viscosity of Oil B1—SAE 5W-30.*

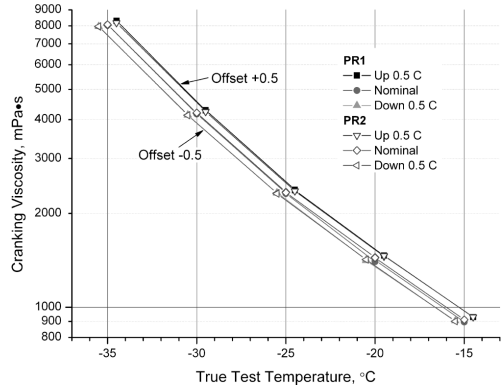

FIG. 6—*Impact of power ratio on apparent viscosity of Oil E1—SAE 5W-30.*

contain twelve data pairs for each offset while Fig. 6 contains 27 data pairs for each temperature offset. The number of pairs exceeding 1 % difference is similar to that seen with the data in Fig. 3.

The previous discussion centered on data from SAE 0W-xx and 5W-xx formulations. Figure 7 shows the viscosity temperature relationship for Oil H1, an SAE 10W-30 formulation. The response of this oil is similar to the response seen in the earlier figures to the temperature offset and different power ratios.

Temperature Sensitivity

Figure 8 shows a plot of indicated test temperature versus cranking viscosity for CLNNR over a narrow temperature range. This is the same data shown in Fig. 3 but with the *x*-axis being indicated rather than true temperature.

Figures 9–12 show the difference in viscosity resulting from the temperature offset from the true temperature. The percent differences are tabulated in Table 5 at indicated test temperatures for some of the oils. CLNNR blend was previously noted as having a large temperature sensitivity. This temperature sensitivity is seen in Fig. 9 and Table 5, where a difference of 6 to 8 % between the −0.5 and and +0.5 temperature offset results. Sample C1, SAE 5W-30 oil, shows a 3 % difference for this range of temperature offsets at the −30°C test temperature. Oil F1 in Fig. 11, a SAE10W-30, shows a percent change at a −25°C test temperature to that seen with Oil C1.

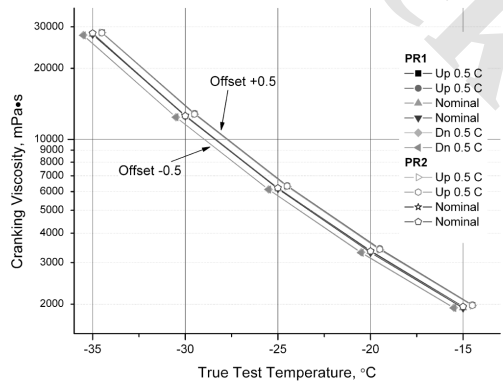

FIG. 7—*Impact of power ratio on apparent viscosity of Oil H1—SAE 10W-30.*

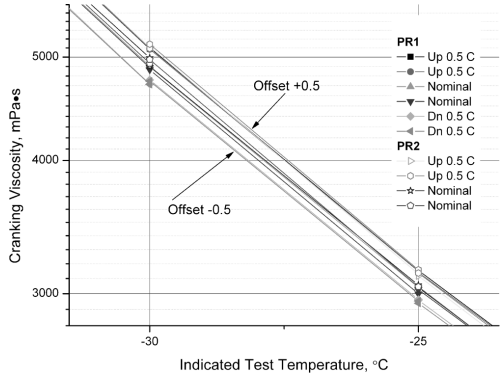

FIG. 8—*Apparent viscosity at indicated temperature for sample CLNNR.*

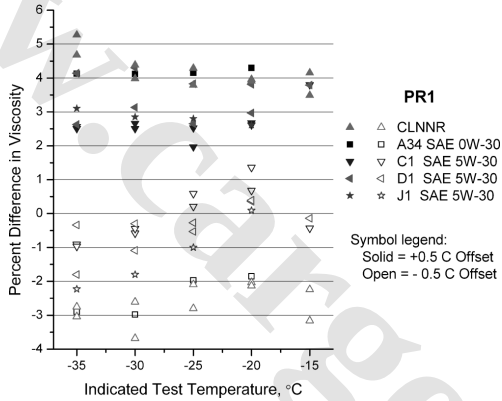

FIG. 9—*Viscosity change with temperature offset with PR1 for Oils CLNNR, A34, C1, D1, J1.*

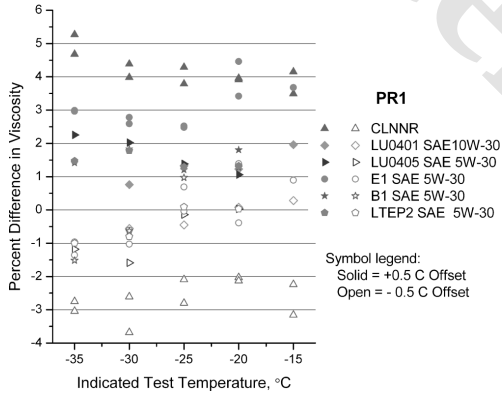

FIG. 10—*Viscosity change with temperature offset with PR1 for Oils CLNNR, LU0401, LU0405, E1, B1, LTEP2.*

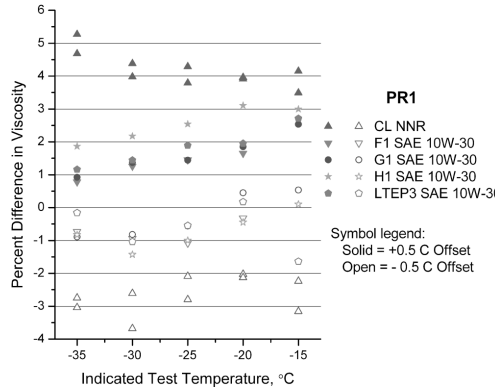

FIG. 11—*Viscosity change with temperature offset with PR1 for Oils CLNNR, F1, G1, H1, LTEP3.*

Thermal Control Comparison

Figure 13 compares viscosity data obtained on a selection of the oils in this program using both the CCS-2100 (thermoelectrically cooled) instrument and a CCS 5 (methanol cooled). The data for the CCS-5 were obtained from a commercial test laboratory. This figure includes data obtained with instrument 3054 using two different rotor-stator pairs. The data from the CCS-5 instrument are used as the reference value in Fig. 13.

Discussion

When this study was initiated, its purpose was to focus on the effect a small temperature offset would have on measured cranking viscosity as made by the CCS instrument. During the preliminary testing it was recognized that the setup of the instrument would need to be tightly controlled. This was due to the fact that the differences in viscosity were expected to be between the repeatability and reproducibility of the test method. For this reason, a significant portion of the testing was done in a single instrument. Thus, by using a single instrument and varying only two variables, power ratio and temperature, it would increase the likelihood of seeing the effect of these variables on CV.

A key parameter controlled in this study was the calibration. With each PR and temperature offset, the instrument was calibrated with a full range of reference oils at each temperature. The measurement of the reference oils was done in duplicate. This approach yielded a minimum of ten data points at each test

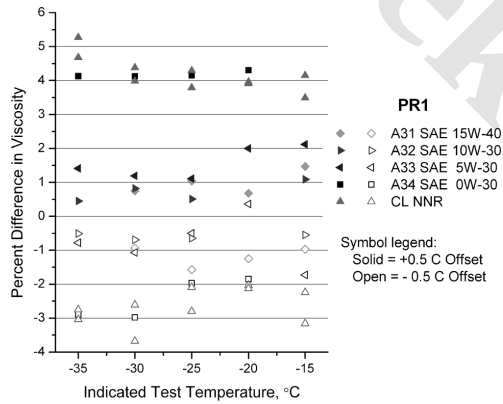

FIG. 12—*Viscosity change with temperature offset with PR1 for Oils CLNNR, A31, A32, A33, A34.*

TABLE 5—*Temperature sensitivity by sample.*

		Viscosity Difference, %	
Oil Code	Temperature, °C	+0.5 Offset	−0.5 Offset
A34	−35	4.13	−2.90
CLNNR	−35	4.68	−3.04
		5.27	−2.75
LTEP 1	−35	3.77	−0.42
CLNNR	−30	4.38	−2.61
		3.98	−3.68
LU 0405	−30	2.02	−1.59
A33	−30	1.19	−1.07
C1	−30	2.51	−0.44
		2.66	−0.58
D1	−30	3.13	−1.09
		4.30	−0.30
LTEP 2	−30	1.78	−0.80
E1	−30	2.78	−1.03
		2.59	−0.61
J1	−30	2.85	−1.80
A34	−30	4.12	−2.98
A31	−25	1.04	−1.57
A32	−25	0.51	−0.65
A33	−25	1.11	−0.50
LU 0401	−25	1.33	−0.45
CLNNR	−25	4.29	−2.09
		3.79	−2.80
F1	−25	1.45	−1.08
G1	−25	1.44	−0.56
LTEP3	−25	1.89	−0.55
T1	−25	1.17	−0.44

temperature, which is more than the four ASTM D 5293-04 [5] currently requires as a minimum. There are several advantages of this approach. First, it minimizes the variance of the correlation as each measured value has a smaller contribution to the calibration constants. Second, it alerts the user to an error in a measured value by its larger deviation. Third, having a consistent set of reference oils in the calibration increases the consistency of the calibration constants. This improved consistency would contribute to reducing the variance seen in viscosity determinations in an instrument and between instruments.

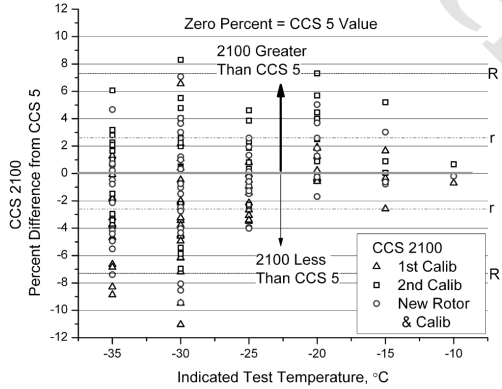

FIG. 13—*Comparison of CCS 5 to CCS 2100 measurements using CCS 5 value as the reference.*

Earlier B_0 was shown to be the primary contributor to the determined viscosity. Using calibration constants based on the data from only four adjacent reference oils, the CV was changed by 5 %. These four data points came from the calibration set used for the constants shown in Table 3 for the second rotor. This narrow selection of reference oils increased B_0 by about 2 % and decreased B_1 by 200 mPa(s). These constants would change a 6000 mPa(s) by ~400 mPa(s). This difference is large enough to potentially cause issues with product labeling compliance and manufacturing tolerances. Thus, one would expect that laboratories using the minimum number of calibration oils may experience the most difficulty in obtaining comparable results in multiple instruments. These differences would likely be within the reproducibility of ASTM D 5293-04 [5].

The importance of running identical calibration procedures between multiple instruments is much more critical when the samples have an increased sensitivity to temperature. The current test method requires the calibration to use only four reference oils. The choice of those calibration oils can have an impact on B_0, as shown in the example above. B_0 is the most significant term in the calibration equation, and depending on the viscosity value, B_1 can also have a large impact on the result. The experience with these instruments has shown that differences between instruments can be reduced by: (1) Increasing the minimum number of data points for calibration. (2) Fixing the viscosity range for the calibration oils at each temperature. (3) Requiring that reference oils used in the calibration be distributed over the entire operating viscosity range. (4) Improving calibration acceptance by limiting the allowable deviation between calibration oil reference value and that calculated by the newest calibration equation. (5) Verifying the actual cell temperature by ensuring the temperature probe is calibrated and properly seated in the cell, and by validating the CCS temperature sensing circuit.

The differences seen in CV between different instruments and laboratories could be reduced if the following were incorporated into the test method. Before beginning a calibration, require verification that the instrument was sensing the correct temperature. The instructions for rotor speed should be expressed in two ways. When calibrating the instrument, the rotor speed setting should be stated as 240 ± 1 r/min at $-20\,^{\circ}\mathrm{C}$ with reference oil CL250. However, when verifying the rotor speed is within operating tolerance after calibration, the rotor speed should be specified as 240 ± 5 r/min. This will accommodate normal day-to-day variation in rotor speed. Using this expression of rotor speed tolerance will help avoid the paradox of a user changing the rotor speed setting while allowing for normal day to day variation.

For this study, the temperature error was artificially introduced by adjusting the probe calibration to create a predetermined offset from the displayed temperature. When the first set of data was analyzed, there was concern regarding the technique used for obtaining the temperature offset. This concern arose because with a positive temperature offset the measured viscosity was higher than the measured viscosity at the true temperature. Reviewing the recorded data from the instrument setup showed the relationship between motor current and offset temperature was correct with CL250. When the current was measured at 240 r/min with each temperature offset, the motor current for 240 r/min decreased with increasing temperature.

This apparent reversal of viscometric response to temperature in the CCS was traced to the basis for the calibration. During calibration, the speed of the rotor was related to the reference oil viscosity at that indicated test temperature. When the temperature was offset in a positive direction, the resulting regression fit of the data yields a larger B_0 value. This anomaly was traced back to the equation used to relate rotor speed and apparent viscosity. With a temperature offset or error, the regression uses the viscosity at the indicated temperature and not the viscosity for the true temperature.

There are several ways for such a temperature offset to manifest in an otherwise normally operating CCS instrument. These will most likely be difficult at best for the user to identify. One cause would be failure to have good thermal contact between the sensing thermistor probe and the copper CCS stator. Often, this problem can be seen as temperature control instability during the viscosity measurement step. Another possible cause is an error made when entering the probe constants into the software. An additional cause could be with the CCS electronics which may drift out of tolerance over time. The authors would like to point out that the manufacturer has made available temperature circuit test plugs for evaluating the performance of the CCS temperature measurement electronics.

In the past ten years, two PR ratios have been used in the instrument. These were noted earlier as being an outgrowth of the LTEP study. As the two PRs have slightly different shear rates, there has been some speculation that this could contribute to the variance seen between instruments. Viscometric data for the

TABLE 6—*Impact of PR on apparent viscosity by sample.*

Oil Code	SAE Grade	Temperature, °C	Viscosity, mPa(s) PR1	Viscosity, mPa(s) PR2	Percent Difference
A34	0W	−35	5440	5495	1.01
LTEP 1	0W	−35	4912	4910	0.04
A34	0W	−30	3205	3235	0.93
CLNNR		−30	4881, 4896	4938, 4963	1.26
LU 0405	5W	−30	5475	5524	0.89
A33	5W	−30	5905	5859	0.78
C1	5W	−30	5788 5775	5837, 5879	1.31
D1	5W	−30	5791 5734	5881, 5860	1.86
LTEP 2	5W	−30	6743	6800	0.84
E1	5W	−30	4177 4172	4206, 4190	0.56
J1	5W	−30	5230	5257	0.51
S1	5W	−30	5823	5853	0.51
B1	5W	−30	5670	5707	0.65
A33	5W	−25	2885	2878	0.24
H1	10W	−25	6191	6213	0.35
A32	10W	−25	5878	5869	0.15
LU 0401	10W	−25	6122	6148	0.42
CLNNR		−25	3021 3034	3051, 3043	0.64
F1	10W	−25	5946	5975	0.49
G1	10W	−25	5914	5936	0.37
LTEP3	10W	−25	6551	6579	0.43
T1	10W	−25	5731	5739	0.14
A31	15W	−20	6138	6130	0.13

two PRs shown in Figs. 3–7 indicate the measured viscosity is identical regardless of the power ratio (PR1, PR2). The percent difference between apparent viscosities determined by the different PRs at some temperatures is shown in Table 6. All of the data are well within the repeatability of this test method (2.6 %). Further, the data implie that the small difference in shear rate between the two PRs has a negligible effect on the measured viscosity. The PR1 ratio corresponds to the ratio used in the CCS instruments prior to the LTEP program. The PR2 ratio was implemented as an outgrowth of the LTEP study to broaden the viscosity range of the instrument. The need for the change in power ratio was driven by the power curve of the motor in use in the earlier instruments. Since then, the original motor has been replaced by one having a longer power curve over the rotor's speed range with either PR.

The data seen in Figs. 9–12 show that the percent viscosity change is close to being constant across the test temperatures −35 to −15°C. There appear to be three general groups of samples when comparing the data in Table 5 in conjunction with the four figures. The group with the greatest increase is CLNNR, LTEP1, and A34, with a greater than 4 % increase with the +0.5 temperature offset. The second group containing C1, D1, E1, and J1 show a 2.5 to 3.5 % increase in viscosity with the +0.5 temperature offset. All of the other samples are less than 2 %. All of these oil formulations are either SAE 0W-xx or 5W-xx multigrades except for CLNNR.

With a −0.5 temperature offset, the groupings and the percent change in CV are different. In nearly all cases the magnitude of the percent change in CV is about 75 % of the increase seen when the offset is in the opposite direction. The only clear grouping with the −0.5 temperature offset is CLNNR and A34.

A cause for the nearly constant temperature sensitivity over the range of test temperatures is difficult to quantify. The only formulation there is detailed knowledge of is CLNNR, which is an OCP VII in PAO. Intuitively, its constant temperature sensitivity could be related to its solubility as VIIs tend to require an increased treat level per unit viscosity increase in formulations with a high PAO content.

In order to determine why some fully formulated formulations have a higher sensitivity to the tem-

perature offset than others would require access to the compositions. Those conducting the study would need access to individual components used in formulations regardless of source. Even then it is possible the source of the temperature sensitivity would not be identified. It would seem that there are two general causes of the temperature sensitivity. One is solubility of the components and the other is component, component interactions. There is a rather large change in base stock molecular size when you go from the 0W and 5W formulations to 10W and higher. Many of the additive components used in an engine oil formulation have a degree of polarity while the environment is very nonpolar. Thus these polar components could link or interact as the temperature decreases resulting in an unexpected viscometric response.

In this paper, most of the attention has been directed toward the PR1 configuration. Similar data were collected using the PR2 configuration in both the 3054 and 3127 instruments, although for brevity it is not included in this paper. The data obtained with the PR2 can be seen in Figs. 3–7, and are nearly identical to that seen with the PR1 configuration. The magnitude of the difference was approximately 1 % or less for the highly temperature sensitive formulations. The data from PR2 configuration confirmed what was seen with the PR1 configuration; that is some SL engine oil formulations, in particular 0W and 5W, are much more sensitive to temperature offset than previous API service categories.

Comparing the open squares and triangles in Fig. 13 shows a visual pattern indicating a lack of bias between instrument models for the population of data tested. The boundaries for repeatability, *r*, and reproducibility, *R*, are shown in Fig. 13. The lines were drawn as if making the comparison between a reference value and another value, where the reference value was the CCS 5 measurement. The variance between the CCS-2100 and CCS-5 appears to increase as the test temperature decreases. The data at −30 and −35°C have a much larger spread than that at the other temperatures. This suggests, in part, that thermal differences increase the further the test temperature is from room temperature.

A temperature difference between instruments of 0.5°C can cause an error in measured viscosity of more than 5 % for engine oils that are exceptionally temperature sensitive. The magnitude of the difference is highly dependent on the specifics of the oil formulation and the viscosity grade. This temperature sensitivity can cause a perception of bias when comparing the data obtained from different instruments. This has been shown to be the case even with instruments having essentially identical calibrations. However, with careful operation of the CCS-2100 instrument in a laboratory, it is possible to obtain repeat measurements that are a small fraction of the published repeatability in ASTM D 5293-04 [5]. Notwithstanding the benefits of improved repeatability, this improved measurement sensitivity can actually exacerbate the effects of subtle temperature differences between two instruments as a consistently observed bias. Interestingly, even with a 0.5°C temperature offset between instruments, the results can still be within the reproducibility of the method but with a consistent bias. An alternative way to look at this result is that instrument A, with temperature offset, would always be expected to be below the average while instrument B, with no temperature offset, would be above when looking at all of the data combined.

The discussion has only dealt with the possibilities of a bias being due to calibration constant differences and or an operating temperature difference. Considering the difference between *r* and *R* for the CCS, it would not be surprising to see an instrument bias between two instruments operated in exactly the same manner.

Based on the experience gained in this study the following operational changes are recommended:

1. Precondition instrument for three minutes before testing samples.
2. Set motor speed at 240 r/min±1 r/min. Verify that speed was within a tolerance of 240±5 r/min during calibration, when CL250 is measured at −20°C and all subsequent checks.
3. Use all reference oils for a particular test temperature when calibrating. Run the oils in duplicate during the calibration. One example for the −25°C test temperature would be to run the following reference oils: CL120, CL140, CL160, CL190, CL220, CL250, CL280, CL320, and CL380 as two consecutive sample sets. An alternative approach would be to run all the reference oils between CL120 and CL320 as a single set, which adds CL130, CL150, CL170, CL200, CL240, CL260, CL300, CL340, and CL420.
4. Reject any calibration data point that recalculates with a viscosity difference larger than 2 % from the reference oils certified viscosity value.
5. When calculating calibration constants, do not reject more than three data points in any dataset consisting of ten or more data points.

6. Use a check oil to monitor measurement performance daily, or each operational cycle when not in daily use.
7. Periodically verify instrument temperature measurement performance. This can be done using special test plugs calibrated and certified by the manufacturer.
8. Recommend running samples in duplicate when time and sample volume permit.
9. Verify calibration or replace CCS thermistor probe annually.

Conclusions

The initial intent of this study was an attempt to understand the magnitude of temperature variance on the measured CV. A second part of this study was to try and understand how much of the variance in precision was attributable to the materials being tested. For this property measurement, there are two broad sources of measurement error. One source is instrument related and the second is sample related.

It is clear from the above data that some API SL commercial engine oil formulations are more sensitive to measurement temperature differences than others. This temperature sensitivity appears to have a grade dependent aspect. The SAE 0W-xx oils tested had percent viscosity difference at specification temperature of 7 % for an API SL oil and 4 % for an API SG oil. SAE 5W-30 SL API oil's had lower temperature sensitivity as shown by the percent viscosity difference which ranged from 2.6 to 4.2 % compared to 7 % for SAE 0W-30 oil. Moving to the next higher viscosity grade (SAE 10W-30) the range is 1.1 to 2.4. Some oils that were tested at temperatures below their specification temperature exhibited increased sensitivity to temperature. Two synthetic SAE 5W-30s (E1, J1) have the highest temperature sensitivity of the group of SAE 5W-30s tested in this study. The difference between the two types of SAE 5W-30s is primarily in the base stock with synthetics typically using API Group 3 or 4 and nonsynthetics using Group 2 or 3. Group 3 are very highly refined and are often considered to be nearly a PAO-like base stock. Group 4 is PAO. The SAE 0W-30 evaluated in this study likely has a significant amount of Group 3 or possibly Group 4 base stock in its composition.

The accuracy of cranking viscosity measurements can be improved by following the recommendations noted in the discussion. However, with tighter instrument precision an operator is much more likely to see two instruments with a nearly constant bias between them. One way to minimize a bias like this is to use an internal standard to adjust the apparent cranking viscosity. This approach has a major difficulty in that it will not be formulation neutral and could cause some formulations to be overcorrected while others are undercorrected. Improving the precision of the cranking viscosity measurement will give the industry more flexibility in formulating their products.

Appendix A-Calibration Matrix

Sample Tray Position	Sample ID	Test Temperature, °C	Sample Tray Position	Sample ID	Test Temperature, °C
1	CL100	−30.0, −35.0	15	CL100	−30.0, −35.0
2	CL120	−25.0, −30.0, −35.0	16	CL120	−25.0, −30.0, −35.0
3	CL140	−20.0, −25.0, −30.0, −35.0	17	CL140	−20.0, −25.0, −30.0, −35.0
4	CL160	−20.0, −25.0, −30.0, −35.0	18	CL160	−20.0, −25.0, −30.0, −35.0
5	CL190	−20.0, −25.0, −30.0, −35.0	19	CL190	−20.0, −25.0, −30.0, −35.0
6	CL220	−15.0, −20.0, −25.0, −30.0	20	CL220	−15.0, −20.0, −25.0, −30.0
7	CL250	−15.0, −20.0, −25.0, −30.0	21	CL250	−15.0, −20.0, −25.0, −30.0
8	CL280	−10.0, −15.0, −20.0, −25.0	22	CL280	−10.0, −15.0, −20.0, −25.0
9	CL320	−10.0, −15.0, −20.0, −25.0	23	CL320	−10.0, −15.0, −20.0, −25.0
10	CL380	−10.0, −15.0, −20.0	24	CL380	−10.0, −15.0, −20.0
11	CL480	−10.0, −15.0, −20.0	25	CL480	−10.0, −15.0, −20.0
12	CL600	−10.0, −15.0	26	CL600	−10.0, −15.0
13	Null		27	CL NNR	−15.0, −20.0, −25.0, −30.0, −35.0
14	CL100	−25.0, −30.0, −35.0	28	CL NNR	−15.0, −20.0, −25.0, −30.0, −35.0

Appendix B-Sample Test Matrix

Sample Tray Position	Sample ID	Test Temperature, °C	Sample Tray Position	Sample ID	Test Temperature, °C
1	A32	−15.0, −20.0, −25.0, −30.0, −35.0	16	G1	−20.0, −25.0, −30.0, −35.0
2	A29	−15.0, −15.0, −20.0	17	J1	−20.0, −25.0, −30.0, −35.0
3	A30	−10.0, −15.0, −20.0, −25.0	18	B1	−20.0, −20.0, −25.0, −30.0, −35.0
4	A31	−15.0, −20.0, −25.0, −30.0	19	LTEP1	−25.0, −30.0, −35.0
5	A32	−15.0, −25.0, −30.0, −35.0	20	LTEP3	−15.0, −20.0, −25.0, −30.0, −35.0
6	A33	−15.0, −20.0, −25.0, −30.0, −35.0	21	LTEP2	−20.0, −25.0, −30.0, −35.0
7	A34	−20.0, −25.0, −30.0, −35.0	22	CLNNR	−15.0, −20.0, −25.0, −30.0, −35.0
8	C1	−20.0, −25.0, −30.0, −35.0	23	BO0406	−20.0, −25.0, −30.0, −35.0
9	S1	−20.0, −25.0, −30.0, −35.0	24	LU0401	−15.0, −20.0, −25.0, −30.0
10	E1	−20.0, −25.0, −30.0, −35.0	25	LU0405	−20.0, −25.0, −30.0, −35.0
11	F1	−20.0, −25.0, −30.0, −35.0	26	C1	−15.0, −20.0, −25.0, −30.0, −35.0
12	T1	−15.0, −20.0, −25.0, −30.0, −35.0	27	E1	−15.0, −20.0, −25.0, −30.0, −35.0
13	H1	−15.0, −20.0, −25.0, −30.0, −35.0	28	D1	−15.0, −20.0, −25.0, −30.0, −35.0
14	B1	−20.0, −25.0, −30.0, −35.0	29	Null	
15	D1	−20.0, −25.0, −30.0, −35.0	30	CLNNR	−15.0, −20.0, −25.0, −30.0, −35.0

Appendix C-Viscosity Data

Power Ratio		Instrument 3054 PR1			Instrument 3054 PR2			Instrument 3127 PR2		
Sample	Nominal Temp. Celsius	−0.5°C Offset	Zero offset	+0.5°C Offset	−0.5°C Offset	Zero offset	+0.5°C Offset	−0.5°C Offset	Zero offset	+0.5°C Offset
		Average Viscosity, mPa(s)			Average Viscosity, mPa(s)			Average Viscosity, mPa(s)		
A70	−15		959.5	1008	916.5	941	966.5	940	980	1020.5
A70	−20		1409.5	1484	1371.5	1409	1444	1403	1445	1491
A70	−25		2142.5	2243.5	2086.5	2147.5	2204.5	2161.5	2248	2303.5
A70	−30		3395.5	3547	3309	3425.5	3523	3494	3615	3724
A70	−35		5807.5	6063	5682	5851.5	6006.5	6094	6269.5	6452.5
A29	−10	5536.5	5531.5	5444.5	5601	5496.5	5544	5727	5652	5525
A29	−15	11643	11541	11461	11667	11501.5	11490	11977	11823.5	11442
A29	−20	27143	26821	26533.5	27375	26837.5	26749	27573.5	27296	26169
A30	−10	2469.5	2483	2503.5	2457.5	2479	2486	2503	2512.5	2529.5
A30	−15	4662	4677	4684.5	4647.5	4653	4668	4792	4768	4772
A30	−20	9890	9926	9972	9890.5	9935.5	9961	10398.5	10349	10360.5
A30	−25	23145	23323	23316	23210.5	23269.5	23410	24559.5	24368	24375.5
A31	−15	3022	3051.5	3096.5	3023	3036.5	3069	3078.5	3089	3112
A31	−20	6061	6138	6179.5	6107	6130	6168	6377	6363.5	6421
A31	−25	13322.5	13535	13675.5	13468.5	13550	13704.5	14327.5	14326.5	14463.5
A31	−30	31793.5	32096.5	32337.5	32082.5	32085	32471	34114.5	34033	34382
A32	−15	1551	1559.5	1576.5	1556.5	1565	1567.5	1548	1561	1565.5
A32	−25	5839.5	5877.5	5907.5	5823	5868.5	5872	6023	6040.5	6054.5
A32	−30	12891	12980	13087	12890	12942.5	12972.5	13433	13451	13494
A32	−35	31235.5	31395	31535	31471.5	31451	31339	32574	32466.5	32707.5
A33	−15	879.5	895	914	891.5	899.5	908.5	903	929.5	934
A33	−20	1527.5	1522	1552.5	1524	1535.5	1543.5	1509	1526.5	1512.5
A33	−25	2870.5	2885	2917	2859	2877.5	2879.5	2878	2905	2876
A33	−30	5842	5905	5975	5847	5898.5	5897	6008.5	6012.5	5987.5
A33	−35	13049	13152	13337.5	13108.5	13092.5	13090.5	13475	13466	13454.5
A34	−20	1323	1348	1406	1311	1340	1382.5	1335	1379	1409
A34	−25	1994.5	2034.5	2119	1983	2049.5	2098	2045.5	2120	2157
A34	−30	3109	3204.5	3336.5	3121.5	3235	3328.5	3280	3395	3468
A34	−35	5282.5	5440	5664.5	5340.5	5495.5	5662.5	5677	5861.5	6000
C1	−20	1567.5	1546.5	1588	1558	1568.5	1580	1570.5	1584	1585
C1	−25	2925.5	2919.5	2977	2919.5	2955.5	2968.5	2965.5	2989.5	2991
C1	−30	5762	5787.5	5933	5797	5878.5	5939.5	5956.5	6017.5	6075

Appendix C-Viscosity Data

Power Ratio		Instrument 3054 PR1			Instrument 3054 PR2			Instrument 3127 PR2		
Sample	Nominal Temp. Celsius	−0.5°C Offset	Zero offset	+0.5°C Offset	−0.5°C Offset	Zero offset	+0.5°C Offset	−0.5°C Offset	Zero offset	+0.5°C Offset
		Average Viscosity, mPa(s)			Average Viscosity, mPa(s)			Average Viscosity, mPa(s)		
C1	−35	12141	12259.5	12567.5	12235	12369	12557	12864.5	12926.5	13120
S1	−20	1452	1437.5	1453	1454.5	1451.5	1440.5	1435	1435	1418.5
S1	−25	2835	2836	2859.5	2824	2849	2842.5	2855	2871	2847.5
S1	−30	5787	5822.5	5884	5801.5	5852.5	5881.5	5942.5	5967	5972
S1	−35	12793.5	12862.5	13057.5	12810	12937	12993	13189.5	13226	13350
E1	−20	1411	1416.5	1465	1421.5	1441.5	1463.5	1442.5	1477	1479.5
E1	−25	2324	2325	2383.5	2323	2342	2361.5	2378.5	2427.5	2434.5
E1	−30	4133.5	4176.5	4292.5	4129.5	4206	4242	4298	4382.5	4428.5
E1	−35	7955	8064.5	8305.5	7964	8072.5	8176	8367.5	8497	8628.5
F1	−20	2966	2975.5	3024.5	2960.5	3008	3018.5	3042.5	3053.5	3056
F1	−25	5881	5945.5	6031.5	5939	5975	6033	6154.5	6172	6177
F1	−30	12979	13101.5	13267	13114.5	13105.5	13239.5	13609.5	13605.5	13659
F1	−35	31327	31556	31801	31854	31656	31723.5	32463.5	32274	32459
T1	−15	1496	1500.5	1525	1505	1511	1520	1496	1514	1504
T1	−20	2812	2811.5	2845	2805	2824.5	2822	2807.5	2812	2784.5
T1	−25	5706.5	5731.5	5798.5	5709.5	5739	5773.5	5834	5823	5802.5
T1	−30	12472	12600	12734.5	12556.5	12573	12670.5	12959	12891.5	12930
T1	−35	29762.5	30108.5	30191.5	30132	30365	30146.5	31104	30830	30912.5
H1	−15	1928	1926	1983.5	1926	1952.5	1973	1961.5	1983.5	1986
H1	−20	3311	3326	3429	3302.5	3361.5	3409.5	3418.5	3449	3483.5
H1	−25	6129	6191	6348	6123.5	6213.5	6321	6410	6464	6530.5
H1	−30	12409	12589	12862	12450.5	12586.5	12784.5	13055	13136.5	13267.5
H1	−35	27654	27885.5	28403	27846.5	28167.5	28322	28900.5	28936	29273
B1	−20	1462.5	1444	1470	1459.5	1464.5	1461.5	1455.5	1458.5	1446.5
B1	−25	2815	2788	2821.5	2789.5	2787	2786	2806.5	2807	2775.5
B1	−30	5634	5669.5	5773	5666.5	5706.5	5714	5834.5	5842	5847.5
B1	−35	12310	12499.5	12675.5	12427.5	12542	12546.5	12889	12837.5	12943
D1	−20	1811	1804	1857.5	1797.5	1824.5	1848.5	1853.5	1876.5	1894.5
D1	−25	3100.5	3117	3199.5	3111	3160.5	3203	3212.5	3268.5	3296
D1	−30	5728	5791	5972.5	5787	5880.5	5988.5	6041	6128	6209
D1	−35	11508	11719	12027	11684	11867.5	12038.5	12289	12428.5	12632
G1	−15	1692	1683	1725.5	1698.5	1714	1719	1689.5	1704.5	1705.5
G1	−20	3016	3002.5	3058	3016.5	3042.5	3050	3028.5	3034	3038.5
G1	−25	5881	5914	5999	5884	5936	5984.5	5984.5	6004	6014
G1	−30	12633	12737.5	12912.5	12674.5	12694.5	12823	12949	12943.5	13038
G1	−35	29464.5	29729	30002	29911	29939.5	29960	30573.5	30378	30630.5
J1	−20	1728.5	1727	1772	1715	1749.5	1772	1768.5	1798	1809
J1	−25	2884.5	2913.5	2995	2874	2934	2969	2996.5	3056	3080.5
J1	−30	5136	5230	5379	5124	5256.5	5344	5424	5517	5600
J1	−35	9803.5	10027.5	10338.5	9881.5	10089.5	10306	10511	10676	10887.5
LTEP6	−15	6874	6895	6970	6941	6980.5	7068.5	7264.5	7218.5	7260.5
LTEP6	−20	14605	14697	14832.5	14964	15092.5	15221	15737.5	15597.5	15650.5
LTEP6	−25	34657	34702	35005	35432	35389.5	35865	37454.5	36861	36905.5
LTEP1	−25	1615	1600	1636	1593	1620.5	1635.5	1664	1717	1726.5
LTEP1	−30	2714.5	2717	2798.5	2695	2733.5	2765.5	2864	2934.5	2969.5
LTEP1	−35	4892	4912.5	5097.5	4824	4910	4989.5	5211	5352.5	5452
LTEP3	−15	1653	1680.5	1726	1664.5	1695.5	1713.5	1703.5	1727	1736.5
LTEP3	−20	3156	3150.5	3212	3155.5	3158.5	3190.5	3301	3292	3287.5
LTEP3	−25	6514.5	6550.5	6674	6547	6579	6643	6896.5	6902.5	6923.5
LTEP3	−30	14590.5	14744	14956.5	14687.5	14718.5	14870.5	15543	15480.5	15518.5
LTEP3	−35	35506.5	35562.5	35974.5	35826	35746	35828	37798	37467.5	37602.5
LTEP2	−20	1664	1663.5	1685.5	1670	1676.5	1682.5	1719.5	1741	1737

Appendix C-Viscosity Data

Power Ratio		Instrument 3054 PR1			Instrument 3054 PR2			Instrument 3127 PR2		
Sample	Nominal Temp. Celsius	−0.5°C Offset	Zero offset	+0.5°C Offset	−0.5°C Offset	Zero offset	+0.5°C Offset	−0.5°C Offset	Zero offset	+0.5°C Offset
		Average Viscosity, mPa(s)			Average Viscosity, mPa(s)			Average Viscosity, mPa(s)		
LTEP2	−25	3219	3216	3257.5	3208.5	3227.5	3243.5	3346.5	3364.5	3372
LTEP2	−30	6688.5	6742.5	6862.5	6742.5	6799.5	6869.5	7082	7123.5	7177.5
LTEP2	−35	15272	15426.5	15652.5	15437	15554.5	15691.5	16366.5	16416.5	16653
CLNNR	−15	1306.5	1336.5	1392	1295.5	1323.5	1369	1317.5	1357	1381
CLNNR	−20	1931.5	1971.5	2048.5	1914	1968.5	2026	1969	2024.5	2068.5
CLNNR	−25	2958	3021	3150.5	2946.5	3050.5	3145	3067	3163.5	3234.5
CLNNR	−30	4753.5	4881	5095	4802	4937.5	5129	5022	5184	5324
CLNNR	−35	8119.5	8374	8765.5	8195	8442.5	8803.5	8657.5	8964	9230.5
BO0406	−20	822	809.5	819.5	838.5	845	842.5	855.5	867.5	870
BO0406	−25	1458.5	1444	1461.5	1466.5	1476.5	1468	1499.5	1516	1507
BO0406	−30	2667	2653.5	2694.5	2664.5	2690	2683.5	2766.5	2788	2776
BO0406	−35	5232.5	5231.5	5348.5	5208	5247.5	5264.5	5477	5509.5	5501.5
LU0401	−15	1633.5	1629	1661	1651.5	1652	1673	1633.5	1646.5	1644.5
LU0401	−20	3000.5	2998	3035	3008	3031	3049.5	3017	3005.5	3002
LU0401	−25	6094	6121.5	6203	6101	6147.5	6196	6219.5	6195	6191
LU0401	−30	13466	13542	13645.5	13537.5	13524	13628.5	13822	13745.5	13774
LU0405	−20	1516.5	1516	1532	1508	1518	1526	1531.5	1551.5	1549
LU0405	−25	2812.5	2816.5	2855.5	2805	2837	2860	2871	2902.5	2898
LU0405	−30	5388	5475	5585.5	5419.5	5523.5	5607.5	5653	5723.5	5784
LU0405	−35	11179.5	11312.5	11567	11237	11365	11561	11794	11905.5	12095
C1	−15	918	922	957	912.5	926.5	951.5	934.5	961	976
C1	−20	1556	1545.5	1586	1549	1562	1570	1561.5	1577.5	1574.5
C1	−25	2919.5	2902.5	2976	2910.5	2949	2962.5	2937	2970.5	2962.5
C1	−30	5741.5	5775	5928.5	5765.5	5837.5	5926.5	5897	5955	6016
C1	−35	12129.5	12241.5	12555.5	12169.5	12315.5	12548.5	12720.5	12838.5	13041
E1	−15	904.5	896.5	929.5	901.5	912	930	926.5	957	961
E1	−20	1420	1400.5	1463	1421.5	1446.5	1456.5	1447.5	1486	1494
E1	−25	2332	2316	2373.5	2315	2334	2359	2384	2435	2442
E1	−30	4146	4171.5	4279.5	4134	4190	4252	4294.5	4377.5	4425.5
E1	−35	7970.5	8047.5	8285.5	7945.5	8032.5	8176.5	8322	8467.5	8620
D1	−15	1094.5	1096	1137.5	1090.5	1103	1120	1117	1147.5	1144
D1	−20	1803.5	1797	1865.5	1784.5	1811.5	1836.5	1830	1861	1866
D1	−25	3095.5	3104	3223	3081.5	3138	3194.5	3177.5	3242	3258.5
D1	−30	5716.5	5733.5	5980	5739.5	5860.5	5960	5965.5	6070.5	6118.5
D1	−35	11507.5	11547	12025	11609	11765	12013.5	12133.5	12308.5	12437.5
CLNNR	−15	1302.5	1345	1392	1290.5	1321	1373	1311.5	1347	1380.5
CLNNR	−20	1929	1971	2049	1910	1960.5	2018	1959	2011	2064.5
CLNNR	−25	2948.5	3033.5	3148.5	2947.5	3043	3127.5	3049	3144	3231
CLNNR	−30	4716	4896	5091	4796.5	4963	5099.5	4999	5153.5	5310
CLNNR	−35	8124.5	8354.5	8794.5	8201	8409.5	8744	8620.5	8899.5	9215.5

Note: Some figures used the individual measurement data rather than the averages shown in the table.

References

[1] Cox, D. B., Manning, R. E., and Kim, D. S., "The Cold Cranking Simulator Method for Viscosity of Motor Oils at Low Temperature," SAE 680067, SAE International.

[2] CRC Report No. 409, "Evaluation of Laboratory Viscometers for Predicting Cranking Characteristics of Engine Oils at 0°F and −20°F," Coordinating Research Council, Inc., 219 Perimeter Center Parkway, Atlanta, GA 30346.

[3] Stewart, R. M., "Engine Pumpability and Crankability Tests on Commercial "W" Grade Engine Oils Compared to Bench Test Results," SAE 780369 and *ASTM STP 621*.

[4] ASTM Standard D 2602, "Standard Test Method for Apparent Viscosity of Engine Oils at Low

Temperature Using the Cold-Cranking Simulator," *Annual Book of ASTM Standards*, ASTM International, West Conshohocken, PA.

[5] ASTM Standard D 5293, "Standard Test Method for Apparent Viscosity of Engine Oils Between −5 and −35°C Using the Cold-Cranking Simulator," *Annual Book of ASTM Standards*, Volume 5.02, ASTM International, West Conshohocken, PA.

[6] Cold Starting and Pumpability Studies in Modern Engines, ASTM Research Report RR-D02–1442, ASTM International, West Conshohocken, PA, 1998.

[7] SAE J300 Engine Oil Viscosity Classification, SAE International, 400 Commonwealth Drive, Warrendale, PA 15096, May 2004.

 Journal of ASTM International, Vol. 4, No. 10
Paper ID JAI100898
Available online at www.astm.org

Mathias Woydt[1]

No/Low SAP and Alternative Engine Oil Development and Testing

ABSTRACT: The use of alternative base oils, like esters or polyglycols, with more intrinsic properties for the lubrication of automobile engines has a potential for ecological and technical advantages. Being in competition with hydrocarbon-based formulations, detailed knowledge of several thermophysical and viscometric properties as well as tribological properties over a large temperature range are required (mapping). The tested polymer-free polyglycols and ester-based formulations displayed no visible tribological weaknesses regarding wear resistance and EP-behavior as well as offering significant advantages in order to meet metal- and ash-free and bio-no-tox criteria. Especially the formulated polyglycols without friction modifiers also showed an intrinsic retention of low coefficients of friction and a hydrodynamic film forming behavior comparable to hydrocarbon-based factory-fill oils. The wear resistance and EP-behavior of low-additivated polyglycols, but also of esters, can be enhanced by means of triboactive materials. Lubricious oxides or triboactive materials and polar base oils, or a combination thereof, may substitute the EP and AW properties realized by the additives, thus enabling long drains and responding to “eco-tox” or “bio-no-tox” requirements as well as restrictions from the “chemical box.”

KEYWORDS: ester, polyglycol, PAG, PPG, factory fill, hydrocarbon, engine oil, bio-oils, eco-lubricants, EAL, bio-no-tox oils, heat capacity, density, viscosity, pressure-viscosity, thermal conductivity, mixed, boundary, lubrication, low sap, mid sap, wear, friction, triboactive materials

Introduction

More and more, engine oils have to minimize or avoid their impact on the durability of particulate filters and catalysts as well as their impact on terrestrial and aquatic environments and to maximize the contribution to fuel economy. Replacing hydrocarbon-based oils with environmental friendly products is one of the ways to reduce adverse effects on the ecosystem caused by the use of lubricants. By means of an analysis of recent technological evolutions and of future trends in engine oil specifications, with the associated consequences for the functional properties performed by base oils and individual additives, the need and potential application of alternative base oils with intrinsic properties will be displayed. The focus of this paper lies on alternative base oils.

The “competition” between hydrocarbons and alternative base oils is not yet technologically decided in favor of hydrocarbons, esters, or polyglycols. In the past, the beneficial contribution of the additive technology and progress in hydrocabon-base oil technology could be demonstrated by an increasing ability to support thermal and oxidative loads of hydrocarbon-based engine oils. From the end of the 1960s until now, the specific loading has increased from $\sim$35 000 kW/km/L^2 to $>$440 000 kW/km/L^2 (kW power/km drain/litre of displacement), which will further increase by heavily supercharged diesel passenger car engines reaching 85 kW/L and upwards in the future.

General Context

The drain intervals in passenger cars have increased in the past 35 years from $\sim$3000–5000 km up to 50 000 km. The associated reduction in oil consumption and drained oil volume was compensated for by much more higher prices for the formulations and a steady-state increase of the total vehicle fleet stabilizing today at $\sim$65 % of the population in G7 countries. A drain of 50 000 km already can be interpreted as “lifetime” fill, since for many passenger car customers it means five years and more, but the original

Manuscript received January 12, 2007; accepted for publication November 1, 2007; published online December 2007. Presented at ASTM Symposium on Automotive Lubricant Testing and Additive Development on 3–5 December 2006 in Lake Buena Vista, FL; Simon Tung, Bernard Kinker, and Mathias Woydt, Guest Editors.
[1] Federal Institute for Materials Research and Testing (BAM), D-12200 Berlin, Germany, e-mail: mathias.woydt@bam.de

equipment manufacturer (OEM) wording is today: “50 000 km or two years.” It is further important to know for the chemical and technical evaluation of the figure of 50 000 km, if manual or automatic top-ups are foreseen are not.

Leasing offers including all maintenance represent a trend today. The OEM will therefore tend to minimize costs related to this incentive by increasing the drain/maintenance intervals.

A drain of 50 000 km and higher per se does not define for passenger cars a technical limit, even respecting “bio-no-tox” criteria, as it has been demonstrated by the RENAULT “ELLYPSE” demonstrator [1,2] seeking a drain between 70 000 to 100 000 km.

OEMs are more and more interested in passenger car engine oils (PCMO) with reduced metal-organic additives, thus contributing to the vision of an environmentally friendly and sustainable car. This is necessary in order to reduce the ash build-up in the after-treatment system caused by engine oils and therefore improve its filter efficiency and lifetime. High fuel efficiency retention and long drain intervals are expected, as well, from the engine oils. Easy removal of bio-no-tox fluids and recycling supports a sustainable development.

As displayed by the RENAULT demonstrator ELLYPSE and the FORD Model U, additional requirements may be demanded in the future, such as:

(a) biodegradability and nontoxicity and
(b) a content of renewables, or both.

The criteria for attribution of the environmental label “EUROMARGUERITE” requires for hydraulic fluids a content of >50 % of renewables. A smaller figure was proposed for engine oils [5]. High fuel efficiency retention, preferably over the drain interval, and long drain intervals (reduced waste volume!) also have an environmental impact.

One of the questions for OEMs is, if the hydrocarbon technologies (base oil+additive packages) as well established products are still robust enough to fulfill all of these requirements or do they need to look towards nonconventional base stocks, like ester or polyglycol base oils? These have more intrinsic properties resulting in a lower additive treat level or “more simple” formulations, which grant a durable application for the next decades also with respect to the EC directive [3] 1999/45/EC regarding the symbol “N” labeling of preparations and U.S.-DA [4] and U.S.-EPA [5] policies.

Also fuel economy targets will increase the demand for low viscosity grades, especially at low temperatures, with high viscosity indices (VI). Direct injecting engines favor formulations without polymeric VI-improvers.

Pure hydrocarbons alone can be U.S. Food and Drug Administration (U.S.-FDA) proof. It is the additive packages, which make hydrocarbons functional, that determine the eco-tox and bio-no-tox and ash formation properties of hydrocarbon based formulations, or a combination thereof. It is obvious to therefore substitute critical additives by others or new functional concepts, such as:

(a) EP/AW properties by triboactive materials and coatings and
(b) Viscosity improvers by the high VI of base oils, like esters and polygycols and
(c) Polar base oil molecules, or a combination thereof.

One of the key questions is: What will the 2010+ engine oil look like?

If now the alternative engine oils represent one direction, what will the engine oil specification for them look like, as the existing items and the individual values are based on long experience defined by the chemical profile of hydrocarbons and the related additive packages?

Engine Oil Specification

The recent new engine oil specifications of RENAULT SAS, DaimlerChrysler AG (DC 229.31), FORD WSS-M2C934-A, and Volkswagen AG (VW 504.00) display an interest in passenger car engine oils (PCMO) with reduced metal-organic additives. The European oil sequence ACEA-C1-04 limits sulfated ash to 0.5 wt.-% (LowSAP) and ACEA-C2-04/C3-07 to <0.8 wt.-% (MidSAP).

This is necessary in order to reduce the ash build-up in the particulate filter and therefore to improve its efficiency and guarantee lifetime. The ash build-up in the after-treatment devices increases the exhaust backpressure leading to a worse effect or penalty on fuel economy [6].

Phosphorus and sulfur are partly related to the anti-wear (AW) and extreme pressure (EP) properties of a hydrocarbon-based formulation, but also to the endurance and efficiency of exhaust after-treatment devices.

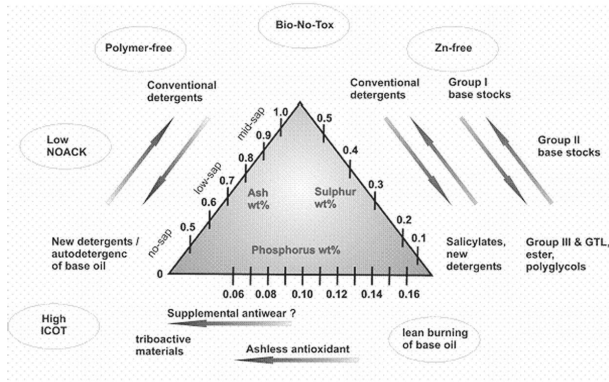

FIG. 1—*What will engine oil look like in 2010 or 2015?*

Figure 1 compiles the SAP-factors with their evolution and potential associated strategies and other factors and trends. Figure 1 presents the whole variety or spectrum of trends, needs, or wishes of OEMs for future engine oils.

The introduction of a "chemical box" will restrict the chemical freedom of engine oil formulations. The chemical box for passenger cars limits phosphorous (ca. <800 ppm [P]), sulfur (<0.3 (<0.2) wt.-% [S]), ash (<0.5/1.0 wt.-%), and the NOACK volatility (<10 % or <13 %), or a combination thereof, as general criteria. Besides, the fragmentation of standardized oil specifications between Europe, Asia, and the U.S. persists, and the diversification in original equipment manufacturer (OEM) specifications is spreading more and more since engine designs requiring specific oil formulations or using specific combustion processes have been released. In general, all specifications are being and will be replaced by new ones on shorter notice, thus spiraling the development costs.

In consequence, the engine oil concepts need to be more robust in order to buffer future developments well and meaningful test procedures outside of engines in order to cut engine bench test costs are needed.

The hydrocarbon-based engine oil formulators have recently reduced the ash content down to 0.7/0.8 wt.-% (MidSAP), some with help of a ester content. Prototype engine oils blended with 30–60 wt.-% esters having 0.5 wt.-% (lowSAP) are under evaluation.

Viscosimetrics

The engine oil specifications of standardization bodies and OEMs refer to kinematic viscosities in mm^2/s and the high-temperature, high-shear viscosity (HTHS) in mPas at a shear rate of $10^6\ s^{-1}$; (see ASTM D 4683, "Standard Test Method for Measuring Viscosity at High Shear Rate and High Temperature by Tapered Bearing Simulator," and D 4741, "Standard Test Method for Measuring Viscosity at High Temperature and High Shear Rate by Tapered-Plug Viscometer").

The kinematic viscosity and the HTHS are seen by OEMs as key properties for safe and durable operation, especially for the crankshaft bearings, as two main tasks for engine lubricants are energy saving (friction) and wear prevention. The dependency of the hydrodynamic design onto the kinematic viscosity and HTHS may be true, if only polymer-containing hydrocarbon-based formulations were considered.

The pressure-viscosity coefficient has up to now not been mentioned in engine oil specifications, but it has a strong influence on the film thickness (see Film Forming Behavior in the Results Section) and in consequence also on the frictional losses associated to the film shearing. It was recently shown that the fuel efficiency [7–9] of an engine is correlated with the pressure-viscosity coefficient. Further correlations exist with viscosity and with the coefficient of friction under mixed/boundary lubrication.

Experimental

Tribotesting Outside of Engines

The tribological performance of "Bio-no-tox&LowAsh" oils interacting with the materials of piston ring/cylinder liner was characterized in several application oriented simulation tests outside of engines based on the BAM [10] and the SRV® test [11].

Piston ring/cylinder liner simulation tests were performed under mixed/boundary lubrication conditions with different lubricants at 170°C and 0.3 m/s of continuous sliding, whereby a thermal-sprayed piston ring segment was pressed with 50 N against a cylinder liner segment (or flat disk) up to a sliding distance of 24 000 m. An oil amount of 0.3–0.5 L was used for each test. The test rig and the piston ring/cylinder liner configuration are shown in Ref. [10] using liner segments.

SRV® tests were additionally performed according to a new ASTM Dyyyy-xx draft method [11] as a cross check. The SRV® sample configuration with piston ring segments and the wear scars used here are shown in Ref. [12]. The BAM and SRV® tests characterize both the friction and wear behavior in the top dead center region.

The resistance against seizure of an iron-based alloy (100Cr6H = AISI 52100) was determined for different lubricants with the SRV® test rig according to ASTM D 5706-05 [13] under conditions of mixed lubrication and quoted as Hertzian contact pressure (last O.K.-pressure before failure). As a measure for the resistance against seizure the critical Hertzian contact pressure is compiled in Figs. 7 and 8.

Testing Oxidative Stability Outside of Engines

Oxidation resistance is one of the limiting factors for long drains and the factor for high-temperature lubrication [14]. The French ICOT test [15] (ICOT = iron catalyzed oxidation test) using 40 ppm iron acetylacetonate ($C_{15}H_{25}FeO_6$) as a diluted catalyzor defines the oxidation resistance at 170°C under an aeration of 10 L/h by three properties:

(a) the viscosity increase (e.g., max. $\Delta\eta < 100$ %),
(b) the increase of an idividual TAN (e.g., max. <7,5 mgKOH/g), and
(c) the evaporation loss at $\Delta\eta = 100$ % due to oxidation.

These set values can differ between OEMs. The ICOT test indicates only the oxidative resistance and gives no hint about the AW/EP-retention of a formulation. The test setup is similar to DIN 51352. For actual factory-fill oils, one ICOT test hour corresponds to ~270–330 km of driving. Comparing the experiences from the field with the test results achieved with the ICOT test using hydrocarbon-based formulations [16], ACEA A3/B3 high-performance grades display an induction time between 72 and 96 h and have a target oil drain interval of ~30 000 km (ACEA A5/B5 > 96 h). This relation has to be established for esters and polyglycols.

Substitution of EP/AW-Additives by Triboactive Materials

Wear protection represents another concern while using "midSAP" or even "lowSAP" oils or oils without or with low contents of extreme pressure (EP) and anti-wear (AW) additives, or both, associated with bio-no-tox properties according to directive EC/1999/45. The EP/AW functions of additives, even also the proven molybdenum-based piston ring coatings, may be substituted by means of "triboactive" or "triboreactive" materials/coatings.

Lubricious oxides (LO) and triboactive materials appeared recently in scientific literature [17] and display estimated functional properties by different approaches. There exists within the scientific community no official consensus about their meaning.

The term "lubricious oxides" was created in 1989 by Gardos [18,19] for TiO_{2-x} as well as thematized by Ref. [20] and aimed for low wear that may also be associated with low dry coefficients of friction. The correct term for TiO_{2-x} is Magnéli-phases of titania, Ti_nO_{2n-1} with $4 \leq n \leq 9$, whereas TiO_{2-x}, with $x \leq 0.01$, describes "Wadsley" defects.

The term "triboactive materials" appeared in Europe at the end of the 1990s describing more of a beneficial reaction between the surface and the lubricant or the ambient enviroment, thus indicating a more overall functional approach. Oxides, hydroxides, or hydrates cover this understanding.

Novel and noncommercial "triboactive" or "triboreactive" materials were selected from Magnéli-type phases, like $TiO_{1.93}$, Ti_nO_{2n-1}, and $Ti_{n-2}Cr_2O_{2n-1}$, as well as substrates, like (Ti, Mo)(C, N) + 23NiMo-binder, which form by triboxidation, γ-Ti_3O_5, Ti_5O_9, Ti_9O_{17}, and $Mo_{0.975}Ti_{0.025}O_2$ as well as double oxides like $NiTiO_3$ and β-$NiMoO_4$.

For more details about the triboactive materials $TiO_{1.93}$, Ti_nO_{2n-1}, $Ti_{n-2}Cr_2O_{2n-1}$, and (Ti, Mo)(C, N) + 23-30NiMo-binder deposited by thermal spraying on piston rings and liner samples, please refer to Refs. [21–23].

Alternative Fluids

Despite the potential future evolution of hydrocarbons by synthesizing novel molecules in order to combine low volatility with low-temperature fluidity, esters and polyglycols were identified as alternative base oils and blended to environmental-friendly prototype engine oils meeting all or most of the following properties:

(a) low viscosity at 40°C and NOACK-volatility,
(b) low contributions to exhaust emissions (lean burning),
(c) high oxidative stability in ICOT test,
(d) high biodegradability (>60 % in OECD 301x) and
(e) low toxicity (bio-no-tox) as well as
(f) low ash or ash-free,
(g) Zn- and Mo-free and
(h) polymer-free.

Synthetic esters are characterized by their polar structure, often low friction, high wear resistance, good viscosity-temperature behavior (high viscosity index VI), their miscibility with most hydrocarbon-based oils and most esters can be classified as environmental friendly and biodegradable (bio-no-tox) and can be synthesized based on renewable resources.

Besides synthetic hydrocarbon lubricants another promising class are polyglycol-based lubricants, which present an "oxygen" polarity in every monomer, where some have high biodegradability and low toxicity. The critique of "thermolysis" and bad eco-toxicity of polyglycols could recently not be confirmed using new polyglycol-based stocks optimized for engine operation [23].

Three factory-fill hydrocarbon-based engine oils considered modern high-performance formulations, FUCHS Titan SL PCX (0W-30), Castrol SLX 0W-30, and TOTAL HC (5W-30), served as references with a HTHS of ~3.0 mPas (target for the prototype oils), for the tribological properties under mixed/boundary lubrication and for the viscosimetrics.

Castrol Greentec LS 5W-30 and the TOTAL HTX 822 15W-50 represented fully-formulated, 100 % ester-based engine oils developed in the mid 1990s and BP VISTRA 7000 5W-40 was a blend of hydrocarbons with esters, commercialized also in the mid 1990s, as can be seen from the HTHS viscosities. They may be considered as fully-formulated and biodegradable engine oils of the first generation.

The commercially available Fuchs Titan GT1 0W-20 with a portion of 50 % ester is listed on the positive list of the German Market Introduction Programme (MIP) for "Biolubricants and Biofuels," funded by the Ministry of Consumer Protection, Food and Agriculture (BMVEL). The ester-based formulation HCE lowSAP of FUCHS conforms with the requirement of >50 % of renewables and to the toxicity criteria of directive EC/1999/45. Also, fully ester-based, prototype Fuchs Titan 100E SAE 0W-20 and TOTAL 100E were blended.

The polyalkyleneglycols PAG 46-1, PAG 46-2, and PAG 46-4, basically formulated according to U.S. 6,194,359, are free of polymers, Zn, and calcium and need no labeling with the symbol "N." The PAGs 46-2/46-3 presents a VI above 200 without using polymeric VI-improvers. The high NOACK volatilities represent a disadvantage of the PAG46-2 and PAG46-3 base oil formulations, but they can be tailored below <13 %.

Additionally, the oxidation resistance of the PAG 46-4 and of PPG 32-2 was boosted by proprietary additive packages "Phopani" and "Phepani." The polymer-free polyalkyleneglycols (PAG) cover a wide range of VI exceeding 200, whereas the polymer-free polypropyleneglycols (PPG 32-2) exhibit as "30" viscosity at 40°C associated with a NOACK below 5 %. The polymer-free PPG 32-2 contained 1.700 ppm sulfur and 200 ppm phosphorus respecting bio-no-tox criteria. Polypropyleneglycol monobutylether (PPG) are classified as "slightly hazard" to water (WGK 1) by the German Environmental Agency (www.um-

TABLE 1—*Viscosimetric and ecotoxicological properties of engine oils and alternative, prototype formulations*

Formulations	$\eta_{40°C}$ [mm²/s]	$\eta_{100°C}$ [mm²/s]	VI	PP [°C]	HTHS [MPas]	NOACK [%]	Algae [mg/L]	Daphnie [mg/L]	Fish [mg/L]	OECD 301x [%]
TOTAL HC FF SAE 5W-30	55.15	9.57	159	−42	3.0	12.8				
FUCHS Titan PCX SyperSyn	53.19	9.44	162	−45	2.95	9				
Castrol SLX 0W-30	57	10.2	168	−57	3.0	8.1				
TOTAL 100E (HTX 822)	111	17.4	184	−36	5.3	5				>60[a]
Greentec LS 5W30	59.3	11.5	187	−39	4.0	5.5				68
BP Vistra 7000	86.9	14.0	167	−45	4.1	10.7	>50	>100	>1,000	~80[a]
TOTAL 100E	40.93	7.6	225	<−42	2.93	4.8	1.780		10,000	62
Fuchs 100E	43.26	8.23	144	−39	2.95	5.5	>100	256	45–55	
TOTAL HCE	46.32	8.41	159	<−42	2.95		>120	>1,000	>1,000	62
Titan GT1 0W20	46.5	8.9	160	−45	2.95	6	>1,000	>1,000	>1,000	61
TOTAL HCE MidSap	57.8	10.4	176	−<48	2.99	6.6	>100	>1,000		~28
FUCHS HCE Low SAP	44	8.8	184	−45	2.9	6	>1,000	>100		78–87
PPG 32−2+2,6	34.5	6.7	*156*	−45	2.78	4.8	>100	600		70.5
PAG 46–2	47.4	9.94	*203*	−31	4.3	19.2	>100	688		64
PAG 46−4+2,6	49.6	8.44	*146*	−33	3.6	6.2	>100	301		80

[a]CEC.

weltbundesamt.de) under the number #3530. All polyglycols used here are ash-free. The amount of phosphor and sulfur is reduced to about 780 ppm [P] and 650 ppm [S] for the PAG46-3/PAG46-2 as well for the PAG46-4 to about 650 ppm [P] and 800 ppm [S]. The PAG46-4 and PPG32-2 prototype formulations meet the ACEA-C1 SAP criteria.

All prototype formulations respond to the symbol "N" criteria and most to a Zn-free philosophy. Ester-based formulations can fail with respect to the biodegradation of >60 % (see Table 1). Most recent ester-based formulations have a "40" viscosity [mm²/s] at 40°C associated with a NOACK evaporation loss below 7 %.

A high viscosity index selecting a "30" viscosity [mm²/s] at 40°C (see PPG32-2) is a fine and right approach followed by the question, if it can be realized by hydrocarbons as polymer-free formulation in order to meet a HTHS of >2.6 or >2.9 mPas?

Results

Film Forming Behavior

In order to differentiate hydrodynamic film forming behavior of alternative oils (hydrocarbons, esters, and polyglycols), the dynamic viscosity taking into account the differences in density and the pressure-viscosity coefficients have to be used. All properties should be determined at least at 150°C. For safe and durable engine operation, the film forming behavior of polyglycols will be compared to those of ester and hydrocarbon-based engine oils. The test methodology and data for densities, viscosities and piezoviscosities measured between 22 and 150°C are detailled elsewhere [24].

The dynamic viscosity considers the range of densities presented by the alternative oils. The report of the viscosity itself in order to rank different engine oil chemistries cannot be considered as sufficient, since the exponents applied to the different parameters for the estimation of film thicknesses are not identical

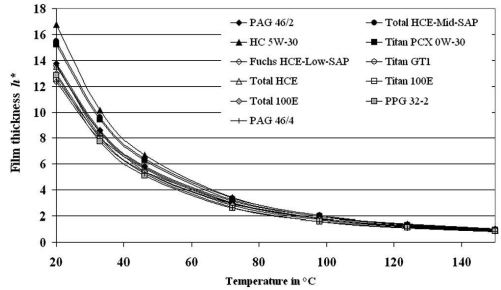

FIG. 2—*Relative film thickness h^* for a line contact over full range of temperatures.*

and is not only limited to viscosity. Three different equations [25] from the literature are referred to in order to calculate the oil film thicknesses. Two of them describe a line contact ($h_{L,1}$ and $h_{L,2}$) and one a point contact (h_P). The proportionalities used are:

$$h_{L,1} \propto \alpha^{0,6} \cdot \eta^{0,7} \text{ (Dowson and Higginson)}$$

$$h_{L,2} \propto \alpha^{0,54} \cdot \eta^{0,7} \text{ (Dowson and Dyson)}$$

$$h_P \propto \alpha^{0,49} \cdot \eta^{0,68} \text{ (Fromm)}$$

For all tested fluids, the relative film thicknesses have been calculated in dependence of the temperature. The value for the factory-fill oil "HC" SAE 5W-30 at 150°C was taken as a reference. Most formulations in Figs. 2 and 3 have a high-temperature high-shear viscosity (HTHS) between 2,8 mPas and 3,0 mPas with exception of the PAG46-2, PAG 46-3, PAG46-4, and PPG 32-2.

The different approaches for film thicknesses produce the same ranking of the formulations [26].

In Fig. 2, the differences in film thickness seems to be at 150°C minor, whereas the enlargement in Fig. 3 reveals at 150°C for some polyglycols a reduced film thickness of up to ~20 %, which fits with the minimal bottom line of twelve hydrocarbon and ester-based formulations as well as blends of hydrocarbons with esters. These results are congruent, since these differ in density and pressure-viscosity coefficient. Figure 2 also shows, that at low temperatures the film thicknesses are unnecessarily high. Thus, engine oils with reduced low temperature viscosities associated with high intrinsic VI are desirable in order to improve fuel economy for city driving and short trips.

Only an increased dynamic viscosity can compensate for the lower pressure-viscosity coefficients of the polyalkylene glycol PAG 46-4 (compare with PPG32-2- and PAG 46-2 in Table 2) or a reduced oil sump temperature or the retention of a smooth surface roughness. As for the PPG 32-2 with a kinematic

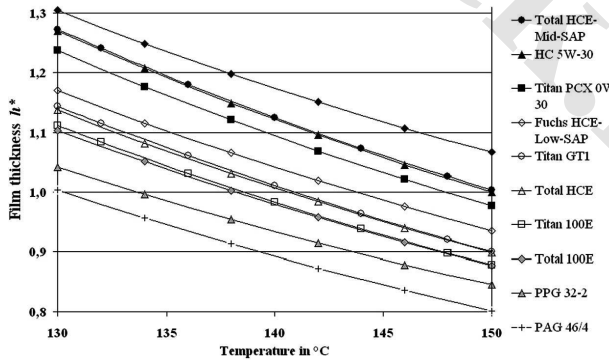

FIG. 3—*Relative film thickness h^* for a line contact for "high" temperatures.*

TABLE 2—*Viscosimetric properties of different factory-fill and prototype engine oils.*

Lubricants	VI	η_{40} [mm^2/s]	η_{100} [mm^2/s]	η_{150} [mm^2/s]	HTHS 150°C [MPa·s]	ν_{150} [MPa·s]	α_p^{1000} 22°C [GPa^{-1}]	α_p^{1000} 150°C [GPa^{-1}]
TOTAL HC 5W-30	159	55.15	9.57	4.197	3.0	3.22	19.8	11.9
Fuchs Titan SL PCX	162	53.19	9.44	4.14	2.95	3.23	18.3	11.8
Castrol SLX 0W-30	168	57.0	10.2	4.42	3.0	3.34	18.2	11.86
TOTAL 100E	156	40.93	7.60	3.46	2.93	2.94	16.9	10.63
Fuchs Titan 100E	166	45.0	8.40	3.64	2.95	2.91	16.9	10.8
TOTAL HCE	159	46.32	8.41	3.73	2.95	2.98	17.3	11.1
Fuchs Titan GT1	164	47.03	8.90	3.78	2.95	2.90	17.6	11.1
FUCHS HCE Low SAP	184	44	8.8	4.26	2.9	3.3	16.8	11.0
TOTAL HCE Mid SAP	170	57.8	10.4	4.53	2.99	3.53	17.96	11.6
PPG 32–2	*156*	34.3	6.7	3.2	2.78	2.87	19.2	10.56
PAG 46–2	*203*	47.4	9.94	4.81	4.3	4.44	14.6	8.8
PAG 46–4	*146*	49.6	8.44	3.7	3.6	3.61	11.76	7.32

viscosity at 40°C of 34,5 mm^2/s, the quite "high" film thickness factor is surprising, which is at 150°C only ~10 % lower as those of the hydrocarbon-based factory-fill oils. This has to be validated in view of the lower coefficients of friction of 0.04–0.06 under mixed/boundary lubrication (see Figs. 8 and 9) and the higher volumetric heat capacity [24,26] as well as the very small sensitivity of the viscosity to high shear rates. The PPG32-2 meets at room temperature the pressure viscosity coefficients of hydrocarbon-based factory-fill oils.

The following Table 2 compiles viscosimetric properties and the pressure-viscosity coefficient determined in a falling ball viscosimeter at 1000 bars of polymer-containing hydrocarbons and hydrocarbon-ester engine oils as well as of polymer-free polyglycol-based and ester-based prototype engine oils. The data show that the lower pressure-viscosity coefficient of polyalkyleneglycol PAG must be compensated for by the higher HTHS in order to give the same film thickness formation behavior of hydrocarbon-based factory-fill engine oils. This should also apply for engine oils composed of 100 % ester, which have at 150°C a pressure-viscosity coefficient equivalent to the polypropylenegylcolmonobutylether PPG32-2.

Comparing the values in the column "HTHS at 150°C" with those of the dynamic viscosity "ν at 150°C," it can be seen that the following qualitative relations exist:

(a) polymer-blended hydrocarbons: HTHS + 9 – 10 % = dynamic viscosity
(b) polymer-free polyglycols, hydrocarbon/ester and ester blends: HTHS + < 3 % = dynamic viscosity, and

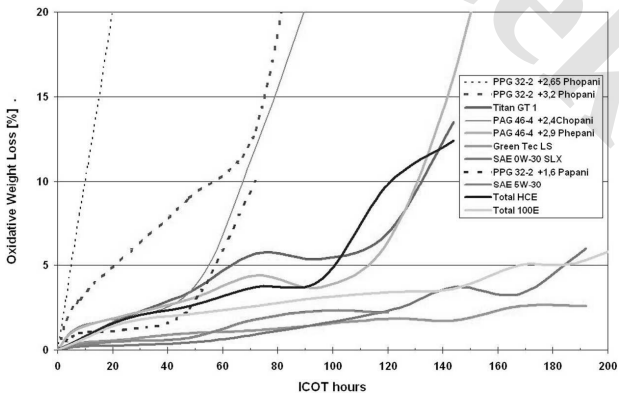

FIG. 4—*Oxidative evaporation losses of different engine oil formulations in ICOT test versus test time (T_{Oil} = 170°C).*

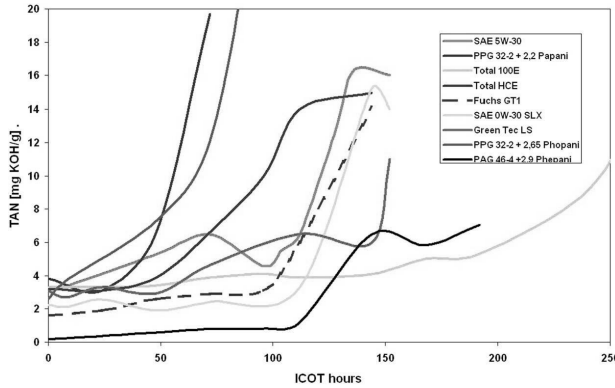

FIG. 5—*Evolution of TAN versus ICOT test time of engine oil formulations ($T_{oil} = 170°C$).*

(c) polymer-blended hydrocarbon/ester blends: HTHS + 12 − 16 % = dynamic viscosity,

which are much smaller than comparing the kinematic viscosity $\eta_{150°C}$ with the HTHS at 150°C, except here also for polymer-free blends.

Table 2 shows that the HTHS is not necessary for describing the viscosimetric behavior of polymer-free alternative engine oils and the dynamic viscosity at 150°C looks sufficient for the film thickness in combination with the pressure-viscosity coefficient. The determination of viscosities at shear rates much above 10^6 s^{-1} with low film heating during testing is desired for the future, as in the tribosystems "crank shaft/Shell" and "Piston ring/cylinder liner" much higher values occur. The loss in viscosity by high shear rates will be lowest or quasi inexistent for polymer-free formulations.

Oxidative Stability (ICOT Test)

For actual factory-fill oils, one ICOT test hour correspond to ~270−330 km of driving. This relation has to be validated for esters and polyglycols. The ICOT life for a 30 000 km drain PCMO based on hydrocarbons lie between 120−140 hours.

The custom-made polyglycols PPG32-2 and PAG46-4 with the proprieraty "boosters" for oxidation resistance have an ICOT lifetime of at least 96 h respecting the bio-no-tox criteria. Overall, "Phopani" is good for 100 h and above and "Phepani" for 130 h and above. The custom made PAG 46-4 base oil reached unadditivated the individual set limit of 7 mgKOH/g at ~48 hours. The evolution of TAN over the test time of the PAG46 − 4 + 2,9 Phepani confirmed, that until 130 hours, even until 192 hours, the set limit of 7,5 mgKOH/g was not passed (see Fig. 5).

The PAG 46 − 4 + 2,6 Phepani reached the same test time for viscosity increase as the ester-based Titan GT1 SAE 0W-20 and presented the same evolution in oxidative weight loss. In contrast, the excessive oxidative weight loss for the "Papani" package is unacceptably high, even the viscosity increase remained stable over test time (see Figs. 4 and 6).

The lowest oxidative weight losses until 200 h (see Fig. 4) were determined for Greentec LS (100 % ester) and TOTAL 100E and even the PAO-based formulation (SAE 0W-30 SLX), reached earlier the drain criteria for TAN and viscosity increase. The highest stability in viscosity until 200 h was determined for TOTAL 100E (see Fig. 6).

Extreme Pressure Behavior in SRV® test

The resistance against seizure of an iron-based alloy (ball bearing 100Cr6H = AISI 52100) was determined for different lubricants with an SRV® test rig[2] according to ASTM D 5706-05 under conditions of mixed lubrication and quoted as Hertzian contact pressure (last O.K.-pressure before failure, see Fig. 7). At

[2]SRV, n-Schwingung, Reibung, Verschleiß (German); oscillating, friction, wear (English translation). Optimol Instruments GmbH, Westendstr. 125, D-80339 Munich, Germany. See ASTM D 5706, D 5707, D 6425 and D 7217.

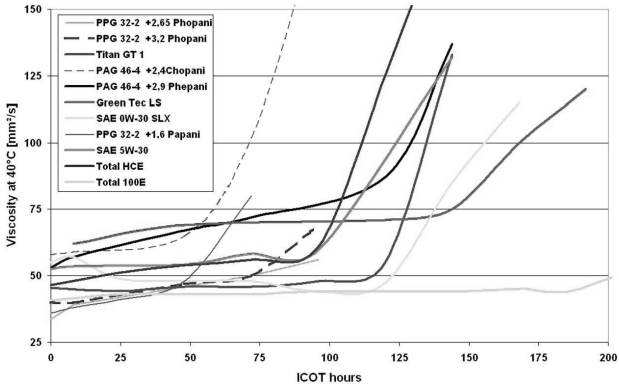

FIG. 6—*Viscosity increase versus oxidation test time ($T_{oil} = 170°C$).*

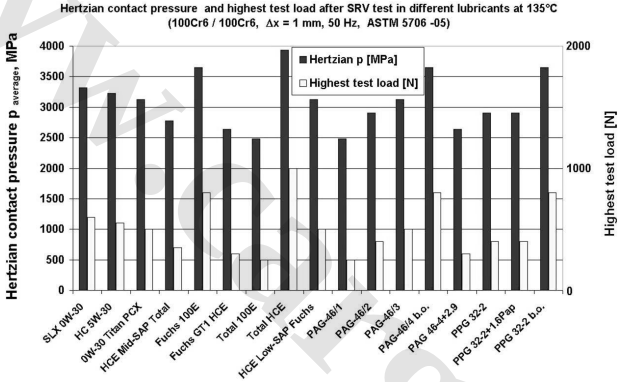

FIG. 7—*Resistance against seizure for different lubricants according to ASTM D 5706-05 using 100/Cr6H/100Cr6H (AISI 52100) at 135°C.*

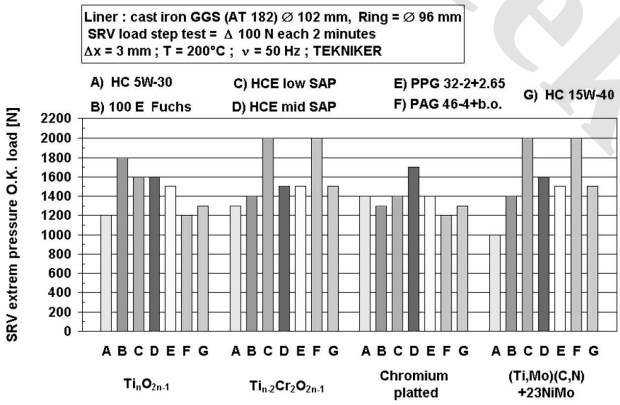

FIG. 8—*SRV™-EP step load test using samples prepared from engines (Note: The HC 15W-40 is an industrial engine oil with 11.630 ppm [S] and a HTHS of 4.2 mPas).*

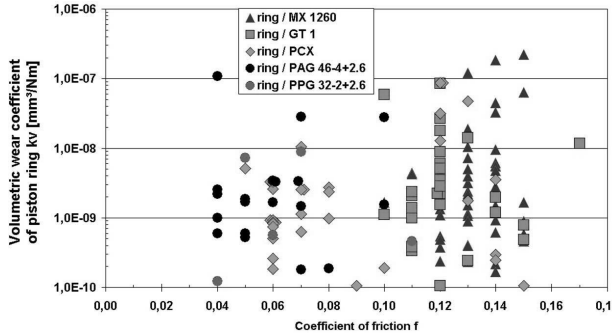

FIG. 9—*Summarizing plot of "coefficient of friction at test end" versus "Wear rate for ring" of sets of different tribo-couples in PAG 46−4+2,6 Phopani, PPG32−2+2,6 Phopani, SAE 5W-30 (HC), PCX 0W-30 and GT1 using the BAM test (F_N = 50 N; υ = 0,3 m/s; T = 170°C; s = 24 km).*

135°C, the factory-fill oils ranged from 3000 MPa to 3500 MPa. The unadditivated polyglycols (base oil=b.o.) PAG46-4 and PPG32-2 achieved the highest values of ~3700 MPa, which were lowered by antioxidants, and were on the same level as the ester-based formulations FUCHS 100E and TOTAL HCE. The formulations with low content of EP-additives or free of "classic" EP-additives displayed no disadvantages exceeding the maximum design limit of today of 2000 MPa. This was confirmed by the SRV® test using a different test condition (higher stroke of 3 mm) with coated pistons rings sliding under linear oscillation against globular cast iron liner specimen (see Fig. 8). The unadditivated PAG46-4 base oil, HCE lowSAP presented highest EP-pressures.

Friction and Wear Behavior in BAM Test

Figures 9 and 10 summarize in a plot the coefficient of friction under mixed and boundary lubrication versus the wear rate of different triboactive and state-of-the-art ring and liner coatings in five oils using the BAM test procedure described in Ref. [10]. The two polyglycols without a fiction modifier and the FUCHS PCX containing an organic friction modifier displayed as a trend the lowest coefficients of friction. The PPG32-2, PAG46-4, and the PCX offer, lubing the appropriate materials, a potential for "zero liner wear," even they are polymer-, Zn-, and Mo-free and respect bio-no-tox criteria (except bio-no-tox for PCX!). More individual details about the friction and wear behavior of alternative oils lubing triboactive and state-of-the-art materials/coatings can be found in Ref [12,22,23].

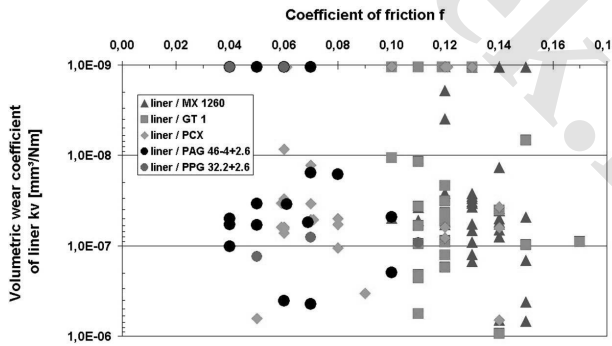

FIG. 10—*Summarizing plot of "coefficient of friction at test end" versus "Wear rate for liner" of a set of different tribo-couples in PAG 46−4+2,6 Phopani, PPG32−2+2,6 Phopani, SAE 5W-30 (HC), PCX 0W-30 and GT1 using the BAM test (F_N = 50 N; υ = 0,3 m/s; T = 170°C; s = 24 km).*

Summary

Overall, the different polymer-free bio-no-tox and low-ash prototype engine oils with reduced additive contents displayed iso-performance regarding the tribological behavior against cast iron with high carbon content and the new triboreactive materials. The polymer-free, alternative proprotype formulations revealed the directions and values of tentative functional improvements of engine oils in the future.

The present results revealed that in engine oil specifications the dynamic viscosity, especially measured under higher shear rates than 10^6 s^{-1}, the heat capacity and the pressure-viscosity coefficients have to be introduced, especially when alternative oils of different chemistries have to be ranked with hydrocarbons. With these data, the oil film thickness of an individual formulation can be calculated. In order to differentiate viscometric properties of alternative oils, the dynamic viscosity taking into account the differences in density has also to be used. All viscometric lubricant properties should be determined at least at 150 °C.

The coefficient of friction under mixed/boundary lubrication is more determined by the lubricants than by the materials or by an individual interaction between lubricants and a specific material or tribopairing.

References

[1] Ellypse, Renault SAS, Direction de la Communication, Pressemappe zum Mondial de l'Automobile in Paris, Sept. 2002, see www.planeterenault.com or www.renault.com>protos>Ellypse.

[2] RENAULT SAS, Dossier Zukunftssichere Entwicklung- "ELLYPSE," Radikal konstruiert-R&D -Wege der Innovation-, Das Magazin für Forschung und Entwicklung, Nr. 26, Oktober 2002 Publisher: Renault SA, Direction de la Communication, rue du Vieux-Pont-de-Sèvres, F-92109 Boulogne-Billancourt (France), ISSN: 1289–009X; also available there in French, English, and Spanish.

[3] Directive 1999/45/EC of the European Parliament and of the Council, "The Approximation of the Laws, Regulations and Administrative Provisions of the Member States Relating to the Classification, Packaging and Labelling of Dangerous Preparations," Official Journal of the European Communities, L200/1, 30.07.1999.

[4] Department of Agriculture, "Guidelines for Designated Biobased Products for Federal Procurement," 7 CFR Part 2902, *Fed. Regist.*, Vol. 68, No. 244, 2003, pp. 70730–70746.

[5] Environmental Protection Agency (EPA), "Oil Pollution Prevention and Responses, Non-Transportation-Related Facilities, Final Rule," 2000, 40 CFR Part 112, 40776–40817.

[6] Sutton, M., "Continued Investigations of Lubricants Effects on Diesel Particulate Filters," *Proceedings, 17th International Colloquium on Tribology*, TAE Esslingen, 2006, ISBN 3-924813-62-0.

[7] Sorab, J., Korcek, S., McCollum, C. B., and Schriewer, K. W., "Sequence VIB Engine Test for Evaluation of Fuel Efficiency of Engine Oils—Part II: Stage Selection and Time Factor Determination," SAE Technical Paper 982624.

[8] Igarashi, J., "The Mineral Oil Industry in Japan," *Proceedings, 13th International Colloguium on Tribology*, Esslingen, Germany, ISBN 3-924813-48-5, Vol. 1, 2002, pp. 13–17.

[9] Taylor, R. I., Dixon, R. T., Wayne, F. D., and Gunsel, S., "Lubricants & Energy Efficiency: Life-Cycle Analysis," *Leeds-Lyon Symposium on Tribology*, Sept. 2004.

[10] Woydt, M., and Kelling, N., "Testing the Tribological Properties of Lubricants and Materials for the System "Piston Ring/Cylinder Liner" Outside of Engines," *Ind. Lubr. Tribol.*, Vol. 55, No. 5, 2003, pp. 213–222.

[11] ASTM D xxxx. yy draft work item "Tribological Characterization of Piston Ring and Cylinder Liner Materials and Lubricants Using the Translatory Oscillation Apparatus (SRV®)."

[12] Woydt, M., and Ebrecht, J., "SRV-Testing of the Tribosystem Piston Ring and Cylinder Liner Outside of Engines," *Proceedings, KSTLE—41st Autumn Conference*, Korea Military Academy, Seoul, 2005, pp. 158–168.

[13] ASTM Standard D 5706-05, "Standard Test Method for Tribological Characterization of Piston Ring and Cylinder Liner Materials and Lubricants using SRV® Test Machine," *Annual Book of ASTM Standards*, ASTM International, West Conshohocken, PA, 2006.

[14] Lansdown, A. R., "High Temperature Lubrication," *Proceedings, 6th International Congress on*

Tribology, Vol. 1, 1993, pp. 56–64.

[15] GFC Lu T 02, Test d'oxydation catalysé par l'acétyle acétonate de fer (ICOT), Groupe Français de Coordination (GFC), Le Consulat, 147, av. Paul Doumer, F-92852 Rueil-Malmaison, gfc@gfc-tests.org; see also IP48/97 (2004) "Determination of oxidation characteristics of lubricating oil."

[16] Fitamen, E., Tiquet, L., and Woydt, M., "Validation of Oxidative Stability of Factory Fill and Alternative Engine Oils Using the Iron Catalyzed Oxidation Test," *J. ASTM Int.*, Vol. 4, No. 8, 2007, pp. 50–79.

[17] Woydt, M., "Review on Lubricious Oxides and Their Practical Importance," *Handbook of Surface Modifications and Processing: Physical & Chemical Tribological Methodologies*, G. E. Totten, Ed., Marcel Dekker, New York, 2004, ISBN 0-9247-4872-7.

[18] Gardos, M. N., "The Effect of Anion Vacancies on the Tribological Properties of Rutile (TiO2-x)," *Tribol. Trans.*, Vol. 32, 1989, pp. 30–31.

[19] Gardos, M. N., "The Effect of Magnéli Phases on the Tribological Properties of Polycrystalline Rutile," *Proceedings 6th International Congress on Tribology*, Vol. 3, 1993, pp. 201–206.

[20] Woydt, M., Kadoori, J., Hausner, H., and Habig, K.-H., "Development of Engineering Ceramics According to Tribological Considerations (bilingual)," Cfi/Ber. DKG, *CFI, Ceram. Forum Int.*, Vol. 67, No. 4, 1990, pp. 123–130.

[21] Woydt, M., Skopp, A., Kelling, N., Hartelt, M., and Berger, L.-M., "Thermal-Sprayed TiO_{2-x}-Coatings Under Mixed Lubrication and Unlubricated Sliding Conditions," *Wear*, Vol. 262, No. 9–10, 2007, pp. 1061–1070.

[22] Landa, J., Illarramendi, I., Kelling, N., Woydt, M., Skopp, A., and Hartelt, M., "Potential of Thermal Sprayed Ti_nO_{2n-1}-Coatings for Substituing Molybdenum Based Ring Coatings," *Ind. Lubr. Tribol.*, Vol. 59, No. 5, 2007, pp. 217–229, or in Proceedings 46. Jahrestagung Gesellschaft für Tribologie, 26.-28.09.2005, Göttingen, Germany, ISBN 3-00-017102-9.

[23] Desplanches, G., Criqui, B., Linnemann, T., and Woydt, M., "Tribological Performances of New Triboactive $Ti_{n-2}Cr_2O_{2n-1}$ and (Ti,Mo)(C,N) as Piston Ring and Cylinder Liner Coatings Interacting with Bio-no-tox Lubricants," Proceedings 17th International Colloguium on Tribology, TAE Esslingen (Plenary paper), 2006, ISBN 3–924813–62–0, or in *Industrial Lubrication and Tribology*, Issue 2, 2008.

[24] Schmidt, R., Klingenberg, G., and Woydt, M., "Thermophysical and Viscosimetric Properties of Environmentally Acceptable Lubricants Industrial," *Ind. Lubr. Tribol.*, Vol. 58, No. 4, 2006, pp. 210–224.

[25] Jones, D. A., "Elastohydrodynamic Lubrication Theory," *Engine Tribology*, Elsevier Science Publishers, Amsterdam, Netherland, C. M Taylor, Ed., pp. 15–50, ISBN 0-444-89755-0.

[26] Schmidt, R., and Woydt, M., Viskosimetrische und thermophysikalische Eigenschaften umweltverträglicher Motorschmierstoffe *Tribol. Schmierungstech.*, (Viscosimetric and thermo-physical properties of environmental friendly engine oils), Vol. 53, No. 2, pp. 16–20.

Journal of ASTM International, Vol. 4, No. 8
Paper ID JAI100912
Available online at www.astm.org

Jian-Qiang Hu,[1,2] *Yi-Qin Hu,*[1] *Guang-Long Liu,*[3] *and Yu-Hong Ma*[3]

Synergistic Tribological Performances of Borate Additive in Lubricants

ABSTRACT: A four-ball tester was used to evaluate the tribological behaviors of nitrogen-containing borate (BNO) combined with zinc dialkyldithiophosphate (ZDDP) and tin dialkyldithiocarbamates (SnDDC) in liquid paraffin or mineral oil, even respectively. The surface analytical tools such as X-ray photoelectron spectrometer (XPS), X-ray diffractometer (XRD), and energy dispersive X-ray (EDX) were used to investigate the chemical states of some typical elements and composition on the rubbing surface of the wear scar. The tribological results show that BNO exhibits better antiwear properties in base oils, and can exhibit good antiwear synergism when it was combined with additives ZDDP and SnDDC, respectively, while the antiwear properties of oil-containing additive packages are optimal under certain concentration ranges. The results of XPS and XRD analyses indicated that BNO can form tribochemical mixed protective films consisting of BN or B_2O_3 compounds on the rubbing surface, and the combination of BNO with SnDDC may form tin, oxides, sulfide, and N-containing compounds on the rubbing surfaces, which contribute to improving the tribological properties of lubricants. A considerable amount of ZDDP can be partially replaced by BNO in synergistic mixtures, or replaced completely by the combination of BNO with SnDDC, which is especially important for ZDDP used in ecologically sensitive applications.

KEYWORDS: borate, additive, antiwear, load carrying, synergistic

Introduction

The addition of extreme pressure (EP) and antiwear (AW) additives is used to improve the friction and wear behavior of lubricants, and to prevent surface damage. In the boundary lubrication regime, the formation of a surface chemical reaction film is the determining factor in minimizing the friction and wear. This depends on the nature and chemistry of additives or tribological effects of their active elements (sulfur, phosphorus, nitrogen, chlorine, etc.) [1,2].

In the field of lubrication, zinc dialkyl dithiophosphate (ZDDP) has been widely utilized as a multifunctional lubricant additive to provide antiwear protection as well as to inhibit the oxidation of petroleum lubricants [3–5]. However, the phosphorus contained in ZDDP has been found to act as a catalyst poison, thus shortening the useful life of the catalytic converter. In addition, the presence of zinc contributes to the emission of particulates in the exhaust.

The International Lubricant Standardization and Approval Committee (ILSAC) introduced the GF-4 Performance Standards that places limits on both phosphorus (0.08 % max.) and sulfur (0.50 % max.) in the finished passenger car engine oil, to improve emissions system compatibility [6,7]. The demand for reducing phosphorus content in engine oils has forced the oil suppliers to modify the formulation of lubricants. So it is desirable to replace ZDDP partially or totally with other nonphosphorus additives without impairing the performance of formulated oils.

Organic borate ester compounds have good antiwear, antifriction properties and oxidation stability as lubricant additives [8–12]. It was reported that oil soluble tin compounds possess good antiwear properties and exhibit good antiwear synergism with other additives containing boron lubricant additives [13–15]. These results show that borate ester and oil soluble tin additives are good candidates to replace ZDDP.

The effect of a particular additive depends on its chemical nature, and its concentration. The wide

Manuscript received November 30, 2006; accepted for publication August 16, 2007; published online September 2007. Presented at ASTM Symposium on Automotive Lubricant Testing and Additive Development on 3–5 December 2006 in Lake Buena Vista, FL; Simon Tung, Bernard Kinker, and Mathias Woydt, Guest Editors.
[1] Department of Aviation Oil, Xuzhou Air Force College, Xuzhou 221000, China.
[2] School of Chemical Engineering, China University of Mining and Technology, Xuzhou 221008, China.
[3] Xuzhou Air Force College, Xuzhou 221000, China.

TABLE 1—*Elemental compositions of three additives.*

	Content (wt. %)					
Additive	B	N	S	P	Zn	Sn
BNO	1.0	0.8				
ZDDP			15.1	8.2	8.2	
SnDDC		1.7	8.1			7.5

variety of positive effects demonstrated by different boron containing compounds in combination with different additives, has motivated the authors to perform systematic studies of the concentration influence of borate additives on the antiwear and extreme pressure properties of S, P compounds.

The required functional action is achieved by appropriate balance. Investigations that can optimize the composition and expand the areas of application of additive packages, are of considerable scientific and practical interest. The present work aims to investigate the antiwear properties and mechanism of nitrogen-containing borate ester additive (BNO). Moreover, the synergistic antiwear and load carrying properties of BNO with ZDDP and tin dialkyldithiocarbamate (SnDDC), respectively, were investigated and offered subsequent exploitation of the results for the development of a synergistic antiwear engine oil composition.

Experimental

Test Basestock and Additives

The organic borate ester additive containing nitrogen (BNO) was synthesized in the authors' laboratory from oleic acid, boric acid, and diethanolamine; BNO synthesized contains oleic acid diethanolamides which was not reacted with H_3BO_3. A boron and nitrogen-containing version was chosen, since several authors have shown the superiority of such additives over additives containing only boron [10,16].

The S, P additives were represented by conventional commercial zinc dibutyl-octyl dithiophosphate (ZDDP) and dibutyl tin dioctyldithiocarbamate (SnDDC), which was prepared according to the following reaction pathway. First, dioctylamine was reacted with carbon disulfide in the presence of sodium hydroxide to yield the corresponding sodium dibutyldithiocarbamates. Further, sodium salt of reactions was neutralized with dibutyl tin dichloride in distilled water. The elemental compositions of the three additives are listed in Table 1.

All concentrations of additives used in the investigation are expressed in percentages by weight if not stated otherwise. The model additives in different proportions were weighed, mixed, and dissolved in an industrial sample of liquid paraffin or mineral base oil 150 SN with kinematic viscosity 5.1 mm^2/s at 100°C.

In the different compositions studied, the original additive, i.e., zinc dialkyl dithiophosphate, was gradually replaced with the borate ester and tin dioctyldithiocarbamates additives, always keeping the sum of the two additive concentrations at the initial level—1.0 % in the particular example. This experimental approach allows for a clear assessment of the synergistic and antagonistic interactions.

Tribological Tests

Tribological properties of base oils containing additives were evaluated with four-ball testers at a rotating speed of 1450 r/min, room temperature of about 25°C. The balls used in the tests were made of GCr15 bearing steel (AISI 52100) at a diameter of 12.7 mm with HRC of 59 to 61.

The antiwear properties were evaluated under loads of 392, 490, and 588 N, respectively, for 30 min according to ASTM D 4172-82 (Standard test method for wear preventive characteristics of lubricating fluid), and the balls were characterized by average wear scar diameters (WSD). The load-carrying capacity of the additive was characterized as maximum nonseizure load (P_B value) and weld load (P_D value) which was evaluated by a short (10 s) extreme pressure test according to ASTM D 2783-88 (Standard test method for measurement of extreme pressure properties of lubricating fluid). Error bars in each experiment represent the 90 % confidence intervals using pooled standard deviations. The relationships between an additive's performance and the tested concentrations are also given.

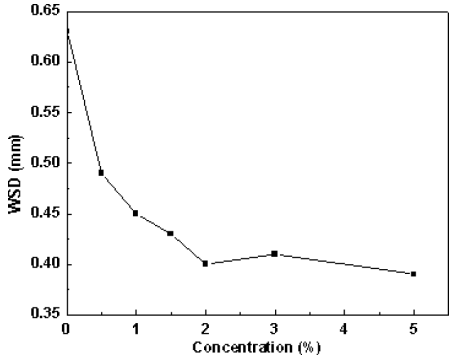

FIG. 1—*Effect of BNO concentration on antiwear property.*

An optical microscope was used to determine the wear scar diameters of the three lower balls with an accurate reading to 0.01 mm. Then, the average of the three wear scar diameters was calculated and cited as the wear scar diameter reported in this paper.

Surface Analysis

The chemical states of the surface film were investigated using a PHI-6100 X-ray photoelectron spectrometer (XPS). The radiation source was Mg Kα line with the pass energy of 29.35 eV. All binding energies were compared with a reference standard of 284.6 eV for carbon. The composition of the surface film was examined by an 18 kW rotating anode X-ray diffractometer (XRD); a small quantity of substance can be detected directly with XRD due to the high energy. Elemental distributions of the worn surfaces were obtained using CSM-950 scanning electron microscopy with energy dispersive X-ray (EDX) analysis

Before XPS, XRD, and EDX analysis, all samples were ultrasonically rinsed with hexane and petroleum ether for 10 min.

Results and Discussion

Antiwear Properties and Mechanism of BNO

The wear tests were performed on the four-ball tester under a load of 392 N. Figure 1 shows the effect of BNO concentration on the antiwear properties in base oil 150 SN. It was found that the antiwear properties increases with increased BNO concentration, although this tendency is less significant for the concentration greater than 2.0 wt.%.

To investigate the antiwear mechanism of the borate ester (BNO), the surface film on the four-ball wear scar was analyzed using X-ray photoelectron spectrometer (XPS). The results are shown in Fig. 2. The B 1 s binding energies on the rubbing surfaces are 198 and 190 eV, which suggests the presence of boron oxide (B_2O_3) and boron nitride (BN) [10,15,17].

To determine the surface composition more precisely, the rubbing surface was investigated by X-ray diffractometer (XRD). The XRD powder diffraction pattern search/match report is shown in Fig. 3. The XRD result indicates that the peaks numbered 1, 2, 3, and 4 are matched very well with the standard powder diffraction pattern of boron nitride (Powder Diffraction File PDF No. 25-1033 and 35-1365), strongly suggesting the presence of boron nitride on the rubbing surface. Boron nitride (empirical formula BN) is a good solid lubricant due to its ordered layer-lattice structure.

Antiwear and Load-carrying Properties of BNO with ZDDP in Liquid Paraffin

Organic borate ester (BNO) and zinc dialkyldithiophosphate (ZDDP) were added to the liquid paraffin; the wear scar diameters (WSD) of the tested balls are reported in Table 2. It shows that BNO and ZDDP possess better antiwear properties than liquid paraffin at each experimental load, and the antiwear prop-

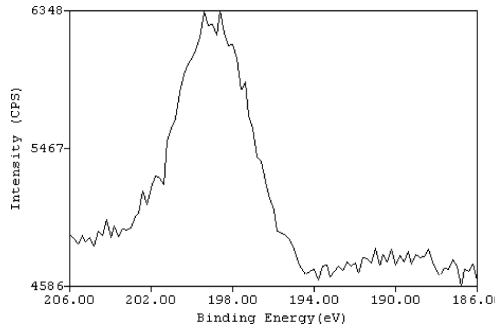

FIG. 2—*B1s XPS diagrams of rubbing surface.*

erties of BNO are better than ZDDP at the loads less than 588 N. No obvious changes are found with the increase of the concentration of BNO and ZDDP. When BNO is combined with ZDDP, the antiwear properties of lubricants are improved compared with each alone. For instance, at constant total concentration of the package, the WSD of the mixtures (at 0.25 % BNO and 0.75 % ZDDP) is lower than that of 1.0 % ZDDP or BNO alone, thus, the antiwear properties of ZDDP can be improved by 31–40 %. The mixtures of 1.0 % BNO with 1.0 % ZDDP show lower WSD than 2.0 % ZDDP or BNO alone.

Figure 4 presents the influence of the additions of BNO and ZDDP on the antiwear properties of liquid paraffin. From Fig. 4 we can see clearly that the wear scar diameter (WSD) varies with the concentration of BNO and ZDDP at loads of 392 and 490 N. With the load higher than 588 N, the wear rate was accelerated, and the protective films formed by tribochemical reactions of this combination cannot prevent thermal decomposition and degradation of ZDDP. The latter produced a large number of active sulfur and phosphorus elements that cause corrosive wear, and the wear scar area was enlarged. The mixture of 0.25

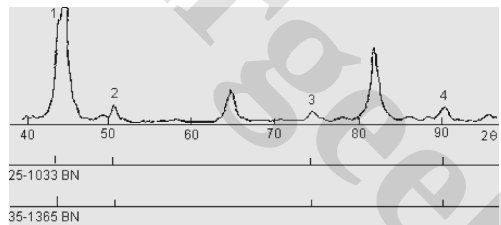

FIG. 3—*Powder diffraction pattern search/match report.*

TABLE 2—*WSD with oils containing BNO with ZDDP.*

Samples	WSD, mm 392 N	490 N	588 N
Liquid paraffin	0.68	1.02	2.35
+1.0 %BNO	0.49	0.69	1.96
+2.0 %BNO	0.50	0.68	1.31
+1.0 %ZDDP	0.62	0.85	1.06
+2.0 %ZDDP	0.61	0.86	0.98
+1.0 %BNO+1.0 %ZDDP	0.33	0. 71	0.92
+0.5 %BNO+0.5 %ZDDP	0.47	0.68	1.67
+0.25 %BNO+0.75 %ZDDP	0.43	0.51	0.83
+0.75 %BNO+0.25 %ZDDP	0.44	0.94	…
+1.0 %BNO+0.5 %ZDDP	0.37	0.86	1.12

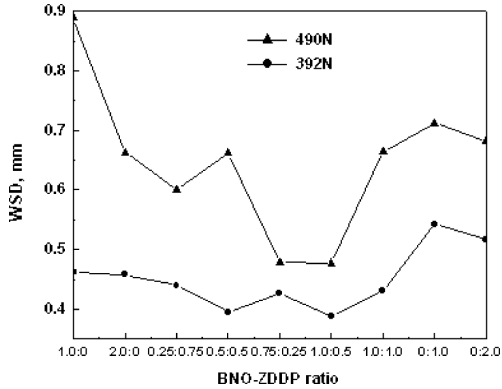

FIG. 4—*Influence of additions of BNO and ZDDP on the antiwear properties.*

% BNO and 0.75 % ZDDP exhibits the best antiwear synergism; secondly, the mixture of 1.0 % BNO and 0.5 % ZDDP is the next best. This approach could provide a method of decreasing the dosage of ZDDP or phosphorus.

The P_B and P_D values of the oils containing different additives are summarized in Table 3; the results show that BNO and ZDDP could all improve the load-carrying properties (enhance P_B and P_D values) of liquid paraffin, and ZDDP is better than BNO. When BNO is combined with ZDDP at constant total concentration of the package, the P_B and P_D values of the lubricants were not improved compared with the same dosage of ZDDP. For instance, the mixtures of 0.25 % BNO with 0.75 % ZDDP are almost equal to 1.0 % ZDDP alone, and also the mixture of 1.0 % BNO compared with 1.0 % ZDDP.

Though BNO possesses better antiwear property than ZDDP, it cannot replace ZDDP completely because ZDDP possesses good antioxidation and corrosion inhibiting properties as a multifunctional lubricant additive. However, the partial replacement of ZDDP with BNO, within a specific narrow range of concentration ratios, evidently decreases the WSD (Fig. 4) and does not reduce the P_B and P_D values. Especially, the WSD of the mixtures of 0.25 % BNO with 0.75 % ZDDP was lower than that of 1.0 % ZDDP alone significantly, and at this synergetic concentration, approximately 0.02 % phosphorus was replaced by approximately 0.0025 % boron. Accordingly, the antiwear synergism of BNO with ZDDP may be attributed to mixed films from decomposition of BNO and ZDDP, such as B_2O_3, BN, phosphate, sulfate, and sulfides.

Antiwear and Load-carrying Properties of BNO with Snddc in Mineral Oil

In order to reduce the phosphorus content in engine oils, the authors selected dibutyl tin dioctylldithiocarbamate (SnDDC) to replace zinc dibutyl-octyl dithiophosphate (ZDDP). BNO and SnDDC were added to

TABLE 3—*Evaluation on load-carrying capacities of BNO mixed with ZDDP.*

Samples	Maximum Nonseizure Load P_B, N	Weld Load P_D, N
Liquid paraffin	392	1236
+1.0 %BNO	647	1569
+2.0 %BNO	804	1961
+1.0 %ZDDP	745	1569
+2.0 %ZDDP	921	1961
+1.0 %BNO+1.0 %ZDDP	921	1961
+0.5 %BNO+0.5 %ZDDP	647	1569
+0.25 %BNO+0.75 %ZDDP	745	1961
+0.75 %BNO+0.25 %ZDDP	647	1569
+1.0 %BNO+0.5 %ZDDP	862	1569

TABLE 4—*WSD with oils containing BNO with SnDDC.*

Samples	WSD, mm 392 N	490 N	588 N
150 SN	0.63	1.12	2.35
+1.0 %BNO	0.45	0.89	1.96
+1.0 %SnDDC	0.52	0.62	1.09
+1.0 %ZDDP	0.54	0.71	1.06
+1.0 %BNO+1.0 %SnDDC	0.39	0.46	0.97
+0.5 %BNO+0.5 %SnDDC	0.40	0.49	0.75
+0.25 %BNO+0.75 %SnDDC	0.39	0.44	0.51
+0.75 %BNO+0.25 %SnDDC	0.42	0.48	0.52
+0.5 %BNO+1.0 %SnDDC	0.38	0.46	0.50

the mineral base oil 150 SN, and the WSD of tested balls under different loads are reported in Table 4. The results show that BNO and SnDDC possess better antiwear properties in 150 SN oil at each experimental load (392 N, 490 N, 588 N), and SnDDC is better than ZDDP at the same condition. When BNO was combined with SnDDC, at constant total concentration of the package, they possess better synergistic antiwear properties; if the concentration of BNO is lower than or equal to that of SnDDC, then good antiwear synergism was obtained. For instance, the mixture of 0.25 % BNO with 0.75 % SnDDC exhibits the best antiwear synergism, and the mixture of 0.5 % BNO with 1.0 % SnDDC is also good. As displayed in Fig. 5, the combination of various amount of BNO and SDDC also clearly illustrates a similar tendency.

The P_B and P_D values of oils containing different additives are summarized in Table 5. The results show that BNO and SnDDC could improve the load-carrying properties (enhance P_B and P_D values), and

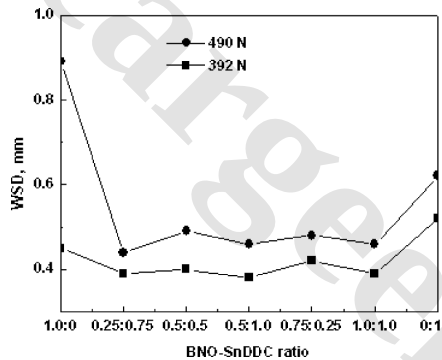

FIG. 5—*Influence of additions of BNO and SnDDC on the antiwear properties.*

TABLE 5—*Evaluation on load-carrying capacities of BNO mixed with SnDDC.*

Samples	Maximum Nonseizure Load P_B, N	Weld Load P_D, N
150 SN	392	1236
+1.0 %BNO	599	1569
+1.0 %SnDDC	745	1961
+1.0 %BNO+1.0 %SnDDC	862	1961
+0.5 %BNO+0.5 %SnDDC	745	1569
+0.25 %BNO+0.75 %SnDDC	745	1569
+0.75 %BNO+0.25 %SnDDC	696	1569
+0.5 %BNO+1.0 %SnDDC	804	1961

TABLE 6—*Binding energy values of elements on the surface and the main components of the reference compounds.*

	Binding Energy, eV					
	B_{1s}	N_{1s}	O_{1s}	Fe_{2p}	S_{2p}	Sn_{3d}
Compounds			Tribo-stressed Sample			
+0.5 %BNO+1.0 %SnDDC	190.3	400.1	529.9	710.8	160.7	484.9
			Reference Compounds			
BN	190.5	398.1				
N-containing compounds		399.8				
FeS				710.8	161.6	
Fe_2O_3			529.6	710.9		
Sn						485.0

SnDDC is better than BNO. With the combinaton BNO with SnDDC, at 1.0 % constant total concentration of the package, the P_B and P_D values of base oils were not improved, compared with the same dosage of 1.0 % SnDDC without impairing the load carrying abilities.

At different concentration ratios of additives BNO and SnDDC, even with the fixed total concentration of the package, they all exhibit good synergistic antiwear properties in the wear test, especially when the concentration of SnDDC is higher than 0.5 % in lubricants. So we could select an economical additive formulation so that maximum efficiency was obtained when they are used in automotive lubricants.

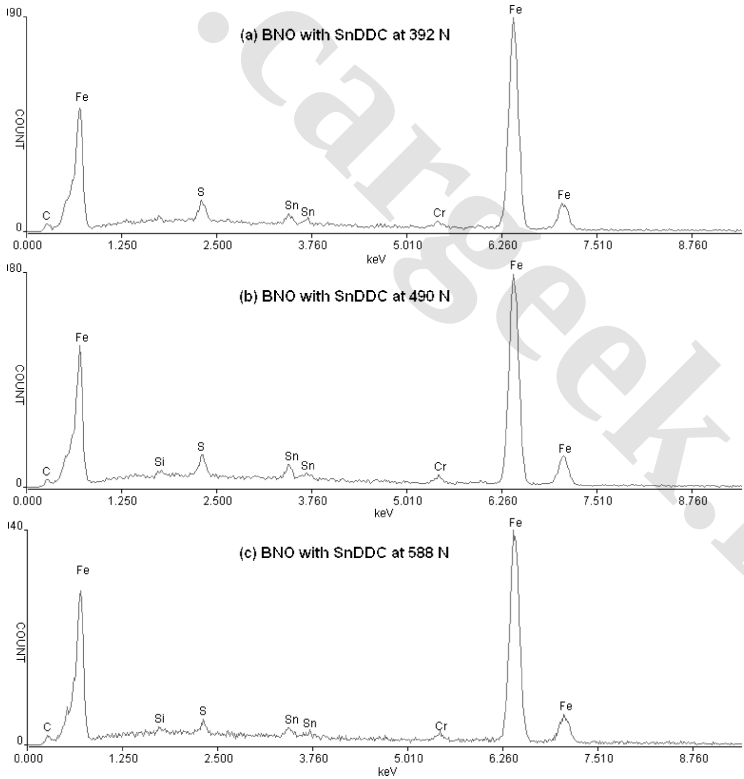

FIG. 6—*EDX spectra of wear scars with BNO and SnDDC under different loads.*

TABLE 7—*Atomic concentration (%) of elements on the wear scar by EDX.*

Analytic Area	C	S	Cr	Fe	Sn
Wear scar at 392 N	2.624	4.342	1.342	90.180	1.512
Wear scar at 490 N	0.558	2.584	1.766	93.218	1.506
Wear scar at 588 N	0.793	1.349	1.330	95.148	0.908

Moreover, it was reported that SnDDC has better antioxidation properties than ZDDP, even better than some phenol antioxidants [18]. It can be seen that this combination is a good method of removing phosphorus from the lubricants.

Surface Analysis

In order to recognize antiwear synergism between BNO and SnDDC the wear surface produced by 150 SN oil containing 0.5 % BNO and 1.0 % SnDDC was analyzed by XPS and EDX. The binding energy of B_{1s}, N_{1s}, O_{1s}, Fe_{2p}, S2p, Sn_{3d} XPS spectra on the tribo-stressed samples under 490 N and the main components of the reference compounds are summarized in Table 6. We can conclude that tin atoms, sulfide, N-containing compound, and iron oxide were formed on the rubbing surfaces in the sliding process.

The elemental distribution on the wear scars at 392 N, 490, 588 N was evaluated using EDX analysis. The EDX spectra are shown in Figs. 6(*a*)–6(*c*) and the atomic concentration of the elements on the wear scars is listed in Table 7. The data in Table 7 were obtained from Fig. 6 using a computer program and normalized to 100 for all given compositions. It was discovered that the contents of S and Sn atoms were decreased with the increase of the applied loads. This change suggests that with the increase of loads, the wear rate increases higher than the super film-forming rate, leading to the decrease of contents of S and Sn. This is consistent with the increase of WSD.

Though SnDDC contains higher contents of S and Sn than the mixture of BNO and SnDDC, the contents of tin on the wear scars from SnDDC under 490 N are less than that of the complex (Sn: 0.820 in Fig. 7).

In view of these observations, the better synergism between BNO with SnDDC can be attributed to formation of the protective layer comprised of tin, sulfide, oxide and N-containing compounds; especially soft tin (0) layer promoted by exoelectron can be catalyzed by borate with electron-deficient p orbits in boron, so that it plays an important role in wear protection. Due to its low melting point, 231.9°C, the authors believe that the tin was deposited in the scratch and served as a “mending material.”

Conclusion

1. The organic borate ester containing nitrogen (BNO) possesses good antiwear properties as a lubricant additive. The surface examination using XPS and XRD indicated that the formation of boron oxide and boron nitride on the rubbing surface contributes to improving antiwear properties of BNO in base oils.
2. When BNO was combined with ZDDP, good antiwear synergism was found at the same dosage without impairing load carrying abilities. Especially, under the optimal proportion of additive

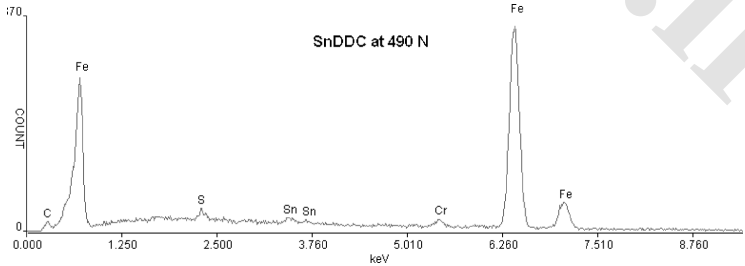

FIG. 7—*EDX spectra of wear scars lubricated with 1.0 % SnDDC under 490 N*

concentrations, the antiwear properties of ZDDP can be improved by 17–35 % by this combination.

3. Dibutyl tin dioctylldithiocarbamate (SnDDC) not only possesses better antiwear properties than ZDDP as a lubricant additive, but also exhibits good antiwear synergism with BNO. The surface examination indicated that tin(0), oxides, sulfide, and N-containing compounds existed on the rubbing surfaces exhibit good antiwear properties.
4. Even with the small additions described above, nearly one-fourth of the phosphorus can be beneficially replaced by approximately eight times the smaller amounts of boron in the blended oil, and the phosphorus in the lubricants may be totally removed with the addition of BNO with SnDDC. This opens up an opportunity for the formulation of ecologically compatible additive packages.

References

[1] Gao, F., Kotvis, P. V., and Tysoe, W. T., "The Surface and Tribological Chemistry of Chlorine and Sulfur Containing Lubricant Additives," *Tribol. Int.*, Vol. 37, 2004, pp. 87–92.

[2] Apay, A. G., "Anti-wear and Extreme Pressure Additives in Lubricants," *Proceedings of 10th International Colloquium*, Vol. II, W. Bartz, Ed., Esslingen 1996, pp. 1093–1099.

[3] Coy, R. C., and Jones, R. B., "The Thermal Degradation and EP Performance of Zinc Dialkyldithiophosphate Additives in White Oil," *ASLE Trans.*, Vol. 24, 1979, pp. 77–90.

[4] Spedding, H. and Watkins, R. C., "The Antiwear Mechanism of ZDDP," *Tribol. Int.*, Vol. 2, 1982, pp. 9–12.

[5] Yamaguchi, E. S., Onopchenko, A., Franciso, M. M., and Chan, C. Y., "The Relative Oxidation Inhibition Performance of Some Neutral and Basic Zinc Dithiophosphate Salts," *Tribol. Trans.*, Vol. 42, 1999, pp. 895–901.

[6] Rolfe, J. H. and Malcolm, W., "Lubricating Oil Composition," U.S. Patent 6500786 B1, 2002.

[7] David, M., "GF-4 Engine Oil Spec Unveiled," *Lube Report*, Vol. 3, 2002, p. 31.

[8] Varlot, K., Kasrai, M., Bancroft, G. M., Yamaguchi, E. S., Ryason, P. R., and Igarashi, J., "X-ray Absorption Study of Antiwear Films Generated from ZDDP and Borate Micelles," *Wear*, Vol. 249, 2001, pp. 1029–1035.

[9] Shen, G. Q., Zheng, Z., Wan, Y., Xu, X. D., Cao, L. L., Yue, Q. X., Sun, T. J., and Liu, A. R., "Synergistic Lubricating Effects of Borate Ester with Heterocyclic Compound," *Wear*, Vol. 246, 2000, pp. 55–58.

[10] Yao, J., "Antiwear Function and Mechanism of Borate-containing Nitrogen," *Tribol. Int.*, Vol. 30, 1997, pp. 387–389.

[11] Dong, J. and Chen, G., "New Concept. Formation of Permeating Layers Nonactive Antiwear Additives," *Lubr. Eng.*, Vol. 50, 1994, pp. 17–22.

[12] Farng, L. O. and Horodysky, A. G., "Mixed Resorcinol-hydroxyester Borates as Antioxidants," U.S. Patent 5006270, 1991.

[13] Ozimina, D. and Kajdas, C., "Antiwear Properties of Complex Compounds of Sn (II) and Sn (IV) in Lubrication of a Bronze-steel Contact," *Lubr. Sci.*, Vol. 4, 1991, pp. 25–33.

[14] Ozimina, D. and Kajdas, C., "Tribological Properties and Action Mechanism of Complex Compounds of Sn (II) and Sn (IV) in Lubrication of Steel," *ASLE Trans.*, Vol. 30, 1996, pp. 508–519.

[15] Yao, J. and Dong, J., "Tribocatalysis Reaction During Antiwear Synergism Between Borates and Sn (IV) Compounds in Boundary Lubrication," *Tribol. Int.*, Vol. 29, 1996, pp. 429–432.

[16] Qiao, Y., Liu, W., Qi, S., Xue, Q., Xu, B., and Ma, S., "The Tribochemical Mechanism of the Borate Modified by N-containing Compound as Oil Additive," *Wear*, Vol. 215, 1998, pp. 165–169.

[17] Wagner, C. D., *Handbook of X-Ray Photoelectron Spectroscopy*, Perkin-Elmer Corporation, Physical Electronic Division, 1979.

[18] Hsu, S. Y. and Horodysky, A. G., "Antioxidants and Antiwear Additives for Lubricants," U.S. Patent 5525248, 1996.

Journal of ASTM International, Vol. 4, No. 9
Paper ID JAI100913
Available online at www.astm.org

B.-R. Höhn,[1] *P. Oster,*[1] *T. Radev,*[2] *and T. Tobie*[1]

The "Practice Relevant Pitting Test"—A New Improved Test Method to Evaluate the Influence of Lubricants on the Pitting Load Capacity of Case Carburized Gears

ABSTRACT: Pitting is a form of fatigue failure which occurs on the flanks of highly loaded case carburized gears. The lubricants, consisting of base oil and additives, influence the pitting lifetime of the gear flanks. Common calculation methods of the pitting load capacity consider, along with the flank roughness and the tangential velocity, only the nominal viscosity of a lubricant as a lubrication relevant influence parameter. The actual lubricant performance and particularly the influence of the additives can be determined only experimentally. Within a FVA-research project a new "Practice Relevant Pitting Test" was developed to evaluate the influence of lubricants on the pitting load capacity of case carburized gears. The new test method is a mechanical test procedure which is based on the existing FVA-FZG-Pitting Test. It is defined as a single stage test which can be extended to an application test by testing the lubricant with a second load stage. In order to improve the practice relevance and to reduce the scatter of the test results the test uses superfinished test gears with adequate profile modifications. The extremely low flank roughness of the new test gears prevents particularly the appearance of undesired micro-pitting and therefore improves the reproducibility of the reached lifetime within the performed test runs. The new pitting test procedure was verified with different gear transmission lubricants and is seen as an improvement of the existing FVA-FZG-Pitting Test. It provides also a possibility to consider the test results for calculation of the pitting load capacity of industrial and automotive transmission gears with an additional factor Z_{Lp} which is to be applied in the calculation method according to DIN 3990. The paper describes the new developed test procedure "Practice Relevant Pitting Test" and discusses the correlation and classification to the existing FVA-FZG-Pitting Test.

Introduction

Pitting is a form of fatigue failure which occurs on rolling-sliding contact surfaces see Fig. 1. Lubricants, consisting of base oil and additives, influence the pitting load capacity of case carburized gears. Common calculation methods of the pitting load capacity of gears like DIN 3990 [1] or ISO 6336 [2] consider, along with the flank roughness and the tangential velocity, only the nominal viscosity of a lubricant as a lubrication relevant influence parameter. The mechanical thermal stresses and the chemical influence of additives on the gear flank surface are dependent on the oil film thickness, the surface structure, and the physical-chemical interaction of surface material and lubricant. These effects are difficult to calculate. The actual lubricant performance and particularly the influence of the additives can be determined only experimentally.

A well known and widely used test method for evaluating the pitting resistance of lubricants in gear drives is the FVA-FZG-Pitting Test [3]. This is a mechanical test procedure which is performed in the FZG back-to-back test rig under defined test conditions using specified test gears. The test result is the pitting lifetime determined with the tested lubricant. It provides also a possibility to consider the test results for calculation of the pitting load capacity of industrial and automotive transmission gears with an additional factor Z_{Lp} which is to be applied in the calculation method according to DIN 3990 [1].

Although the FVA-FZG-Pitting Test has proved itself as an appropriate test method for pitting load capacity, there was a demand from the gear and lubricant industry for improvement and further develop-

Manuscript received November 14, 2006; accepted for publication August 17, 2007; published online October 2007. Presented at ASTM Symposium on Automotive Lubricant Testing and Additive Development on 3–5 December 2006 in Lake Buena Vista, FL; Simon Tung, Bernard Kinker, and Mathias Woydt, Guest Editors.
[1] Technical University of Munich, Institute for Machine Elements, Gear Research Centre (FZG), Botzmannstr. 15, 85748 Garching, Germany
[2] Volkswagen AG, Dr. —Rudolf-Leiding-Platz 1, 34225 Baunatal Germany

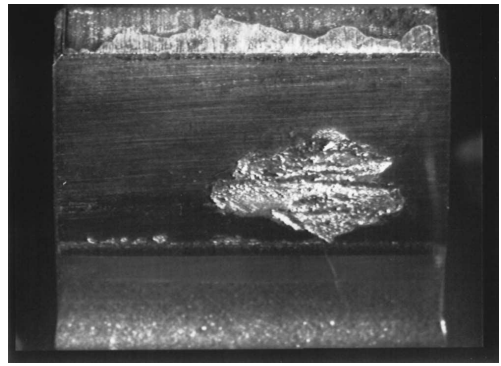

FIG. 1—*Typical pitting damage.*

ment of the test method. Within the scope of a FVA research project a new "Practice Relevant Pitting Test" [4–6] was developed, which is seen as an improvement of the existing FVA-FZG-Pitting Test, particularly regarding practice relevance, reproducibility, and reliability.

The FVA-FZG Pitting Test According to FVA 2/IV

Test Definition

The standard FVA-FZG-Pittig Test according to Ref. [3] is defined as a single load stage test, performed in the FZG standard gear test rig with a center distance of $a = 91.5$ mm (see Fig. 2). The applied torque depends on the nominal viscosity of the tested lubricant. The test procedure is respectively designated as follows:

- PT C/9/90—(Load Stage 9) for low viscosity gear oils below ISO VG 100
- PT C/10/90—(Load Stage 10) for medium and high viscosity gear oils of ISO VG 100 or higher.

The test conditions and the geometry of the test gears are summarized in Figs. 3 and 4.

The result of the standard pitting test is the pitting lifetime LC_{50} for 50% failure probability, which shall be evaluated from at least three individual test runs according to Fig. 5. This value can be compared with the LC_{50} values of reference lubricants and allows a ranking for different candidate lubricants.

Furthermore, the result of the pitting test PT can be also considered by the lubricant performance factor Z_{Lp50T} into the standardized calculation method for rating the pitting load capacity of gears according to DIN 3990 [1] and ISO 6336 [2] respectively. Z_{Lp50T} is calculated based on the determined pitting lifetime LC_{50} and defines a new strength branch of the SN-curve compared to the calculated SN-curve for this oil, which considers only its nominal viscosity (see Fig. 6). Assuming that the influence of lubricant

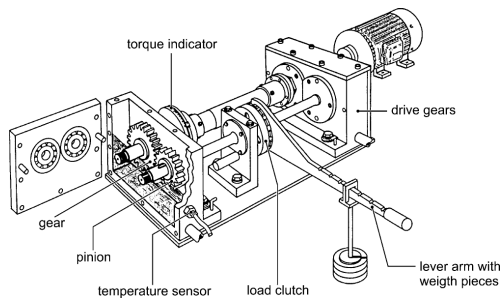

FIG. 2—*FZG standard gear test rig (a = 91.5 mm) according to DIN 51354, Part 1 [8].*

Test gears:	Type FZG-C-PT, R_a = 0,3 ± 0,1 µm
Pinion torque:	PT C/9/90 – T_1 = 302 Nm PT C/10/90 – T_1 = 372 Nm
Speed of rotation:	n_1 = 2250 min^{-1} (8,3 m/s pitch line velocity)
Lubrication type:	Dip lubrication
Oil temperature:	ϑ_{oil} = 90 ± 3 °C controlled
Duration	until reaching of failure criterion, maximally 40·10⁶ load cycles of pinion ≈ 300 h
Failure Criterion:	Pitting area on the most damaged tooth at least 4% of the active flank (ca. 5 mm^2)

FIG. 3—*Test conditions for the standard FVA-FZG-Pitting Test according to Ref. [3].*

additives in the range of endurance limit decreases again, the influence of the factor Z_{Lp50T} is limited to the range of finite life and the endurance level (load cycle range $N > N_\infty$) is kept constant.

Improvement Potential

Test experience shows that the test method PT is able to discriminate the pitting load capacity of different gear lubricants but that the test results are often influenced by some additional, undesired phenomena.

Optical inspection of the gear flanks proves that depending on the lubricant performance and the surface roughness, many test runs are accompanied by more or less strong micro-pitting. Profile deviations

Parameter	Designation	Value	Unit
Centre Distance	a	91,5	mm
Face Width	b	14	mm
Pitch Diameter	d_{w1} d_{w2}	73,2 109,8	mm mm
Tip Diameter	d_{a1} d_{a2}	82,45 118,35	mm mm
Module	m	4,5	mm
Number of Teeth	z_1 z_2	16 24	- -
Addendum Modification Faktor	x_1 x_2	0,1817 0,1715	- -
Preassure angle	α α_w	20, 22,44	° °
Helix angle	β	0	°

FIG. 4—*Geometry of the pitting test gears type FZG-C-PT.*

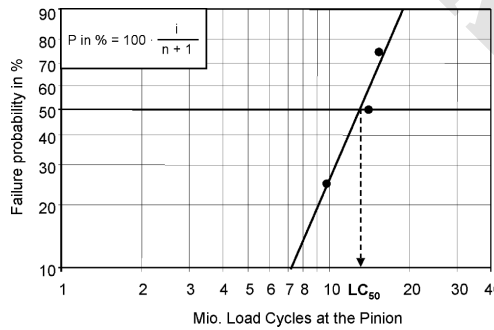

FIG. 5—*Evaluation of the test results of the standard FVA-FZG-Pitting Test (example).*

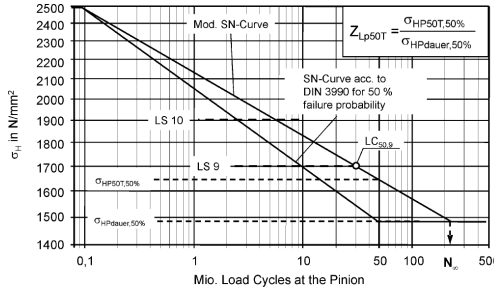

FIG. 6—*Modified SN-curve based on the test result of the standard FVA-FZG-Pitting Test PT.*

due to micro-pitting may lead to a change of the local contact stress distribution on the gear flanks as well as to increased dynamical forces. Consequently the test conditions are not constant any more. Furthermore micro-pitting also affects the location where the pitting damage starts. The gear flank shown in Fig. 7(*a*) has only a small amount of micro-pitting and the pitting damage has started near to the beginning of the of tooth contact. The gear flank shown in Fig. 7(*b*) is characterized by a noticeable micro-pitting. In this case the location where the pitting damage has started has clearly shifted to the border of the micro-pitted area.

In some cases micro-pitting during the pitting test seems to delay the pitting damage but in other cases strong micro-pitting can also reduce the pitting lifetime. Consequently, undesired micro-pitting may lead to an increased scattering of the pitting test results and to some uncertainty regarding the evaluation of the reached pitting lifetime.

Another undesired phenomenon which influences the damage mechanism and the pitting lifetime in the pitting test is a scrape mark which is observed in the root flank area where the tooth contact begins. Scrape marks are caused by a premature contact of the unmodified gear flanks of the gears type C-PT and lead to a decreased pitting lifetime. In the most practical applications scrape marks are avoided by appropriate modifications on the gear flanks.

Therefore more praxis-oriented test gears with adequate profile modifications and a higher micro-pitting load capacity were desired to improve the reliability and the acceptance of the test procedure in the practice.

Although the FVA-FZG-Pitting Test allows the discrimination of gear lubricants according to their pitting load capacity, the test results are based on the pitting lifetime only at one load stage. This allows the users to obtain a test result in a relatively short time but nevertheless in many cases the evaluation of the lubricant performance in a wider load range is necessary, particularly if it shall be considered in the load capacity calculation of transmissions gears of the practical application. Therefore an optional extension of the standard single stage test by a second load stage was desired by the lubricant users and gear designers in the industry as a way to improve the reliability of the test results.

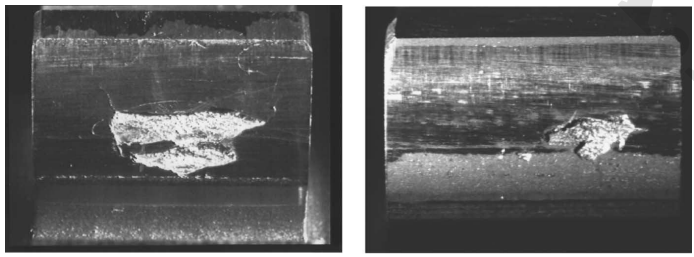

FIG. 7—*Gear flanks used in the standard FVA-FZG-Pitting Test with the test gears C-PT—influence of the micro-pitting on the location where the pitting damage starts.*

Development of the Practice Relevant Pitting Test (According to FVA 371)

Within the scope of an FVA research project the standard FVA-FZG-Pitting Test (PT) was further developed to a new test method called FVA-FZG-Practice Relevant Pitting Test (PTX) [5]. The aim of this project was the improvement of the existing test procedure particularly regarding:

- practice relevance of the test gears and test results,
- prevention of undesired micro-pitting,
- higher reliability of the test results based on additional testing at a second load stage. The new test procedure PTX was defined on the basis of the existing pitting test PT and uses modified test gears and test conditions. The main aspects within the development of the new test procedure are described below.

Modification of the Test Gears

In order to improve the practice relevance of the pitting test the influence of different modifications on the basis of the standard reference test gears type FZG-C-PT were theoretically investigated and experimentally tested in the test rig. The results showed that appropriate tip and root relief can prevent the premature contact and the scrape mark in the beginning of the tooth contact. On the other hand, profile modifications lead to an increased pitting lifetime and the duration of the test procedure exceeds the required ranges for a short time test method.

This effect was compensated by an additional lengthwise crowning which increases the contact stress and reduces the pitting lifetime back to load cycles comparable to the unmodified reference gears. On the basis of the performed investigations, the pitting test gears were modified by adequate profile and lengthwise modifications and were designated as C-PTX (see Fig. 8). Figure 9 compares the contact stress distribution of the standard test gears C-PT and the modified test gears C-PTX along the path of contact.

The experience of many performed pitting tests at the FZG has shown that the flank roughness has a significant influence on the amount of micro-pitting and the resulted profile deviations during the test runs.

gears type:	FZG-C-PTX
material: heat treatment: base geometry:	Identical with FZG-C-PT
grinding method:	form grinding
flank modifications:	test pinion: unmodified test gear: tip and root relief: $C_a = C_f = 50 \pm 4$ µm lengthwise crowning: $C_b = 30 \pm 3$ µm
flank surface:	both test gears superfinished, $R_a = 0{,}1 \pm 0{,}05$ µm

FIG. 8—*Specification of the test gears type C-PTX.*

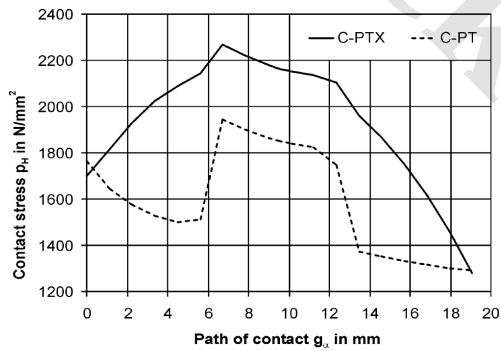

FIG. 9—*Comparison of the contact stress distribution of the test gear types C-PT and C-PTX along the path of contact.*

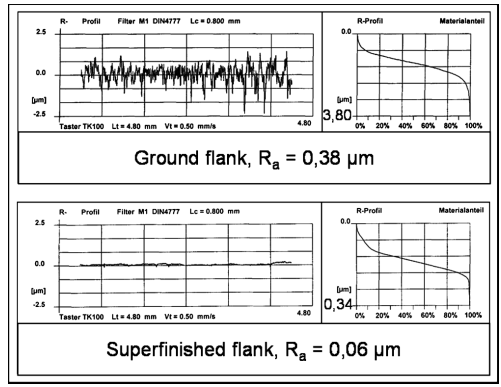

FIG. 10—*Surface roughness profile of ground only and ground and superfinished test gears (example).*

In order to reduce the flank roughness the new test gears C-PTX are implemented with a superfinished flank surface as a final processing after grinding. The superfinishing procedure is specified as a mechanical removal of roughness peaks performed in neutral pH-range. Figure 10 shows representative roughness measurement results of a ground only and a ground and superfinished test gear flank. The results approve a significantly lower surface roughness and an improved material ratio after superfinishing without changing the flank geometry and the performed profile and lengthwise modifications.

In order to compare the micro-pitting resistance of the reference test gears type C-PT and the modified test gears type C-PTX the micro-pitting safety factor S_λ according to Ref. [7] was calculated for both gear types as a function of the viscosity class and the determined failure load stage of the lubricant in the FZG-micro-pitting test. The results are shown in Fig. 11.

The displayed curves for the gears C-PT show that only lubricants with a high micro-pitting resistance (GFT-high) reach a calculated micro-pitting safety factor $S_\lambda > 1$. The calculation results correlate with the experience that only lubricants with a sufficient micro-pitting resistance should be tested in the pitting test PT in order to assure an acceptable profile deviation during the test runs. Due to the extremely low flank roughness the new superfinished test gears type C-PTX provide always a calculated micro-pitting safety factor $S_\lambda > 1$ and even $S_\lambda > 2$ for lubricants with a micro-pitting failure load stage higher than six (such lubricants are still classified as GFT-low). The calculation results approve the experimentally approved insensibility of the superfinished test gears regarding micro-pitting. Therefore also lubricants with a low micro-pitting performance can be tested in the new pitting test procedure PTX.

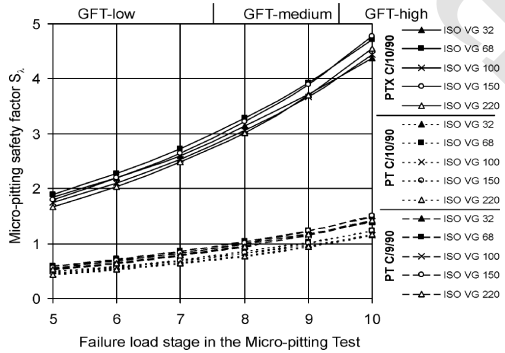

FIG. 11——*Micro-pitting load safety factor S_λ according to [7] for the test gears type C-PTX and C-PT depending on the viscosity class and the determined failure load stage of the lubricant in the FZG micro-pitting test.*

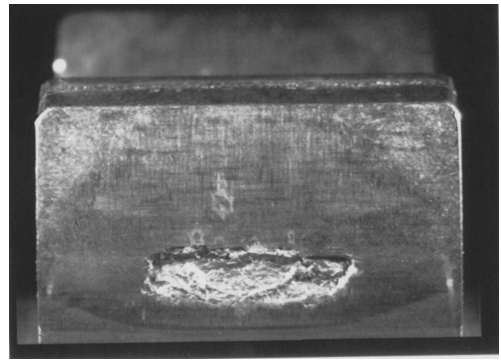

FIG. 12—*Typical pitting damage on a gear flank of the gears type FZG-C-PTX.*

The experience of the performed experimental test with the new superfinished test gears type C-PTX provide a typical pitting damage without micro-pitting appearance (Fig. 12). The results have proved that due to the superfinished flank surface micro-pitting can be almost completely avoided in the pitting test. This ensures a constant tooth profile during the course of the test procedure and eliminates a considerable factor for a large scatter of the test results.

Modification of the Test Condition

The PTX test is performed in the FZG back-to-back test rig with a center distance of 91.5 mm. The test conditions are comparable to the FVA-FZG-Pitting Test according to FVA 2/IV and are summarized in Fig. 13.

Depending on the application profile the new test method PTX is defined as single stage test (for lubricant developers) which can be extended to an application test (for lubricant users and gear designers):

- Single Stage Test PTX C/10/90: Unlike the standard pitting test PT where the used load stage depends on the nominal viscosity of the tested lubricant (PT C/9/90 or PT C/10/90), the new single stage test procedure PTX C/10/90 is performed always with the load stage 10 independent on the lubricant viscosity.
- Application Test PTX C/SNC/90: The application test is an extension of the single stage test by additional testing of the lubricant at a second load stage. The second load stage is determined depending on the results of the single stage test. For lubricants with a lower pitting load capacity the additional testing is performed at load stage 9, lubricants with a higher pitting load capacity are tested at load stage 11.

A detailed description of the test procedure is to be found in Ref. [4]. The pitting test PTX is basically performed at 90 °C oil sump temperature. Optionally the test temperature can be adjusted according to the

Test gears:	Type FZG-C-PTX, R_a = 0,1 ± 0,05 µm
Single stage test: Application test:	PTX C/10/90: T_1 = 372 Nm PTX C/SNC/90: T_1 = 302 Nm (LS9) if $LC_{50,10} = 15 \cdot 10^6$ T_1 = 405 Nm (LS11) if $LC_{50,10} > 15 \cdot 10^6$
Speed of rotation:	n_1 = 2250 min^{-1} (8,3 m/s pitch line velocity)
Lubrication type:	Dip lubrication
Oil temperature:	ϑ_{oil} = 90 ± 3 °C controlled
Duration	until reaching of failure criterion, maximally $40 \cdot 10^6$ load cycles of pinion ≈ 300 h
Failure Criterion:	Pitting area on the most damaged tooth at least 4% of the active flank (ca. 5 mm²)

FIG. 13—*Test conditions for the Pitting Test PTX according to Ref. [4].*

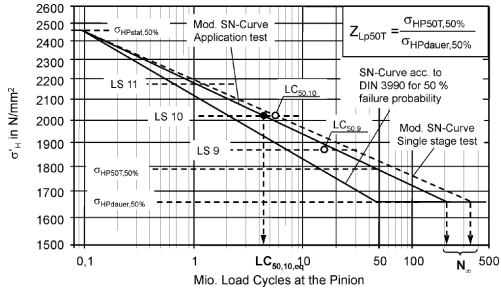

FIG. 14—*Determination of the factor Z_{Lp50T} from the test results of the pitting test PTX.*

temperature range of the actual practical application. It is recommended to perform at least three test runs within the single stage test and in case of an extended application test at least two additional test runs at the second load stage.

Evaluation of the Results and Determination of the Factor Z_{Lp}

The results of the single stage test PTX C/10/90 is the pitting lifetime $LC_{50,10}$ obtained at load stage 10. Similar to the standard pitting test according to FVA 2/IV the factor Z_{Lp50T} can be calculated from the results of the new pitting test as well and can be considered in the calculation method for pitting load capacity according to DIN/ISO. In order to ensure a better coverage in the range of limited fatigue strength of the SN-curve it is recommended to extend the single stage test to the application test. In this case Z_{Lp50T} is calculated as a function of the equivalent lifetime at load stage 10 ($LC_{50,10,eq}$) taking into consideration the determined lifetime at load stage 10 ($LC_{50,10}$) and the determined lifetime at the second load stage ($LC_{50,9}$ or $LC_{50,11}$) as shown in Fig. 14.

Within the development of the new pitting test PTX different lubricant samples were investigated. The results have shown that the PTX test is suitable to discriminate lubricants regarding their pitting load capacity. The scatter of the test results has to be expected equal or even lower than in the standard pitting test method PT. As an example Fig. 15 shows the test results for one lubricant sample that was tested in the new test procedure PTX according to FVA 371 and for comparison also in the test procedure PT according to FVA 2/IV. Figure 16 summarizes the results of both test procedures.

The results prove a good correlation of the determined Z_{Lp50T}-values for the different test methods. For the calculation of Z'_{LP50T} in the test procedure PTX the influence of profile roughness as well as the influence of profile modifications compared to the test method PT were considered. The Z'_{LP50T}-value obtained in the application test PTX C/SNC/90 considers the test results from both tested load stages LS10

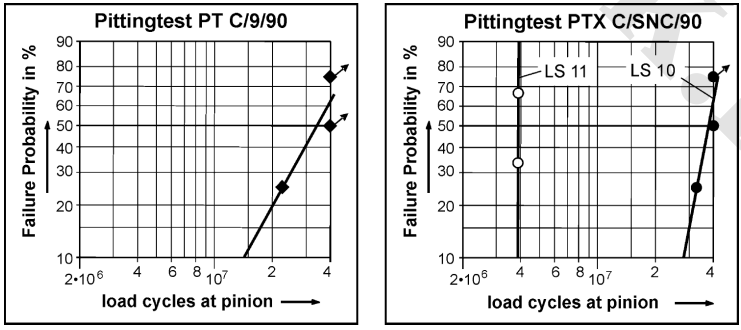

FIG. 15—*Test results of the pitting test PT C/9/90 compared to the new test method PTX C/SNC/90 for one lubricant sample (example).*

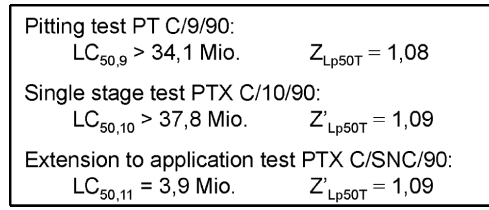

FIG. 16—*Comparison of test results of the pitting test methods PT and PTX for the lubricant sample according to Fig. 15.*

and LS11. The correlation of the two test methods is expected to be as better as less strong undesired phenomena like micro-pitting have influenced the test results in the test method PT.

Summary

Pitting is a gear fatigue failure that is strongly influenced by the lubricating conditions and lubricant properties. The actual lubricant performance regarding pitting load capacity can be determined only experimentally. A well known and widely used pitting test procedure is the standard FVA-FZG-Pitting Test PT. Within an FVA research project this test method was improved and further developed to a new pitting test called "Practice Relevant Pitting Test PTX." Depending on the application profile the new advanced test method is defined as a single stage test—recommended for lubricant developers and as an extended application test—recommended for lubricant users. The pitting test PTX uses superfinished test gears with suitable flank modifications. Therefore the influence of undesired phenomena like micro-pitting or scrape marks on the pitting life time can be minimized. The practice oriented test gears ensure a closer correlation of the test results to practical gear applications. The extended application test offers the possibility of a higher reliability of the test results compared to the single stage test by an additional testing at a second load stage.

References

[1] DIN 3990: *Tragfähigkeit von Stirnrädern*, Beuth Verlag, 1987.
[2] ISO 6336: Calculation of the Load Capacity of Spur and Helical Gears, International Organization for Standardization, 2003.
[3] FVA-Information Sheet No. 2/IV "Pitting Test," *Forschungsvereinigung Antriebstechnik e.V.*, 1997.
[4] FVA-Information Sheet No. 371 "Practice Relevant Pitting Test," *Forschungsvereinigung Antriebstechnik e.V.*, 2003.
[5] Radev, T., Entwicklung eines praxisnahen Pittingtests, *FVA-Forschungsvorhaben Nr. 371, Heft 710*, 2003.
[6] Radev, T., Einfluss des Schmierstoffes auf die Grübchentragfähigkeit einsatzgehärteter Zahnräder—Entwicklung des Praxisnahen Pittingtests, Dissertation TU München, 2005.
[7] Schrade, U., Einfluss von Verzahnungsgeometrie und Betriebsbedingungen auf die Graufleckentragfähigkeit von Stirnrädern, Dissertation TU München, 2002.
[8] DIN 51354, Teil 1: *Prüfung von Schmierstoffen—FZG-Zahnradverspannungs-Prüfmaschine. Allgemeine Arbeitsunterlagen*, Beuth-Verlag, 1990.

Journal of ASTM International, Vol. 4, No. 10
Paper ID JAI100916
Available online at www.astm.org

Bernard G. Kinker,[1] *Raymond Romaszewski,*[1] *and Pamela A. Palmer*[1]

ROBO—A Bench Procedure to Replace Sequence IIIGA Engine Test

ABSTRACT: A constant quest but a difficult goal is replacement of expensive and lengthy engine tests with more cost effective bench tests. This paper will report on development of a bench test, the ROBO, as a potential replacement for the Sequence IIIGA, an oxidative oil thickening engine test now part of ILSAC GF-4 specifications. Sequence IIIGA, a gasoline fueled engine running under severe conditions, is used to condition oils prior to determining TP-1 MRV viscosity, a cold temperature and low shear rate measurement. After Sequence IIIGA conditioning, candidate oils must meet SAE J300 pumpability limits at no more than 5°C warmer than its original SAE W grade. The ROBO bench procedure has been developed to potentially replace Sequence IIIGA engine aging by mimicking, to the degree possible, oxidative conditions found in the engine conditioning procedure. ROBO conditions were developed by employing the three Sequence IIIG ASTM matrix oils and comparing their used oil rheologies from multiple Sequence IIIG and ROBO runs. The results from the final ROBO conditions compare well not only for TP-1 MRV but also for KV 40°C and CCS. To further test the correlation of bench to engine conditioning, a set of diverse oils (various SAE viscosity grades and DI chemistries) have been examined; these viscometric data from ROBO and Sequence IIIG also compare favorably with only a few anomalies. Finally, the status of industry acceptance of ROBO will be discussed.

KEYWORDS: oxidation, Sequence IIIGA, pour point depressant, MRV TP-1

Sequence IIIG Engine Test

Gasoline engine lubricants are certified after exhaustive testing for rheological, chemical, and physical properties, but most importantly for their performance in controlled engine tests. For International Lubricant Standards and Acceptance (ILSAC) Gasoline Fuel (GF) specification series and American Petroleum Institute (API) "S" and "C" categories, the engine tests are carefully developed and documented [1]. Currently there are five different "Sequence" gasoline engine tests, each dedicated to evaluating different specific performance parameters under relevant conditions. An important part of this engine testing sequence is the Sequence IIIG. This test is the current version of the Sequence III procedure first developed over 45 years ago to evaluate primarily the oxidative stability of engine oils in severe service. Anecdotally, it was meant to simulate towing a heavy load under hot desert-like conditions.

The current Sequence IIIG evaluates oil thickening, oil consumption, valve train wear, and piston deposits by simulating high speed service under relatively high ambient conditions. It is an important element of ILSAC GF-4 [2] and API SM [3] specifications. It also appears in heavy duty diesel specifications such as API CJ-4 [4] and an earlier version, the Sequence IIIF, appears in certain ACEA specifications [5].

The test itself utilizes a fired 1996/1997 GM Series III V-6 engine of 3800 cc displacement operating on a dynamometer [6]. Unleaded gasoline fuel induction is accomplished by a modified GM port fuel injection system, which sets the air to fuel ratio to a nominal value of 15+1. The overhead valve train uses a single camshaft operating both intake and exhaust valves via pushrods and hydraulic valve lifters in a sliding-follower arrangement. There is a 10 min oil-leveling period followed by a 15 min ramp up to operating conditions during which operational and oil checks are conducted. After this the test operates at 3600 r/min, 125 bhp, and 150°C oil temperature for 100 hours. At 20-h intervals oil samples are taken and a corresponding oil replenishment aliquot is added [7].

Manuscript received November 20, 2006; accepted for publication September 19, 2007; published online November 2007. Presented at ASTM Symposium on Automotive Lubricant Testing and Additive Development on 3–5 December 2006 in Lake Buena Vista, FL; Simon Tung, Bernard Kinker, and Mathias Woydt, Guest Editors.
[1] Senior Technical Fellow, Principal Scientist, and Senior Technologist, respectively, RohMax USA, Horsham, PA.

Sequence IIIGA Engine Test

The Sequence III engine procedure, evolving through many versions up to "G" now, has a long history of measuring oil thickening after engine oxidative conditioning. The actual determination of viscosity has been and still is conducted at 40°C in a kinematic viscometer [8]. While this test has served well over the years it did not detect certain problems noted in the field with high power density engines running in severe service [9]. The same research identified a more appropriate tool to detect these problems, namely the TP-1 version of the Mini Rotary Viscometer (MRV) operating at cold temperature [10]. The TP-1 MRV procedure is normally employed to measure viscosity related low-temperature pumpability of fresh oils as defined in SAE J300 engine oil viscosity classification [11].

Thus, a new measurement was added to the protocol for used oil evaluation after Sequence IIIG aging. End-of-test oils are evaluated for low-temperature rheology via the TP-1 MRV procedure. When this is done the engine test is coded as the Sequence IIIGA but the test protocol and operating conditions remain exactly the same as a Sequence IIIG. The renaming and registration of a Sequence IIIGA procedure allows one to run and measure used oil's low-temperature rheology independently of the other pass/fail criteria, if so desired. Prior to the Sequence IIIGA, used oil TP-1 MRV was a "rate and report" parameter after Sequence IIIF.

It is obviously necessary to define the temperature of measurement when discussing viscometric determinations. For the issue at hand, TP-1 MRV viscosity of Sequence IIIGA used oils is determined at the oil's original SAE W pumpability temperature as defined by SAE J300 or at one W grade higher. The measurement at one W grade higher (5°C higher) is allowed if the used oil's Cold Cranking Simulator (CCS) viscosity no longer meets the limits of the fresh oil W grade imposed by SAE J300. The potential need to measure used oils at one SAE W grade higher is certainly understandable as used, oxidized oil often thickens to one SAE W grade higher in the CCS. The CCS is a low-temperature measurement associated with engine oil rheology as it relates to cold-temperature engine starting [12]. The viscometric limits of Sequence IIIGA used oils are the same values found in SAE J300, i.e., 60 000 mPa·s maximum and no detectable yield stress, i.e., <35 Pascals, under the conditions of the TP-1 MRV test.

So far through this discussion, an unanswered question about the referenced field problems [9] has probably arisen. Why was the 40°C kinematic viscosity (KV) inadequate and conversely why is the TP-1 MRV determined at the SAE W viscosity grade temperature better. One hypothesis to explain excessive TP-1 MRV viscosity is that severe oil oxidation can lead to the formation of polar molecular species which associate to form gel-like structures at relatively cold temperatures but not necessarily at warmer temperatures. Such gel-like structures may be detected under low-temperature, low-shear rate conditions such as those in the TP-1 MRV. The same gel-like structure may not be detected at the warmer temperatures employed in determining kinematic viscosity. Nor may they be detected in a CCS measurement for despite its cold-temperature operation it is a high-shear rate operation which would presumably destroy any gel structure.

As stated above, oil that has undergone excessive oxidative thickening can be first identified by low-temperature, low-shear rate viscosity as measured by TP-1 MRV. In an effort to avoid this behavior and ultimately to provide adequate low-temperature pumpability, the ILSAC GF-4 specification includes a TP-1 MRV measurement on the end-of-test used oil drained from the Sequence IIIGA engine test.

Cold Temperature Rheology Testing

The TP-1 MRV rheology measurement discussed above is normally associated with fresh oil pumpability as defined in SAE J300. In this use, it identifies cold temperature *wax gel* structuring and ultimately to demonstrate control over such structures by their absence under test conditions. In a similar vein, the Sequence IIIGA and attendant TP-1 MRV identifies cold temperature *polar molecule* structuring and ultimately to demonstrate control over such structures by their absence. Thus a common test, the TP-1 MRV, is used to measure both low-temperature structuring phenomena. But, it is important to keep in mind that there are two very different structuring mechanisms involved: nonpolar wax crystallization versus polar molecule agglomerations. Since a single rheology test is involved, a brief summation of its evolution is worthwhile.

Over the past 30 years cold-temperature pumpability limits have been investigated and introduced into specifications for fresh, unused engine oils. SAE J300 Engine Oil Viscosity Classification first included a

laboratory bench measurement of pumpability related properties in the September 1980 version [13] based on engine testing conducted by ASTM [14]. The test procedure, ASTM D 3829 [15,16], utilized the same MRV instrument mentioned above, but had a relatively fast cool down to the final test temperature as defined by an oil's SAE "W grade." Two measurements were made: first *yield stress* to simulate an oil's potential inability to flow because of wax-gel structure; second *viscosity* to understand an oil's potential inability to be pumped.

Unfortunately, the test conditions were found to be deficient as some oils that met specification experienced pumpability field failures [17]. The problem was related to the fast cooling cycle which was too rapid to fully allow wax crystallization [18]. The tonic to this problem was slower cooling to better allow creation of a wax-gel matrix and wax particles, or both, that contribute to excessive viscosity. In answer, the TP-1 MRV procedure was developed and has been specified in all versions of SAE J300 since 1985. The TP-1 MRV still measures *yield stress* and *viscosity* but uses a slow cooling rate, i.e., 0.33°C per hour through the typical wax crystallization temperature range so as to improve the likelihood of creating wax-gel structure.

A later study in the 1990s was conducted to evaluate low-temperature starting and pumping properties of more modern engines and lubricants. Most engines in the study were found to cold start much more easily than the previously studied 1970s era engines. To provide better starting and pumping protection, all SAE J300 W grades were redefined by lowering both CCS and TP-1 MRV test temperatures by 5°C. Pumpability viscosity limits were doubled to the current 60 000 mPa seconds but yield stress remained the same at $<$35 Pascals [19].

Numerous other low-temperature low-shear rate pumpability test procedures exist and are often employed to build further assurance of good performing lubricants. For instance, Gel Index via Scanning Brookfield technique (ASTM D 5133) is a part of the ILSAC GF-4 specification. However, TP-1 MRV is the most widely recognized, utilized, and available low-temperature test because of its inclusion in the global SAE J300 viscosity classification. Therefore its selection for use after Sequence IIIGA is quite appropriate not only for its low-shear rate but particularly for the very slow cooling rate to allow potential structure to build from polar molecular aggregation.

Bench Testing Versus Engine Testing

With the above background in mind, it is clear that the Sequence IIIGA is an oxidative stressing tool and that the actual measurement of how much stress is conducted in a TP-1 MRV instrument which is extraneous to the engine. Also, obvious is that rating of actual engine parts for parameters such as wear, scuffing, deposits, or corrosion is not an issue. So, could a bench oxidation condition procedure simulate the engine conditioning procedure? There are numerous bench oxidation procedures in the literature. Just to name a few there is the well known RBOT [20] normally applied to turbine oils and the ABOT [21] for application to automatic transmission fluids. In fact, there are reports of attempts to simulate internal combustion engine oxidation such as Sequence III. Two such examples are provided by Roby [22] and Mazzamaro [23].

There has been a previous successful substitution of a bench test for an Sequence gasoline engine test, i.e., the Ball Rust Test in place of the Sequence IID rust test. This test was developed in 1997 [24,25] and incorporated into ILSAC GF and API Category S specifications.

There are obvious advantages for bench tests over full-scale dynamometer engine tests. These include: the convenience of normal laboratory bench operation versus a specialized engine laboratory facility; just the reduction in complexity should be of value; and most importantly cost control. A Sequence IIIGA test is priced at about US$ 36 000 while a ROBO is in the range of US$ 1500 to 2000 depending on the analytical tests requested beyond the usual viscometrics.

Simulating Engine Conditions in Glassware

Duplicating the environment and the effects of an engine in laboratory glassware seems a daunting task. But, if the chemical and physical processes can be understood at a basic level, then there is a possibility that they can be mimicked at least to a certain degree. So setting out to duplicate a Sequence IIIG with respect to its oxidative environment, we determined that the following were of importance. First, an obvious consideration is to bring together the main reactants oil and oxygen (air); an overriding chemical

TABLE 1—*ROBO and Sequence IIIG conditions.*

ROBO Ingredient	Engine Simulation	Effect	ROBO Setting
Test fluid	Lube oil	Substrate for reaction	200 g
Iron ferrocene	Wear metals	Catalyst	15 ppm
Nitrogen dioxide	Blow-by gas	Catalyst	2 mL over 12 h
Dry air	Air	Oxygen source	185 mL/min
Agitation	Churning	Mixing	200 r/min
Vacuum	Volatility (Exhaust stroke)	Remove light ends	0.61 Barr (18 in. Hg)
Temperature	Operational condition	Reaction driver	170°C
Time	Drain interval	Sufficient reaction time	40 h

consideration is catalysis such as from the wear metals (iron) and from blow-by gas (NO_2). The above reactants and catalytic materials then need to be subjected to intimate mixing and high temperature over a sufficient period of time to drive the reaction forward. Finally evaporative loss (related to oil consumption), a very significant physical process in engines and in particular the Sequence IIIG needs to be simulated. This is obvious for any procedure attempting to reproduce used oil rheology. Without removal of lighter oil fractions it is not possible to get all the rheology measurements correct and in line with each other. There are three components: reactants {oil and air}, catalysts (Fe and NO_2), and conditions (time, temperature, mixing, and vacuum). A tabular form of these factors and their intent in ROBO is shown in Table 1.

Critical Parameters

ROBO was developed over a period of a few years and a detailed chronology or exhaustive description of the experimentation leading to its current state would be detailed, voluminous, and not enhance the quality of this discussion. Keep in mind that these conditions work in concert to produce used oil quite similar to the used oil from the Sequence IIIG engine. One cannot consider these conditions as isolated factors as a change in only one will have a significant impact. So, let us start at the end and discuss briefly the key variables: what are they, what are their settings, and what are important associated factors.

Oil Amount—Test oil is simply added to the reactor at 200 g per individual run. Choice of this amount is in large part a function of vessel size and head room needed to accommodate vigorous stirring, bubbling air, and the application of vacuum. Also, it is desirable for the reaction to yield sufficient used oil for rheology or other desired determinations. Amounts from 200 to 300 g were evaluated.

Air Flow—House supplied air is first dried then metered into the reaction mixture at a flow rate of 185 mL per minute through a subsurface feed. Dry air is utilized in order to avoid any effects of variable amounts of moisture present in the air supply. Rates from 100 to 1000 mL per minute were investigated.

Nitrogen Dioxide Catalyst—The importance of this powerful oxidation catalyst cannot be over stated. The ROBO conditions have been set to deliver 2.0 mL of gaseous high purity NO_2 over the first 12 h of the reaction. The gas is fed along with dry air through the subsurface feed system. Range finding experiments went from 0 all the way up to 20 mL; 0 giving very little oxidation. Feed times of 12 to 48 h were studied.

Temperature—This is fundamental to the rate of reaction and hence to the final condition of the oil. Temperature is set at 170°C, 20°C warmer than a Sequence IIIG, and after heat up is carefully controlled throughout the reaction. Temperatures as low as 150°C and up to 175°C have been examined.

Time—Of course, time keys with the other critical parameters most particularly with temperature. The setting is 40 h versus the 100 h of a Sequence IIIG. The shorter duration of the ROBO is helpful in extracting more runs per work week. Reaction times studied ranged from as short as 24 h up to as long as 100 h.

Vacuum—The use of vacuum is another extremely important aspect in that light end, lower viscosity molecules must be removed just as in the engine. Volume velocity of 56.6 L/min is set in the equipment at a pressure is set at 0.61 Barr (18 in. Hg) which produces evaporative losses similar to those in a Sequence IIIG. Studies of vacuum pressure were conducted at 0.67 to 0.54 Barr.

Less Critical Parameters

There are several aspects of ROBO procedure that are not critical in the sense that small to medium variation does not cause significant change in the measured responses. Nonetheless, it is important to apply these to the reaction as their complete absence would be problematic.

Stirring is such a parameter. The normal rate of 200 r/min and the type of stirrer (45° pitched blade turbine) are less important than being sure to create strong agitation throughout the reaction period.

Wear metal catalyst is another such factor. Iron ferrocene (15 ppm) is a surrogate for the ubiquitous presence of a wear metals in used oil. This particular compound was chosen for its oil solubility and decomposition to yield Fe at a temperature approaching that in ROBO. Brief studies with other oil soluble iron compounds and with more iron ferrocene (200 ppm) did not substantially alter measured responses.

Parameters Not Used

Two other parameters were considered; one was investigated and abandoned while the other was rejected even prior to any experimentation.

Addition of Strong Oxidizers—We investigated the addition of strong oxidizing compounds such as an acid and peroxides to the reaction mixture. Nitric acid from 0.05 up to 1 % was evaluated. Several peroxides were examined; these were selected to cover a range of thermal decompositions from very fast to slow at ROBO reaction temperature (170°C), i.e., t-butyl peroxy 2-ethylhexanoate $t1/2 = 0.02$ min; t-butyl peroxy benzoate $t1/2 = 1.1$ min; and cumyl hydroperoxide $t1/2 = 42$ min. Concentrations ranged from 0.25 to 1.0 %. Addition strategies of a single oxidizer compound, mixtures of peroxides of different half lives, and addition of both acid and peroxide were examined. The experimentation included adding these compounds at the beginning of the reaction and also in aliquots during the reaction. Ultimately this strategy was abandoned as the quality of the results was not enhanced by addition of these oxidants.

Fuel Dilution—It is well known that lubricant in normal engine operation is diluted by fuel from piston blow-by and that fuel can be an important substrate for oxidation. However, it is debatable how important fuel dilution might be when the lubricant is held at a constant 150°C for 100 h such as in the Sequence IIIGA. Under the conditions of the experiment in both the engine and the ROBO fuel would rapidly volatilize. Thus, we did not attempt to incorporate or even investigate the use of gasoline dilution in ROBO; additionally we avoided the serious safety concerns associated with gasoline.

Equipment

The ROBO is a fairly complex assembly of individual equipment most of which is available from commercial sources. The main reactor is a specially prepared one litre, glass, round-bottomed reactor equipped with a bottom sample/drain valve and an outside heating element. The reactor is fitted with a specially machined metal head with ports to accept a stirrer bearing, a gas feed tube, a vacuum regulator, a thermocouple, and also with entrance (filling) and exit (vacuum) ports. There are systems for the controlled delivery of dry air; for the application and control of vacuum; for heating and accurate control of temperature; and for the very accurate delivery of high purity nitrogen dioxide over a set time interval. Less sophisticated systems provide appropriate agitation and water cooling of the vacuum condensers. See Fig. 1 for a visual of the assembled ROBO apparatus.

Responses

Of course, the key response to follow in a procedure simulating Sequence IIIGA would be the TP-1 MRV. CCS viscosity is also determined in order to set the appropriate MRV temperature. In addition and just as in the Sequence IIIG, we determine kinematic viscosity at 40°C in belief that the procedure should

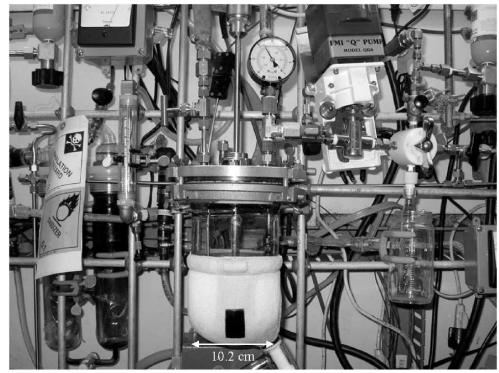

FIG. 1—*ROBO equipment setup.*

reasonably simulate the entire engine caused rheologies. We also determine infrared oxidation {1700 cm-1} and nitration {1635 cm-1} by the peak height method but will not delve into this information now.

Test Fluids

When a new or substantially revised engine test is introduced, a specially selected set of oils are subjected to repeat tests in order to assemble precision data. In the case of the Sequence IIIG (IIIGA) three ASTM Matrix oils are available from the ASTM Test Monitoring Center and the extensive engine test results have been published [26]. These fluids were used in exhaustive experimentation to develop the conditions now utilized in ROBO to provide satisfactory reproduction of Sequence IIIG used oil rheology.

In addition to the ASTM oils, numerous oils with known Sequence IIIG rheology behavior were "donated" for ROBO conditioning prior to determination of used oil rheology. To date 34 oils have been ROBOed and the results compared to the used oil rheology after Sequence IIIG. Many of these oils were donated by fellow ACC members along with pertinent data. It should be noted that all ROBO data reported in this paper came from the RohMax laboratory.

Results with ASTM Sequence IIIG Matrix Oils

After achieving the final set of conditions described in this paper, the three matrix oils were subjected to repeat ROBO runs under set conditions so as to generate a significant body of data for comparison to the Sequence IIIG engine data. ASTM Matrix fresh oil rheology data are summarized in Appendix I while the used oil information follows in Appendix II; note the results are laid out in order of lowest to highest result and not in any chronological or run order. Of the three ASTM oils, one (435) gives consistently failing results in MRV via the presence of yield stress as well as viscosity >60 000 mPa seconds; KV 40°C increases also routinely fail with results of >150. Another oil (438) provides excellent results in both rheological measurements, while the third (434) yields generally passing results. These conclusions are true for the engine as well as the laboratory procedures. There does appear to be one obvious outlier with oil 434; one engine result was an abysmal failure in MRV and KV increase (*also known by the industry term of pVis*). Comparing the outlier values to the average values for all the engine results, pVis 250 high versus 121 average and MRV 84 400 high versus 46 500 average it is reasonable to conclude this one value is a spurious result. Comparative graphics of ROBO versus engine results are provided in Fig. 2 (MRV) and Fig. 3 (pVis). It is apparent that ROBO and the Sequence engine procedure provide oils with comparable used oil rheology.

It is these data that convinced the American Chemistry Council (ACC) to sponsor ROBO for evaluation as a potential replacement for the next generation of the Sequence IIIGA (presumably Sequence IIIHA) in next generation ILSAC GF-5 specifications. The same data persuaded ILSAC/Oil to list ROBO as a potential replacement for Sequence IIIHA in next generation ILSAC GF series specifications. How-

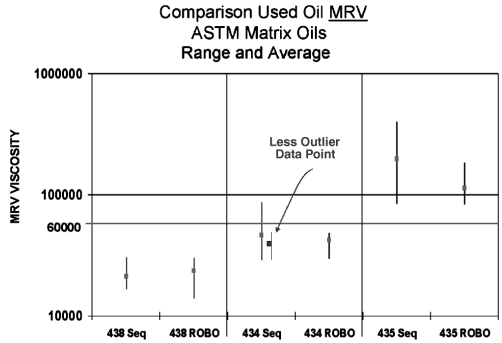

FIG. 2—*ROBO versus Sequence Engine Test results—Range (bar) and average (point) for MRV [60 000 = pass/fail limit].*

ever, the development of the replacement Sequence IIIH has been canceled; despite this, ROBO remains a valid, potential replacement for Sequence IIIGA in next generation ILSAC GF series specifications.

MRV Results with Additional Oils

In addition to the above ASTM Matrix oils, 34 other oils, primarily donated by various ACC member companies, have been conditioned by ROBO and the resulting used oil rheologies compared to the same from Sequence IIIG. The detailed data are listed in Appendix III. The MRV Sequence IIIG versus MRV ROBO results are displayed graphically in Fig. 4 along with linear regression statistics. Note that two points in the upper right-hand corner are not drawn to scale. These are very poor performers with very high MRV viscosities such that an on-scale representation would heavily compress the scales to a visually unsatisfying point. The engine (Seq) and ROBO values are listed along with these data points. Pass/fail lines at the 60 000 mPa·s maximum limit have been placed on the graph for reference.

A simple visual inspection shows the engine and ROBO data appear to be reasonably correlated. However, there are two clear outliers where the engine MRV data points are much higher than those derived from the bench. The oils and underlying data have been thoroughly investigated in order to understand why only these two points are so grossly mismatched. The only fact noted to explain the engine behavior of oil 211 is that it had very high oil consumption, but the test was a valid run regarding oil consumption. High oil consumption would most likely cause higher viscometric responses. Still there has been no complete resolution of the discrepancy introduced by these two oils and their attendant data. Data from multiple repeat ROBO are not substantially different, and unfortunately the Sequence IIIG has not been rerun due to the high cost of the engine test. The repeat ROBO data are shown in Table 2.

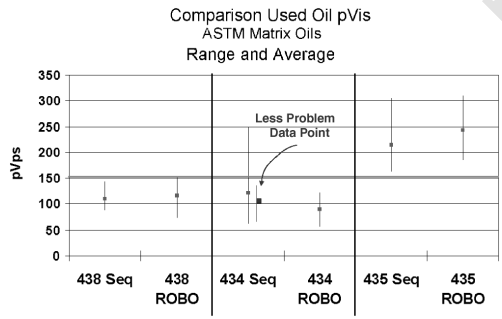

FIG. 3—*ROBO versus Sequence Engine Test results—Range (bar) and average (point) for pVis [150 = pass/fail limit].*

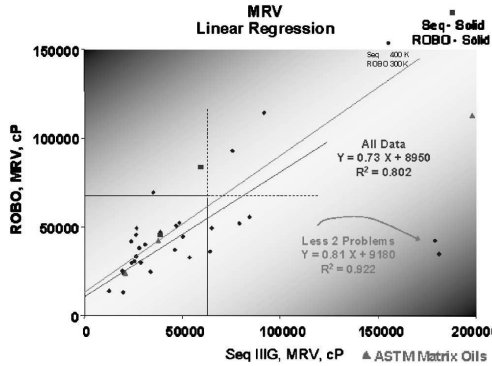

FIG. 4—*MRV via ROBO and Sequence IIIG for 37 oils (including averages for three ASTM Matrix oils).*

Linear regression lines, equations and data are included in Fig. 4 and considering all data, an r-square of 0.802 is not unreasonable for comparison to an engine procedure. While engine testing is a vital part of oil qualification and can be done reasonably and usually reliably, such testing is not a precision tool. If the two problem data points were eliminated then the r-square rises to 0.922, a fairly impressive value considering the above engine precision discussion. If one compares the equations resulting from the complete dataset versus the data less the two problems, there is not a great change between the two. Without the problem points, the slope more closely approaches unity, but the intercept is little affected.

While not apparent from the raw data or the graphical representation, an important statistical conclusion is that the source of the 34 ACC oils cannot be discerned. Said another way, the source of the additive chemistry is not a factor in the data. Keeping in mind that the oils were donated by five different ACC companies, the fact that oil source is not a factor strongly indicates that there are no known chemistry biases in the results.

pVis Results with Additional Oils

Recollect that in Fig. 3, pVis data assembled from engine and bench testing of ASTM Matrix oils provided reason to further evaluate ROBO with regard to this viscometric response. Data from the engine and bench conditioning procedures are assembled in Appendix III and these same data are displayed graphically in Fig. 5. There is one point in the upper right-hand corner not drawn to scale because of its extremely high pVis values in both conditioning procedures. Pass/fail lines have been drawn at the limit of 150 maximum for reference.

The same conclusions, as discussed above with MRV, on the source of oil apply to the pVis response as well indicating additive chemistry is not being distinguished by ROBO.

Once again there is a problem data point that does not fit the trend described by all other data. In the case of pVis response there is only one such data point and it is from one of the problem MRV oils, i.e.,

TABLE 2—*Repeat ROBO runs on the two oils giving problematic data points.*

	Sequence IIIG		ROBO	
Oil SAE VG	pVis	MRV YS/Viscosity mPa·s	pVis	MRV YS/Viscosity mPa·s
260 SAE 5W-30	120	Yes/179 000	70	No/42 200
			115	No/67 700
211 SAE 10W-30	253	Yes/181 000	134	No/35 000
			133	No/36 000
			122	No/36 000
			136	No/29 000

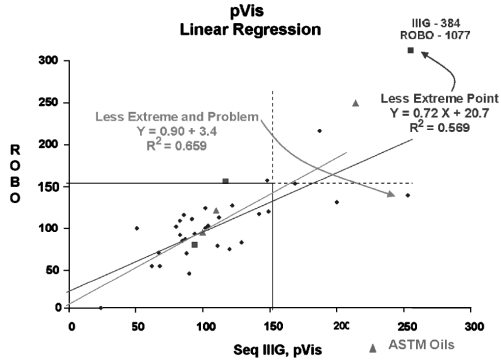

FIG. 5—*pVis via ROBO and Sequence IIIG for 37 oils (including averages for three ASTM Matrix oils).*

oil 211. Recollect this oil had very high oil consumption in the Sequence IIIG but that the test was nevertheless a valid test. Just as with MRV there is no known reason for the discrepancy; repeat ROBO data have already been given in Table 2.

pVis linear regression lines, equations, and data were assembled excluding the extremely high data point since such huge values abnormally skew the linear regression results. R-square for all data minus the high point is 0.569. Further exclusion of the problem data point alluded to above gives an R-square of 0.659. Also without these points, the slope is 0.90 (approaching unity) while the intercept of 3.4 is close to the origin.

Category Prediction Analysis—MRV

A final statistical consideration is a category prediction analysis. Simply stated, this is the measure of ROBO's ability to predict the pass/fail outcomes of the Sequence IIIG. Such an analysis is shown in Fig. 6. Note the data point with the notation "ROBO YS;" this is to indicate that the MRV measurement of viscosity after ROBO had Yield Stress which is a failure irrespective of the actual viscosity (oil 250). So, this data point is counted as a fail and thus as an accurate category prediction of the engine result. The analysis is summarized in the upper left-hand corner with ROBO giving an 81 % prediction rate. Also note there are two data points annotated "borderline" because of their just failing viscosity by the engine procedure (oils 160 and 503). The point here is, that a marginal change to a lower value would cast these two points into the accurate prediction category. For the MRV measurement repeatability is 10.3 % of the

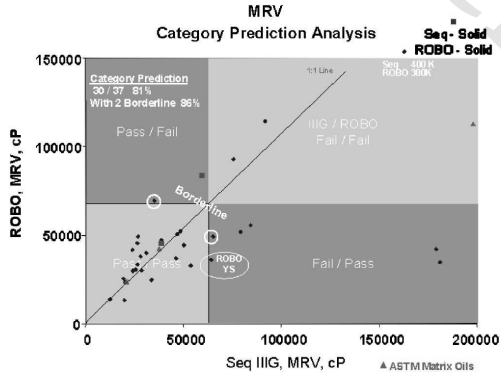

FIG. 6—*MRV category prediction analysis—ROBO versus Sequence IIIG.*

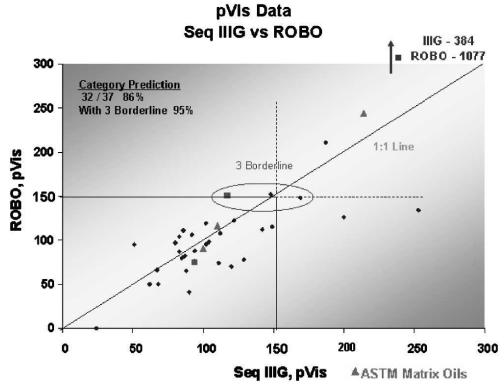

FIG. 7—*pVis category prediction analysis—ROBO versus Sequence IIIG.*

mean at −25°C and reproducibility is 20.8 %; neither r nor R are reported at −30°C (10). Inclusion of the two borderline points as accurate predictions would yield a prediction accuracy rate of 86 % compared to an 81 % rate imposed by a hard pass/fail limit.

Category Prediction Analysis—pVis

The same analysis applied to the pVis parameter is displayed and summarized in Fig. 7. In this case, ROBO gives an even higher accuracy prediction rate of 86 % (compared to MRV—81 %). For pVis there are three "borderline" oils. Note in particular one data point at the intersection of the pass/fail limits for Sequence IIIG (148) and ROBO (152). Inclusion of these three cases as accurate predictions gives a rate of 95 % compared to the rate of 86 % imposed by a hard pass/fail limit.

Status

As of this writing ROBO is a strong candidate to replace Sequence IIIGA in next generation GF-5 PCMO specifications. The same data as discussed in this paper are the basis of ROBO's strong consideration by ILSAC/Oil. It has also been suggested that ROBO be "fast tracked" in order to enter current ILSAC GF-4 specifications. EMA has endorsed evaluating ROBO as a potential replacement for Sequence IIIG in Heavy Duty Diesel Oil specifications, but data from heavy duty oils must be obtained.

Conclusions

- ROBO equipment and conditions have been developed to simulate Sequence IIIG conditions and oxidative aging of oils.
- Results from ASTM Matrix oils reasonably duplicate Sequence IIIG used oil rheology.
- Statistics derived from 34 ILSAC GF-4 type oils and three ASTM Matrix oils via ROBO compared to Sequence IIIG used oil rheology are quite encouraging.
- Results from 34 ILSAC GF-4 type oils and three ASTM Matrix oils have a high rate of predicting Sequence IIIG pass/fail rheology of aged oils.
- ILSAC/Oil is considering ROBO as a substitute for Sequence IIIGA used oil MRV.

Acknowledgments

The authors wish to express their gratitude to Doug Anderson of the American Chemistry Council for compiling and organizing the raw data. Also, we wish to thanks Todd Dvorak of Afton Chemical for his expert statistical analysis and helpful suggestions.

Appendix 1: ASTM Precision Matrix Fresh Oil

	434 *SAE 5W-30*	*435* *SAE 5W-20*	*438* *SAE 5W-20*
KV 100°C, mm^2/s	10.14	8.38	8.74
KV 40°C, mm^2/s	57.45	45.29	48.85
CCS −30°C, mPa·s	4500	4950	4200
MRV −30°C, mPa·s	11 700	9800	8100
MRV −35°C, mPa·s	22 400	21 400	15 200

Appendix 2: ASTM Precision Matrix Used Oil Rheology Results

	Sequence IIIG			*ROBO*		
	pVis % 40°C Vis Increase	TP-1 MRV, −30°C Yield Stress/Visc Yes - No/mPa·s	CCS, −30°C mPa·s	pVis % 40°C Vis Increase	TP-1 MRV, −30°C Yield Stress/Visc Yes - No/mPa·s	CCS, −30°C mPa·s
Oil 434	63	No/29 000	20 600	57	No/29 900	13 100
SAE	87	No/34 200	19 000	59	No/32 500	13 400
5W-30	90	No/31 900	15 600	94	No/43 300	12 600
	99	No/45 600	19 500	118	No/48 000	14 000
	127	No/49 200	23 600	122	No/57 600	18 100
	133	No/48 900	17 200			
	250	No/86 400	22 500			
Range	63–250	29.0–86.4 K	15.6–23.6 K	57–122	29.9–57.6 K	12.6–18.1 K
Average	121	46 500	19 800	90	42 300	14 200

	Sequence IIIG			*ROBO*		
	pVis % 40°C Vis Increase	TP-1 MRV, −30°C Yield Stress/Visc Pa/mPa·s	CCS, −30°C mPa·s	pVis % 40°C Vis Increase	TP-1 MRV, −30°C Yield Stress/Visc Pa/mPa·s	CCS, −30°C mPa·s
Oil 435	163	Yes/84 800	11 400	185	Yes/99 300	18 600
SAE	168	Yes/110 000	15 600	226	Yes/83 500	18 500
5W-20	172	Yes/84 500	16 200	256	Yes/183 000	19 700
	176	Yes/91 900	14 000	310	Yes/85 400	22 000
	222	Yes/300 000	19 400			
	230	Yes/294 000	17 200			
	279	Yes/211 000	8530			
	305	Yes/400 000	17 500			
Range	163–305	84.5–400 K	8.5–19.4 K	185–310	83.5–183 K	18.6–22.0 K
Average	214	198 000	15 000	244	113 000	19 700

	Sequence IIIG			*ROBO*		
	pVis % 40 °C Vis Increase	TP-1 MRV, −30°C Yield Stress/Visc Yes - No/mPa·s	CCS, −30°C mPa·s	pVis % 40°C Vis Increase	TP-1 MRV, −30°C Yield Stress/Visc Yes - No/mPa·s	CCS, −30°C mPa·s
Oil 438	88	No/16 700	8300	74	No/16 600	7400
SAE	90	No/18 000	8600	101	No/14 100	8800
5W-20	92	No/19 000	9200	109	No/21 100	9100
	102	No/19 300	10 200	113	No/26 400	11 400
	112	No/20 500	9900	127	No/30 000	9800
	121	No/20 500	10 500	133	No/29 800	8700
	133	No/23 700	9900	152	No/27 300	10 800
	144	No/30 400	15 400			
Range	88–144	16.7–30.4 K	8.3–15.4 K	74–152	14.1–30.0 K	7.4–11.4 K
Average	110	21 000	10 200	116	23 600	9400

Appendix 3: Donated Oils—Used Oil Rheology

Oil Code	*SAE VG*	*Sequence IIIG*		*ROBO*	
		pVis	MRV YS/Visc, mPa·s @ °C	pVis	MRV YS/ViscmPa·s@°C
100	5W-30	85	Yes/ > 400 000@-30	80	Yes/298 670@-30
110	5W-30	104	Yes/91 743@-30	98	Yes/114 270@-30
120	5W-30	83	No/31 003@-30	87	No/40 000@-30
130	5W-30	92	No/23 858@-30	106	No/41 750@-30
131	10W-30	200	No/53 724@-30	126	No/32 740@-30
140	5W-20	122	No/28 600@-30	122	No/30 070@-30
150	5W-30	67	No/46 200@-30	66	No/37 020@-30
160	10W-30	170	No/65 100@-25	148	No/49 150@-25
170	10W-30	149	Yes/84 300@-25	115	No/55 630@-25
180	5W-20	90	No/19 800@-30	41	No/13 180@-30
190	5W-30	68	No/19 400@-30	50	No/25 320@-30
211	10W-30	253	Yes/180 700@-25	143	No/34 670@-25
220	5W-30	86	No/26 700@-30	111	No/49 240@-30
230	5W-30	88	No/26 400@-30	65	No/22 750@-30
240	5W-30	80	No/48 500@-30	97	No/52 240@-30
250	10W-30	51	Yes/64 200@-25	95	Yes/36 160@-25
260	5W-30	120	Yes/178 600@-30	70	No/42 210@-30
270	5W-30	94	No/38 700@-30	88	No/47 110@-30
280	5W-30	94	Yes/75 600@-30	76	Yes/92 900@-30
290	5W-30	87	No/28 800@-30	82	No/30 000@-30
291	10W-30	129	No/33 700@-25	78	No/24 670@-25
292	10W-30	102	No/26 500@-25	119	No/33 370@-25
500	10W-30	142	No/24 200@-25	112	No/29 740@-25
501	10W-30	112	No/28 094@-25	108	No/38 040@-25
502	10W-30	102	No/25 500@-25	95	No/30 530@-25
503	10W-30	187	No/35 200@-25	211	No/69 440@-25
504	5W-20	62	No/12 800@-30	50	No/13 850@-30
505	5W-50	24	No/29 500@-30	0	No/44 440@-30
506	0W-20	83	No/20 200@-35	104	No/23 370@-35
507	0W-30	111	No/79 200@-35	74	No/51 920@-35
508	10W-30	148	No/46 800@-25	152	No/50 590@-25
509	5W-30	117	No/59 300@-30	151	No/83 680@-30
510	5W-30	384	Yes/TVTM	1078	Yes/TVTM
511	5W-30	94	No/38 700@-30	75	No/45 380@-30

References

[1] ASTM Standard D 4485, "Standard Specification for Performance of Engine Oils," *Annual Book of ASTM Standards*, ASTM International, West Conshohocken, PA, 2006.

[2] International Lubricant Standardization and Approval Committee, "ILSAC GF-4 Standard for Passenger Car Engine Oils," January 14, 2004.

[3] American Petroleum Institute, Washington, API Publication 1509, "Engine Oil Licensing and Certification System," Service [S] Category.

[4] American Petroleum Institute, Washington, API Publication 1509, "Engine Oil Licensing and Certification System," Commercial [C] Category.

[5] Association des Constructeurs Europèen d'Automobiles, Brussels, BE–ACEA European Oil Sequences, 2004.

[6] Clark, S. L., Olree, R. M., Lang, P., Leverett, C., and Bowden, D. H., "Development of the Sequence IIIG Engine Oil Certification Test," SAE Paper 2004-01-2987.

[7] Intertek web site Sequence IIIG test, http://fluidsciences.perkinelmer.com/catalog/Product.aspx?ProductID=cp-iiig

[8] ASTM Standard D 445, "Standard Test Method for Kinematic Viscosity of Transparent and Opaque Liquids," *Annual Book of ASTM Standards*, ASTM International, West Conshohocken, PA, 2006.

[9] Bartko, M., Florkowski, D., Ebeling, V., Geilbach, R., and Williams, L., "Lubricant Requirements of an Advanced Designed High Performance, Fuel Efficient Low Emissions V-6 Engine," SAE Paper *2001-01-1899*.

[10] ASTM Standard D 4684, "Standard Test Method for Determination of Yield Stress and Apparent Viscosity of Engine Oils at Low Temperature," *Annual Book of ASTM Standards*, ASTM International, West Conshohocken, PA, 2006.

[11] SAE J300, May 2004, "Engine Oil Viscosity Classification System," *SAE Handbook*, Vol. 1, 2006.

[12] ASTM Standard D 5293, "Test Method for Apparent Viscosity of Engine Oils Between −5 and −35°C Using the Cold Cranking Simulator," *Annual Book of ASTM Standards*, ASTM International, West Conshohocken, PA, 2006.

[13] McMillian, M. L. and Stambaugh, R. L., "The Development of a Viscosity Classification System Based on Engine Performance—A Review of SAE and Related ASTM Activities," *Paper EL/4/3 presented at CEC International Symposium*, June 3–5, 1981.

[14] ASTM Data Series Publication 57, "Low-Temperature Pumpability Characteristics of Engine Oils in Full-Scale Engines," ASTM International, West Conshohocken, PA, Sept. 1975.

[15] Shaub, H., Smith, M. F., and Murphy, C. K., "Predicting Low Temperature Engine Oil Pumpability with the Mini-Rotary Viscometer," SAE Paper *790732*.

[16] ASTM Standard D 3829, "Standard Test Method for Predicting the Borderline Pumping Temperature of Engine Oil," *Annual Book of ASTM Standards*, ASTM International, West Conshohocken, PA, 2006.

[17] Stambaugh, R. L., "Engine Oil Viscosity Classification Task Force Low Temperature Report," SAE Subcommittee 2 Meeting Minutes Attachment, June 9, 1981.

[18] Stambaugh, R. L. and O'Mara, J. H., "Low Temperature Flow Properties of Engine Oils," SAE Paper *820509*.

[19] Shaub, H., Ed., "Oil Flow Studies at Low Temperatures in Modern Engines," *ASTM STP 1388*, 2000.

[20] ASTM Standard D 2272, "Standard Test Method for Oxidation Stability of Steam Turbine Oils by Rotary Pressure Vessel," *Annual Book of ASTM Standards*, ASTM International, West Conshohocken, PA, 2006.

[21] Ford Laboratory (FLTM) BJ 110-04, "Aluminum Beaker Oxidation Test."

[22] Roby, S. H., Mayer, R. J., Ruelas, S. G., Martinez, J., and Rutherford, J. A., "Development of a Bench Test to Predict Oxidative Viscometric Thickening in the Sequence IIIG Engine Test," SAE Paper *2004-01-2985*.

[23] Mazzamaro, G. A., "Using Laboratory Tests to Predict Oxidation in Today's Engine Lubricating Oil," *Lubricating Oil*, Vol. 19, No. 6, 2004, pp. 6–11.

[24] ASTM Standard D 6557, "Standard Test for Evaluation of Rust Preventative Characteristics of Automotive Engine Oils," *Annual Book of ASTM Standards*, ASTM International, West Conshohocken, PA, 2006.

[25] Kim, C., Kuo, C. C., and Marchand, D. M., "Development of the Ball Rust Test—A Laboratory Test to Replace the Sequence IID Engine Test," SAE Paper *97-2861*.

[26] ASTM Test Monitoring Center website, http://www.astmtmc.cmu.edu/

 Journal of ASTM International, Vol. 4, No. 10
Paper ID JAI100926
Available online at www.astm.org

Jin Yuansheng,[1] *Yang He*,[2] *and Li Shenghua*[3]

Mechanochemical Additive-Assisted Reconditioning Effects and Mechanism on Worn Ferrous Surfaces

ABSTRACT: An additive package of reconditioning functionality for worn ferrous surfaces has been designed in light of the mechanochemical reaction principle. The package is formulated from a fine-powdery multicomponent mixture of Serpentine minerals, surfactants, and catalysts. The main reconditioning component in the package is magnesium silicate hydroxide ($Mg_6(Si_4O_{10})(OH)_8$), with the surfactants for dispersing the main component into bulk lubricant and the catalysts for facilitating interfacial mechanochemical reactions, particularly oil pyrolysis and carbonization. With commercial fully-formulated engine oils as benchmark, the reconditioning effects of the reconditioner package have been demonstrated in both laboratory tribotestings and in real-world heavy-duty (locomotive diesel engine) scenarios. Surface examination of sampled worn surfaces on both laboratory test specimens and cylinder bore of locomotive diesel engine has shown that a nano-crystalline layer has been generated which possesses nanometric roughness, higher surface hardness, and proper H/E ratio. Advanced analyses have indicated that the layer is composed of Fe_3O_4 and FeOOH nanoparticles which are dispersed on the Fe-C matrix. The smoother surface mitigates asperity interlocking which would otherwise induce high friction; the high surface hardness and appropriate H/E ratio result in less elastic deformation within nanocrystalline contact regions, which effectively lessens friction and wear arisen from plastic plowing and adhesion. Further characterization of sampled worn cylinder bore surface and analysis of used oils have suggested that generation of the nanocrystalline layer in presence of $Mg_6(Si_4O_{10})(OH)_8$ involves three interwoven processes: oxidative mechanical polishing, lubricant carbonization and graphitization, and mechanical alloying.

KEYWORDS: lubricant additives, nanocrystalline layer, surface modification, catalysis, mechanical alloying, mechanochemical reaction

Introduction

Emission, efficiency, and performance are fundamental considerations in designing advanced combustion engines and mechanical systems. Reduced engine-out/tailpipe emissions, increased fuel economy, and extended machinery lifetime are driven, respectively, by stringent environmental regulations, decreased dependence on petroleum resources, and improved reliability. Advanced combustion and lubrication mechanisms, together with compatible fuels, lubricants, and additives chemistry, are among the well recognized technology enablers to achieve these missions.

Academia and industry have devoted concentrated efforts to develop triboadditives chemistry to enable advanced lubrication mechanisms. Traditional triboadditives, which include oiliness agents, antiwear additives, extreme pressure additives, and friction modifiers, are integral components of fully-formulated lubricating oils for reduced friction coefficient, lowered wear rate, and increased load-carrying capacity. One inadequacy of the traditional triboadditive family members is that they are performing their designed functions when only mild wear exists or there is no real surface damage [1]. When tribosystems come into the surface-damage but still reconditionable wear region, the current triboadditives fail to function except that certain extreme pressure additives can manage to delay the incurring of surface damage wear [1]. To repair the surface damage wear so that the geometrical morphology or mechanical performances of tribopairs can be effectively and efficiently restored, wear reconditioning additives are needed. Traditional

Manuscript received December 11, 2006; accepted for publication August 28, 2007; published online November 2007. Presented at ASTM Symposium on Automotive Lubricant Testing and Additive Development on 3–5 December 2006 in Lake Buena Vista, FL; Simon Tung, Bernard Kinker, and Mathias Woydt, Guest Editors.

[1] State Key Laboratory of Tribology, Tsinghua University, Beijing 100084, China, e-mail: jinys@tsinghua.edu.cn.

[2] Research Institute of Petroleum Processing, China Petroleum & Chemical Corporation (SINOPEC), Beijing 100083, China, e-mail: yanghe@ripp-sinopec.com.

[3] Maxtor Corporation, 2001 Fortune Drive, San Jose, CA 95131, e-mail: Shenghua_Li@maxtor.com.

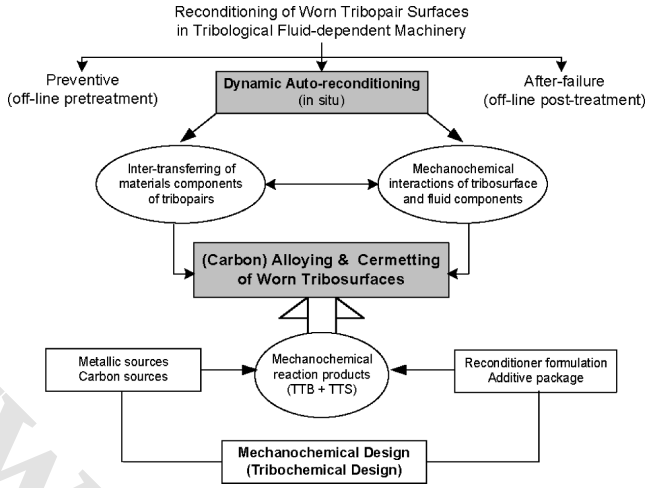

FIG. 1—*In situ mechanochemical reconditioning principle and design strategy of wear reconditioner package.*

triboadditives prevent or delay surface damage wear and wear reconditioners repair or rehabilitate damaged surfaces.

Wear-related surface damage and degraded or contaminated lubricants are among the most threatening factors for premature catastrophic failures in tribosystems. Many practical maintenance technologies, breakdown, preventive, predictive, and proactive maintenance, are available depending on fault/failure modes [2]. These technologies can be performed based on machinery fluids diagnostics and are meant to *detect* but not to *repair* wear damage that has already occurred. Russian scientists and technologists are among the pioneers in patenting the earliest known worn surface rehabilitation technologies [3–5]. We developed a dynamic auto-reconditioning mechanochemical technique which can be initiated by the tribosystem itself in a real-time manner and *in situ* in presence of a proprietary reconditioner package, as shown in Fig. 1 [6].

Mechanochemical reconditioning takes advantage of the more energetic, reactive damaged surface and nascent surface/debris contributed from the damaging process, such as fine wear particles, degraded lubricant species, and the reconditioner chemistry in particular. The mechanochemical reactions in the damaged regions yield tribochemical third bodies (TTB). In tribosystems TTB will be processed *in situ* into tribologically transformed structures (TTS) of self-adaptation, self-compensation, and self-rehabilitation nature [6,7].

This paper presents a simple description of the mechanochemical reconditioner package developed from the mechanochemical reconditioning principle. Emphasis will be given to the demonstration of the reconditioning effects of the reconditioner package when blended into commercial fully-formulated engine oils and applied in laboratory and field scenarios. A three-stage action mechanism of the mechanochemical reconditioner is suggested based on structural and compositional analyses from reconditioned tribosurfaces and in-service lubricating oils.

Mechanochemical Reconditioner Chemistry

Magnesium silicate hydroxide of empirical formula $Mg_6(Si_4O_{10})(OH)_8$ is the main component of the mechanochemical reconditioner package, and it is mechanochemically synthesized from Serpentine phyllosilicates and finely ground into micron-sized powder. Bulk Serpentine phyllosilicates assume sheet-stacked configurations, as shown in Fig. 2. The basic structure of Serpentine phyllosilicates is based on interconnected six-member rings of complex ion $(SiO_4)^{4-}$ tetrahedron that extends outward in infinite sheets (Fig. 3). Three apical oxygen atoms from each tetrahedron are shared with other tetrahedron. This

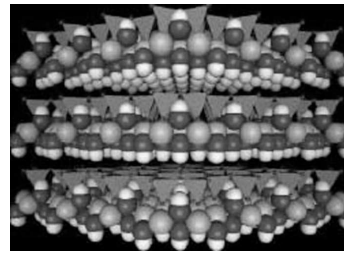

FIG. 2—*Structural model of Serpentine (Lizardite).*

leads to a basic structural unit of $(Si_2O_5)^{2-}$. Most phyllosilicates contain hydroxyl ion (OH^-) located at center of the six-member ring. Thus, the group becomes $Si_2O_5(OH)^{3-}$. When Mg^{2+} cations in octahedron are bonded to the SiO_4 sheets, they share the apical oxygen atoms and the OH ions through weak electrovalent bonding.

While being mechanically acted, Serpentine phyllosilicates display basal cleavage releasing associative oxygen and free water. Such inherent structure and property impart Serpentine phyllosilicates potential lubricity performance in thermally or mechanically affected tribosystems.

The mechanochemical reconditioner package is a fine-milled multicomponent mixture. Morphological feature and size distribution of the powdery reconditioner is ferrographically analyzed and displayed in Fig. 4. The reconditioner package contains serpentine minerals as the main components as well as catalysts and metallurgical activation agents which facilitate the mechanochemical reactions, especially oil pyrolysis and carbonization.

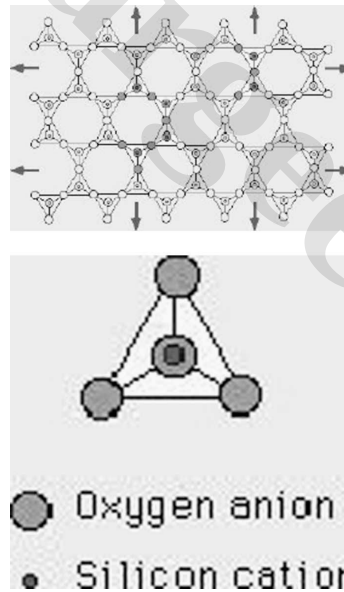

FIG. 3—*Configuration of SiO_4 tetrahedral rings. (Sources of Figs. 2 and 3: Goldberg and Romanosky, National Energy Technology Laboratory, Pittsburgh, PA; Chen, Science Applications International Corporation, McLean, VA; Nelson, Tulane University, Louisiana.)*

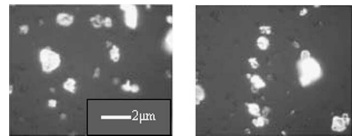

FIG. 4—*Powdery reconditioner on ferrogram.*

Experimentation

Laboratory Tribotesting

Laboratory tribostesting for demonstrating reconditioning effect of the reconditioner package was conducted on a Falex-1506 Tribotester. Figure 5 presents the tribopair installation and dimensions of the lower and upper specimen. The contact area between the upper and lower cast iron specimen is 506 mm^2. Critical experimental conditions were loads of 1∼5 LB, lever ratio of 10+1, and revolution of 500 ∼3000 r/min. The corresponding applied forces and average contact pressures were 44.45∼222.26 N and 0.088∼0.439 N/mm^2, respectively. The corresponding average linear speeds were 1.23∼7.35 m/s. The lubricant was a blend of API SD/CC SAE40 engine oil formulated with the reconditioner at a concentration of 1.6 g/L.

The Falex tribotesting matrix was designed to validate the formation of reconditioned layers on cast iron tribosurfaces in sliding contact as compared to the reconditioned layers generated in locomotive field trials (see below). The Falex tribotesting was performed through a load-speed cycle in three periods with each period lasting for 24 hours, as shown in Table 1.

After completion of the Falex tribotesting, the tribopairs were disassembled and sectioned for surface analyses of reconditioning effects.

Laboratory tribostesting for demonstrating the friction reducing effect of the reconditioned layers was conducted on an SRV Tribometer. The reconditioned piston ring-cylinder bore pair was sectioned from real piston rings and cylinder bores after the locomotive field trialing, and they are sectioned to fit for the geometrical requirements of the tribopairs on the SRV tribotester. Operation parameters of SRV friction testing include: loading: 20, 30, 40, 50 and 60 N; stroke: 0.3∼0.6 mm; frequency: 50 Hz; maximum mean pressure: 1.43 N/mm^2; maximum sliding speed: 0.1 m/s. All SRV testing was conducted in oil free conditions so as to demonstrate the inherent lubricious effect offered by the reconditioned layers. The coefficients of friction are continuously recorded under all changed operation parameters on the SRV Tester. Figure 6 displays the configuration, installation, and contact geometry of the tribopair. As compared with the reconditioned layers, the coefficient of friction with untreated piston ring-cylinder bore pair is also measured and recorded under the same test conditions.

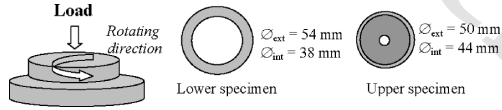

FIG. 5—*Upper and lower specimens for Falex tribotest.*

TABLE 1—*Norm of Falex tribotesting.*

	500 r/min	1000 r/min	1500 r/min	2000 r/min	2500 r/min	3000 r/min
1 LB	10 min	10 min	10 min	10 min	10 min	10 min
2 LB	10 min	10 min	10 min	10 min	10 min	10 min
3 LB	10 min	10 min	10 min	10 min	10 min	10 min
4 LB	10 min	10 min	10 min	10 min	10 min	10 min
5 LB	10 min	10 min	10 min	10 min	10 min	50 min
5 LB	10 min	10 min	10 min	10 min	10 min	500 min
5 LB	10 min	10 min	10 min	10 min	10 min	500 min

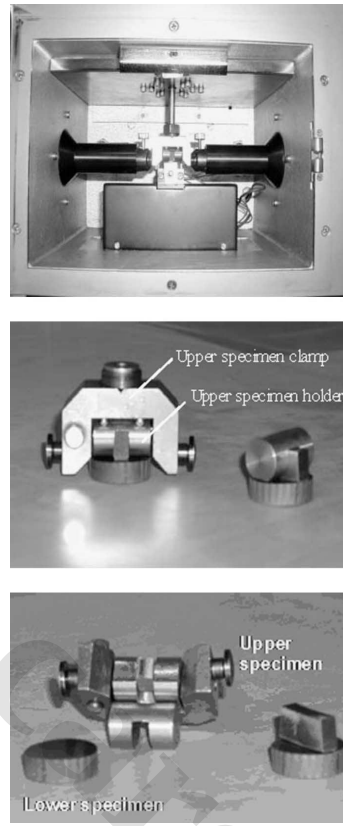

FIG. 6—*Tribopair configuration, installation, and contact geometry in SRV tribotest.*

Locomotive Field Trials

Locomotive field trials were conducted in Beijing Diesel Locomotive Depot on two DF11 series diesel locomotives, DF11-0063 and DF11-0163, and the locomotives were operated by model 16V280 diesel engines of 3600 kw power [6]. The reconditioner package was blended into the crankcase oil at concentration of 0.04 g/L when the engines had just gone through overhauling. After an extended operation of 150 000 km, the engines were disassembled for inspecting visual appearance of main engine components and validating the reconditioned layers formed on cylinder bore by surface examination. Details of locomotive field trials were reported in Ref [6].

Surface Analyses

Detailed analyses of reconditioned layers generated both in laboratory and in trial conditions were designed and conducted to understand the reconditioning effects of the reconditioning layers in terms of surface features (SEM), mechanical properties (Profilometer and Nano-hardness indentor), chemical compositions (EDS, ESCA) and phase structures (TEM, HRTEM) [6–8]. Details of surface characterization of reconditioned layers can be found in Refs [6–8].

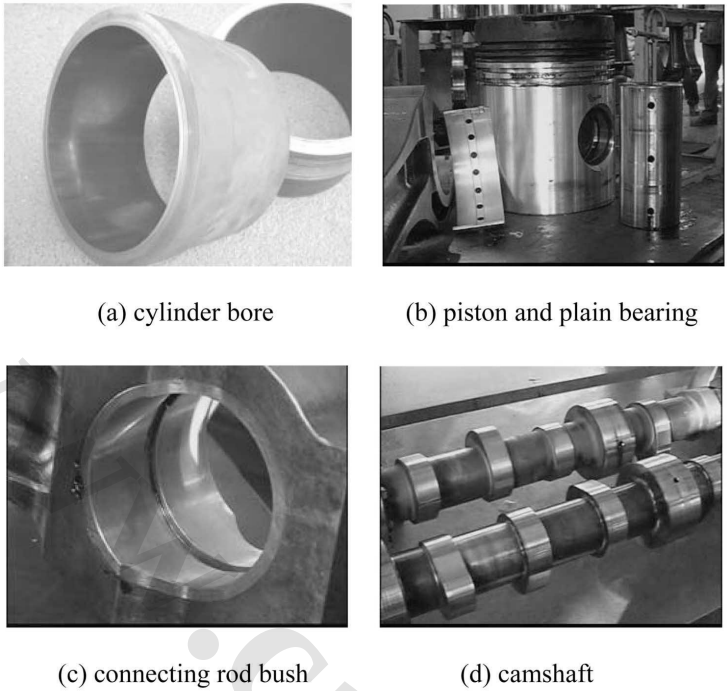

FIG. 7—*Component parts in powertrain systems of locomotive diesel engine.*

Results

Morphological Restoration

In Fig. 7 the real component parts of 16V280 diesel engine in DF11-0063 locomotive after an extended operation of 150 000 km are displayed. Measurements on the dimensions and clearances indicated that there was no wear on both piston rings and cylinder bores, and original dimensions of other tribological parts were maintained [6].

Figure 8 displays the SEM observation of the cross sections of the real cylinder bore from the locomotive diesel engines (a) and the cast iron specimen from the laboratory Falex tribotesting (b). For comparison, the cross section image of cast iron sample cut off from cylinder bore of a 16V280 diesel engine in which the additive was not blended in the crankcase oil after locomotive running for 150 000 km was also presented as shown in Fig. 8(*c*), under the title of nontested cast iron sample. It is clearly seen that reconditioning layers with a certain thickness were generated which adhered seamlessly onto the cast iron substrates in both the Falex test and the field test.

The capability of the reconditioned layer in restoring the morphological features of the tribosurfaces was validated by the roughness measurement of the reconditioned cylinder bore from the locomotive field trials, as shown in Fig. 9. The surface roughness $Ra = 69.40$ nm, suggesting an ultra-smooth reconditioned surface which is processed with ultra super-grinding, super-polishing, and mirror surface milling.

Performance Restoration

The coefficient of friction of the reconditioned piston ring-cylinder bore pair is maintained at 0.005 under all operation parameters on the SRV friction tester. Comparatively, the coefficient of friction with untreated piston ring-cylinder bore pair is always over 0.1.

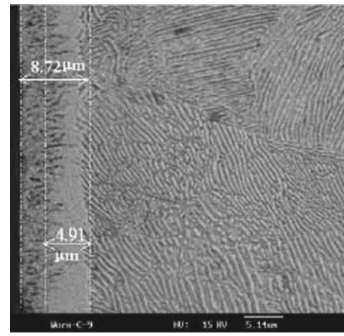

(a) cast iron cylinder bore

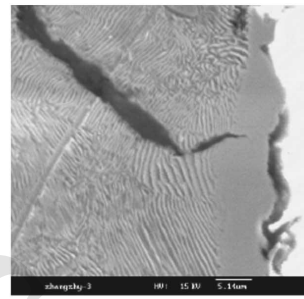

(b) cast iron specimen in Falex

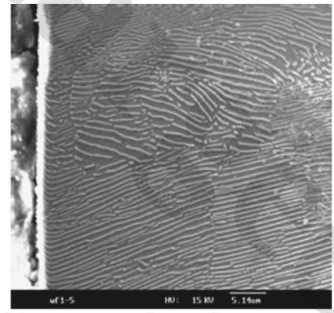

(c) non-tested cast iron sample

FIG. 8—*SEM image of cross section of reconditioned layers on cast iron.*

The nano-hardness of the reconditioned layer and cast iron substrate on the cylinder bore from the locomotive field trials was measured with a CSEM Nano-hardness indentor, as indicated with the 3-D images in Fig. 10. The average hardness from six measurement positions on the reconditioned layer is 1119 Hv_{20mN}, nearly twice as hard as the cast iron substrate (524 Hv_{20mN}).

Table 2 is a summary of the critical mechanical properties of the reconditioned layers on the cast iron substrate that are averaged from reconditioned layers generated in laboratory Falex tribotesting and locomotive field trials.

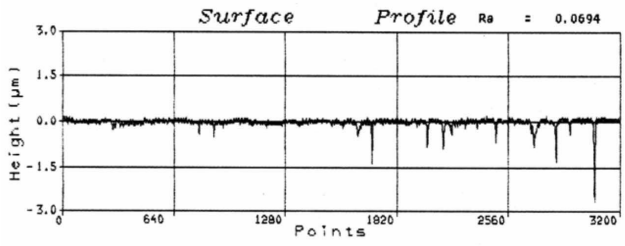

FIG. 9—*Surface roughness of reconditioned cast iron cylinder bore.*

Chemical Compositions

SEM/EDS analyses of reconditioned layers on cylinder bores from the locomotive field trials, as shown in Fig. 11, indicate that Fe, C, and O are the main elements. Atoms Mg and Si from serpentine reconditioner were hardly detected.

ESCA analyses in Table 3 present the chemical status of the three main atoms, Fe, C, and O throughout the reconditioned layers on cylinder bore of locomotive diesel engines. When bonding with C and VO, Fe assumes higher valencies in the outer layer but it assumes lower oxidation states in the inner layer. In terms of chemical compounds, the reconditioned layer is made from the complicated mixtures of iron oxides and iron carbides.

Phase Structures

A JEM-2000FX Model TEM and a JEOL JEM-2010F Model HRTEM were applied to identify the phase structures of the reconditioned layers. Images in Figs. 12 and 13 suggest the coexistence of magnetite (Fe_3O_4) and iron oxyhydroxide (FeOOH) in the reconditioned layer and dispersion of the iron oxide nanoparticles on the Fe-C compound (Fe_3C) nanocrystal matrix. Figures 14 and 15 display finer phase structure features of the dispersed iron oxides nanoparticles and the iron carbide matrix.

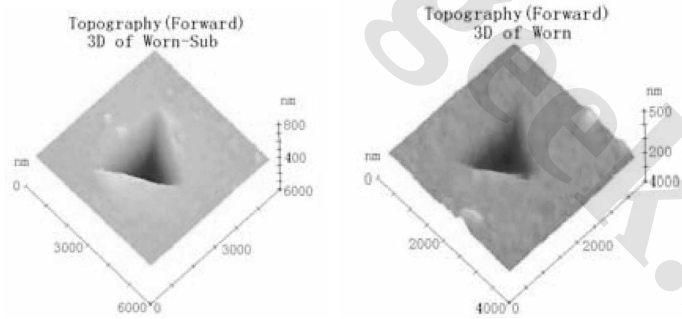

FIG. 10—*Three-dimensional images of cast iron substrate (left) and reconditioned layer (right).*

TABLE 2—*Average mechanical properties of reconditioned layers.*

	Reconditioned Layer on Cast Iron Specimen in Laboratory Falex Tribotesting	Reconditioned Layer on Cast Iron Cylinder Bore in Locomotive Field Trials
Hv_{20mN}, min.	13.32 GPa	12.73 GPa
E, max.	240 GPa	210 GPa
H/E	0.0555	0.0606

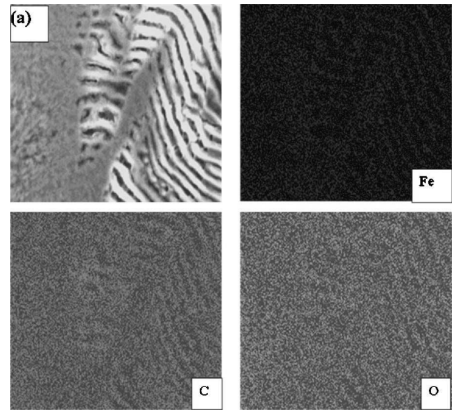

FIG. 11—*Elemental composition and distribution on reconditioned layers on cast iron cylinder bore of locomotive diesel engines.*

Discussion

Suggested Origins of Ultra-low Friction of Reconditioned Layer [7,8]

As mentioned above, the reconditioned layers could be considered as special nanocrystalline coatings with grain sizes in nanometer range (less than 100 nm) and with smoother surface (*Ra* at nanometer scale). The smoother surface of the reconditioned layer was responsible for the reduction of the coefficients of friction, as some factors that cause high friction, such as asperity interlocking and plowing, were eliminated.

TABLE 3—*Compound compositions throughout the reconditioned layer on cast iron cylinder bore of locomotive diesel engines.*

Sputtering Time (min)	$Fe2p_{3/2}$(eV)	O1s (eV)	C1s (eV)
2	FeOOH	FeOOH	Organic Species
	Fe_2O_3	Fe_2O_3	
12	Fe_2O_3	Fe_2O_3	Graphite
	Fe_3O_4	Fe_3O_4	Organic Species
22	Fe_3O_4; FeO	Fe_3O_4; FeO	Graphite
32	FeO; Fe_3C	FeO	Graphite; Fe_3C
42	FeO	FeO	Graphite
	Fe_3C, Fe		Fe_3C
Substrate	Fe_3C; Fe		Graphite (less) Fe_3C

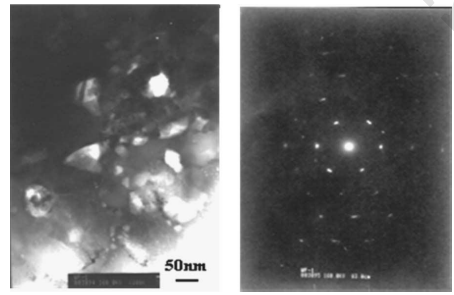

FIG. 12—*TEM photograph and SAD pattern of reconditioned layer on cast iron cylinder bore of locomotive diesel engines.*

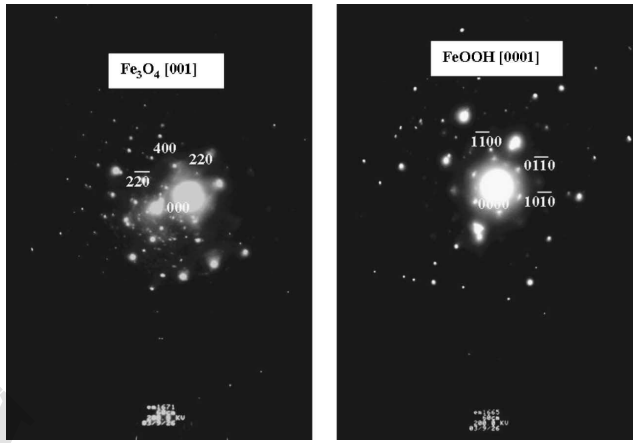

FIG. 13—*SAD pattern of iron oxides nanoparticles in reconditioned layer on cast iron cylinder bore of locomotive diesel engines.*

The combined effects of hardness (H) and elasticity (E), the H/E ratio, of coating materials can help understand the frictional behavior of the reconditioned layers. The significance of H/E ratio in optimizing tribological performances of nanocrystalline coating has been well recognized [9,10]. From our measurement of the mechanical properties, the reconditioned layers assume high "ceramic" hardness (H = 13.32 GPa or more) but retain the elastic properties of metals (E = 240 GPa or lower), and their H/E ratios are similar to the values of typical nanocrystalline ceramic coating materials. High surface hardness and reasonable H/E value of the reconditioned layers result in very small elastic deformation within the nanocrystalline contact region, and plastic plowing and adhesion are effectively reduced.

It has been reported that formation of both oxides and hydroxide by tribochemical reactions can lead to extreme low friction [11–14]. The dramatic reduction of the coefficient of friction by hydroxides is owing to formation of weak hydrogen bonds in hydrates. In the present case, it is assumed that Fe_3O_4 nanoparticles dispersed on the Fe-C matrix act as lubricious oxides, and FeOOH nanoparticles supply the weak hydrogen bonds as hydrates between layers and on the counter surface. This is probably another route by which the reconditioned layers have demonstrated ultra-low friction.

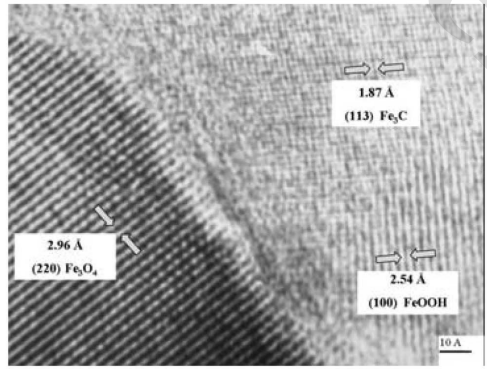

FIG. 14—*HRTEM images of the nanocrystal reconditioned layer on cast iron cylinder bore of locomotive diesel engines.*

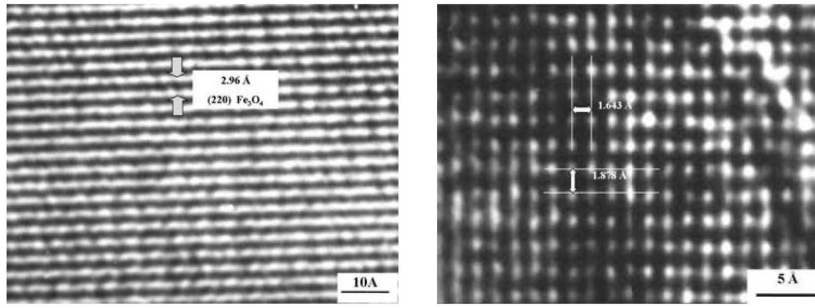

(a) (b)

FIG. 15—*HRTEM image of plane spacing in the reconditioning layer on cast iron cylinder bore of locomotive diesel engines. (a) plane spacing of Fe_3O_4 nanoparticles (b) plane spacing in Fe_3C matrix.*

Suggested Routes of Reconditioned Layer Generation [15]

Oxidative Mechanical Polishing—It has been claimed that oxy-acids can release active oxygen atoms and thus bring about a polishing effect on metal surfaces [16]. Under high shear stress and flush temperature at friction contact points the main component of Serpentine auto-reconditioner, undergoes the cleavage fracture detaching to SiO_2 and Mg^{2+}, and release O^{-2} and activated free water by hydroxyl drop-off. Then, FexOy and Fex(OH)y are produced by an oxidative effect of O^{-2} and the free water on surface asperities and wear debris. The mechanical polishing results from SiO_2 and FexOy particles, and oxidative polishing results from surface asperities oxidation. The entire process could be summarized as follows:

$$Mg_6Si_4O_{10}(OH)_8 \rightarrow 6Mg^{2+} + 4SiO_2 + 4H_2O + 6O^{2-}$$

$$Fe^0, Fe^{n+}(EEE) + O^{2-} \rightarrow Fe_xO_y$$

$$Fe^0, Fe^{n+}(EEE) + H_2O + O_2 \rightarrow Fe_x(OH)_y$$

Fe^0 (Novel-fresh iron surface); Fe^{n+} (EEE) (Exo-Electron Emission iron surface)

Lubricant Carbonization and Graphitization—Carbonization and graphitization of the powdery reconditioner formulated lubricant has occurred to a much higher extent than in the absence of the reconditioner. The increased carbonization in the presence of the reconditioner is contributed by the active constitutes in the reconditioner package, catalytic ferrous surface, and the active elements from the traditional additive package in the lubricant. Figure 16 displays a fine layer on the cast iron plate surface after the crankcase simulation experiment. The layer is corroborated by SEM/EDX analysis to be composed of nano-sized carbon particles, ca. 10–20 nm. XRD analysis indicates that they are microlite and amorphous carbon. Nano-sized carbon particles were also detected in the crankcase oil of a locomotive diesel engine after 25 000 km of real-world operation, as exhibited in Fig. 17. Figure 17(*b*) displays nano-sized carbon particles detected in the crankcase oil of locomotive diesel engine after 25 000 km of real-world operation. As a comparison, almost no carbon nanoparticles were detected at 0 km operation as shown in Fig. 17(*a*). The yielded carbon nanoparticles are active and could reduce iron oxides to atom Fe. The iron atoms further react with carbon nanoparticles generating Fe_3C and graphite, as illustrated below.

$$Fe_2O_3 + C \rightarrow Fe + CO.CO_2$$

$$Fe + C \rightarrow Fe_3C$$

$$Fe_3C \rightarrow Fe\uparrow + C \text{ (easy to graphitization)} \rightarrow \text{graphite}$$

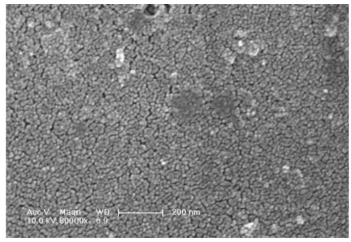

(*a*)

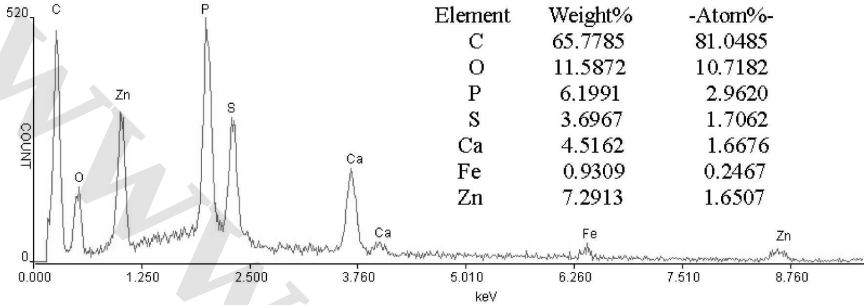

Element	Weight%	-Atom%-
C	65.7785	81.0485
O	11.5872	10.7182
P	6.1991	2.9620
S	3.6967	1.7062
Ca	4.5162	1.6676
Fe	0.9309	0.2467
Zn	7.2913	1.6507

(*b*)

FIG. 16—*SEM image of cast iron plate surface after crankcase simulation experiment. (a) Fine carbon layer SEM image on cast iron plate surface (b) EDS analysis results of cast iron plate surface.*

Mechanical Alloying

Interactions of oxidative mechanical polishing and carbonization of lubricating oil result in mechanochemical reactions which involve fresh surfaces with high activity and numerous nanoparticles of iron oxides, iron carbides, and a large quantity of carbonaceous species. These nanoparticles are agglomerated on freshly exposed worn surfaces. The nanoparticle clusters accumulated in the surface valleys are repeatedly subjected to extreme shearing and extrusion stresses resulting in mechanical alloying.

CONCLUSIONS

1. An additive package of Serpentine auto-reconditioner with reconditioning functionality for worn ferrous surfaces has been developed. The main component of the auto-reconditioner is magnesium silicate hydroxide, $Mg_6Si_4O_{10}(OH)_8$.
2. The additive package of Serpentine auto-reconditioner reveals reconditioning effects in both laboratory tribotesting (Falex) and in real-world heavy-duty (locomotive diesel engine) scenarios.

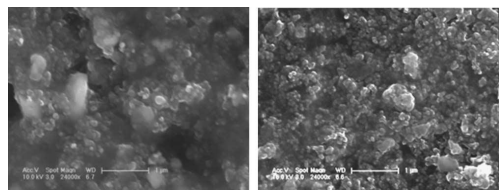

FIG. 17—*Field emission SEM photos of carbonaceous matters from crankcase oil. (a) 0 km (b) 25 000 km.*

3. The reconditioned layer is composed of three elements of Fe, C, and O, and assumes nanocrystalline phase structure of improved mechanical and tribological behaviors.

References

[1] Fein, R. S., "A Perspective on Boundary Lubrication," *Ind. Eng. Chem. Fundam.*, Vol. 25, 1986, pp. 518–524.

[2] Zeng, S. W., "Discussion on Maintenance Strategy, Policy and Corresponding Maintenance Systems in Manufacturing," *Eur. J. Oper. Res.*, Vol. 138, No. 3, 2002, pp. 554–568.

[3] Агафонов, А. К., Арацкий, П. Б., Бахматов, С. И., Гамидов, Е. А., Никитин, И. В. and Слободяню, А. А., Способорного безрборного восстановления трущихся соединений. Па*м*енм *N*o *97107224* (*Russian Patent No. 97107224*), 1997.

[4] Ермаков, В. И., Нежданов, В. И., and Никитин, И. В., Способ обрзования заещитного покрытия, избирательно компенсирующего износ поверхностей трения и контакта деталей машин. Па*м*енм *N*o *2155638* (*Russian Patent No. 2155638*), 1998.

[5] Балабин, В. Н., Ермаков, В. И., Какоткин, В. З., and Нежданов, В. И., Способ модификации железосоржащих поверхностей узлов трения. Па*м*енм *N*o *2001117721* (*Russian Patent No. 2001117721*), 2001.

[6] Jin, Y. S., Li, S. H., Zhang, Z. Y., Yang, H., and Wang, F., "In situ Mechanochemical Reconditioning of Worn Ferrous Surfaces," *Tribol. Int.*, Vol. 37, 2004, pp. 562–567.

[7] Jin, Y. S., Yang, H., Wang, F., Minfray, C., and Li, S. H., "Phase Structure and Lubricity of In-situ Generated Protective Layer on Worn Metal Surfaces in Presence of $Mg_6Si_4O_{10}(OH)_8$," *Proceedings of WTC2005, Word Tribology Congress III*, WTC2005-63927, 2005.

[8] Jin, Y. and Li, S., "Superlubricity of in situ Generated Protective Layer on Worn Metal Surfaces in Presence of $Mg_6Si_4O_{10}(OH)_8$," *Superlubricity Book* Chapt. 24, Ali Erdemir and Jean-Michel, Martin, Eds., 2007.

[9] Leyland, A. and Matthews, A., "On the Significance of the H/E Ratio in Wear Control: A Nanocomposite Coating Approach to Optimized Tribological Behavior," *Wear*, Vol. 246, 2000, pp. 1–11.

[10] Holmberg, K. and Matthews, A., "Tribology of Engineered Surfaces," Submitted to MEP book, Gwidon Stachowiak, Ed., *Wear—Materials, Mechanisms and Practice*, 2004.

[11] Erdemir, A., "A Crystal-chemical Approach to Lubrication by Solid Oxides," *Tribology Letters*, Vol. 8, 2000, pp. 97–102.

[12] Erdemir, A., "A Crystal Chemical Approach to the Formulation of Self-Lubricating Nanocomposite Coatings," *Surface & Coatings Technology*, Vol. 200, 2005, pp. 1792–1796.

[13] Itoa, K., Martin, J., Minfray, C., and Kato, K., "Low-friction Tribofilm Formed by the Reaction of ZDDP on Iron Oxide," *Tribol. Int.*, Vol. 39, 2006, pp. 1538–1544.

[14] Scott, F. H. and Wood, G. C., "The Influence of Oxides on the Friction and Wear of Alloys," *Tribol. Int.*, Vol. 11, 1978, pp. 211–218.

[15] Jin, Y. and Yang, H., "The Generation Mechanism of Nanocrystalline Protective Layer on Worn Ferrous Metal Surface in Presence of $Mg_6Si_4O_{10}(OH)_8$," *Proceedings of ASIATRIB 2006 Kanazawa, Japan*, 2006, pp. 837–838.

[16] Fox, P. G., "Review Mechanically Initiated Chemical Reactions in Solids," *J. Mater. Sci.*, Vol. 10, 1975, pp. 340–360.

Journal of ASTM International, Vol. 4, No. 7
Paper ID JAI100937
Available online at www.astm.org

T. Haque,[1] *A. Morina,*[1] *A. Neville,*[1] *R. Kapadia,*[2] *and S. Arrowsmith*[2]

Study of the ZDDP Antiwear Tribofilm Formed on the DLC Coating Using AFM and XPS Techniques

ABSTRACT: To meet the challenge of the increasing demand of fuel economy, in recent years low friction nonferrous coatings such as diamond-like carbon (DLC) coatings have become very popular for automotive tribo-components. The interaction of lubricant additives, which are designed for ferrous surfaces, with nonferrous coatings is an important issue for the automotive and lubricant industries. The aim of this paper is to establish a link between the evolution of antiwear zinc dialkyl dithiophosphate (ZDDP) tribofilm and the tribological performance of a DLC coating under boundary lubrication conditions. Experiments were performed in a pin-on-plate reciprocating tribotester to produce the tribofilm. Atomic force microscopy (AFM) was used to record high resolution topographical images of the ZDDP films while chemical analysis of the ZDDP tribofilms was performed using X-ray photoelectron spectroscopy (XPS). Results in this study show that the ZDDP tribofilm consists of short chain zinc pyrophosphate ($Zn_2P_2O_7$) and zinc metaphosphate ($ZnOP_2O_5$), and it is formed along the raised portion of the initial marks of the DLC surface.

KEYWORDS: DLC coating, boundary lubrication, zinc dialkyl dithiophosphate, atomic force microscopy, X-ray photoelectron spectroscopy

Introduction

Zinc dialkyl dithiophosphate (ZDDP) additive has been used in engine oil for over 50 years, chosen particularly for its excellent antiwear and antioxidant properties. It is known that this additive provides tenacious antiwear film on sliding surfaces under boundary lubrication conditions. Extensive research has been carried out into the mechanism of formation, chemical composition, and structure of the ZDDP-derived tribofilm. Most of the related works published so far were done on ferrous materials since most engine components used so far have been made of cast iron/steel.

In the published studies, the structural analysis of ZDDP tribofilm formed on the ferrous surface are mostly done by the AFM technique. Pidduk et al. [1] showed long smooth features aligned along the sliding direction along with scattered micro-pits of various densities in the tribofilm. By measuring the pit depths, they estimated that the ZDDP tribofilm was in the range of 100–140 nm. Aktary et al. [2] observed the precipitation of ZDDP that forms long chain polyphosphate islands surrounded by the underneath short chain polyphosphate. In some other works [3,4], it has been reported that the ZDDP antiwear tribofilm is a combination of white patches and the dark strips [4] formed along sliding direction. Nicholls et al. [5] suggested that the white area is the long chain antiwear film while the dark area represents the short chain polyphosphates and unreacted ZDDP.

Literatures published show a difference in the mechanisms of the formation ZDDP tribofilms on the ferrous surface. Some research works claim that the presence of Fe_2O_3 at the sliding surface is required for the formation of ZDDP antiwear tribofilm [6–8], while others show the presence of Fe_2O_3 is not necessary [9]. The most recent argument was made by Martin et al. [6] where they proposed a thermo-oxidative mechanism based on the hard and soft acid base (HSAB) principle. The oxidative degradation of ZDDP forms a polymer-like long chain zinc polyphosphate film on the metal surface and liberation of organic sulfur species in the solution. Then the iron oxide coming from the metal surface as wear debris reacts with the zinc-thiophosphate polymer and forms a mixed iron and zinc phosphate glass and metal sulfides.

Manuscript received December 4, 2006; accepted for publication July 9, 2007; published online August 2007. Presented at ASTM Symposium on Automotive Lubricant Testing and Additive Development on 3–5 December 2006 in Lake Buena Vista, FL; Simon Tung, Bernard Kinker, and Mathias Woydt, Guest Editors.
[1] Institute of Engineering Thermofluids, Surfaces and Interfaces (iETSI), School of Mechanical Engineering, University of Leeds, Leeds, LS 2 9JT, UK, E-mail: menth@leeds.ac.uk.
[2] Infineum UK Limited, 1 Milton Hill Abingdon, Oxfordshire, UK.

Therefore, it is necessary to have a ferrous surface or some ferrous elements in the wear scar to produce such ZDDP derived glass-like antiwear films. On the other hand, Fuller et al. [9] proposed a different mechanism of the formation of ZDDP tribofilm where they showed that the presence of Fe_2O_3 was not necessary to form the ZDDP antiwear tribofilm. They exclaimed that the ZDDP is adsorbed onto the metal surface and is converted into linkage isomer (LI) of ZDDP followed by thermal degradation of the adsorbed LI isomer of ZDDP by O_2 or ROOH to form long chain polyphosphate $Zn(PO_3)_2$. Finally, hydrolysis of long chain polyphosphate by the water forms short chain polyphosphate ($Zn_7(P_5O_{16})_2$). This explanation gives an indication of how a ZDDP antiwear tribofilm could potentially form on nonferrous surfaces.

In recent years, low friction carbon-based coatings have been used for the improvement of fuel economy and for the reduction of dependence on the harmful components of lubricants. Diamond-like carbon (DLC) coating has been found as the most popular nonferrous coating due to its high hardness, excellent wear resistance, high corrosion resistance, high thermal and chemical stability, low friction properties [10,11], and excellent running-in property [10,12]. Since no antiwear additive has been designed so far for nonferrous coatings, it is necessary to understand how the existing ZDDP additive interacts with the DLC coating which may give a clue about designing new antiwear additives for nonferrous materials/coatings.

Kano et al. [13] reported the chemical inertness of the DLC coating deposited by CVD (chemical vapor deposition) when oil containing ZDDP and molybdenum dialkyldithiocarbamate (MoDTC), or both, were used. They noticed that no ZDDP tribofilm was formed on the DLC coating while it was observed on the steel counterbody. Barros'bouchet et al. [14] used plasma-assisted chemical vapor deposition (PACVD) coated DLC containing 50 at. % hydrogen sliding against steel counterbody and reported that the tribofilm formed by ZDDP was strongly depleted in P while they found a significant amount of Zn in the tribofilm. Haque et al. [15] observed similar results where they used ZDDP-containing lubricant and a DLC coating that contained 30 at. % hydrogen. In contrast, Ban et al. [16] performed XPS analysis on the boundary layer formed by the oil containing ZDDP on the Si-doped DLC sliding against steel ball and showed the presence of P that remained in the form of $FePO_4$. Thus, results in the literature are found to be quite contradictory and the ZDDP/DLC interaction is yet to be clearly understood.

Similar to a ferrous surface, the structural analysis of the ZDDP tribofilm on the DLC coating can be performed using the AFM technique. The AFM study on the tribofilm formed on DLC was done by Miyake et al. [17]. In their study they performed AFM analysis on the tribofilm formed on Ti-DLC by MoDTC/ZDDP containing lubricant to understand the viscoelastic characteristics of the tribofilm. They observed lower shearing resistance reactant on the DLC wear tract and claimed that those were derived from MoDTC/ZDDP of lubricants. As far as the authors know, no other work reported the structural and topographical analysis of the ZDDP tribofilm formed on the DLC coating. Therefore, a systematic analysis of ZDDP tribofilm on the DLC coating using AFM has been performed in this study.

In this paper, the topographical analysis of the ZDDP tribofilm will be performed using the AFM technique and such information will be supported by the chemical analysis of the tribofilm using XPS. Results in this study will give a clear idea about the antiwear performance of ZDDP additive on the DLC coating.

Experimental

Materials and Coatings

In this work, a hybrid PACVD process was used to deposit the DLC coating on the polished AISI 52100 steel plate material and uncoated BS 1452 cast iron (CI) was used as the pin material. Before depositing the coating, the plates were polished with polishing paper in the sequence of P320, P600, P800, P1000, and P1200 to achieve roughness R_q 0.05 μm. The sliding end of the pin had a radius of 40 mm and the roughness of the pin varied in the range of from R_q 0.7–0.9 μm. For comparison of results, an uncoated steel/CI combination was also used in this study. The properties of DLC coating, uncoated (UC) steel, and CI counterbody are given in Table 1.

TABLE 1—*Physical properties of plate (substrate, coatings) and counterbody materials.*

Properties of Coating/ Specification	Uncoated Steel Plate/Substrate AISI 52100	Cast Iron Counterbody BS 1452	DLC Coated Plate Hydrogenated DLC
Thickness of the coating	…	…	~1 μm
Hardness	8 GPa	4.5 GPa	14.5 GPa
Atomic percentage of hydrogen	…	…	14–16%
Roughness, R_q	0.04–0.06 μm	0.7–0.9 μm	0.04–0.06 μm
Reduced Young's modulus	218 GPa	134 GPa	130–200 GPa

Lubricants

In this study, a poly-alpha-olefin (PAO) base oil containing ZDDP antiwear additive was used and the properties of the lubricants and respective film thicknesses are given in Table 2. The film thickness and lambda ratio were calculated using Eq 1 and Eq 2, respectively.

The minimum film thickness,

$$h_{\min} = 3.63 \times R \times U_{\Sigma}^{0.68} \times G_{\Sigma}^{0.49} \times W_{\Sigma}^{-0.073}(1 - e^{-0.68k_e}) \quad (1)$$

where $U_{\Sigma} = \frac{\eta_0 u_s}{E^* R}$; $G_{\Sigma} = \alpha_p E^*$; $W_{\Sigma} = \frac{P}{E^* R^2}$ and R is the radius of the pin (40 mm), u_s is the sliding velocity (0.015 m/s), P is the normal load (326 N), E^* is the effective modulus of elasticity and k_e is the elliptical parameter which is equal to 1.0339 for a sphere on flat type of contact.

$$\Lambda = \frac{h_{\min}}{\sqrt{R_c^2 + R_p^2}} \quad (2)$$

where R_c is the roughness of the coating and R_p is the roughness of the pin end.

The calculation gives the lambda ratio well under the unity (0.003) that means the lubrication occurred in boundary lubrication regime.

Pin-on-Plate Tests

Tests were performed using a reciprocating pin-on-plate tribotester using an oil containing antiwear additives in boundary lubrication conditions. The contact point of the plate and pin was submerged under a static volume of lubricant (3 mL) at 100°C and the average sliding speed was 0.015 m/s. A load of 326 N was used that gave initial Hertzian contact pressure of 704 MPa which provides the similar pressure range of cam/follower contact of gasoline engine. The friction force data were collected every 5 min for 2 s (120 data points) that corresponds to two strokes of cycles and the duration of the tests was six hours.

Surface Analysis

Wear Measurement—The wear volume of DLC coating was measured using a WYKO light interferometer and the wear volume of pin material was measured by measuring the radius of the wear scar in the optical microscope and using Eq 3.

TABLE 2—*Lubricant components and additive compositions.*

Lubricant	P (ppm)	ZDDP wt %	Base Stock (PAO) wt %	Dynamic Viscosity at (η_0), Pa-s	Viscosity-pressure Coefficient (α_p), Pa^{-1}	Minimum Film Thickness (h_{min}), m
Base oil (PAO) + ZDDP	500	0.64	99.36		@100°C	
				4.03×10^{-3}	1.1×10^{-8}	2.4×10^{-9}

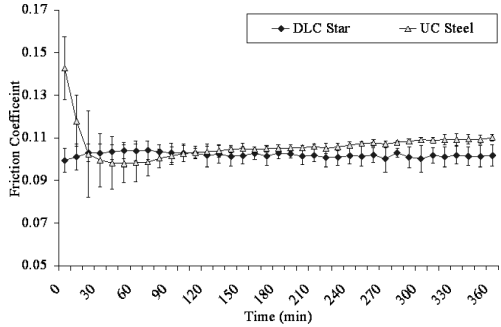

FIG. 1—*Friction coefficient as a function of time.*

$$V_{pin} = \frac{1}{6}\pi h[3r^2 + h^2] \tag{3}$$

where $h = R - \sqrt{R^2 - r^2}$, R=Tip radius of the pin=40 mm, $r = d/2$=Radius of the wear scar measured (m), V_{pin}=Volume loss of pin material (m^3), h=Height of the sphere of pin worn after the wear test.

Topographical/Structural Analysis of the Tribofilm—Analysis of nano-thickness tribofilm by AFM provides lateral and vertical resolution less than 0.1 nm while the scanning electron microscopy gives lateral resolution of 3 nm but does not provide vertical resolution [18]. In addition, the analysis in AFM can be done in ambient condition. Therefore, in this study, the AFM technique has been adopted to do topographical analysis of the tribofilm. The scanning probe microscope (SPM) used was a Topometrix TMS 2000 explorer (TM Microscopes). This equipment also provided lateral force microscopy (LFM) that helps to understand the frictional homogeneity of the surface. The scanner had a maximum scan range of 100 by 100 by 8 μm in the *x*, *y*, and *z* directions, respectively. Scans were carried out in contact mode using a silicon nitride cantilever with a nominal spring constant of 0.03 Nm−1. A constant force of 30 nA was employed by the cantilever during scanning.

Chemical Analysis of Tribofilm—The elemental analysis of the tribofilm was performed by the surface sensitive XPS technique that can probe as small as a few nanometers (5 nm) depth in the tribofilm. The samples were cleaned using *n*-heptane to remove residual oil and contaminants before doing XPS analysis. An area of 500 μm by 500 μm in the wear scar of the plates has been analyzed using a monochromatized AlK_{α} source in the XPS. Spatial mode was chosen to acquire the spectra and an argon etching was performed using an ion gun set at beam energy 3 keV and 1 μA in an area of 1 mm^2 on the wear scar. CasaXPS software [19] was used to fit the curves on XPS peaks obtained from long scans and the quantitative analyses of the peaks were performed using peak area sensitivity factors. A handbook of XPS [20] has been used to find the chemical species at the respective binding energies.

Results and Discussion

Friction and Wear

Friction results given by the lubricant used in this experiment (PAO+ZDDP) are given in Fig. 1. Both DLC coating and UC steel sliding against CI counterbody provided similar friction coefficients (0.10–0.11). The friction coefficient of the UC steel/CI combination increased gradually from 0.1 to 0.11 with time while the DLC/CI combination showed steady friction coefficient at 0.10. The running-in period for UC steel was found around two hours while the DLC coating provided excellent running-in performance showing steady-state friction within a few minutes after starting the test. The friction results given by the oil shows

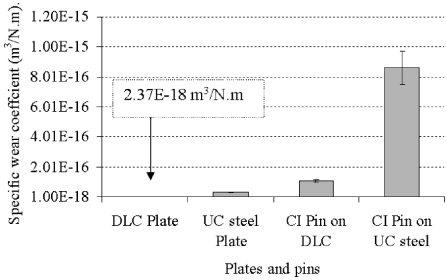

FIG. 2—*Specific wear coefficient of plate and pin materials.*

good agreement with the results published by Kano et al. [13] where they used a CVD-coated DLC sliding against the steel counterbody. It should be noted that, in contrast to this study, they did not detect any ZDDP derived tribofilm on the DLC coating.

The wear coefficient for both plate and pin materials are given in Fig. 2. For the DLC/CI combination, the DLC-coated plate showed one order of magnitude lower than that of uncoated steel while both cast iron counterbodies sliding against DLC coating and UC steel showed wear coefficients in the same order of magnitude; however, the counterbody sliding against DLC coating showed around eight times lower wear rate than that of UC steel. Thus the ZDDP-containing lubricant provided improved wear characteristics for both DLC coating and its CI counterbody compared to the UC steel/CI system. This result can be compared with the published results [14] where the trend has been found that the steel counterbody of the steel/steel combination showed two times higher wear rate than that of the DLC/steel combination. It is interesting to note that DLC coating is much harder than UC steel and use of oil containing ZDDP did not give significant improvement in friction performance as compared to UC steel; however, it provided improved wear performance for its CI counterbody. The possible reason for such result is the longer running-in period of UC steel than DLC coating where the CI sliding against UC steel experienced high friction (>0.10) for initial 30 min. During this time, the CI pin may experience plastic deformation resulting in high wear.

AFM Analysis of the Antiwear Tribofilm

The AFM and LFM images of the DLC coating used in this study are given in Fig. 3(*a*) and 3(*b*), respectively. The topography with uniform *cobblestone*-like distribution can be noticed and it has been reported that such distribution and structure provide long life under slip-rolling tests [21]. In Fig. 4(*a*), micro/nanoscale polishing marks were observed on the UC steel; however, the LFM of both DLC and UC steel surfaces show similar range of lateral forces as given in Fig. 3(*b*) and 4(*b*), respectively.

The AFM image of the wear scar of the DLC coating (Fig. 5(*a*)) shows the presence of tribofilm which is formed along the direction of the original marks left on the DLC coating. It is clearly visible from the LFM image in Fig. 5(*b*) that the deposition or growth of the tribofilm occurs at the raised areas of the

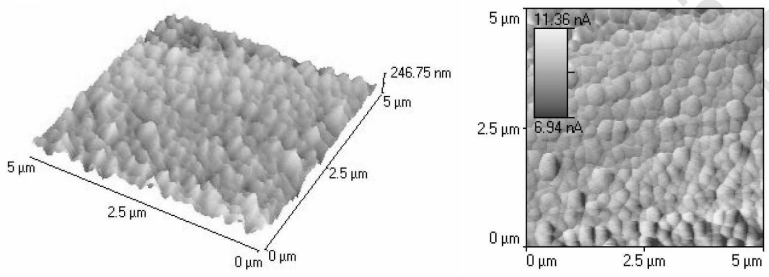

FIG. 3—*(a) AFM image, and (b) LFM image of a typical surface DLC coating.*

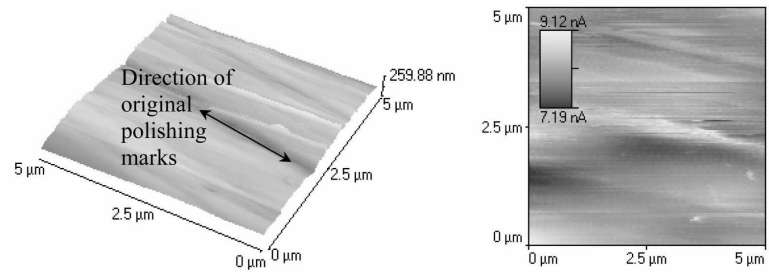

FIG. 4—*(a) AFM image, and (b) LFM image of a typical surface of UC steel.*

coating while it did not properly cover the valleys showing grains of the DLC coating. It is interesting to note that the sliding action could not remove the polishing marks of the DLC coatings and this could be because of high hardness of the coating or the antiwear performance of ZDDP additive.

On the other hand, in case of UC steel as shown in Fig. 6(*a*), polishing marks coming from the sample preparation are not visible on the wear scar and this could be because of the plastic deformation of the raised areas at the sliding surface. Both AFM and LFM images (Figs. 6(*a*) and 6(*b*)), give evidence of the formation of smooth tribofilm with some scattered micro-pits along the sliding direction and thus supports the findings of Pidduck et al. [22]. The film thickness of the tribofilm has been found in the range of 100 nm (distance from the exposed grains to the peaks of the tribofilm) which gives good agreement with the findings of this research group.

The AFM analysis clearly indicates that the features of the tribofilm on the DLC coating are quite different from that of UC steel. In the case of DLC coating, the formation of tribofilm was uniform along

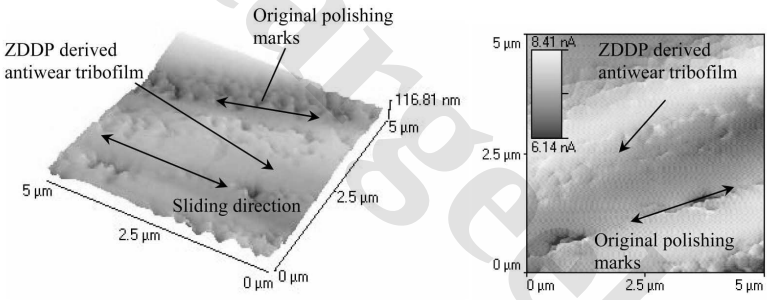

FIG. 5—*(a) AFM image, and (b) LFM image of the ZDDP tribofilm formed on the DLC coating.*

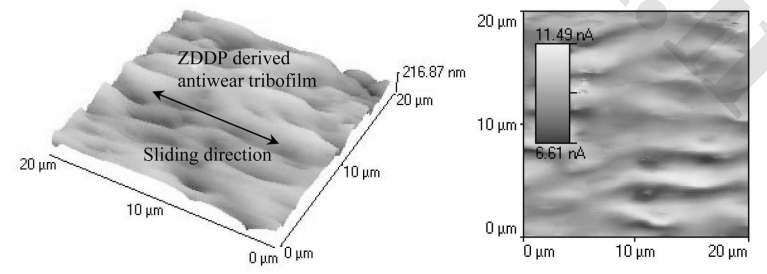

FIG. 6—*(a) AFM image, and (b) LFM image of a tribofilm formed on the UC steel.*

TABLE 3—*Chemical quantification of the ZDDP antiwear tribofilm formed on the DLC coating.*

Chemical Elements	DLC Coating at. %	Uncoated Steel at. %
P2p	1	4.2
S2p	1.2	1.6
C1s	62.1	3.1
O1s	3.8	13.4
Cr2p	0	1.4
Fe2p	0	2
Zn2p	31.9	74.2

the raised portion of the initial marks on the surface. This could be because the raised portions come into severe tribo-contact and thus promote chemical reaction to occur facilitating the formation of tribofilm. In contrast, a patchy distribution of film was observed on the UC steel showing some randomly distributed *micro-pits*. However, the LFM images of both DLC and UC steel in the wear scar indicates a similar range of lateral force distribution. This result indicates that the frictional homogeneity of the ZDDP tribofilms formed on both DLC and UC steel by showing very small variation in the lateral force.

Chemical Analysis of the Tribofilm

XPS analysis of the ZDDP tribofilm formed on the DLC coating was performed to know the chemical composition as well as the compounds formed by the additive. Results of the tribofilm formed on the UC steel have been provided to make a good comparison with those of the DLC coating. The chemical quantification of the tribofilm as given in Table 3 shows that Zn, P, and S were found in the wear scar of the DLC coating and those are believed to be derived from the decomposition of ZDDP additive. It appears that the amount of those elements is lower than that of UC steel. Although the CI counterbody sliding against the DLC coating experienced wear loss (Fig. 2), no Fe was found in the wear scar of the DLC coating. Similar results can be found in the elemental composition of the tribofilm reported by Barros'bouchet et al. [14]. The absence of Fe in the tribofilm could be either because the wear of the CI counterbody was too low to form chemical compounds or the surface of the DLC coating may not be a favorable surface to form ferrous compounds. The source of Cr in the wear scar of DLC coating could be from the adhesion-promoting layer. The absence of Cr in the wear scar indicates that no delamination of the DLC coating occurred.

The binding energy (BE) of C1s peak (284.6 eV) as given in Table 4 represents either hydrocarbon carbon (284.2 eV–285 eV) or graphite (284.4 eV) [23]. The possibility of the presence of graphite in the wear scar of the DLC coating is visible because the structure of DLC is inherently metastable and the heat generated at the sliding contact from the tribo-friction can easily transform sp^3 structure into sp^2 structure (graphite-like) [24].

Figure 7 and Table 4 show the XPS spectra and the binding energies of C1s, O1s, P2p, S2p, and Zn2p peaks. The BE 531.8 eV of O1 s represents the nonbridging oxygen (-P-O-Zn, Zn-O-Zn, Zn-OH) while the BE 533.4 eV represents the bridging oxygen (P-O-P) [25]. The BE of P2p peaks indicate that the

TABLE 4—*Binding energies of the XPS peaks and the corresponding chemical bonds of the ZDDP tribofilm formed on DLC coating.*

Peaks	Binding Energy, eV	FWHM	Chemical Bond
C 1s	284.6 (100 %)	1.43	Carbon/Graphite
O 1s	531.8 (59.7 %)	1.75	NBO
	533.4 (34.88 %)		BO
	529.78 (5.65 %)		Oxide
P 2p	133.1 (76.84 %)	1.48	Pyrophosphate
	134.9 (29.17 %)		Metaphosphate
S 2p	161.3 (42.92 %)	1.57	Sulfide
	163.0 (56.9 %)		Sulfide
Zn 2p	1022.5 (100 %)	1.51	ZnS/ZnO/Zinc Phosphate

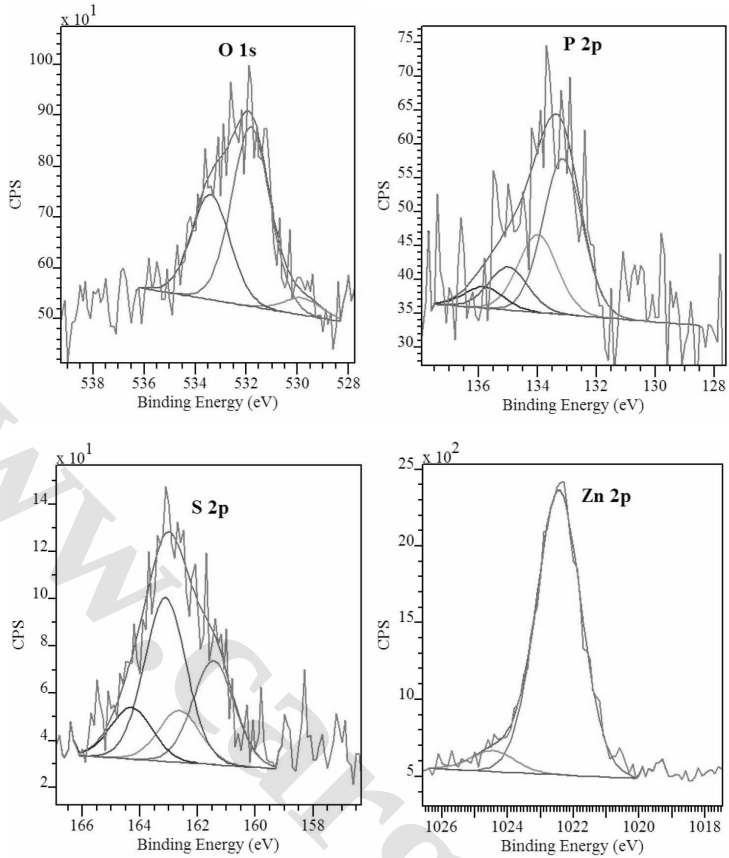

FIG. 7—*XPS peaks recorded in the tribofilm formed on DLC coating: (a) O1s peaks, (b) P2p peaks, (c) S2p peaks, and (d), Zn2p peak.*

tribofilm formed on the DLC coating was composed of pyrophosphate and metaphosphate [20]. Both S2p peaks represent the formation of sulfide compounds. The BE 1022.5 eV of Zn 2ppeak is attributed to the formation of ZnS, ZnO [20] and zinc phosphate glass [25]. From published studies, it has been found that the binding energy of O1s and Zn2p peaks for Zn-OH are 531.6 eV [26], and 1022.7 eV [27], respectively, and those values are close to the corresponding values of NBO and Zn 2p peaks found in this study. Therefore, apart from zinc phosphate there is a possibility of formation of other zinc species.

The chemical compounds formed in the wear scar of UC steel are given in Table 5. Similar to the DLC

TABLE 5—*Binding energies of the XPS peaks and the corresponding chemical bonds of the ZDDP tribofilm formed on UC steel coating.*

Peaks	Binding Energy, eV	FWHM	Chemical Bond
O 1s	531.6 (81.20 %)	1.62	NBO
	533.3 (18.8 %)		BO
P 2p	133.3 (95.83 %)	1.76	Pyrophosphate
	134.9 (4.17 %)		Metaphosphate
S 2p	161.9 (42.92 %)	1.51	Sulfide
	163.7 (56.9 %)		Sulfide
Zn 2p	1022.4 (87.92 %)	1.58	ZnS/ZnO/Zinc Phosphate

coating, the binding energies of ZDDP elements found on the wear scar, show the formation of a phosphate glass [20,28] showing agreement with other works [8,28]. An important parameter for glass characterization is the ratio of bridging oxygen (P-O-P) to nonbridging oxygen (-P=O and P-O-Zn) [29], which is equal to:

$$\frac{BO}{NBO} = \frac{(n-1)}{2(n+1)}. \tag{4}$$

where $n=1$ is an orthophosphate, $n=2$ is a pyrophosphate, and in the case that n is higher than 2 it is a metaphosphate. The curve fitting of O1s peak shows that no oxides are observed in the top layers of ZDDP tribofilm which is in agreement with other results published elsewhere [30]. However, the curve fitting of the O1s peak in the case of the DLC coating did show the presence of oxide. Calculation shows that the glass polymerization number for the UC steel is 2.7 which indicates the presence of metaphosphate and it is claimed that such glass like ZDDP tribofilm is made of iron and zinc phosphate matrix containing sulfide species [31]. Similar calculations for the DLC coating show that the value of n is under unity which does not signify any of the predicted glass phases. Now the question arises if only glass like zinc phosphate glass is formed on the DLC coating or whether some other zinc species are also formed which may be responsible for such value of the glass polymerization number. This will be the subject of a subsequent paper.

According to the mechanism described by Fuller et al. [9], the formation of zinc phosphate compounds on the DLC coating is possible without the presence of Fe_2O_3. In this case, because of thermal oxidation the linkage isomer of ZDDP forms zinc polyphosphate and the hydrolysis of zinc phosphate forms short chain zinc pyrophosphate ($Zn_2P_2O_7$) and zinc metaphosphate ($ZnOP_2O_5$). These results contradict with the findings of Haque et al. [15] and Barros'bouchet et al. [14] where they did not find any ZDDP derived P on the DLC coating. However, DLC coatings used by those two groups contained 30 at. % and 50 at. % of hydrogen, respectively. In contrast, in this work, the DLC coating used contained 14–16 at. % of hydrogen, and therefore, the presence of hydrogen in DLC may play a key role in the formation of zinc pyrophosphate and zinc metaphosphate, and further investigation is necessary to verify these findings.

Conclusions

From the qualitative and quantitative analysis of the ZDDP tribofilm formed on the DLC coating, the following conclusions can be drawn:

1. Use of ZDDP antiwear additive on DLC coating offers better wear protection to its CI counterbody than that of UC steel.
2. DLC coating having 14–16 at. % hydrogen shows the formation of ZDDP antiwear tribofilm under boundary lubrication condition.
3. AFM analysis shows that ZDDP tribofilm forms along the raised portion of the original marks left on the DLC surface; those experience severe tribo-contact during sliding and thus facilitates tribo-chemical reaction.
4. The presence of Zn, O, and P in the tribofilm confirms decomposition of ZDDP additive on the DLC coating.
5. The ZDDP antiwear tribofilm on the DLC coating remained as short chain zinc pyrophosphate ($Zn_2P_2O_7$) and zinc metaphosphate ($ZnOP_2O_5$).

References

[1] Pidduck, A. J. and Smith, G. C., "Scanning Probe Microscopy of Automotive Antiwear Films," *Wear*, Vol. 212, 1997, pp. 254–264.

[2] Aktary, M., McDermott, M. T., and Torkelson, J., "Morphological Evolution of Films Formed from Thermo-oxidative Decomposition of ZDDP," *Wear*, Vol. 247, No. 1, 2001, pp. 172–179.

[3] Morina, A., Green, J. H., Neville, A., and Priest, M., Surface and Tribological Characteristics of Tribofilms Formed in the Boundary Lubrication Regime with Application to Internal Combustion Engines," *Tribol. Lett.*, Vol. 15, No. 4, 2003, pp. 443–452.

[4] Ye, J., Kano, M., and Yasuda, Y., "Evaluation of Local Mechanical Properties in Depth in MoDTC/ZDDP and ZDDP Tribochemical Reacted Films Using Nanoindentation," *Tribol. Lett.*, Vol. 13, No. 1, 2002, pp. 41–47.

[5] Nicholls, M. A., Do, T., Norton, P. R., et al., "Chemical and Mechanical Properties of ZDDP Antiwear Films on Steel and Thermal Spray Coatings Studied by Xanes Spectroscopy and Nanoindentation Techniques," *Tribol. Lett.*, Vol. 14, No. 3, 2003, pp. 241–248.

[6] Martin, J. M., "Lubricant Additives and the Chemistry of Rubbing Surfaces: Metal Dithiophosphates Triboreaction Films Revisited," *Jpn. J. Tribol.*, Vol. 42, No. 9, 2002.

[7] Martin, J. M., "Antiwear Mechanisms of Zinc Dithiophosphate: A Chemical Hardness Approach," *Tribol. Lett.*, Vol. 6, 1999, pp. 1–8; Martin, J. M., Crossiord, C., Varlot, K., et al., "Synergistic Effects in Binary Systems of Lubricant Additives: A Chemical Hardness Approach," *Tribol. Lett.*, Vol. 8, 2000, pp. 193–201.

[8] Martin, J. M., Grossiord, C., Mogne, T. L., et al., "The Two-Layer Structure of Zndtp Tribofilms Part I: Aes, Xps and Xanes Analyses," *Tribol. Int.*, Vol. 34, 2001, pp. 523–530.

[9] Fuller, M. L. S., Kasrai, M., Bancroft, G. M., et al., "Solution Decomposition of Zinc Dialkyl Dithiophosphate and Its Effect on Antiwear and Thermal Film Formation Studied by X-Ray Absorption Spectroscopy," *Tribol. Int.*, Vol. 31, No. 10, 1998, pp. 627–644.

[10] Ronkainen H., Varjus S., Holmberg K. "Friction and Wear Properties in Dry, Water- and Oil-Lubricated DlC Against Alumina and DLC Against Steel Contacts," *Wear*, Vol. 222, No. 2, 1998, pp. 120–128.

[11] Kodali, P., Walter, K. C., and Nastasi, M., "Investigation of Mechanical and Tribological Properties of Amorphous Diamond-Like Carbon Coatings," *Tribol. Int.*, Vol. 30, No. 8, 1997, pp. 591–598.

[12] Podgornik, B., Jacobson, S., and Hogmark, S., "DlC Coating of Boundary Lubricated Components-Advantages of Coating One of the Contact Surfaces Rather than Both or None," *Tribol. Int.*, Vol. 36, No. 11, 2003, pp. 843–849.

[13] Kano, M. and Yasuda, Y., "The Effect of ZDDP and Modtc Additives on Friction Properties of DlC-Coated and Steel Cam Follower in Engine Oil," http://www.oetg.at/website/wtc2001cd/html/m-27-11-230-kano.pdf(accessed on 22 June 2006).

[14] Barros'Bouchet, M. I. D., Martin, J. M., Le-Mogne, T., and Vacher, B., "Boundary Lubrication Mechanisms of Carbon Coatings by Modtc and ZDDP Additives," *Tribol. Int.*, Vol. 38, No. 3, 2005, pp. 257–264.

[15] Haque, T., Morina, A., Neville A., Kapadia, R. and Arrowsmith S., "Non-Ferrous Coating/Lubricant Interactions in Tribological Contacts: Assessment of Tribofilms," *Tribol. Int.* (in press).

[16] Ban, M., Ryoji, M., Fuji, S., and Fujioka, J., "Tribological Characteristics of Si-Containing Diamond-Like Carbon Films under Oil-Lubrication," *Wear*, Vol. 253, No. 3–4, 2002, pp. 331–338.

[17] Miyake, S., Saito, T., Yasuda, Y., et al., "Improvement of Boundary Lubrication Properties of Diamond-Like Carbon (DLC) Films Due to Metal Addition," *Tribol. Int.*, Vol. 37, No. 9, 2004, pp. 751–761.

[18] GRC, N., "Surface Interface Analysis Capability," http://www.grc.nasa.gov/WWW/SurfSci/ssb-siac.html(accessed on 22 Nov. 2006).

[19] Fairley, N., "Casaxps Version 2.1.25,"

[20] Moulder, J. F., Stickle, W. F., Sobol, P. E., and Bomben, K. D., "Handbook of X-Ray Photoelectron Spectroscopy," *Minnesota: Pelmir-Elmer Corporation*, 1992.

[21] Klaffke, D., Santner, E., Spaltmann, D., and Woydt, M., "Influences on the Tribological Behavior of Slip-Rolling DLC-Coatings," *Wear*, Vol. 259, No. 1–6, 2005, pp. 752–758.

[22] Pidduck, A. J. and Smith, G. C., "Scanning Probe Microscopy of Automotive Antiwear Films," *Wear*, Vol. 212, 1997, pp. 254–264.

[23] Hellgren, N., Guo, J., Luo, Y., et al., "Electronic Structure of Carbon Nitride Thin Films Studied by X-ray Spectroscopy Techniques," *Thin Solid Films*, Vol. 471, No. (1-2), 2005, pp. 19–34.

[24] Neville, A., Morina, A., Haque, T., and Voong, M., "Compatibility between Tribological Surfaces and Lubricant Additives—How Friction and Wear Reduction Can Be Controlled by Surface/Lube Synergies," *Tribol. Int.* (in press).

[25] Onyiriuka, E. C., "Zinc Phosphate Glass Surfaces Studied by XPS," *J. Non-Cryst. Solids*, Vol. 163, No. 3, 1993, pp. 268–273.

[26] Pokhmurs'kyi, V. I., Zin, I. M., Laion, S. B., and Bilyi, L. M., "Surface Films on Zinc-Plated Steel Formed on Holding in Aqueous Extracts of Anticorrosion Pigments," *Mater. Sci.*, Vol. 39, No. 4, 2003, pp. 511–516.

[27] Wagner, C. D., Naumkin, A. V., Kraut-Vass, A., et al., "NIST X-ray Photoelectron Spectroscopy Database," http://srdata.nist.gov/xps/(accessed on 30 Nov. 2006).

[28] Morina, A., Green, J. H., Neville, A., and Priest, M., "Surface and Tribological Characteristics of Tribofilms Formed in the Boundary Lubrication Regime with Application to Internal Combustion Engines," *Tribol. Lett.*, Vol. 15, No. 4, 2004, pp. 443–452.

[29] Minfray, C., Martin, J. M., Esnouf, C., et al., "A Multi-Technique Approach of Tribofilm Characterization," *Tribol. Lett.*, Vol. 447, No. 1, 2004, pp. 272–277.

[30] Grossiord, C., Martin, J. M., and Mogne, T. L., "Friction-Reducing Mechanisms of Molybdenum Dithiocarbamate-Zinc Thiophosphate Combination: New Insights in Mos2 Genesis," *J. Vac. Sci. Technol. A*, Vol. 17, No. 3, 1999, pp. 884–890.

[31] Minfray, C., Martin, J. M., Barros, M. I. D., et al., "Chemistry of ZDDP Tribofilm by Tof-Sims," *Tribol. Lett.*, Vol. 17, No. 3, 2004, pp. 351–357.

Journal of ASTM International, Vol. 4, No. 8
Paper ID JAI100938
Available online at www.astm.org

Eric Fitamen,[1] *Laurent Tiquet,*[1] *and Mathias Woydt*[2]

Validation of Oxidative Stability of Factory Fill and Alternative Engine Oils Using the Iron Catalyzed Oxidation Test

ABSTRACT: Oxidation resistance is one of the limiting factors for long drains, bionotox, LowSAP or NoSAP engine oils. The French iron catalyzed oxidation test (ICOT) uses 60 ppm iron acetylacetonate as diluted catalyst under an aeration of 10 L/h at 170°C. The ICOT ranks the oxidation stability of oils according to three properties: a. the viscosity increase (e.g., max. $\Delta\eta^{40°C}<100$ % or $\Delta\eta^{100°C}<100$ %), b. the increase to an individual TAN (e.g., max. 7.5 mgKOH/g) and c. the oxidative evaporation losses of max. 10 % at $\Delta\eta=100$ % due to oxidation. This paper describes the ICOT method standardized as GFC Lu 36T 03 and the obtainable accuracy. Also, results are compiled achieved with this test for factory fill engine oils as well as alternative prototype engine oils based on esters, blends of esters with hydrocarbons, and polyglycols.

Introduction

In order to reduce the costs related to testing and to meet the shortened development time schedules, especially OEMs are more and more interested in methods which do not require an engine for testing functional properties of lubricants and piston ring/liners materials/coatings. Recently, an increasing number of criteria have been placed for the engine oils to meet. This continuously reduces the time available to address the new demands and turn them into functional solutions.

Most lubrication applications expose lubricants to oxygen in some manner. They are therefore susceptible to oxidation and, in the case of usage as engine oils, are additionally subjected to NOx and SOx.

In general, the purpose of oxidation testing is to study, evaluate, and meaningfully rank the oxidation as well as the thermal performance of lubricant additives, base oils, and candidate formulations under simulated operating conditions with the aim to predict as close as possible the performance of those lubricants in real world applications.

A number of oxidation and thermal stability tests suitable for engine oils have been developed by ASTM, DIN, JASO, IP, and French GFC:

a. ASTM D 4742 (AFNOR NF T 60-182), “Standard Test Method for Oxidation Stability of Gasoline Automotive Engine Oils by Thin-Film Oxygen Uptake,” thin film oxygen uptake test (TFOUT),
b. DIN 51352, “Testing of lubricants; determination of aging characteristics of lubricating oils; increase in Conradson carbon residue after aging by passing air through the lubricating oil,”
c. IP 48, “Oxidation characteristics of lubricating oils,”
d. ASTM D 6335, “Standard Test Method for Determination of High Temperature Deposits by Thermo-Oxidation Engine Oil Simulation Test,” thermo-oxidation engine oil simulation test (TEOST),
e. CEC L-48-A-00, “Bulk oxidation test” (same as GFC T-021-A-90),
f. JSAE JASO M333, “High temperature oxidation stability test procedure for evaluating automobile gasoline engine oils,” or
g. ASTM D 7098, “New Standard Test Method for Oxidation Stability of Lubricants by Thin-Film Oxygen Uptake (TFOUT)1 Catalyst B2.”

Manuscript received December 4, 2006; accepted for publication June 18, 2007; published online September 2007. Presented at ASTM Symposium on Automotive Lubricant Testing and Additive Development on 3–5 December 2006 in Lake Buena Vista, FL; Simon Tung, Bernard Kinker, and Mathias Woydt, Guest Editors.
[1] RENAULT SAS, F-78288 Guyancourt
[2] Federal Institute for Materials Research and Testing (BAM), D-12200 Berlin

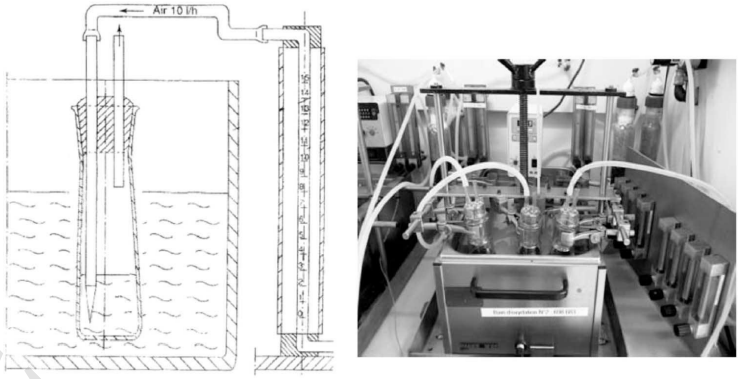

FIG. 1—*Schematics and photos of the test equipment used for the ICOT.*

It has to be noted, that many companies have proprietary methods they use in-house. The French GFC standardized "ICOT" developed by the GFC working group "LM2/SG6" can be considered as an OEM-driven in-house test of the two French car makers, Renault SAS and PSA Peugeot Citroën, with a clear emphasis on car engines, which actually attracts the attention of other European car manufacturers.

Other OEMs, like FORD with the FOAT [1] "Ford Oil Aging Test," developed also a proprietary engine oxidation test which reflects the OEMs-specific needs. FOAT intends to simulate the ASTM-sequence IIIE and is suited for the homologation of engine oils according to the FORD Double IIIE specification. The viscosity increase was limited to +50 % after 128 h.

The ICOT is attractive overall for benchmarking factory fill oils of competitors and suppliers as wells as ranking alternative engine oil concepts prior to engine testing. Basically, the combined intrinsic functional properties of ICOT are its valued attraction.

Test Method

Apparatus

The French ICOT [2] (ICOT = iron catalyzed oxidation test, see Fig. 1) uses 60 ppm iron acetylacetonate ($C_{15}H_{25}FeO_6$) as the diluted catalyst. The initial amount of oil needed is 150 g, with air bubbling through this specimen at a rate of 10 L/h for a period of test time which is a function of the oil performance expected (usually 0, 12, 24, 48, 72, 96 h, etc.). In order to perform an ICOT with a duration of 96 h, six tubes are needed.

Drain Criteria (Oil Changes Intervals)

The ICOT defines the oxidation resistance of a lubricant at 170°C under an aeration of 10 L/h for three properties: viscosity, TAN, and oxidative evaporation loss. A lubricant is considered to have reached the end of its lifetime or lost its resistance to oxidation, if:

The viscosity increase is larger than e.g., $\Delta\eta > 100$ %,

1. the increase of an individual TAN exceeds 7.5 mgKOH/g and (or?)
2. the oxidative evaporation losses at $\Delta\eta = 100$ % exceed 10 %. The actual times for these three properties of a lubricant tested to reach the above conditions may differ, but all three give a quite clear indication about the oxidation processes. The oxidative evaporation losses should not be higher than 10% at the criteria of a viscosity increase of $\Delta\eta = 100\%$.

The induction times of the ICOT properties can differ among the OEMs, e.g., 50 to 200 % for the viscosity increase at 40 or 100°C. The ICOT indicates only the oxidative resistance and gives no hint about the AW/EP-retention of a formulation. For actual factory fill oils, one ICOT hour corresponds to

TABLE 1—*Accuracy Statements for the French ICOT (7 Co-operators).*

Precision statement from RR tests		
Repeatability	r=0.05×H	or 96 h±5 h
Reproducibility	R=0.15×H	or 96 h±15 h

Note: H is the interpolated hour with × % increase of the chemical characteristic.

~270–330 km of driving. This relation has to be validated for esters and polyglycols. The ICOT life of PCMO based on hydrocarbons for a drain of 30 000 km lies around 100 hours.

Accuracy of ICOT Results

In order to assess the accuracy of the ICOT, the philosophy of the French working group is to actually use the duration option for comparison. Although the duration of ICOT exceeds other tests by far, its results are more representative than calculating the respective accuracy based on a one-hour test only. After one hour, the lubricant is still far from the end of its lifetime which, however, is the best condition to appreciate the accuracy of the method (see Table 1).

Results

Factory Fill Oils

Comparing Fig. 2 with the experiences gained in the field with the test results obtained with the ICOT, the following extrapolations can be made:

a. ACEA A2/B2 classified lubricants have an ICOT lifetime below 48 h which converts to a maximum oil change interval of <20 000 km,
b. ACEA A3/B3 ones have an ICOT lifetime between 48 and 72 h converting to an oil change interval of between 20 000 and 30 000 km,
c. ACEA A3/B3 high performance grades exhibit an ICOT lifetime between 72 and 96 h and have a target oil change interval of ~30 000 km,
d. ACEA A5/B5 grades have an ICOT lifetime above 96 h and a potential oil change interval of ~40 000 km.

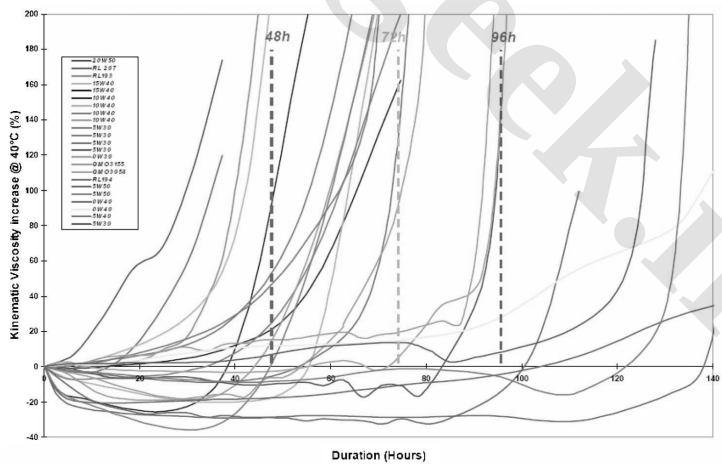

FIG. 2—*Viscosity increase versus oxidation test time (T=170°C) of different factory fill oils (red curves=ACEA A2/B2, blue curves=A3/B2 and A1/B1; green curves=A5/B5)*

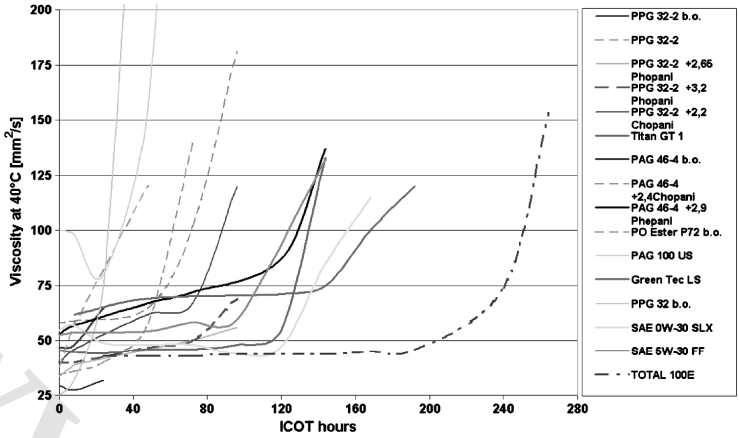

FIG. 3—*Viscosity increase versus oxidation test time (T = 170°C) of different alternative oils and factory fill oils.*

Figure 2 suggests that the performance level of factory fill oils can be ranked semi-quantitatively by the ICOT test. It is also interesting to note that some formulations display a loss or drop in viscosity which is a concern for the hydrodynamic design of the tribosystems. Therefore, the viscosity increase as criteria may also be put into relation to this drop in viscosity.

Alternative Oils

Figure 3 displays the viscosity increase versus test time and Fig. 4 the oxidative evaporation losses during ICOT used for validation of alternative engine [3] oils (the respective base oils used are esters, polyglycols as well as blends of esters with hydrocarbons).

The GreenTec LS (100 % ester base oil) as well as the best "bio-no-tox" formulations GT1 (a blend of hydrocarbons with esters, which conforms with VW 50300/50600), PPG 32-2 + Phopani or PAG 46-4

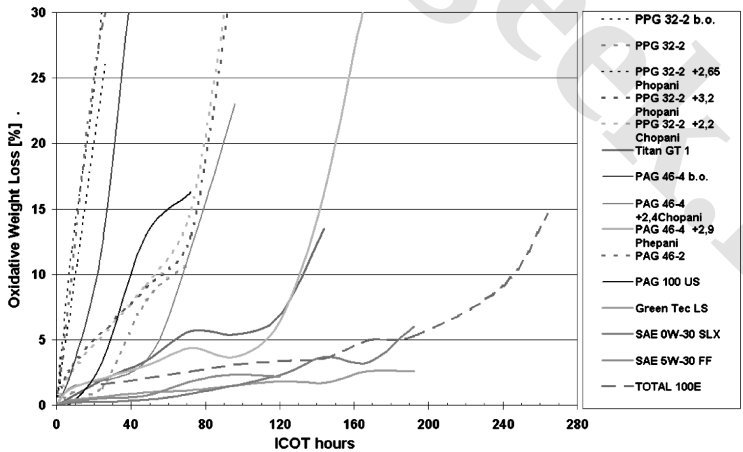

FIG. 4—*Oxidative evaporation losses of different engine oil formulations versus ICOT time (T = 170°C).*

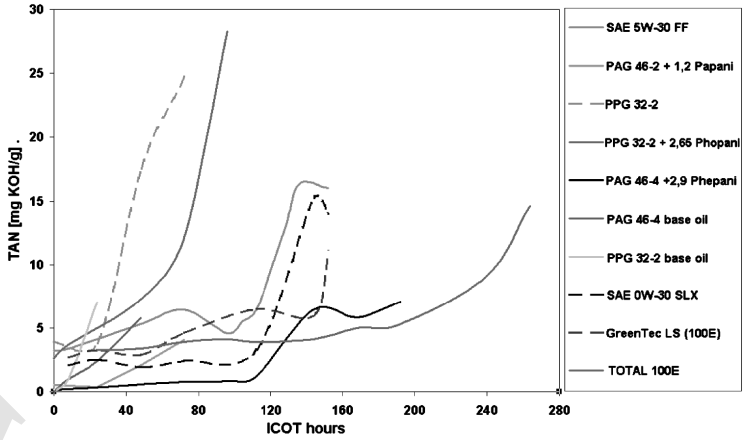

FIG. 5—*Evolution of TAN versus ICOT time of polyglycols.*

+Phepani achieves between 100 and 160 h of lifetime before reaching one of the criteria of the ICOT for long duration. For convenience, the artificial names “Phopani” and “Phepani” are used as abbreviations for the respective additive packages.

The custom-made polyglycols PPG32-2 and PAG46-4 with the proprieraty “boosters” for oxidation resistance have an ICOT lifetime of at least 96 h respecting the bionotox-criteria (biodegradable and nontoxic). Overall, “Phopani” ensures 100 h and “Phepani” even 130 and more hours of lifetime.

The contribution of a properly selected polyglycol base becomes obvious by comparing the evolution of the oxidative evaporation losses of the PAG 46-4 base oil (b.o.) to the additivated PAG 46-2. The PAG 46-4 base oil reached one of the drain criteria after 30 h. Further comparison reveals that the “Papani”- and “Phopani”-package can stabilize viscosity increase for up to 100 h, but not the oxidative breakdown resulting in excessive weight losses. In contrast, the “Phepani”-package in a proprietary polyglycol boosts the respective lifetime up to ~130 h concerning all three ICOT drain criteria, viscosity and TAN increase as well as evaporation loss.

The PAG 46-4+ 2,6 Phepani achieved the same ICOT lifetime concerning the viscosity increase as the ester-based Titan GT1 SAE 0W-20 (Fig. 3) and exhibited the same evolution in oxidative weight loss (see Fig. 4). The evolution of the oxidative weight losses gives a good indication of the protecting effect of the antioxidant package against breakage of the molecules of the base oil.

The custom made PAG 46-4 base oil in its unadditivated form reached the individually set limit of 7 mgKOH/g for the TAN criterion after ~48 h (see Fig. 5). Adding 2.9 Phepani to the PAG 46-4, the evolution of TAN over ICOT time impressively demonstrated that the set limit for the TAN criterion was not passed after 130 h or even 192 h.

Even the candidates for ultra-long oil change intervals, namely Greentec LS (100 % ester) and TOTAL 100E (100 % ester) followed by the PAO-based formulation (SAE 0W-30 SLX), exhibiting the lowest oxidative weight losses after 200 h (see Fig. 4), reached the drain criteria for TAN and viscosity earlier.

Conclusions

Without the need of engines, ICOT proves the feasibility to evaluate the oxidative stability within a reasonable test time. Combining the three criteria viscosity increase, TAN, and evaporation loss, ICOT allows a deep insight into the oxidation kinetics.

The new GFC method is the best way to screen the ACEA oil performances in relation to their on-road performances. This test is discriminative to the entire range of engine oils and the information is available in a short time. With this laboratory test, it is possible to extrapolate the oil change interval. However, oxidation performance is only one parameter of oil degradation. The thickening observed after engine

testing is an additional effect also related to the volatility and soot intake of the oil. Also the dilution by fuels.

The ICOT can also be applied in order to screen Low-/NoSAP, polymer, and metal-free alternative engine oils in relation to their bionotox properties.

References

[1] Korcek, S., Jensen, R. K., and Johnson, M. D., "Assessment of Useful Life of Current Long Drain and Future Low Phosphorus Engine Oils," *Proceedings International Tribology Conference*, September 2001, Vienna.

[2] GFC Lu 36T 03, Test d'oxydation catalysé par l'acétyle acétonate de fer (ICOT), Groupe Français de Coordination (GFC), Le Consulat, 147, av. Paul Doumer, F-92852 Rueil-Malmaison, gfc@gfc-tests.org; see also IP48/97 "Determination of Oxidation Characteristics of Lubricating Oil," 2004.

[3] Desplanches, G., Criqui, B., Linnemann, T., and Woydt, M., "Tribological Performances of New Triboactive (Ti,Mo) (C,N) and $Ti_{n-2}Cr_2O_{2n-1}$ as Piston Ring and Cylinder Liner Coatings Interacting With Bio-no-tox Lubricants," *Plenary paper at 15th Int. Coll. Tribology, TAE Esslingen, 17–19 January 2006*, ISBN 3-924813-62-0 or in Industrial Lubrication and Tribology, Issue 2, 2008.

Journal of ASTM International, Vol. 4, No. 4
Paper ID JAI100941
Available online at www.astm.org

Paul W. Michael,[1] *Thomas S. Wanke,*[1] *and Michael A. McCambridge*[1]

Additive and Base Oil Effects in Automatic Particle Counters

ABSTRACT: The U.S. Military specifies the use of Mil-PRF-2104 engine oil in the hydraulic system of certain nontactical military vehicles. Skid-steer loaders and other heavy equipment also use engine oils in their hydraulic systems. These vehicles are required to meet roll-off cleanliness specifications in order to improve hydraulic equipment reliability. Automatic particle counters are used to verify the cleanliness of these systems. Occasionally, particle counters detect phantom particles that cannot be removed by filtration. This paper examines the possible role of base oil and additive selection in the appearance of phantom counts. Filtered Group I and Group III base oils were doped with the components of an engine oil formulation. Particle levels were monitored before and after filtration using an on-line automatic particle counter. The results show that base oil selection has minimal bearing upon appearance of phantom counts while additive selection is a significant factor. Results from three different particle counters are compared. Two laser particle counters that operate by the light-blockage principle were found to produce phantom counts from polydimethylsiloxane antifoam additives. A direct-imaging laser particle counter classified antifoam particles as water droplets and was less susceptible to phantom particle interferences from silicone antifoam additives.

KEYWORDS: Hydraulic Fluid, Engine Oil, Additives, Particle Counting

Background

Reducing Built-in Contamination

The first step in achieving roll-off cleanliness targets is to reduce built-in contamination from hydraulic pumps, connectors, cylinders, and reservoirs. This is vitally important because built-in contaminants, particularly welding slag from fabrication processes, abrasives from cylinder honing operations, and chips from valve manifold machining can irreversibly damage hydraulic components within the first minutes of machine operation. Once these sources of contamination are reduced, the new fluid itself must be eliminated as a contributor to hydraulic system contamination. Often the contamination level of new hydraulic fluids is more than an order of magnitude greater than the contamination limits specified by hydraulic component manufacturers. In order to reduce built-in contamination from new hydraulic fluid, lubricant manufacturers have devised procedures for producing “surgically clean” hydraulic fluid.

Measuring Fluid Cleanliness

Automated white-light and laser particle counters are used to quantify the contamination level of hydraulic fluids. The basic concept of these particle counters is simple; a beam of light is projected through a narrow stream of the sample fluid, when a particle blocks the light, voltage pulse that is proportional to the equivalent diameter of the particle is produced. In our earlier work we found that these sensors can be susceptible to producing phantom counts [1]. Recently LaserNet Fines (LNF), a direct imaging laser particle counter, was developed by the U.S. Naval Research Laboratory and commercialized by Lockheed Martin [2]. This instrument is an optically-based particle analyzer that uses an artificial neural network to analyze pixilated images of wear particles that are projected onto a ccd chip. A schematic diagram of the instrument’s operating principle is shown in Fig. 1. LNF measures the distribution of particles from 4 to 100 μm and classifies contaminants larger than 20 μm based upon their shape. Through the use of mathematical algorithms LNF is able to differentiate images of:

Manuscript received December 12, 2006; accepted for publication March 17, 2007; published online May 2007. Presented at ASTM Symposium on Automotive Lubricant Testing and Additive Development on 3–5 December 2006 in Lake Buena Vista, FL; Simon Tung, Bernard Kinker, and Mathias Woydt, Guest Editors.
[1] Milwaukee School of Engineering, Milwaukee, WI.

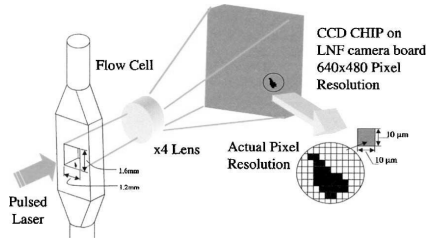

FIG. 1—*Schematic diagram of LaserNet Fines particle imaging system.*

- Cutting wear particles
- Fatigue wear particles
- Sliding wear particles
- Water and air bubbles
- Fibers and nonmetallic contaminants

The ISO Contamination Code

ISO 4406 describes a method of coding the level of solid particles in an oil sample [3]. The code number corresponding to a contamination level comprises three scale numbers, which permits the differentiation of the dimension and distribution of the particles. The first scale number represents the number of particles per milliliter (mL) of fluid ≥ 4 microns (μm). The second scale number represents the number of particles per mL of fluid ≥6 μm. The third scale number represents the number of particles per mL of fluid ≥14 μm. A step ratio of two has been established between the upper and lower limits for each scale number (Table 1). For example, an ISO code of 17/15/12 indicates that there are 641–1300 particles ≥4 μm/mL, 161–320 particles ≥6 μm/mL, and 21–40 particles ≥14 μm/mL of fluid.

Changes in Base Oil Dewaxing Processes

For many years solvent refined paraffinic oils were the primary base stocks used in hydraulic fluids and engine oils. Over the past decade, demand for reduced emissions and enhanced oxidation stability in diesel and passenger car motors oils has led many refineries to convert base oil production from solvent extrac-

TABLE 1—*Ranges for ISO 4406 scale numbers (abridged).*

	Particles per mL	
Scale Number	More than	Less or equal
22	20 000	40 000
21	10 000	20 000
20	5000	10 000
19	2500	5000
18	1300	2500
17	640	1300
16	320	640
15	160	320
14	80	160
13	40	80
12	20	40
11	10	20
10	5	10
9	2.5	5
8	1.3	2.5
7	0.64	1.3
6	0.32	0.64

TABLE 2—*API base oil classifications.*

Base Oil Type	Sulfur %	Saturates %	Viscosity Index
Paraffinic			
Group 1	>0.03	<90	80–120
Group II	<0.03	>90	80–120
Group III	<0.03	>90	>120
Group IV		All Polyalphaolefins	

tion to catalytic dewaxing processes. In catalytic base oil dewaxing, the feedstock is reacted with hydrogen in the presence of a catalyst at high temperatures (400°C) and pressures (3000 psi). This results in:

- Removal of compounds containing sulfur, nitrogen, and oxygen
- Conversion of aromatic hydrocarbons to saturated cyclic hydrocarbons
- Breaking up of higher molecular weight polycyclo-paraffins into lower molecular weight saturated hydrocarbons

The lubricating oils that are produced by this method have higher levels of saturated hydrocarbons and lower levels of sulfur. The American Petroleum Institute (API) categorizes lubricating oils based upon the sulfur and saturated hydrocarbon content (Table 2) [4]. These catalytically processed or hydrocracked base oils provide twice the oxidation life of traditional solvent refined paraffinic oils [5]. This improvement in oxidation stability is the direct outcome of reduced sulfur and unsaturated hydrocarbon levels. While elimination of these components improves oxidation stability, it also reduces the solvency of the base oil and, to some extent, additive solubility [6]. The effect of base oil solubility on particle count results is examined in this paper by comparing Group I and Group III base oils.

Additive Descriptions and Concentrations

Additives are an integral part of modern hydraulic fluid formulations. Some additives, such as dispersants, detergents, antiwear agents, and corrosion inhibitors react with metals and oxidation products to reduce wear and maintain system cleanliness. Other additives such as foam inhibitors and viscosity index improvers enhance the physical properties of lubricants critical to performance. Table 3 describes the additives evaluated in this study and the percent by weight of additive blended into the base oils.

Experimental

Procedure

In this study particle counts for blends of individual additive components were compared to those of a fully-formulated diesel engine oil dispersant-inhibitor (DI) additive system. These additives were mixed into commercial Group I and Group III paraffinic base oils at concentrations similar to what might be found in a typical engine oil. The reservoir was charged with 10 gal of base oil and the pump flow was adjusted to 10 gal/min in order to achieve a nominal circulation rate of one "turn" per minute. The test circuit is depicted in Fig. 2. An MP Filtri LPA-2 on-line particle counter with dual laser sensors was used to monitor the fluid's contamination level at five minute intervals throughout the test. Bottle samples were

TABLE 3—*Additive descriptions and concentrations*

Chemical Description	Function	Weight %
50 TBN calcium sulfonate	Rust inhibitor	1.6
400 TBN calcium sulfonate	Detergent	1.2
Succinimide	Dispersant	1.1
Zinc dithiophosphate	Antiwear agent	1.1
Boronated succinimide	Dispersant	0.9
Polyacrylate	Foam inhibitor	0.05
Polydimethylsiloxane	Foam inhibitor	0.02
Detergent-Inhibitor Package	DEO additive (75 % conc.)	18.8

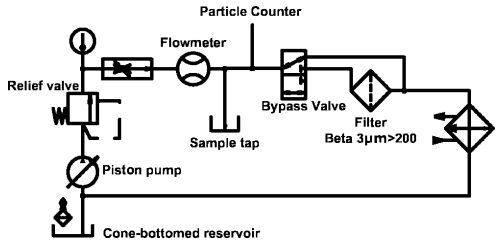

FIG. 2—*Circuit used to assess additive effect in automatic particle counters.*

also collected for off-line analysis. The base oil was circulated through a filter until it reached ISO -/16/13 or cleaner. After the fluid reached ISO -/16/13 and 100°F, the filter-bypass valve was opened and the additive was measured into the cone-bottomed reservoir. After ≥30 min of mixing via circulation the filter bypass valve was closed and the filtration was initiated. (*Note*: The filtration step was omitted if introduction of the additive did not raise the ISO code above -/15/12.) Filtration was discontinued when the ISO Code reached -/15/12 or 30 min, whichever came first. If the fluid did not reach ISO -/15/12 or cleaner within 30 min, the system was drained and flushed with mineral spirits prior to charging it with fresh base oil.

Foam Testing

The ASTM D 892 Standard Test Method for Foaming Characteristics of Lubricating Oils was used to determine if filtration caused depletion of foam inhibitor. In this test, an oil sample is equilibrated at 24°C (75°F). Air is bubbled through the oil for five minutes, and then any foam produced is allowed to settle for ten minutes. The volume of foam is measured at the end of both periods. If all of the foam collapses within ten minutes the collapse time is recorded. The test is repeated at 93.5°C (200°F) and again at 24°C (75°F) after the foam breaks. Various levels of foaming tendency are permitted by industry standards, but stable foam is generally not tolerated.

Particle Counter Calibration

In order to compare particle counter results a second series of tests was performed on the Group I base oil/DI additive combination. In this series of tests a 1 μm, $\beta > 75$ filter was used to filter the fluid, rather than the 3 μm, $\beta > 200$ filter that was used in the prior series of tests. In addition to the MP Filtri LPA-2 on-line particle counter, bottle samples were evaluated using Hiac 8000A and Spectro LaserNet Fines particle counters. Calibration was verified with an ISO 2806 Medium Test Dust secondary reference fluid prior to analysis [7]. The results are shown in Table 4.

Results

The unfiltered Group I and Group III base oils were relatively clean prior to introduction of the additive. In both instances the base oils were found to be cleaner than a typical commercial lubricant. As can be seen in Table 5, blending additives into the base oil increased particle counts to varying degrees. The greatest increase was seen with the diesel engine oil additive and the polydimethylsiloxane antifoam. In terms of absolute counts, the effect of the other additives was less significant. More importantly, these

TABLE 4—*Results of particle counter validation tests with ISO 2806 Medium Test Dust.*

	Reference Fluid			Particle Counter		
Size	C of A	Lower Range	Upper Range	LPA 2	8000A	LNF
≥4 μm counts/mL	6172	5028	8382	5484	6323	6158
≥6 μm counts/mL	2283	1856	3413	2083	2365	2448
≥14 μm counts/mL	170.3	87	439	152	173.6	202

TABLE 5—*Particle count results for additives blended into Group I and Group III base oils.*

Additive	Group I, ISO Code			Group III, ISO Code		
	Base Oil at Start of Test, 100°F	Filter Off 15 Min After Additive Addition	After 30 Min of Filtration	Base Oil at Start of Test, 100°F	Filter Off 15 Min After Additive Addition	After 30 Min of Filtration
50 TBN calcium sulfonate	15/13/<7	13/11/9	13/12/9	15/13/10	15/13/10	15/14/10
400 TBN calcium sulfonate	15/13/10	15/14/11	13/9/<7	13/12/11	15/13/10	15/13/10
Succinimide	13/11/8	16/14/11	16/14/11	15/13/10	15/14/10	15/13/10
Zinc dithiophosphate	16/15/12	17/15/11	17/15/12	15/14/10	15/14/10	14/12/9
Boronated succinimide	16/14/11	17/15/11	17/15/11	13/12/7	14/12/10	14/13/11
Polyacrylate	14/12/8	16/12/10	17/14/12	12/10/<7	15/12/11	15/12/11
Polydimethylsiloxane	15/13/9	>28/22/21	>28/22/16	15/12/10	>28/24/21	21/19/12
Diesel engine additive package	17/14/<7	22/19/14	20/16/7	18/14/<7	22/19/15	21/16/7

other additives responded to filtration in a predictable manner. Typical contamination-versus-time profiles for are depicted in Fig. 3.

In the comparison test of particle counters addition of the DI package to Group I base stock increased all counts substantially. As can be seen in Table 6, there was less agreement between the results after

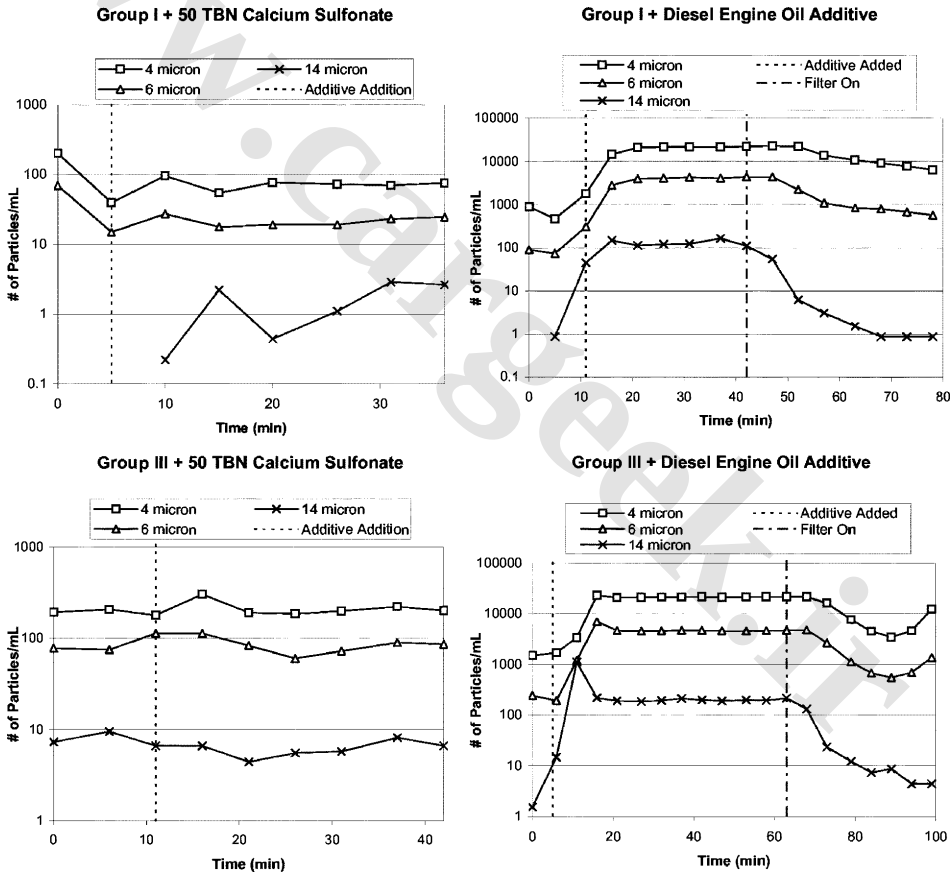

FIG. 3—*Typical contamination versus time profile.*

TABLE 6—*Group I base oil + DI package, comparison of particle counts for three instruments.*

	Instrument		
Description	LPA-2	8000 A	LNF
Group I Base Oil @ 120°F	13/9/<8	15/11/9	13/11/<10
Addition of DI Package	22/20/13	23/21/16	23/21/15
	22/20/16	23/21/16	23/21/15
Begin Filtration	20/15/10	21/15/9	17/14/10
	19/14/9	21/14/<8	16/13/<10
	18/13/8	20/14/9	15/13/10

filtration. The LaserNet Fines particle counter detected numerous hollow spherical particles as shown in Fig. 4. The majority of these particles were classified as water-droplets by the LNF artificial neural network.

Since silicone additives increase particle count significantly the DI-blend was evaluated for foam stability and tendency via ASTM D 892. As can be seen from Table 7, filtration had a slightly increased the foaming tendency and stability of the oil. However, these results are well within acceptable limits for Mil-L-2104 Grade 10 engine oil. ICP spectroscopic analysis performed at a commercial oil analysis laboratory indicated that the change in silicon concentration for the diesel engine oil was $\leq$1 ppm. The precision of this measurement is unknown.

Discussion

The results above indicate that the silicone antifoam agent is the most likely source of phantom counts in light-blockage laser particle counters. Foaming occurs when gas rises to the fluid surface and forms stable bubbles that do not immediately break. Silicone antifoams function by forming an insoluble micelle within air bubble walls that reduces the surface tension of foam and causes thinning of the bubble wall and its collapse. In order to accomplish this, an antifoam must have a surface tension lower than that of the fluid, be insoluble in the fluid, and disperse into small droplets within the fluid [8]. Evidently the insoluble nature of these additives can lead to the appearance of phantom counts in light-blocking laser particle counters.

According to "Form B" data provided by the additive supplier, the DI package contains 6 ppm silicon when diluted in base oil. Silicone fluids have the general structural formula depicted in Fig. 5. In polydimethylsiloxane antifoam additives, R=CH_3 and the number of repeating groups (n) is large. Based upon the structure of the repeating groups, dimethyl silicone compounds contain approximately 38 % silicon, plus carbon, oxygen, and hydrogen. Thus a lubricant that contains 6 ppm silicon in fact contains 16 ppm silicone. Since the density of silicone (0.971 g/cm^3) is greater than that of mineral oil (0.876 g/cm^3), 16 ppm weight is equivalent to ~14 ppm (vol). While 14 ppm might not seem like enough to affect particle count results, each mL of a fluid that is formulated with silicone at a treat rate of 14 ppm by volume contains 14×10^6 cu μm of silicone. Assuming the silicone forms six micron spherical micelles, each micelle contains 113 cu μm per spherical "particle." Thus, if all of the silicone antifoam in the DI package were to form 6 μm micelles, the particle count at the six micron level would exceed

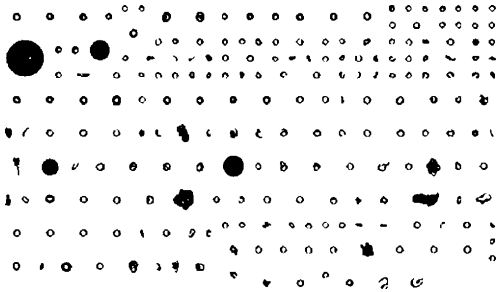

FIG. 4—*LaserNet Fines images produced by DI additive package.*

TABLE 7—*Foam test results before and after filtration.*

		Group I Before/After		Group III Before/Times	
		Tendency	Collapse Time	Tendency	Collapse Time
Seq.	Temp.	mL	Seconds	mL	Seconds
I	24.0°C	0/0	0/0	0/10	0/0
II	93.5°C	20/30	11/16	20/40	10/18
III	24.0°C	0/0	0/0	10/20	12/31

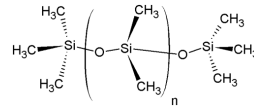

FIG. 5—*Structural formula of polydimethylsiloxane foam inhibitor.*

120 000 particles/mL. As can be seen from Fig. 3, the DI additive produced counts in excess of 120/mL at ≥14 μm, 4000/mL at ≥6 μm and 21 000/mL at ≥4 μm 15 minutes after additive addition. The total volume of these particles is less 1.3×10^6 cu μm, assuming the particles are spherical and there is no significant overlap between the size ranges. This accounts for less than 10 % of the total 14×10^6 cu μm of silicone present in the diesel engine oil. Since there was no appreciable increase in the foam stability of the fluid after filtration and ICP analysis indicated that the change in silicon content was 1 ppm or less, it appears that 90 % of the silicone antifoam remains dispersed in the fluid at a particle size less than 4 μm.

Conclusion

Filtered Group I and Group III base oils were doped with the components of an engine oil formulation. Particle levels were monitored before and after filtration using an on-line automatic particle counter. The results show that base oil selection has minimal bearing upon appearance of phantom counts while additive selection is a significant factor. Results from three different particle counters are compared. Two laser particle counters that operate by the light-blockage principle were found to produce phantom counts from polydimethylsiloxane antifoam additives. A direct-imaging laser particle counter classified antifoam particles as water droplets and was less susceptible to phantom particle interferences from silicone antifoam additives.

References

[1] Michael, P. W. and Wanke, T. S., "Surgically Clean Hydraulic Fluid—A Case Study," *Proceedings of the 47th National Conference on Fluid Power*, National Fluid Power Association, Milwaukee, WI, 1996, pp. 129–136.

[2] Reintjes, J., Tucker, J., et al., "LaserNet Fines Wear Debris Analysis Technology: Application and Mechanical Fault Detection," *AIP Conference Proceedings*, No. 657B, 2003, pp. 1590–1597.

[3] ISO 4406:1999 Hydraulic Fluid Power—Fluids Method for Coding the Level of Contamination by Solid Particles.

[4] American Petroleum Institute Publication 1509, *Engine Oil Licensing and Certification System*, 13th ed., 1995.

[5] Michael, P. W., *Standards for Hydraulic Fluid Testing, Handbook of Hydraulic Fluid Technology*, G. E. Totten, ed., 2000, Marcel Dekker, NY, p. 1189.

[6] Givens, W. A. and Michael, P. W., *Fuels & Lubricants Handbook*, G. E. Totten, ed., ASTM International, West Conshohocken, PA, p. 335.

[7] ISO 11171:1999 Hydraulic Fluid Power—Calibration of Automatic Particle Counters for Liquids.

[8] Friesen, T. V., "Transmission-Hydraulic Fluid Foaming," SAE Technical Paper 871624, 1987.

Journal of ASTM International, Vol. 4, No. 10
Paper ID JAI100956
Available online at www.astm.org

Michael Müller,[1] *Jingyan Fan*,[2] *and Hugh Spikes*[2]

Design of Functionalized PAMA Viscosity Modifiers to Reduce Friction and Wear in Lubricating Oils

ABSTRACT: Polyalkylmethacrylates (PAMAs) are widely used as both viscosity index improvers and dispersant boosters in engine, hydraulic, and transmission oils. Since they are employed in a relatively high concentration in these roles, it is desirable that they be able to enhance other characteristics of a lubricant and, in particular, its boundary lubricating properties. A series of functionalized PAMAs have been synthesized that can adsorb from oil solution onto rubbing surfaces to produce thick boundary films. These films enhance lubricant film formation in slow speed and high temperature conditions and thus make a significant contribution to their lubricating ability. The current paper describes a systematic study of the influence of functionalized PAMAs on boundary lubrication performance. The high frequency reciprocating test rig (HFRR) was applied to investigate friction and wear under pure sliding. A new test method has been developed which allows wear to be monitored in a rolling and sliding contact based on the mini traction machine (MTM). This, in combination with other tests, is employed to investigate the influence of polymer architecture, functionality, concentration and molecular weight on friction and wear in a range of lubricant formulations. This enables the tailored design of polymers which offer low friction and wear properties.

KEYWORDS: tribology, friction, wear, PAMA, viscosity modifier

Introduction

Polyalkylmethacrylates (PAMAs) are widely used as both viscosity index improvers and dispersant enhancers in engine, hydraulic and transmission oils. Although the main role of these polymers is generally to influence the bulk rheological properties of their blends, it has been shown that some are also able to form boundary lubricating films [1,5]. Previous work has found that some dispersant functionalized PAMAs (d-PAMAs) can form quite thick, adsorbed boundary films in rolling/sliding, high pressure, lubricated contact and that these films have a significant effect on reducing friction in mixed rolling-sliding conditions. This effect is especially marked when the functionality is clustered, as in block copolymers, rather than being statistically distributed. These phenomena have been explained by the adsorption of the polar groups of polymers on metal surfaces [1].

The current paper describes a systematic study of the influence of functionalized PAMAs on boundary lubrication performance. A new test has been developed which allows wear to be monitored in a rolling and sliding contact. This, in combination with other tests, is employed to investigate the influence of PAMA functionality, molecular weight, and concentration on friction and wear.

Test Methods

A High Frequency Reciprocating Rig (HFRR, PCS Instruments), as shown in Fig. 1, was used to measure friction and wear under pure sliding, boundary lubrication conditions.

In this test, a 6.0-mm diameter steel ball is held in a chuck and loaded downwards on the flat face of a 10.0-mm diameter steel disk. The disk is held in a bath which contains lubricant so that the contact between the ball and flat is fully immersed. The bath has heaters and a control system so that the temperature can be set at any required value between room temperature and 200°C. Friction is monitored

Manuscript received January 12, 2007; accepted for publication November 1, 2007; published online December 2007. Presented at ASTM Symposium on Automotive Lubricant Testing and Additive Development on 3–5 December 2006 in Lake Buena Vista, FL; Simon Tung, Bernard Kinker, and Mathias Woydt, Guest Editors.
[1] RohMax Additives GmbH, D-64293 Darmstadt, Germany
[2] Tribology Group, Department of Mechanical Engineering, Imperial College, London SW7 2AZ, UK.

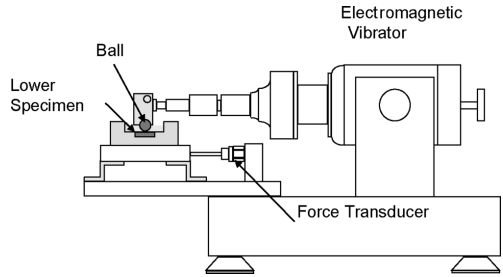

FIG. 1—*Schematic diagram of the HFRR.*

continuously while wear is determined from the wear scar on the steel ball at the end of the test by averaging the scar diameters transverse and along the rubbing direction.

The test conditions used in this work are listed in Table 1.

A Mini Traction Machine (MTM, PCS Instruments) was employed to measure friction in mixed sliding-rolling. In this test rig, the rubbing contact is a steel ball on a steel disk as shown in Fig. 2.

Ball and disk are driven independently so that any required sliding/rolling speed combination can be achieved. Friction is measured by a load cell attached to the housing of the ball drive bearing. Friction testing was carried out at an applied load of 30 N (corresponding to a maximum Hertz contact pressure of 0.93 GPa), a temperature of 120°C, and a fixed slide-roll ratio of $SRR=0.5$. Slide roll ratio is defined as the ratio of the sliding speed to the entrainment speed, i.e., $(u_b+u_d)/U$ where u_b and u_d are the surface speeds of the ball and disk respectively, and U is the entrainment or mean rolling speed given by $(u_b+u_d)/2$. Friction was measured over a range of entrainment speeds and since elastohydrodynamic film thickness depends on $U^{0.67}$ [2], this produces a Stribeck curve, showing how friction varies from boundary/mixed lubrication at slow speed to full-film elastohydrodynamic lubrication at high entrainment speed.

For wear tests, the MTM was used in the bidirectional mode, with the ball rotating in the opposite direction to the disk to give a slide roll ratio greater than the "pure sliding" case of $SRR=2$. In this study, $SRR=5$ was employed. The advantage of this is that it enables tests to be run at very low entrainment speed (and thus in mixed or boundary lubrication) while still being at reasonably high sliding speeds, thus producing significant sliding distance (and thus wear) in a test of reasonable duration. Periodically during the test, samples of oil were extracted and analyzed for iron content using Inductively Coupled Plasma

TABLE 1—*HFRR test conditions.*

Test load	200 g
Test temperature	120°C
Stroke length	2000 microns
Frequency	20 Hz
Test duration	75 min
Ball properties	AISI 52100, 800 VPN
Disk properties	AISI 52100, 650 VPN

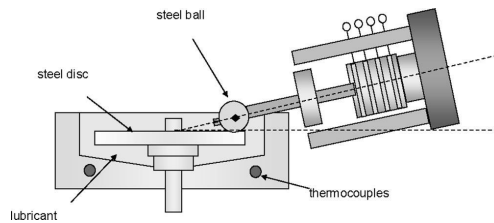

FIG. 2—*Schematic diagram of the MTM rig.*

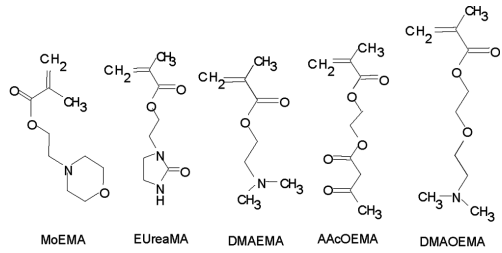

FIG. 3—*Structures of functionalized PAMAs studied.*

Atomic Emission Spectroscopy (ICP-AES), to monitor the extent of wear. This test method is able to monitor mild wear and is fully described in Ref. [3].

Test Materials

A range of dispersant-functionalized PAMAs (d-PAMAs) having different functional groups were synthesized and Fig. 3 shows the structures of those used in the tests reported in this paper.

The polymers contained typically 4 to 8 % of functionalized monomer units, with the rest being alkylmethacrylates. The functionalized units were either statistically distributed in the d-PAMA chains or clustered in block copolymer form. Table 2 lists the main types of polymers studied.

These polymers were blended in one base fluid for study. This was an API Group 1 mineral oil with properties listed in Table 3 (BO). The polymer concentrations used were such as to give a blend in base oil having a viscosity of *ca* 9.2 mm^2/s at the test temperature of 120°C. A base oil also having viscosity of 9.2 mm^2/s at 120°C was blended from two API Group I base stocks to serve as a polymer-free reference oil (RO), as indicated in Table 3

Table 4 lists the various polymer solutions studied. A nonfunctionalized PAMA was included for comparison with the d-PAMAs. All of the d-PAMAs in this paper had block copolymer architecture except for one, designated MoEMA-stat.

Tests were also carried out to explore the influence of molecular weight and concentration of functionalized polymer on friction and wear. The solutions used are listed in Table 5. For varying concentrations, the same 9.2 mm/s^2 viscosity was maintained by replacing some of the d-PAMA by an appropriate proportion of nonfunctionalized PAMA.

TABLE 2—*Functionalities studied.*

	Abbreviation
Nonfunctionalized alkyl methacrylate	NFPAMA
d-PAMA containing functionality	
Dimethyaminoethyl methacrylate	DMAEMA
Dimethylaminoethoxyethyl methacrylate	DMAEOMA
Morpholinylethyl methacrylate	MoEMA
Acetoacetoxy methacrylate	AAcOEMA
Methacryloyl oxyethyl ethylene urea	EUreaMA

TABLE 3—*Base oils used.*

	Description	KV40 mm^2/s	KV100 mm^2/s	KV120 mm^2/s
BO	SN150 mineral oil	30.53	5.180	3.567
RO	Bright stock in SN600 blend having same KV120 as polymer solutions	152.5	14.69	9.241

TABLE 4—*Types of polymer solution used.*

Abbrev.	Mw	Architecture	Conc. wt. %	KV40 mm^2/s	KV100 mm^2/s	KV120 mm^2/s
NFPAMA			28.35	92.56	13.62	9.196
DMAEMA	86000	block	12.2	82.05	13.63	9.149
DMAEOMA	…	block	18.8	81.24	13.79	9.288
MoEMA-stat	84000	statistical	17.9	81.79	13.70	9.208
MoEMA	87000	block	17.0	103.0	14.21	9.246
AAcOEMA	164000	block	8.4	77.31	13.48	9.124
EUreaMA	77000	block	11.6	77.62	13.60	9.211

Friction Properties of d-PAMAs

Friction Reducing Effect of Block, Functionalized Polymer

Figure 4 compares the MTM friction behavior of two MoEMA solutions, one with block architecture and the other statistical. Also shown is the friction response of the reference oil. It can be seen that the statistical MoEMA solution has no beneficial effect on friction compared to the polymer-free oil of similar viscosity, but the block copolymer produces a very marked reduction in friction at intermediate and low speeds.

This behavior is similar to that found previously [1] and its origin is believed to be as shown schematically in Fig. 5. The block functionalized polymer molecules adsorb on polar surfaces to form a

TABLE 5—*Solutions with different concentrations and MWts.*

Functionality	Mw	Conc. d-PAMA wt. %	KV40 mm^2/s	KV100 mm^2/s	KV120 mm^2/s
DMAEMA	23000	26.0	94.01	13.92	9.165
DMAEMA	46000	19.9	83.14	13.68	9.167
DMAEMA	86000	12.2	82.05	13.63	9.149
DMAEMA	146000	8.2	81.64	13.65	9.172
DMAEMA	86000	1.52	93.85	14.01	9.235
DMAEMA	86000	2.83	92.03	13.93	9.204
DMAEMA	86000	5.05	89.99	13.79	9.132
DMAEMA	86000	9.0	85.19	13.70	9.147
MoEMA	87000	1.58	93.81	13.91	9.160
MoEMA	87000	3.04	93.98	13.99	9.218
MoEMA	87000	5.66	94.06	13.98	9.209
MoEMA	87000	11.6	97.37	14.17	9.299
MoEMA	87000	17.0	100.9	14.15	9.232

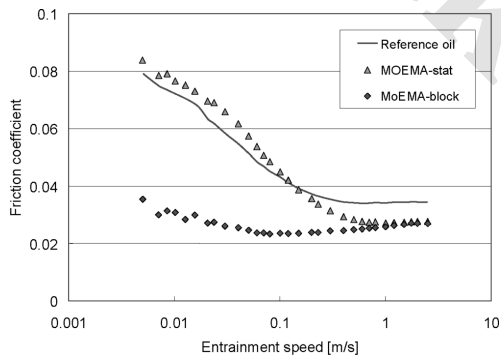

FIG. 4—*Comparison of MTM friction performance of block and statistical MoEMA solutions.*

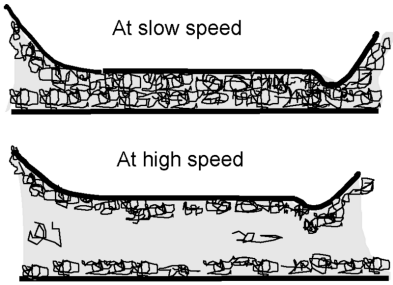

FIG. 5—*Proposed mechanism of film formation and friction reduction by d-PAMAs.*

brush-type layer. This layer has a thickness of the same order of the polymer coil diameter with much higher viscosity than the bulk solution. At low entrainment speeds, when the predicted EHD film thickness based on the viscosity of the bulk solution would otherwise be very low, the contact inlet is actually filled with much higher viscosity, adsorbed, polymer-concentrate, so the resultant entrainment and thus film thickness is much higher than expected. In effect the surfaces remain fully separated by a fluid (concentrated polymer solution) film rather than the negligible film that would be present if there were no surface viscosity enhancement.

From Fig. 4 it can be seen that the high-speed friction of both polymer solutions is considerably less than that of the reference base oil. This indicates that the polymer solutions have a lower EHD friction or "traction" coefficient, probably because the PAMA molecules, being significantly more flexible than most mineral base oil molecules, markedly reduce the EHD traction coefficient of their blends [4].

Effect of a "Spacer" Group on MTM Friction

Figure 6 compares the friction behavior of two functionalized block polymers. Both have a dimethylamine group and the only difference between the two is that in the DMAOEMA, ethoxy groups separate the potentially-adsorbing dimethylamine group from the main polymer chain. This has the effect of reducing the friction at low speeds, suggesting stronger adsorption of this polymer. This may be because the ethoxy groups hold the adsorbing amine group away from the main polymer chain, so that they have easier access to solid surfaces.

Effect of a Chelating Groups on MTM Friction

Figure 7 shows the friction behavior of two d-PAMAs with functional groups that are designed chelating, i.e., to have more than one absorbing group in close proximity on the molecule so that both can participate in forming bonds with the surfaces. It can be seen that both are very effective in reducing friction.

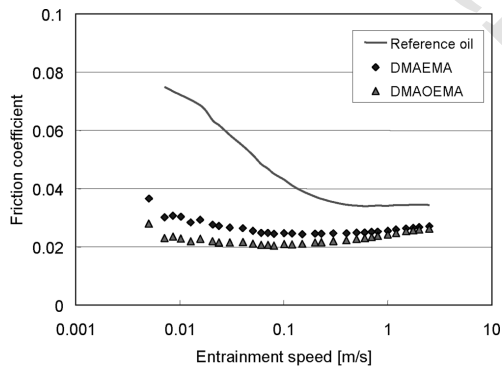

FIG. 6—*MTM friction performance of two d-PAMAs, one with "spacer" group.*

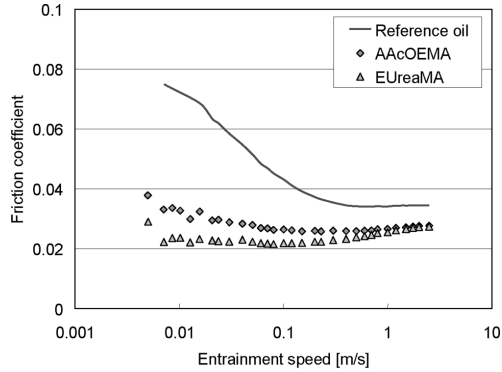

FIG. 7—*MTM friction performance of two chelating d-PAMAs.*

Effect of Polymer Molecular Weight and Concentration on MTM Friction

Figure 8 shows the influence of polymer molecular weight (Mw) on MTM friction for block DMAEMA polymer solutions. There is a very clear effect, with high molecular weight giving lower friction at low entrainment speeds. This probably reflects the greater thickness of adsorbed films of higher molecular weight polymer and consequently greater ability to separate the solid surfaces at low speeds.

Figures 9 and 10 show the influence of functionalized polymer concentration on friction for DMAEMA and MoEMA, respectively. For all solutions the bulk solution viscosity was kept constant by substituting nonfunctionalized PAMA for d-PAMA. For both polymer types, increased concentration produces a reduction in low-speed friction, but this is minor compared to the effect of viscosity. It appears that both polymer types are effective even at polymer concentrations of less than 2 % wt.

Effect of Polymer Molecular Weight and Concentration on HFRR Friction

Figure 11 shows how friction coefficient varies during HFRR tests on MoEMA solutions of various concentrations. The initial effect of the polymer is small, only reducing friction coefficient of the reference oil (0.185) by 8 %. However, after about a 20-min rubbing, the higher concentration polymer solutions produce a marked, but irregular, further reduction in friction. The relative lack of effectiveness of the polymer solutions may indicate that the polymers form films which, while able to reduce friction in mixed sliding-rolling due to enhanced entrainment, are unable to withstand full boundary conditions where there

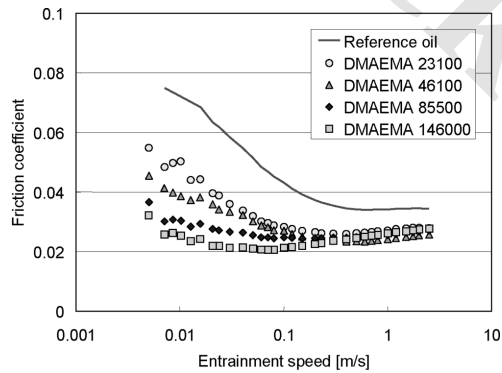

FIG. 8—*Influence of polymer molecular weight on MTM friction for DMAEMA block polymers.*

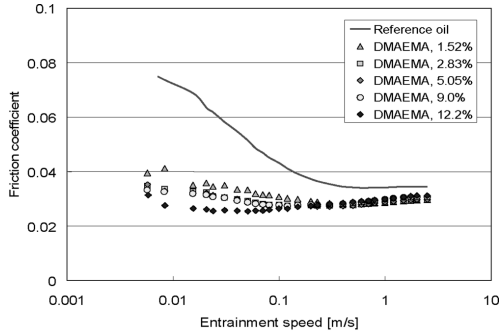

FIG. 9—*Influence of polymer concentration on MTM friction for DMAEMA block polymers.*

is negligible fluid entrainment, as will occur during stroke reversal in the HFRR. The effectiveness of the polymers after prolonged rubbing may then indicate tribochemical reactions of the polymer to form a film that is more strongly bound to the rubbing surfaces.

Similar tests were carried out on the various DMAEMA concentrations. These also showed a small and almost concentration-independent immediate reduction in friction, similar to the MoEMA, but no evidence of a further, time-dependent effect.

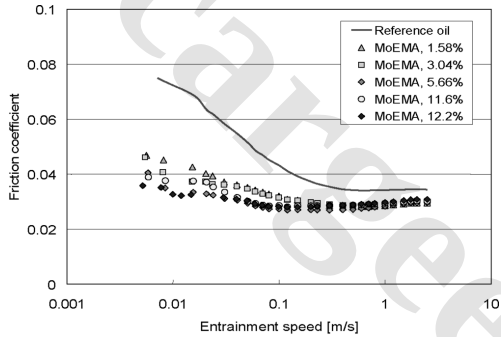

FIG. 10—*Influence of polymer concentration on MTM friction for MoEMA block polymers.*

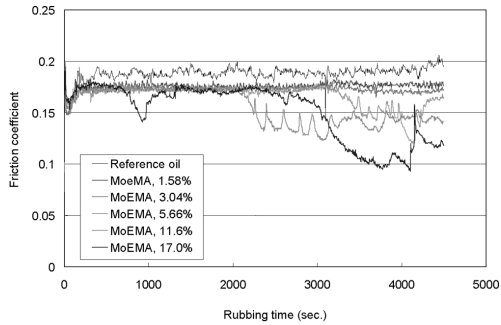

FIG. 11—*HFRR friction behavior of various concentrations of MoEMA block polymers.*

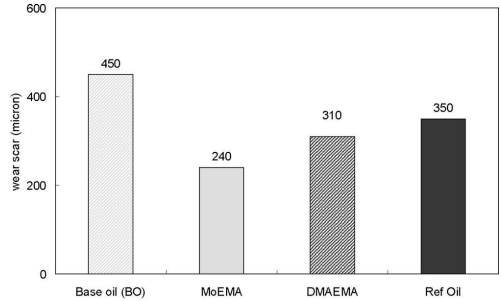

FIG. 12—*HFRR wear performance of 17% wt. solution of MoEMA.*

Wear Results

HFRR Wear Results

Figure 12 compares the HFRR wear performance of solutions of MoEMA and DMAEMA with both the reference oil and the polymer solution base oil (BO). It can be seen that both d-PAMAs significantly reduce wear compared to the reference oil. The wear of the base oil alone is higher than that of the reference oil, probably because the former's viscosity is lower and also possibly because the reference oil contains slightly more naturally-occurring polar species, since it contains higher viscosity base oil fractions.

Figure 13 shows how HFRR wear varies with d-PAMA concentration for both the block DMAEMA and block MoEMA. Also shown is the wear scar diameter for the polymer-free reference oil. The DMAEMA produces a significant reduction in friction even with the lowest polymer concentration and no further benefit is obtained from higher concentrations. This is consistent with the HFRR friction results. For MoEMA, the higher polymer concentrations produce a further wear-reducing benefit, which correlates with the ability of these solutions to produce a further reduction with friction during prolonged rubbing, as seen in Fig. 11.

MTM Wear Results

Figure 14 shows MTM-ICP wear results for various polymer solutions and also the polymer-free reference base oil. The block d-PAMA gives very low, almost immeasurable wear over the whole four hour test while the statistical d-PAMA gives higher wear, but still much lower than the reference oil. It is interesting to note that the nonfunctionalized PAMA (NFPAMA) gives no reduction in wear compared to the reference oil for the first half hour of rubbing but that wear then effectively ceased, as indicated by there being no further increase in iron content of the lubricant. This may be because the NFPAMA molecules are

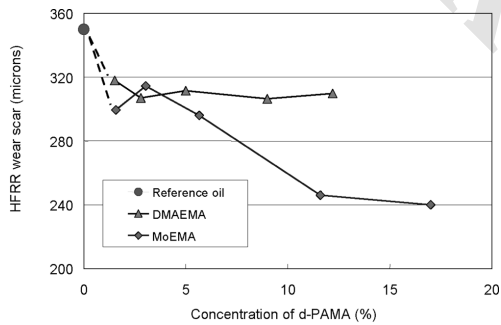

FIG. 13—*Influence of polymer concentration on HFRR wear performance for MoEMA and DMAEMA.*

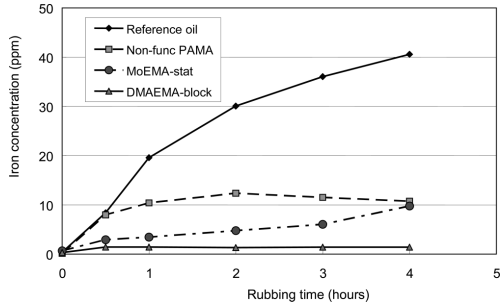

FIG. 14—*MTM wear performance of various PAMA solutions.*

partially broken down within the rubbing contact to form adsorbing species or because wear exposes an active surface on which the NFPAMA molecules themselves are then able to adsorb. One other possibility is that wear of the surfaces in the first half hour leads to an increase in surface conformity and thus a reduced contact pressure, to the extent that weakly-adsorbed NFPAMA molecules are able to withstand the pressure in the contact. This is, however, unlikely since in the rolling-sliding MTM test, both surfaces move with respect to the contact so wear is evenly distributed around wear tracks rather than being localized within the contact, as is the case when one surface is stationary [3].

Discussion

The above results confirm previous work to show that functionalized PAMAs in which the functionality is grouped, such as in the case of block co-polymer architecture, can adsorb on rubbing surfaces to give very pronounced reductions in friction in mixed rolling-sliding steel-on-steel contacts. These reductions can be optimized by judicious choice of functionalities, for example, by using chelating groups. These reductions in friction are believed to result from the adsorption of polymer molecules on the steel surfaces to form viscous surface layers of thickness up to 20–30 nm. The reduction in friction is quite strongly dependent on molecular weight but, for the range of concentrations studied, only slightly dependent on d-PAMA concentration. This suggests that strong adsorption to form a viscous surface film occurs even at bulk polymer concentrations as low as 2 % wt.

Although these polymers are very effective at reducing friction in rolling-sliding MTM contact, they have a much less dramatic effect in the reciprocating, sliding conditions present in HFRR tests. In the latter, contact conditions are much more severe than in the MTM, since the reversal of motion promotes full breakdown of any fluid film and thus almost complete boundary lubrication conditions. It appears that these polymers are less effective in producing protective boundary films under these conditions than in unidirectional, although there is still some benefit on both friction and wear.

Conclusions

The friction and wear-reducing properties of some functionalized PAMA solutions have been studied. It has been shown that significant reductions in friction and wear can be produced by appropriate design and concentrations of these polymers, especially in rolling-sliding contact conditions.

References

[1] Müller, M., Topolovec-Miklozic, K., Dardin, A., and Spikes, H. A., “The Design of Boundary Film-Forming PMA Viscosity Modifiers,” *Tribol. Trans.* Vol. 49, 2006, pp. 225–232.

[2] Hamrock, B. J. and Dowson, D., *Ball Bearing Lubrication. The Elastohydrodynamics of Elliptical Contacts*, John Wiley & Sons, New York, 1981.

[3] Jingyun, F. and Spikes, H. A., “New Test to Measure the Wear-Reducing Properties of Engine Oils,”

Presented at STLE Annual Meeting, Las Vegas, May 2005, and accepted for publication in *Tribol. Trans.*

[4] Smeeth, M., Gunsel, S., Korcek, S. G., and Spikes, H. A., "The Elastohydrodynamic Friction and Film-Forming Properties of Lubricant Base Oils," *Tribol. Trans.* Vol. 42, 1999, pp. 559–569.

[5] Smeeth, M., Gunsel, S., and Spikes, H. A., "Boundary Film Formation by Viscosity Index Improvers," *Tribol. Trans.* Vol. 39, 1996, pp. 726–734.

Journal of ASTM International, Vol. 4, No. 9
Paper ID JAI101079
Available online at www.astm.org

Kazuhisa Miyoshi,[1] *Kenichi Ishibashi,*[2] *and Manabu Suzuki*[2]

Surface Characterization Techniques in Wear of Materials

ABSTRACT: To understand the benefits that tribological engineering materials or surface modifications provide, and ultimately to devise better ones, it is necessary to study the topographical, mechanical, physical, and chemical characteristics of surfaces. This paper reviews advanced surface analytical techniques for measuring surface topography and hardness of engineering surfaces. The primary emphases are on the use of these techniques as they relate to measurements of wear volume loss and nanohardness of materials using optical profilometry and nanoindentation in conjunction with atomic force microscopy, respectively.

KEYWORDS: nanohardness, wear volume measurement, lunar dust simulant, interference microscopy, surface topography

Introduction

Many material properties are actually surface properties. For example, wear, abrasion, erosion, oxidation, corrosion, adhesion, bonding, friction, fatigue, and cracking are all affected by surface properties [1–4]. By modifying surfaces, depositing thin films, or producing multiple-layered coatings, the designer can enhance performance, such as resistance to wear, abrasion, erosion, oxidation, corrosion, and cracking, as well as biocompatibility or environmental compatibility [5,6].

Surface characterization (diagnostic) is important for verifying the success of the selection of tribological materials, lubricants, or the surface preparation process including a coating process or surface treatment, for controlling the surface quality, and for identifying the surface effects that can either enhance or inhibit. Surface characterization techniques are now available for measuring the topographical, micromechanical, chemical, and physical properties, composition, and chemical states of any solid surface. Because the surface plays a crucial role in many mechanical, chemical, physical, and thermal processes, such as adhesion, friction, lubrication, wear, erosion, oxidation, and corrosion, these characterization techniques have established their importance in a number of scientific, industrial, and commercial fields.

Selecting the proper analytical tool and method is crucial to obtaining the right information. To select the proper tool, the researcher must know the size of the specimen, the sampling area, the sampling depth, the spatial resolution, the detection sensitivity, whether quantitative or qualitative results and destructive or nondestructive analysis are desired, and many other factors. Each technique has its strengths and weaknesses. Therefore, no single tool can provide the answers to all problems. In many cases, it will be necessary to use multiple tools to reach an answer. The reader will find the practical applications as well as the basic principles and instrumentation details for a wide range of analytical tools in the literature [e.g.,[7]]. However, the analytical instrumentation field is moving rapidly, and within a year current spatial resolutions, sensitivities, imaging and mapping capabilities, accuracies, and instrument cost and size are likely to be out of date. Therefore, these specifications should be viewed with caution.

This paper generally provides a review of advanced surface characterization techniques for measuring (1) surface topography, and (2) hardness of tribological engineering surfaces. The primary emphasis in the first section is the ways in which noncontact, optical profilometry can be usefully applied to measure wear volume loss of tribological materials, coatings, or films. The primary concern of the second section is the

Manuscript received March 2, 2007; accepted for publication September 12, 2007; published online October 2007. Presented at ASTM Symposium on Automotive Lubricant Testing and Additive Development on 3–5 December 2006 in Lake Buena Vista, FL; Simon Tung, Bernard Kinker, and Mathias Woydt, Guest Editors.
[1] National Aeronautics and Space Administration, Glenn Research Center, Cleveland, Ohio 44135
[2] Nippon Institute of Technology, Saitama, Japan

nanohardness measurements of compacted lunar dust simulants, thin ceramic films, and monolithic ceramics using a Berkovich nanoindenter in conjunction with atomic force microscopy.

Shape of Tribological Surfaces

Surface topography, such as roughness, waviness, and error of form or lay, has a great influence on the surface properties and phenomena of materials, such as surface area, thermal conductivity (or heat contact resistance), electrical conductivity (or electrical contact resistance), bearing area, wear, erosion, corrosion, adhesion, and friction [e.g.,[2]]. Surface roughness is an important parameter in characterizing engineering surfaces used in industrial and commercial applications. Surface texture controls the performance of the product. Surface roughness occurs at all length scales. The advanced surface characterization techniques, such as optical profiler and atomic force microscopy, are available today for three-dimensional profilometry of tribological surfaces, quantitative measurements of film thickness, and wear measurements.

Interference Microscope (Optical Profiler)

The single most useful tool available today to lubrication engineers, surface engineers, and tribologists interested in studying surface texture and topography, surface damage, wear, and erosion of engineering surfaces is undoubtedly the optical profiler, such as scanning interference microscopy and laser scanning microscopy [e.g.,[8–10]]. The noncontact optical profiler can profile an extremely wide range of surface heights and can measure surface features without contact while preserving the sample.

In vertically scanning interference microscopy (also called noncontact, optical profilometry, noncontact, vertical-scanning, white-light interferometry, or noncontact, vertical scanning, laser interferometry), light reflected from the surface of interest interferes with light from an optically flat reference surface. Deviations in the fringe pattern of bright and dark lines produced by the interference are related to differences in surface height. If an imaging array is used, three-dimensional information can be provided. In general, optical profilers have some advantages—nondestructive measurement, no specimen preparation, and short analysis time under ambient conditions—but also some disadvantages. If the surface is too rough (roughness greater than 1.5 mm), the interference fringes can be scattered to the extent that topography cannot be determined. If more than one matrix is involved (e.g., multiple thin films on a substrate), or if the specimen is partially or very transparent to the wavelength of the measurement system, measurement errors can be introduced. Multiple-matrix specimens can be measured if coated with a layer that is not transparent to the wavelength of light used. The shape of a surface can be displayed by a computer-generated map developed from digital data derived from a three-dimensional interferogram of the surface. Computer processing and frequency domain analysis result in a quantitative three-dimensional image. Such a map shows details of individual features and the general topography over an area and describes surfaces. Optical profilometry characterizes and quantifies surface roughness, step height, bearing ratio, height distribution, critical dimensions (such as area and volume of damage, wear scars, wear tracks, and eroded craters), and other topographical features. It has three-dimensional profiling capability with excellent precision and accuracy; for example, profile heights ranging from <0.1 nm to 8 mm at speeds to 100 μm/s with <0.1-nm height resolution, and large profile areas to 50 by 50 mm or 100 by 100 mm.

There has been no easy, accurate way to measure the wear loss produced on a tribological surface or a multilayered surface coating (topcoat/bond coat) system. An even more subtle, yet critical, problem is that these tribological surfaces or protective surface coatings contain two or more materials with different densities. Therefore, simply measuring the specimen mass loss before and after wear or erosion will not provide an accurate gage of the volume losses of the multistructured materials or multilayered coating system. Consequently, wear volume losses have been obtained by measuring cross-sectional areas, determined from stylus tracings using stylus profilometry, across the wear scars. In addition, wear volumes of materials and coatings have been determined from cross-sectioning the wear scars and observing the cross sections by optical microscopy. Both techniques are time consuming. Wear measurement by optical microscopy requires sample destruction and does not provide a comprehensive measure of the entire wear volume loss.

Figure 1 shows optical interferometry images taken from the damaged surface of a typical nickel-based superalloy pin after contact with a gamma titanium aluminide flat (Ti-48Al-2Cr-2Nb in atomic percent) under fretting. Clearly, the surface damage consisted of deposited counterpart material (material

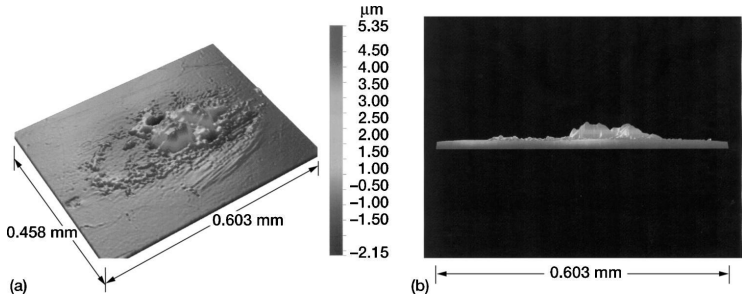

FIG. 1—*Optical interferometry images of damaged surface of nickel-based superalloy pin fretted against gamma titanium aluminide flat (Ti-48Al-2Cr-2Nb in atomic percent) in air. Fretting frequency, 50 Hz; slip amplitude, 150 μm; number of fretting cycles, 1 million; load, 30 N; temperature, 823 K. (a) Three-dimensional view. (b) Side view. Volume of material transferred, 1.35 × 10^5 μm^3.*

transfer), pits, grooves, fretting craters, wear scars, and plastic deformation. Also, the combination of data taken from the optical profilometry, scanning electron microscopy (SEM), and X-ray analysis using energy-dispersive X-ray spectroscopy (EDS) (or wavelength-dispersive X-ray spectroscopy (WDS) could be used) verified the presence of Ti-48Al-2Cr-2Nb on the nickel-based superalloy pin (Fig. 2). The Ti-48Al-2Cr-2Nb failed either in tension or in shear because some of the interfacial adhesive bonds were stronger than the cohesive bonds in the Ti-48Al-2Cr-2Nb. In this fretting wear and fatigue study, the failed Ti-48Al-2Cr-2Nb debris subsequently transferred to the nickel-based superalloy surface in amounts ranging from 10 to 60 % of the nickel-based superalloy contact area at all fretting conditions. The thickness of the transferred Ti-48Al-2Cr-2Nb ranged up to 50 μm. The computer directly processed the quantitative volume and thickness of the transferred material.

Figure 3 presents a three-dimensional view of the Ti-48Al-2Cr-2Nb wear scar at slip amplitude of 200 μm and a temperature of 296 K. In the wear scar are large, deep grooves where the wear debris particles have scratched the Ti-48Al-2Cr-2Nb surface in the slip direction under fretting. The volume loss of this particular wear scar, calculated from the three-dimensional image, was 4.83×10^6 μm^3. Figure 4 shows the volume loss measured by the optical interferometer as a function of slip amplitude for Ti-48Al-2Cr-2Nb in contact with nickel-based superalloy at temperatures of 296 and 823 K. The fretting wear volume of Ti-48Al-2Cr-2Nb generally increased as the slip amplitude increased. An increase in amplitude tends to produce more metallic wear debris, causing severe abrasive wear in the contacting metals, as shown by Fig. 4.

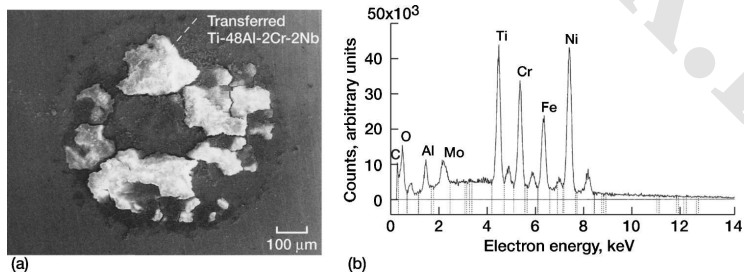

FIG. 2—*SEM backscattered electron image (a) and X-ray energy spectrum (b) of wear scar on nickel-based superalloy pin fretted against Ti-48Al-2Cr-2Nb flat in air at 823 K. Fretting frequency, 80 Hz; slip amplitude, 50 μm; number of fretting cycles, 1 million; load, 1.5 N; temperature, 823 K.*

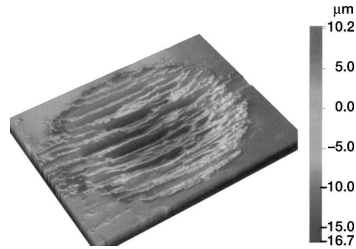

FIG. 3—*Optical interferometry three-dimensional image of damaged surface of gamma titanium aluminide (Ti-48Al-2Cr-2Nb) flat fretted against nickel-based superalloy pin in air. Fretting frequency, 50 Hz; slip amplitude, 200 μm; number of fretting cycles, 1 million; load, 30 N; temperature, 296 K.*

Confocal Microscope (Optical Profiler)

The popularity of confocal microscopy in characterizing surface damage, such as surface cracks, fracture pits, wear scars and craters, scratches, oxides and debris, and material transfer, arises from its ability to produce blur-free, crisp images of thick specimens at various depths [11]. This method improves resolution and contrast by eliminating scattered and reflected light from out-of-focus planes. In contrast to a conventional microscope, apertures are used to eliminate all light but that from the focused plane on the specimen; a confocal microscope projects only light coming from the focal plane of the lens. Light coming from out-of-focus areas is suppressed. An extended-focus image is obtained by recording the maximum signal at the focal setting, without sacrificing the lateral resolution. Thus, information can be collected from much defined optical sections perpendicular to the microscope axis. Confocal imaging can be performed only with point-wise illumination and detection, which is the most important advantage of using confocal laser scanning microscopy. Confocal optics give a high resolution (e.g., 0.25 μm), far exceeding that of normal light microscopes. The confocal microscope can optically section thick specimens in depth, generating stacks of images from successive focal planes. Subsequently, the stack of images can be used to reconstruct a three-dimensional view of the specimen. The brightness of a pixel depends on the intensity of the light measured from that point in the specimen. Like the optical interferometry system, an image of the whole area of interest is collected by either moving the specimen on computer-controlled scanning stages in a raster scan or moving the beam with scanning mirrors to move the focused spot across the specimen in a raster scan. In either case, the image is assembled pixel by pixel in the computer memory as the scan proceeds. The resolution obtained with the confocal microscope can be a factor of 1.4 better than the resolution obtained with the microscope operated conventionally. By memorizing the stage position at maximum intensity with respect to each scanned pixel, noncontact surface profiling is possible.

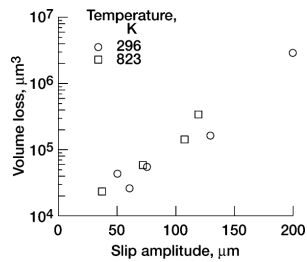

FIG. 4—*Wear volume loss as function of slip amplitude, measured by optical interometry for Ti-48Al-2Cr-2Nb flat fretted against nickel-based superalloy pin in air. Fretting frequency, 50 Hz; number of fretting cycles, 1 million; load, 30 N.*

Atomic Force Microscope (Stylus Profiler).

An atomic force microscope (AFM), also called a scanning force microscope (SFM), can be considered as a derivative of the stylus profilometer. It can measure the force of interaction between a specimen surface and a sharp probe tip. The tip, a couple of micrometers long and often less than 10 nm in diameter, is located at the free end of a cantilever 100 to 200-mm long. When the tip comes within a few angstroms of the specimen surface, repulsive van der Waals forces between the atoms on the tip and those on the specimen cause the cantilever to deflect, or bend. A detector, such as the position-sensitive photodetector measures the cantilever deflection as the tip is scanned over the specimen or the specimen is scanned under the tip. As a piezoelectric scanner gently traces the tip across the specimen (or the specimen under the tip), the contact force causes the cantilever to bend to accommodate changes in topography. The shape of a surface can be displayed by a computer-generated map developed from digital data derived from many closely spaced parallel profiles taken by this process. Such a map shows details of individual features and the general topography over an area and describes surfaces. Many engineering surfaces have height distributions that are approximately Gaussian (i.e., they can be described by the normal probability function). It is also useful to describe surfaces in terms of the integral of the distribution (bearing ratio), which gives the fraction of the surface at or below each height. The well known Abbott's bearing curve, which gives the contact area that would exist if the hills were worn down to the given height by an ideally flat body, is the fraction of the surface at or above each height. Many modern surface analyzers provide chart or video displays of height histogram and bearing ratio (Abbott's bearing curve or bearing area curve) as standard features.

Atomic force microscopes can be used to study insulating and semiconducting materials as well as electrical conducting materials. Most atomic force microscopes currently used detect the position of the cantilever with optical techniques. The position-sensitive photo detector itself can measure light displacements as small as one nm. The ratio of the path length between cantilever and detector to the length of the cantilever itself produces a mechanical amplification. As a result, the system can detect even 0.1-nm vertical movements of the cantilever tip. Other methods of detecting cantilever deflection rely on optical interference, a scanning tunneling microscope tip, or piezoresistive detection (fabricating the cantilever from a piezoresistive material).

Nanohardness and Microhardness of Solid Surfaces

Hardness measurements are a quick, reliable means of quantifying the mechanical properties and performance of modified surfaces, thin films and coatings, and engineering materials. Hardness values measured with a specific method represent a scale by themselves, evaluating the mechanical properties and allowing the comparison of materials. Hardness measurements can quickly yield quantitative information about the elastic, plastic, viscous, and fracture properties of a great variety of both isotropic and anisotropic solids. Hardness measurements can be used to determine the hardness, yield strength, and fracture toughness of a material in a nondestructive manner. The tools used are simple and the specimen sizes needed are typically small, sometimes submicroscopic. It is not necessary to have large specimens to measure strength properties, and it is possible to measure the properties of various microscopic particles within the matrix phase of a polyphase (multiple phase) metal, polymer, mineral, or ceramic as well as a coated material. Therefore, hardness may be considered to be a mechanical properties nano-probe or micro-probe. Many indenters are available for use in hardness measurements. The indenter, being made of diamond, suffers little deformation during the indentation, and the constraint developed is essentially elastic. Researchers tend to work mainly with nanohardness using a Berkovich indenter and with microhardness using a Vickers (or sometimes Knoop) indenter or a spherical indenter.

Nanoindentation Hardness Measurement

Nanohardness measurement, such as by a mechanical properties nanoprobe, is today ideal for thin lubricating coatings, surface-modified materials, multiple-phase materials, composites, and particles on almost any type of material: hard, soft, brittle, or ductile. Hardness, Young's modulus, and time-dependent indentation creep can be determined at penetration depths as small as a few tens of nanometers [e.g., [12]].

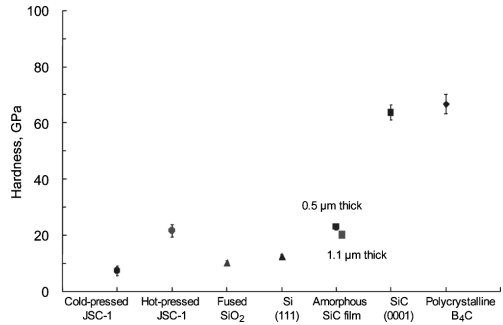

FIG. 5—*Nanoindentation hardnesses for JSC-1 lunar soil simulants and other ceramic materials. Load, 1000 μN.*

An indenter tip, normal to the specimen surface, with a known geometry (e.g., Berkovich or Vickers indenter) is driven into the specimen by applying an increasing load up to some preset value. The load is then gradually decreased until partial or complete relaxation of the specimen has occurred. The load and displacement are recorded continuously throughout this process to produce a load-displacement curve from which the micro-mechanical properties can be calculated. The applied load and penetration depth data can be analyzed to provide the hardness and elastic modulus of the specimen.

Figure 5 presents the nanoindentation hardness for JSC-1 lunar dust simulants and other ceramic materials and coatings. The measured hardness, elastic modulus, and maximum contact depth, obtained from more than 25 indentations, of cold-pressed JSC-1 were 7.3 GPa, 78.0 GPa, and 83.5 nm, respectively. The combination of a quantitative depth-sensing nano-indenter with atomic force microscopy can provide nanometre-scale images of indentation, revealing the imprint of the indents and other surface features with nanometer resolution.

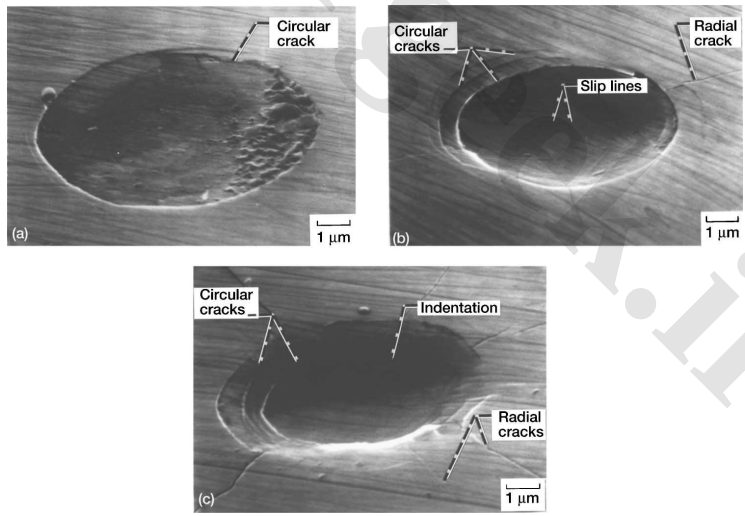

FIG. 6—*Scanning electron micrographs of indentation and cracks on silicon carbide {0001} surface generated by hemispherical indenter. (a) Indenter radius, 0.1 mm; load, 10 N. (b) Indenter radius, 0.02 mm; load, 5 N. (c) Indenter radius, 0.008 mm; load, 2 N.*

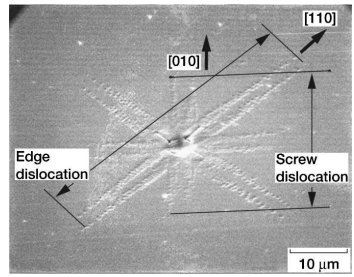

FIG. 7—*Distribution of dislocation etch pits on MgO {001} surface around indentation made by Vickers diamond indenter at load of 0.1 N.*

Microindentation Hardness Measurement

Pyramidal indenters (Vickers, Knoop, and Berkovich indenter) produce square, rhombohedral, and triangular indentations, respectively, that are plastically deformed. Indentation microhardness measures the plastic strength of the material (i.e., the amount of plastic deformation produced). All the pyramidal indenters have a further advantage in that they yield values, in terms of units of pressure, that can be compared directly with other mechanical properties, such as yield stress, yield strength, and Young's modulus, as described in the previous section.

It has already been established that the hardness measured for a crystalline solid is very much dependent on the indenter shape, normal load, temperature, crystallographic orientation of the material with respect to the indented plane, and impurities. For a given crystal, the Vickers and Berkovich indenters give similar results.

Spherical indenters develop tensile stresses around the contact area that encourage brittle fracture rather than plastic flow (Fig. 6). Fracture stresses and spherical indenters can evaluate crack patterns.

The indentation process imposes a considerable hydrostatic stress on the material, a great advantage when indenting brittle materials. The hydrostatic pressure suppresses fracture and makes an otherwise difficult measurement routine. In other types of mechanical tests, such as bend or tensile testing, careful machining is required so that surface defects do not create stress raisers and affect the test. The microhardness test also eliminates the difficulties associated with machine and fixture alignment.

Figure 7 shows the distribution of dislocation etch pits on a well-defined, single-crystal magnesium oxide (MgO) surface. The MgO bulk crystals were first cleaved along the {001} surface in air and then subjected to hardness indentation in air at 298 K, which introduced a certain amount of plastic deformation into the {001} surface. Next, the MgO surfaces were chemically etched in a solution of five parts saturated ammonium chloride, one part sulfuric acid, and one part distilled water at room temperature. Then scanning electron micrographs were taken of the etched surfaces. The dislocation-etch-pit pattern on the indented surface (Fig. 7) contains screw dislocations in the [010] direction and edge dislocations in the [110] direction. The screw and edge dislocation arrays are 4.9 and 7.7 times wider, respectively, than the average length of the two diagonals of hardness indentation.

Figure 8 shows the length of the dislocation row and the length of the diagonal of indentation as functions of load on a log-log scale. As expected, the gradient of the diagonal length is approximately 0.5 because the Vickers hardness is independent of indentation load. Almost the same gradient is shown for the length of edge dislocations. However, the gradient for the screw dislocations is slightly smaller, possibly, because cross slips occur easily at higher loads. The row of edge dislocations is always longer than that of screw dislocations for the hardness indentations.

Cracking and fractures around the indents can affect the accuracy of microhardness measurements. The energy absorbed by plastic deformation far exceeds that released by cracking for many materials. Although it can make accurate measurements difficult, indentation cracking can reveal important material parameters. Indentation cracking can be related to the fracture toughness of the material.

The cracks can be one of two basic types, median or lateral. Median cracks, which form on loading, are deep halfpenny-shaped cracks with the fracture plane normal to the surface. Lateral cracks, which form on unloading, are shallow cracks with a fracture plane approximately parallel to the surface.

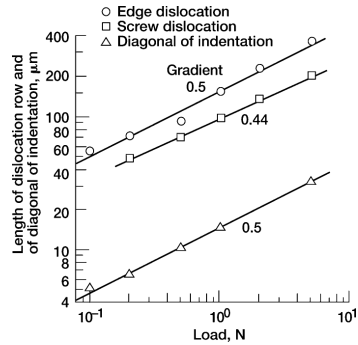

FIG. 8—*Lengths of dislocation row and diagonal of indentation as function of load.*

Concluding Remarks

A wide variety of surface characterization techniques is available for assessing the topographical, mechanical, physical, and chemical properties of surfaces. Each measurement and characterization technique provides unique information. It should be possible to coordinate the different pieces of information provided by these measurement and diagnostic techniques into a coherent self-consistent description of the surface and bulk properties.

References

[1] Miyoshi, K., *Solid Lubrication: Fundamentals and Applications*, Marcel Dekker, New York, 2001.

[2] Miyoshi, K. and Chung, Y. W., Eds., *Surface Diagnostics in Tribology: Fundamental Principles and Applications*, World Scientific Publishing Co., River Edge, NJ, 1993.

[3] Burnnell-Gray, J. S. and Datta, P. K., Eds., *Surface Engineering Casebook, Solutions to Corrosion and Wear-Related Failures*, Woodhead Publishing Limited, Cambridge, UK, 1996.

[4] Erdemir, A. and Martin, J. M., Eds., *Superlubricity*, Elsevier Science, Amsterdam, 2007.

[5] Holmberg, K. and Matthews, A., *Coatings Tribology: Properties, Techniques and Applications in Surface Engineering*, Tribology Series 28, D. Dowson, Ed., Elsevier, Amsterdam, 1994.

[6] Kumar, A., Chung, Y.-W., Moore, J. J., and Smugeresky, J. E., Eds., *Surface Engineering: Science and Technology 1*, The Minerals, Metals, & Materials Society, Warrendale, PA, 1999.

[7] Brundle, C. R., Evans, C. A., Jr., and Wilson, S., Eds., *Encyclopedia of Materials Characterization*, Butterworth-Heinemann and Manning, Stoneham, MA, 1992.

[8] Miyoshi, K., Street, K. W., Jr., Sanders, J. H., Hager, C. H., Jr., Zabinski, J. S., Vander Wal, R. L., Andrews, R., and Lerch, B. A., "Wear Behavior of Low-cost, Lightweight TiC/Ti-6Al-4V Composite Under Fretting: Effectiveness of Solid-film Lubricant Counterparts," NASA/TM-2007–214468, Available electronically at http://gltrs.grc.nasa.gov, 2007.

[9] Miyoshi, K., Sutter, J. K., Horan, R. A., Naik, S. K., and Cupp, R. J., "Assessment of Erosion Resistance of Coated Polymer Matrix Composites for Propulsion Applications," *Tribol. Lett.*, Vol. 17, No. 3, 2004, pp. 377–387.

[10] Miyoshi, K., Farmer, S. C., and Sayir, A., "Wear Properties of Two-phase Al_2O_3/ZrO_2 (Y_2O_3) Ceramics at Temperatures from 296 to 1073 K," *Tribol. Int.*, Vol. 38, No. 11–12, 2005, pp. 974–986.

[11] Chandrasekaran, V., Yoon, Y. I., and Hoeppner, D. W., "Analysis of Fretting Damage Using Confocal Microscope," *Fretting Fatigue: Current Technology and Practices*, ASTM STP 1367, D. W. Hoeppner, V. Chandrasekaran, and C. B. Elliott, III, Eds., ASTM International, West Conshohocken, PA, 2000, pp. 337–351.

[12] Corcoran, S. G., "Nanoindentation of Tribological Coatings on Steel," Hysitron Incorporated, Minneapolis, MN, 1997, Available electronically at http://www.hysitron.com, 2007.

www.astm.org

ISBN: 978-0-8031-4505-4
STOCK #: STP1501